University of Alberta

Reactivity and Hemilability of *ortho*-Phosphinoaniline Complexes of Rhodium and Ruthenium

by

Lindsay James Hounjet

A thesis submitted to the Faculty of Graduate Studies and Research
in partial fulfillment of the requirements for the degree of

Doctor of Philosophy

Department of Chemistry

Spring, 2011
Edmonton, Alberta

Examining Committee

Martin Cowie
Department of Chemistry
University of Alberta

Jeffrey M. Stryker
Department of Chemistry
University of Alberta

Eric Rivard
Department of Chemistry
University of Alberta

Christopher W. Cairo
Department of Chemistry
University of Alberta

Arno de Klerk
Department of Chemical and Materials Engineering
University of Alberta

Michael D. Fryzuk
Department of Chemistry
University of British Columbia

Abstract

Molecular transition metal catalysts offer unique potential for the production of fine chemicals. Chemical processes carried out in the presence of well defined molecular catalysts often only require mild, easily accessible conditions, fewer sacrificial reagents, and can selectively produce a desired product with minimal waste. The active site of a transition metal catalyst can be varied by the use of a hybrid ligand, which employs a combination of groups with different binding affinities for the metal center. Hybrid ligands possessing both substitutionally inert and labile donors, called "hemilabile" ligands, offer an added dimension to catalysis since the weakly binding donor can be displaced from the metal center by a substrate to facilitate the chemical transformation. However this labile donor, in conjunction with an inert donor, can also offer chelate stabilization of the catalyst in the event of coordinative unsaturation at the metal center, a feature which can serve to enhance catalyst longevity.

A major goal of the research reported herein is to understand the mechanisms by which hemilabile processes occur within *ortho*-phosphinoaniline complexes of rhodium and ruthenium and, in turn, how such features might affect catalytic characteristics. To this end, a comparison of catalytic activities of related hemi- and non-labile complexes has been carried out. The ability for two metal atoms held in close proximity to have a cooperative effect on substrate activation or catalysis has also inspired the generation of a series of binuclear compounds bridged by bis(*ortho*-phosphinoaniline) ligands. In addition to hemilabile and

catalytic features, many unique ligand geometries and coordination modes are also observed, particularly by altering the substituents on labile amine donors.

Non-labile complexes can also be prepared by deprotonation of labile amine donors to produce *ortho*-phosphinoanilido species, which display reactivity patterns and structural features distinct from the those of their hemilabile congeners. The amido complexes, which are effective toward ketone transfer hydrogenation and olefin silylation reactions, display interesting features, and in the first case, the possibility of a reaction mechanism unprecedented for transition metal catalysts is discussed. Evidence supporting the operation of such an unexpected mechanism could have important implications for the design and operation of new and more effective transition metal catalysts.

Acknowledgements

Numerous individuals have been instrumental to the completion of this work and, while some have contributed more directly to its development by offering unique scientific perspectives, others have been more influential to my personal development. Over the past four years my PhD supervisor, Martin Cowie, has acted as an outstanding mentor and role model for all of his students, both as a hard-working, meticulous scientist and as an understanding, respectful human being. While Marty's careful criticisms of his students' work have always been thorough and warranted, they has never carried sarcastic or condescending undertones – a quality that I shall always admire. Thanks to former postdoctoral researcher Matthias Bierenstiel who laid the foundation for many of my scientific endeavors and left organized and detailed notes before pursuing a faculty position at Cape Breton University. Throughout my studies, I have had the pleasure of expanding upon his work while keeping him informed of progress at the annual Canadian Society for Chemistry Conference. I thank X-ray crystallographers Robert McDonald and Michael J. Ferguson, whose immense scientific contributions cannot be overstated. It has been a pleasure to work just across the hall from them.

I would like to thank former graduate student colleagues and friends Rahul G. Samant and Owen C. Lightbody, who have both made scientific contributions through intellectual discussions. Coworkers and close friends, Matthew T. Zamora, Michael E. Slaney, Tiffany J. Ulmer, Md. Hosnay Mobarok and Kyle D. Wells for thousands of hours of stimulating discussions, practice presentations, chalk talks and lunch beers – thank you all for an enjoyable experience in the Cowie group. I would also like to thank Jason Cooke for the opportunity to instruct the inorganic chemistry laboratory and for exposing me to the finer details of synthetic chemistry, laboratory maintenance and scientific pedagogy. Many thanks are also due for the exceptional assistance offered by various personnel working within departmental NMR spectroscopy, mass spectrometry,

microanalytical, electronics, machine and glassware facilities, particularly Mark Miskolzie, Don Morgan, Angela Morales-Izquierdo, Guy Bernard and Wayne Moffat, for technical assistance and training.

I would like to thank my wonderful family for their unwavering support and for encouraging my academic pursuit from an early age. I thank my father, Larry W. P. Hounjet, for always teaching me to be open-minded, determined, honest and respectful. Dad and I share a passion for music, and I'd like to thank him for all the wisdom, patience and encouragement he has provided. I would like to thank my mother, Dianna D. Hounjet, truly one of the kindest people I know and with whom I share a unique sense of humor, for continually inspiring me to be thoughtful, self-motivated and happy. I thank my sister, Ashley R. Hounjet, for many brief (but equally hilarious) road trips in Mom's Honda, and for reminding me to be a conscious role model and a caring person.

Many thanks go out to my grandparents, (Lawrence, Alice, Joseph and Doreen), aunts and uncles (Lorraine, Ed, Vivian, Verne, Brenda, Marven, Shirley, Gordon, Karen, Randy, Philip, Diane, Wayne, Joyce, Rex, Emily and Dean) and cousins (Brent, Christy, Trevor, Erin, Nicole, Andrea, Neil, Camille, Clinton, Jody, Tammy, Robyn, Ryan, Renae, Tania, Clayton, Jennifer and Victoria) of the Hounjet and Meier families, for always providing a strong sense of community and purpose. I would also like to thank my close friends, Martin T. Rankin, Jeffrey D. Wukovits and Christopher M. Sadek who are always willing to lend an ear or a hand during the best and worst of times. Finally, I would like to thank Carley T. Canuel for sharing the past three years with me – they have truly been the happiest of my life. Her companionship, sense of humour and continuous encouragement have certainly inspired the completion of this work.

Table of Contents

Table of Figures

Chapter 4

Chapter 5

Table of Schemes

Chapter 1

Chapter 2

Chapter 3

Chapter 4

Chapter 5

Table of Tables

Table of Charts

Chapter 1

Chapter 5

List of Abbreviations

Å	Ångström
Ar	*ortho-N*-methylanilinyl
Ar’	*ortho-N*,*N*-dimethylanilinyl
Bipy	bipyridine
Bu	butyl
cm	centimeter
COD	cyclooctadiene
d	day
DCM	dichloromethane
dmapm	bis(di(*ortho-N*,*N*-dimethylanilinyl)phosphino)methane
dppe	bis(diphenylphosphino)ethane
EI	electron impact
ESI	electrospray ionization
Et	ethyl
FT	Fourier transform
g	gram
GCOSY	gradient correlation spectroscopy
GHMQC	gradient heteronuclear multiple quantum coherence
GHSQC	gradient heteronuclear single quantum coherence
h	hour
HRMS	high resolution mass spectrometry
Hz	Hertz
IR	infrared
K	Kelvin or equilibrium constant
kcal	kilocalorie
kg	kilogram
kJ	kiloJoule
M	moles per liter
m	meter

mapm	bis(di(*ortho*-*N*-methylanilinyl)phosphino)methane
mg	milligram
MHz	megaHertz
min	minute
mL	milliliter
mm	millimeter
mmol	millimole
mol	mole
MS	mass spectrometry
m/z	mass to charge
NBD	norbornadiene
NMR	nuclear magnetic resonance
OAc (AcO)	acetate
ORTEP	Oak Ridge Thermal Ellipsoid Plot
OTf (TfO)	triflate
Ph	phenyl
Pr	propyl
ppm	parts per million
Py	pyridine
s	second
THF	tetrahydrofuran
Tol	Tolyl
w/w	by weight
μg	microgram
μL	microliter
μmol	micromole
Ω	Ohm
°	degree
°C	degree Celsius
$[M^+]$	molecular ion
%	percent

Chapter 1: Introduction

1.1 Transition Metals as Catalysts

Transition metals are valuable substances with a wide range of applications. In their elemental forms, they are generally dense, lustrous, malleable solids with high melting points and superb electrical and thermal conductivities. In addition to the physical features that make transition metals useful as components of construction materials, machinery, electronic devices and jewelry, these substances are also valuable because of their unique chemical properties, particularly as they pertain to catalysis.

Transition metals have been instrumental to the development of modern chemical technologies with their remarkable ability to catalyze chemical transformations, facilitating the synthesis of value-added products from less expensive feedstocks.[1-4] These metals are effective as catalysts because of their variable oxidation states, availability of low-lying vacant orbitals and partial occupation of valence d-orbitals, allowing them to accept electron density from coordinated substrates while offering π-density in return. In such a manner, transition metals can be used to access anti-bonding orbitals of coordinated substrates, facilitating bond cleavage within the reactants – a necessary prerequisite for any chemical reaction, generally referred to as "activation." By lowering the energetic barrier to substrate activation, such catalysts enable chemical reactions to occur much faster and under less forcing conditions than would be possible in their absence. While more benign reaction conditions are economically favorable from an energetic perspective, they can also block other potentially accessible reaction pathways to prevent the occurrence of undesirable side reactions. The resulting improvement of product selectivity can reduce the production of waste, or minimize the need for subsequent separations of products.[5] Furthermore, many fundamental chemical processes simply cannot

occur in a single step due to mismatches between the electronic orbital symmetries of reactants (i.e., olefin hydrogenation), making the use of a catalyst absolutely essential for permitting stepwise transformations of substrates.

Late transition metals, as well as low-valent early transition metals with partially occupied d-orbitals, can achieve substrate activation by oxidative addition, in which d-electrons are used to create new bonds with a substrate while cleaving a pre-existing bond therein (Scheme 1.1). The increase in formal

Scheme 1.1. Oxidative Addition/Reductive Elimination and σ-Bond Metathesis

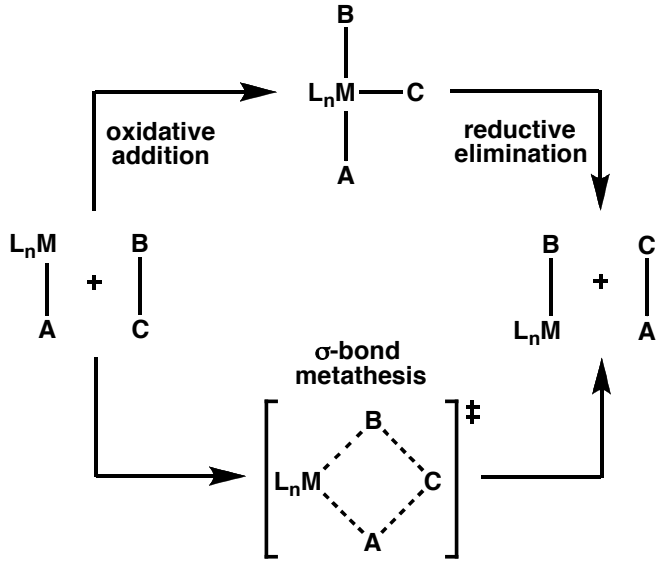

oxidation state of a metal that accompanies an oxidative addition can be reversed by reductive elimination, and indeed both processes are operable in many reactions catalyzed by both late and early metals containing d-electrons. Conversely, high-valent, early transition metals lacking d-electron density are not able to undergo oxidative addition, and are more likely to activate substrates by σ-bond metathesis (a single-step, double-displacement process)[5] or by other means that do not involve a change in the metal's formal oxidation state.

The second row platinum group metals (ruthenium, rhodium and palladium) have an exceptionally rich chemistry as catalysts. Like their third row congeners (osmium, iridium and platinum), these metals can access higher

oxidation states, however they tend to stabilize fewer valences, making them more labile and hence, more active as catalysts.[5] For example, Wilkinson's catalyst, [$RhCl(PPh_3)_3$], is effective toward the hydrogenation of olefins, while the iridium analogue is completely inactive due to the stronger Ir–P bond, which is not labile and hence, does not permit both the required oxidative addition of H_2 and olefin coordination necessary for subsequent hydrogenation.[5] Compared to their first row analogues (iron, cobalt and nickel), the larger size and lower energy valence electrons of second row metals can accommodate softer, more sterically demanding ligand environments, generally rendering these metals more suitable for use in homogeneous catalytic processes as discrete molecular complexes. For example, while [$RuCl_2(PPh_3)_3$] is a well-known hydrogenation catalyst,[6] the corresponding iron analogue is unknown (although the bis(phosphine) derivative, [$FeCl_2(PPh_3)_2$] is stable),[7] presumably due to the smaller size of iron, which cannot accommodate such a sterically demanding ligand environment.

Catalysts can be broadly divided into two classes: heterogeneous, in which the catalyst is in a different phase from the reactants, and homogeneous, in which the catalyst and reagents are in the same phase. Heterogeneous catalysts, which often consist of finely divided, metal-containing solids with high surface areas, are predominantly used for the industrial-scale production of fine chemicals because of the relative ease of their preparation, separation from reaction mixtures and recyclability. However, the active sites of exposed metal surfaces on these materials are usually of poor uniformity, and the different reactivities of these sites can lead to the generation of unwanted side-products. By contrast, the uniformity of well defined active sites within discrete metal complexes, used in homogeneous catalysis, is maximized owing to ligand control over both steric and electronic environments at each metal atom. The high degree of homogeneity between individual active sites of a molecular catalyst encourages consistent reactivity patterns, thereby resulting in enhanced product selectivities. Not only do ligands ensure complex homogeneity, but their features often profoundly alter product selectivities, allowing for a range of reactivities through ligand variation.

Although heterogeneous processes are generally preferred by industry, there have been notable successes using homogeneous catalysts. Examples of economically advantageous chemical processes that involve the application of molecular transition metal catalysts include the Monsanto[8] and Cativa[3] processes, which convert methanol and carbon monoxide into acetic acid using rhodium or iridium/ruthenium complexes, respectively. Another example is the Shell Higher Olefin Process (SHOP), which employs a nickel phosphine complex to effect the oligomerization of alkenes.[9] The pharmaceutical industry benefits from ruthenium complexes bearing chiral diphosphine and diamine ligands that have been used in asymmetric ketone (transfer) hydrogenation catalysis.[10-12] In the synthesis of L-DOPA (a compound used for the treatment of Parkinson's disease), a rhodium complex containing a chiral diphosphine is used for the hydrogenation of a prochiral precursor.[13] Ziegler-Natta polymerization, which constitutes the single largest process for the production of polyethylene, often utilizes organometallic titanium or zirconium complexes in conjunction with organoaluminum species as catalysts.[14] Finally, one of the largest chemical processes utilizing homogeneous catalysts is the "oxo" process, in which the hydroformylation of olefins to aldehydes occurs. This process commonly employs either cobalt carbonyl[15] or rhodium phosphine[4] complexes. These examples, among many others, serve to highlight the importance of molecular transition metal catalysts in the context of modern chemical infrastructure.

1.2 Phosphorus- and Nitrogen-Containing Ligands

1.2.1 Comparing Phosphines and Amines

As alluded to above, one advantage of homogeneous catalyst systems includes the ability to fine-tune reactivity by varying the ligands attached to a metal. Ligands require a pair of electrons available for donation into vacant metal orbitals. For this purpose, ligands containing group 15 elements as donor atoms are ubiquitously employed within molecular catalysts. Phosphorus- and nitrogen-

containing ligands, have found extensive application within transition metal complexes. Ligands based on trivalent donor atoms, such as those found in phosphines and amines offer enormous flexibility since their size, stereochemistry and electronic properties can be readily tuned by alteration of the substituents at phosphorus and nitrogen.[16] Phosphine ligands have been widely used in rhodium-catalyzed olefin hydrogenation,[17] oxidative (dehydrogenative) silylation,[18] hydrosilylation[18,19] and hydroformylation,[4] as well as ruthenium-catalyzed olefin metathesis,[20] ketone hydrogenation[10-12] and alcohol dehydrogenation reactions.[21] While the softer phosphines tend to bind more strongly to late transition metals in low oxidation states by very effective σ-donation, the harder amine donors are better suited for coordination to high-valent, early transition metals. Nevertheless, amines have also been used within low-valent, late metal complexes[22] despite their weaker donor character, which imparts less stability than the corresponding phosphine ligands.

Arguably the most well-known, phosphine-containing catalyst is Wilkinson's compound, $[RhCl(PPh_3)_3]$,[17] which is known to undergo facile oxidative addition of hydrogen after initial phosphine dissociation to afford a more reactive 14 e^- intermediate, $[RhCl(PPh_3)_2]$ (Scheme 1.2). Since Wilkinson's report of $[RhCl(PPh_3)_3]$ in 1966, Schrock and Osborn have generated related

Scheme 1.2. Mechanism for Alkene Hydrogenation by Wilkinson's Catalyst[23]

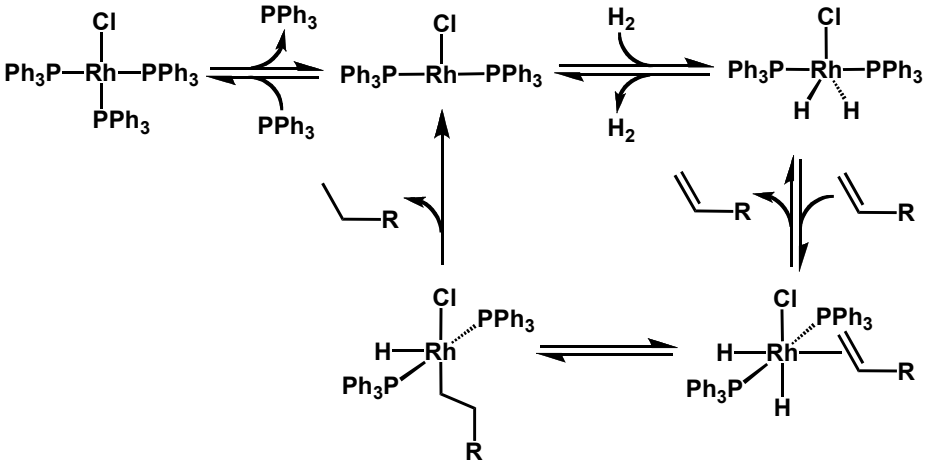

cationic species of the types $[Rh(diolefin)(phosphine)_2]^+$ and $[Rh(diolefin)(diphosphine)]^+$ (Chart 1.1, left and middle, respectively), in which

Chart 1.1. Catalysts Developed by Schrock, Osborn (left and middle) and Crabtree (right)

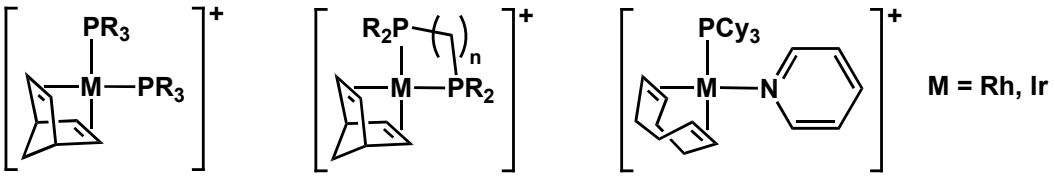

one of the phosphines and the chloro ligand of Wilkinson's catalyst have been replaced by a chelating diolefin (i.e., 1,5-cyclooctadiene or 1,4-norbornadiene).[24] These complexes show comparable hydrogenation activities to Wilkinson's catalyst but are more soluble in polar solvents. Crabtree's complex, $[Ir(COD)(PPh_3)(Py)][PF_6]$, an iridium derivative of Schrock and Osborn's complexes in which one of the phosphine donors is replaced by a relatively labile nitrogen donor (Chart 1.1, right), demonstrated superior activity over the related bis(phosphine) system, $[Ir(COD)(PPh_3)_2][PF_6]$, showing that the use of mixed donors had a positive affect on hydrogenation activity.[25] With this idea in mind, the possibility of incorporating both strongly and weakly coordinating donors into single bi- or multidentate systems, referred to as "hybrid" ligands, has become an attractive endeavor.

1.2.2 Hybrid Phosphorus-Nitrogen (*P*,*N*)-Ligands

The use of hybrid ligands (those containing more than one type of donor functionality)[26] has several distinct advantages in catalysis compared to the use of a number of different monodentate ligands. For example, Roundhill *et al*. have shown that complexes containing bidentate *P*,*N*-ligands were more effective for the hydrogenation of 1-hexene than an analogous complex containing two monodentate *P*-donor ligands (Scheme 1.3).[27] In addition to their chelate stabilization, hybrid ligands can also be designed so that their donor sites are forced into a particular arrangement (i.e., mutually *cis*) about the metal center without complications arising from isomerization to other coordination geometries (i.e., mutually *trans*). Futhermore, the desired stoichiometric ratio of

each type of coordinated ligand is maintained at the metal center by tethering different donors together into a single-ligand system.

Scheme 1.3. Iridium Phosphine and Phosphine-Amine Hydrogenation Catalysts

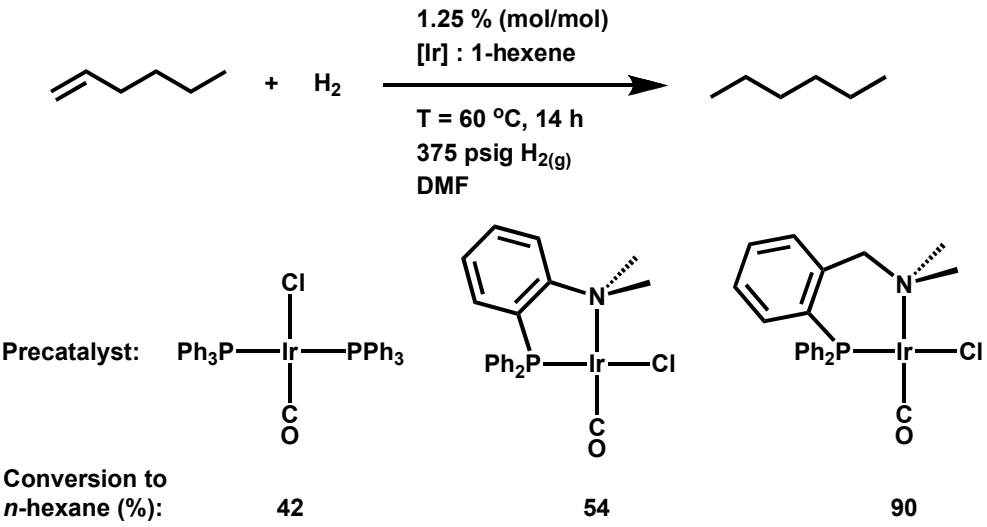

The chelation of a bi- or multi-dentate ligand system to a metal atom is an entropically favorable process that stabilizes the resulting complex to a greater extent than coordination of the equivalent number of independent monodentate ligands. Should one of the donors of a chelating ligand be displaced from the inner coordination sphere, another donor within this chelate serves as an anchor, thereby preventing diffusion of the displaced end from the metal and encouraging re-coordination of this labile group, effectively restoring complex stability. The relative binding strength of the donors of a hybrid ligand can be varied to allow one or more of these donors to act preferentially as a labile group while the other acts as an inert or "anchored" donor, firmly associated with the metal center. The use of both strongly and weakly binding donors within a single hybrid ligand can allow for the generation of a vacant coordination site (by displacement of the labile donor), as required during a catalytic process, but does not result in any permanent coordinative unsaturation because the pendent, labile group is tethered to the complex by its association to the inert donor. Thus, the labile donor, in a state of flux, rapidly dissociating from and recoordinating to the metal center, enhances reactivity without sacrificing complex stability. In theory, this

phenomenon should be beneficial to both catalyst activity and longevity. Such hybrid ligands, which possess both substitutionally labile and inert groups are often referred to as "hemilabile"[28] ligands, and have recently found extensive utility in catalytic processes.[29] However, solid, direct evidence demonstrating that hemilability can enhance catalytic activity remains quite scarce.[30]

1.2.3 Hemilability of Hybrid Ligands

Evidence suggests that the *P*,*N*-ligands depicted in Scheme 1.3 are indeed hemilabile at iridium,[27] although it is uncertain whether such hemilability results in the superior catalytic capabilities of their iridium complexes, or if other characteristics of these hybrid ligands (i.e., coordination geometry) can account for the observed improvements over Vaska's complex, $[IrCl(CO)(PPh_3)_2]$.[31] *P*,*N*-Complexes can exhibit hemilability by a number of mechanisms that can be broadly divided into three categories as defined by Braunstein and Naud (Scheme 1.4).[26] Type I hemilability involves reversible rupture of a dative bond between a

Scheme 1.4. Examples of Hemilabile Equilibria. "**A**" is the inert donor, "**B**" and "**C**" are labile donors and "**S**" is an external donor or substrate.

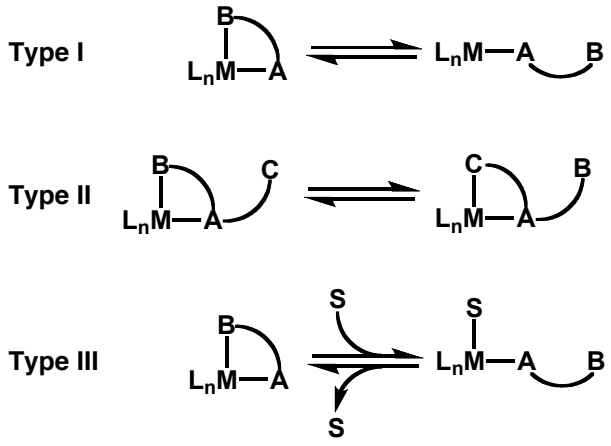

labile donor and a metal center to generate a transient, coordinatively unsaturated complex. This type of hemilability has been observed by variable temperature ^1H NMR spectroscopy within complexes of the general formula, $[NiX(PN_3)]^+$, in which PN_3 is a multidentate ligand containing one phosphine and three amine donors.[32] In this case, the five-coordinate cation is in equilibrium with a four-

coordinate, square-planar species by reversible coordination of one of the labile amine groups (Scheme 1.5). Type II hemilability occurs when two or more labile

Scheme 1.5. Type I Hemilability of a Nickel Phosphine-Triamine Complex

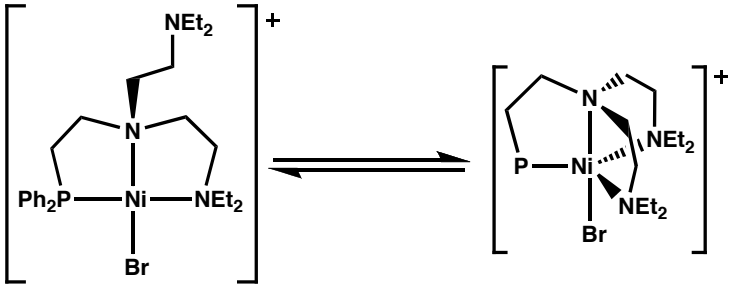

donors compete for a single coordination site, as has been spectroscopically observed for anisyl-pyridyl-phosphine complexes of rhodium, in which labile oxygen and nitrogen donors are shown to displace each other at the metal center.[33] Examples of hemilability that should have the most profound implications for catalysis involve displacement of a labile donor by an external group or substrate; these are referred to as Type III hemilabile processes. A ligand that can provide a labile donor to exert coordinative stability upon a complex, but can also allow for its displacement from the inner coordination sphere by substrates, can impart both enhanced stability and reactivity to a compound – features necessary for sustained molecular catalysis. Lindner *et al*. have uncovered indirect evidence that the Type III hemilability involving the phosphine-ether ligands illustrated in Scheme 1.6 gives rise to enhanced rates of oxidative addition and methyl migration within rhodium-catalyzed methanol carbonylation reactions.[34]

Although hemilability is a seemingly attractive feature for catalysis, the ability of a substrate to displace a labile donor does not always result in improved performance. For example, a comparison of methanol carbonylation activities for hemilabile phosphorus-oxygen *versus* non-labile phosphorus-sulfur ligands within rhodium complexes showed superior performance of the latter.[35] Gusev *et al*. have also concluded that hemilability is relatively unimportant in their ketone hydrogenation system by a comparison of catalytic activities of hemilabile *PNN*- versus non-labile *PNP*-complexes of iridium.[36] Similarly, Bischoff *et al*. observed

no general catalytic improvements of hemilabile phosphine-phosphonate rhodium complexes for methanol carbonylation relative to non-hemilabile catalysts.[37]

Scheme 1.6. Type III Hemilability of a Rhodium Phosphine-Ether Catalyst

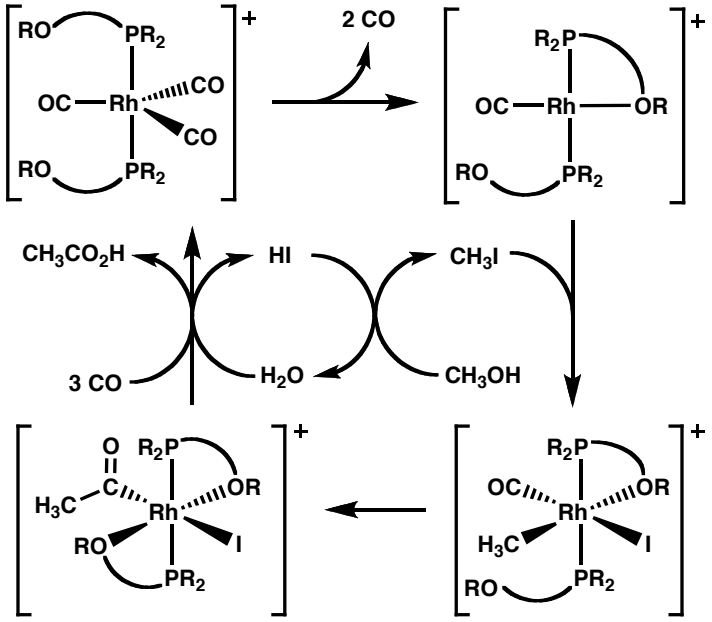

Although much is still not understood about the roles and effects of these fluxional processes in many catalytic cycles, several examples of hemilabile compounds have found other applications, particularly as chemical sensors.[38]

1.2.4 Non-Labile Phosphine-Amido Ligands

The versatility of *N*-donor ligands is truly immense. As described above, amines are weakly coordinating groups to soft transition metal centers and are attractive ligands because their labilities can be varied by changing the substituents bonded to the nitrogen atom, which alters the steric and electronic properties of the donor.[39] Additionally, if incompletely substituted amines are used as ligands, deprotonation at the nitrogen atom (Scheme 1.7) produces strongly coordinating,

Scheme 1.7. Equilibrium Between Amine (left) and Amido Complexes (right)

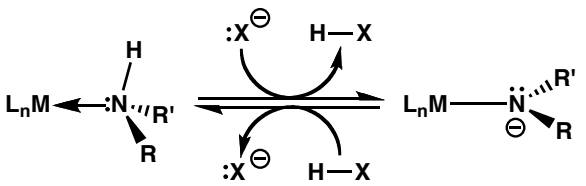

non-labile amido groups, which can donate both σ- and π-electron density to stabilize late metal complexes. The coordinating strength of an electron-donating nitrogen atom can thereby be tuned by altering the acidity of a reaction mixture to influence the pH-dependent equilibrium depicted in Scheme 1.7.

Late metal phosphine-amido complexes have been used in a variety of interesting stoichiometric activations of small molecules. The anionic amido group is strongly basic, especially when incorporated into a chelating ligand system with phosphine donors. Coordination of these highly electron-donating ligands to late transition metals can produce very electron-rich complexes, which are understandably reactive. Fryzuk *et al.* have shown that low-valent phosphine-amido complexes of rhodium and iridium can undergo traditional oxidative additions of methyl halides (Scheme 1.8).[40] However, one of the more recent applications of late metal-amido complexes is the ability for such species to bring about heterolytic bond cleavage by the late metal-amido functionality, i.e., the activation of molecular hydrogen to generate hydrido-amine complexes, many of which are intermediates in the (transfer) hydrogenation of polar unsaturates. Grützmacher *et al.* have demonstrated that structurally distinct phosphine-amido

Scheme 1.8. Oxidative Addition to Iridium Phosphine-Amido Complexes

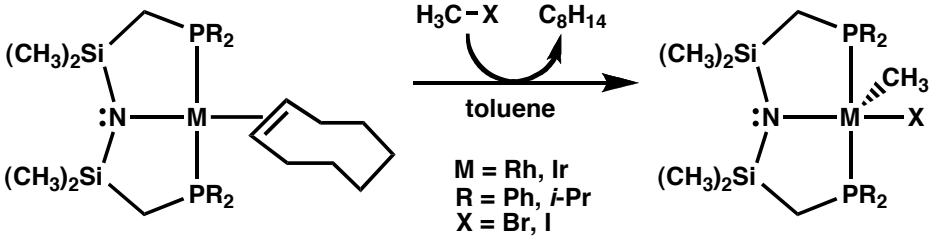

complexes of rhodium can effortlessly react with molecular hydrogen[41] and alcohols[42] (Scheme 1.9) to generate hydrido-amines by substrate heterolysis. These examples serve to illustrate that the reactivities of late metal phosphine-amido complexes can be varied by alteration of the ligands, which affects the steric and electronic properties of the system. The ability for the complex depicted on the left of Scheme 1.9 to heterolytically activate molecular hydrogen has been attributed to the coordination geometry of the tridentate ligand, which prevents a

trigonal planar geometry about the amido nitrogen, forcing the groups around this atom into a more reactive pyramidal arrangement. In this case, the geometry at the

Scheme 1.9. Heterolytic Activation by a Rhodium Phosphine-Amido Complex

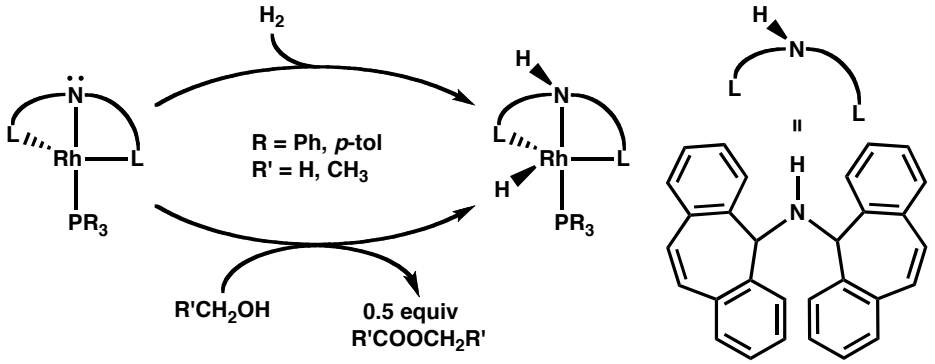

amido nitrogen atom is such that the lone pair becomes more accessible to reagents, making the complex more reactive toward relatively inert substrates.[41] Interestingly, Fryzuk *et al.* have also shown that iridium phosphine-amido complexes can activate molecular hydrogen by both oxidative addition and heterolytic processes (Scheme 1.10).[43]

Scheme 1.10. Simultaneous Oxidative and Heterolytic H_2 Activation

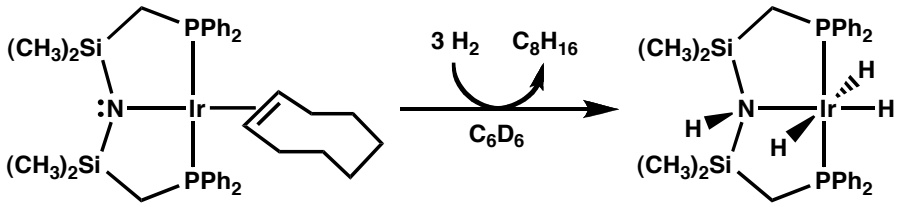

1.3 Binuclear Complexes

1.3.1 Metal-Metal Cooperativity

The local environment of a transition metal atom in a mononuclear, molecular complex (used in homogeneous catalysis) is quite different from that found on a solid-phase surface (used in heterogeneous catalysis). In the former situation, the metal atom is in contact with a less reactive ligand framework comprised of main-group elements, so that each isolated metal center encounters substrates in a

similar fashion, thereby maximizing the availability of structurally identical, catalytically active components in reaction mixtures. Conversely, metal atoms found on the surface of a solid-phase material are surrounded by other catalytically active metal atoms rather than a relatively inert ligand environment. Surface defects present in solid-phase catalysts give rise to a number of active sites, each with different catalytic properties, and these can result in poor product selectivities. Compared to molecular complexes, solid metal catalysts can act as electron-reservoirs for substrates, allowing greater potential for substrate oxidation or reduction. Within heterogenous catalysts, atoms not directly exposed to the solid's surface are unable to come into contact with the surrounding solution, meaning that a significant portion of the metal used does not participate in the catalytic process. Despite the inevitable sacrifice of potentially useful catalyst material, the mutual proximity of metal atoms on a surface has, in some cases, been ascribed to an enhancement of reactivity by acting as a scaffold on which to assemble and support reagents.[44] For example, the Fischer-Tropsch process,[45] which involves the hydrogenation of carbon monoxide bound to a metallic surface, uses adjacent metals to initially cleave the C–O bond, and is subsequently believed to operate by the coupling of surface-bound methylene units with methylene-derived hydrocarbyl fragments on adjacent metal nuclei[44] to afford a range of hydrocarbons.

The detailed study of molecular processes carried out on metallic surfaces is fraught with complications, and attempts have been made to study the cooperative effects of adjacent metal atoms on chemical reactivity by designing and examining the behaviours of molecular complexes containing two or more closely spaced metal nuclei. Although in most cases such complexes serve as poor models for metallic surfaces due to numerous effects imposed by ligand substitution, chemical transformations carried out by cooperating metals in molecular systems can be studied more easily by spectroscopic techniques. Stanley *et al*. have shown that binuclear complexes of rhodium (see for example Scheme 1.11, bottom-right), in which the close approach of the metal nuclei is

made possible, display vastly improved catalytic activities and selectivities for olefin hydroformylation reactions relative to analogous mononuclear complexes, illustrating a synergistic effect of the adjacent metal centers.[46] This study shows that high catalytic activities, characteristic of metal surfaces, can be emulated by molecular complexes, effectively combining some of the advantages associated with heterogeneous and homogeneous systems.

Scheme 1.11. Mono- and Binuclear Rhodium Hydroformylation Catalysts.

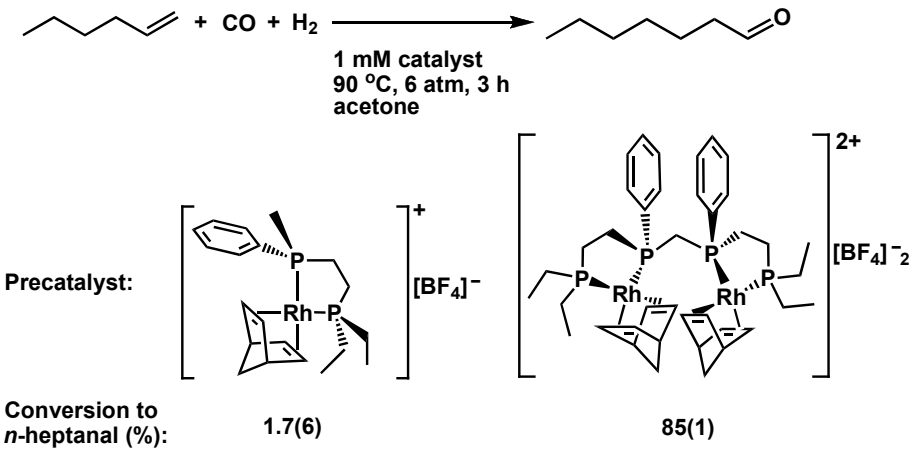

1.3.2 Amine-Functionalized Diphosphines as Bridging Ligands

Stanley's binuclear rhodium complex, alluded to above (Scheme 1.11), which contains a tetraphosphine ligand that simultaneously bridges a pair of metals while chelating to them,[46] inspired the generation of a new series of hemilabile, amine-functionalized diphosphines. James *et al.* developed syntheses of amine-containing diphosphine ligands, bis(di(*ortho*-*N*,*N*-dimethyl-anilinyl)phosphino)methane (dmapm, Scheme 1.12) and other hemilabile

Scheme 1.12. Synthesis of dmapm

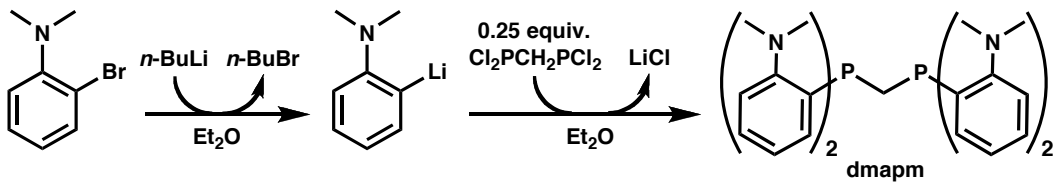

derivatives thereof.[47] This group then used the dmapm ligand for the syntheses of homo- and heterobinuclear complexes, particularly those incorporating platinum

and/or palladium.[48] Interestingly, the dipalladium(I,I) complex, [Pd_2Cl_2(μ-*P*,*N*,*P'*,*N'*-dmapm)], is able to add thiols across the metal-metal bond to place thiolato and hydrido ligands on opposite metals.[48] The possibility for metal-metal cooperativity within these hemilabile systems has been demonstrated for Heck coupling reactions in which the binuclear species are found to be more active per equivalent of metal than similar mononuclear species.[49] Subsequent to this work, the Cowie group demonstrated that the dmapm ligand can also be used to form hemilabile, heterobimetallic complexes of rhodium and either iridium or ruthenium (although the latter combination could not be produced as an isolable substance due to complex instability).[50] To help stabilize these very fluxional complexes, the group began to explore the possibility of a less labile analogue of the dmapm ligand that could provide stronger coordinative saturation when necessary. The installment of less bulky, less labile, incompletely *N*-methylated amine functionalities could result in enhanced complex stability while allowing deprotonation of the coordinated amines to afford non-labile amido groups. Together, the concepts of metal-metal cooperativity and tunable hemilability as means for developing more effective catalyst systems have inspired much of the work described in this dissertation.

1.4 Some Applications of Molecular Late Metal Catalysts

1.4.1 Ketone Hydrogenation

Hydrogenations of unsaturated polar bonds, like those found in ketones, aldehydes and imines, have been carried out most successfully using ruthenium-containing catalysts in which the metal does not necessarily undergo changes in formal oxidation state throughout the catalytic cycle.[51] While the traditional oxidative addition of dihydrogen at a metal center is generally a homolytic process (i.e., $H_2 \rightarrow 2\ H\bullet$) creating two distinct M–H bonds, heterolytic processes for the activation of dihydrogen (i.e., $H_2 \rightarrow H^+ + H^-$) have proven to be exceedingly useful for the catalytic hydrogenation of unsaturated polar bonds.

Although heterolytic H_2 cleavage is currently an active area of research, it is not new. The earliest reports of heterolytic activation of dihydrogen by copper salts are summarized in a review by Halpern.[52] Heterolysis may (or may not) involve initial coordination of dihydrogen to a metal center, via a σ-complex, followed by proton abstraction by a strongly basic, ligand (i.e., an amido group; Scheme 1.13,

Scheme 1.13. Outer-Sphere Ketone Hydrogenation by an Amido Complex

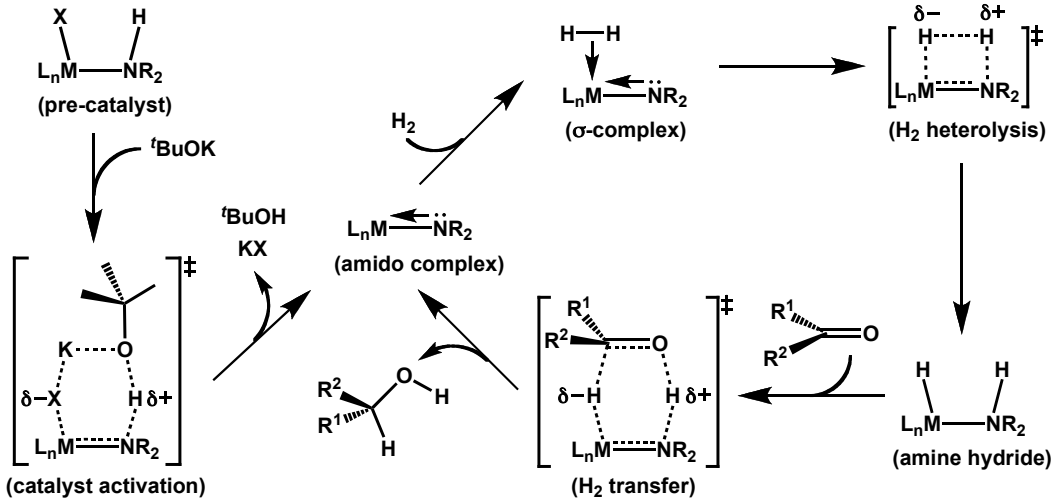

top-right). The result is a protonated ligand and a metal-bound hydride (bottom-right). Because both protic and hydridic atoms are generated by the heterolysis of dihydrogen, unsaturated substrates with a local dipole can form favorable interactions with the hydride and the acidic proton on a neighboring ligand, resulting in facile transfer of hydrogen to the unsaturated bond without requiring substrate coordination (bottom-middle). This so-called "outer-sphere" or "metal-ligand bifunctional" hydrogenation mechanism was proposed by Ryoji Noyori who, in 2001, won a Nobel Prize in Chemistry for his work on stereoselective hydrogenations.[53]

In addition to the amine ligands used in Noyori's catalysts, many of these ruthenium complexes also contained phosphines (see Scheme 1.14).[54] By employing chiral, chelating diamines and diphosphines, the asymmetric hydrogenation of prochiral alcohols could be carried out very effectively by maintaining a chiral environment at the ruthenium-nitrogen bond. In the case of

the catalyst depicted in Scheme 1.14, substrate hydrogenation by the complex produces an amido functionality by the generalized mechanism illustrated in Scheme 1.13.[54]

Scheme 1.14. Enantioselective Ketone Hydrogenation by a Chiral Catalyst

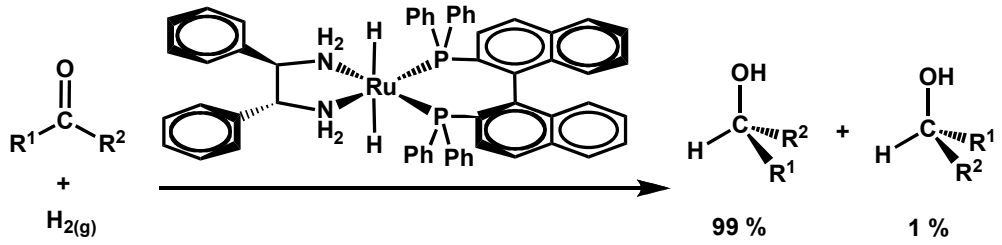

The use of molecular hydrogen in the direct reduction of ketones (and other unsaturates) is a process that usually requires high temperatures, along with specialized, high-pressure equipment to encourage the solubility of hydrogen within the reaction mixture. An alternative means of hydrogenation involves transfer of hydrogen atoms from a sacrificial donor reagent. In the case of ketone transfer hydrogenation catalysis, a less expensive secondary alcohol (i.e., isopropanol; see Equation 1.1) can act as an indirect, liquid-phase source of

$$RR'C(O) + (CH_3)_2CH(OH) \rightarrow RR'CH(OH) + (CH_3)_2C(O) \qquad (1.1)$$

hydrogen, negating the use of energy-intensive conditions. However, the costs associated with the use of a sacrificial donor and the separation of resultant byproducts usually make direct hydrogenation reactions more economically practical in the long-term for the pharmaceutical industry.[55] Nevertheless, the study of (often applied) transfer hydrogenation processes can provide important mechanistic insights about catalyst operation on a molecular scale.

The outer-sphere mechanism for dihydrogen heterolysis can also be applied to transfer hydrogenation, in which transfer of "H_2" from a sacrificial alcohol to an amido complex occurs by the microscopic reverse of the ketone hydrogenation step depicted in Scheme 1.13. However, other mechanisms of transfer hydrogenation are also known. A classical "inner-sphere" mechanism[51]

proceeds by β-hydride elimination from a coordinated alkoxide to generate a metal hydride complex (Scheme 1.15, top-right). A ketone is then inserted into the M–H bond to generate a new alkoxo species (bottom-right), which is then protonated by the sacrificial alcohol, ejecting the product alcohol from the complex.

Scheme 1.15. Inner-Sphere Transfer Hydrogenation

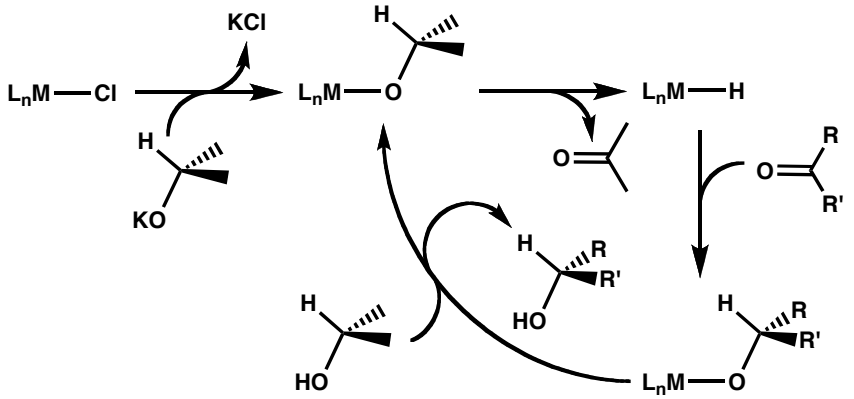

A third mechanism for transfer hydrogenation reactions, which has not yet been demonstrated by ruthenium catalysts, but is known to occur with aluminum-containing complexes, is the Meerwein–Ponndorf–Verley–Oppenauer (MPVO) mechanism (Scheme 1.16).[51] This reaction occurs via the intermediacy of alkoxo/

Scheme 1.16. Transition State for Hydride Transfer in an MPVO Mechanism[51]

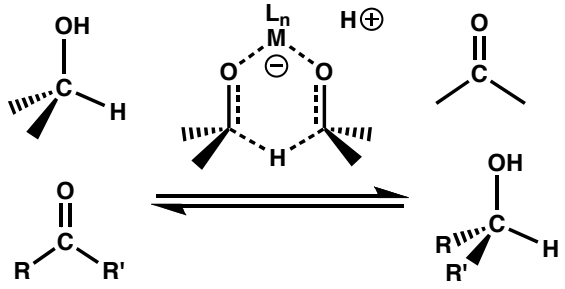

ketone species, but avoids the generation of hydrido ruthenium intermediates. Rather than allowing for β-hydride elimination from the alkoxide, a vacant coordination site is instead occupied by a ketone substrate. The alkoxide then transfers its hydride to the electrophilic carbon of the adjacent ketone and subsequent protonation by the incoming reagent alcohol liberates the product alcohol. In this case, although the hydrogenation mechanism proceeds via

coordination of substrates to the metal, the hydride transfer step does not take place within the inner-coordination sphere.

1.4.2 Olefin Hydrosilylation

The reaction of an olefin with a silane (containing at least one Si–H bond), referred to as hydrosilylation (Scheme 1.17), is similar in many respects to the

Scheme 1.17. The Chalk-Harrod Mechanism[55] for Alkene Hydrosilylation. In this case, Markovnikov and *anti*-Markovnikov regioisomers (in addition to *R*- and *S*-stereoisomers of the former) are possible products.

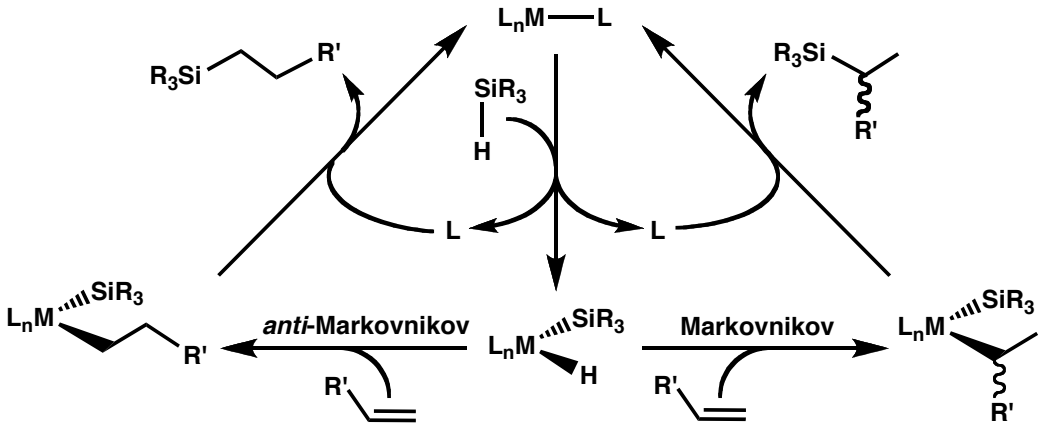

hydrogenation of an alkene, discussed earlier in section 1.2.1. However, olefin hydrosilylation reactions differ from analogous hydrogenations in that stereo- and regiochemical features of the products are more prevalent in the former owing to the addition of both silicon and hydrogen (rather than just hydrogen) atoms to unsaturated substrates. The variable product distributions generated by such silylation reactions provide a more in-depth understanding of catalytic mechanisms since changing either the catalyst or the reaction conditions can influence the ratio of various isomers produced.[5] The Chalk-Harrod mechanism[56] can be invoked to demonstrate one means by which hydrosilylation can proceed. This mechanism, illustrated in Scheme 1.17, involves oxidative addition of silane to a coordinatively unsaturated complex, followed by insertion of the olefin into the M–H bond; subsequent reductive elimination of metal-bound alkyl and silyl substituents generates the alkylsilane product. Speier's catalyst, $H_2[PtCl_6]$, reputed as one of the most active hydrosilylation catalysts known, can easily accomplish millions of catalytic turnovers,[57] although there is some speculation about the

nature of the active species,[5] with strong evidence in support of a heterogeneous process by colloidal platinum.[58] Karstedt's platinum(0) catalyst (Figure 1.1) however, appears to operate quite successfully via the intermediacy of molecular species.[59] The products of olefin silylation reactions have potential applications to the polymer and electronics industries.[60]

Figure 1.1. Karstedt's Catalyst

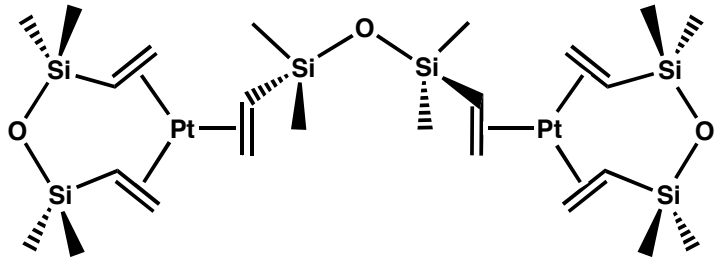

1.4.3 Dehydrogenative Silylation of Olefins

As alluded to above, olefin hydrosilylation reactions can proceed by more than one possible mechanism. In addition to the Chalk-Harrod mechanism depicted in Scheme 1.17, an alternate possibility (illustrated in Scheme 1.18) can be envisioned in which insertion of the alkene into the M–Si bond (rather than the

Scheme 1.18. Alternative Mechanism for Alkene Hydrosilylation. This mechanism accounts for the possibility of dehydrogenative silylation.

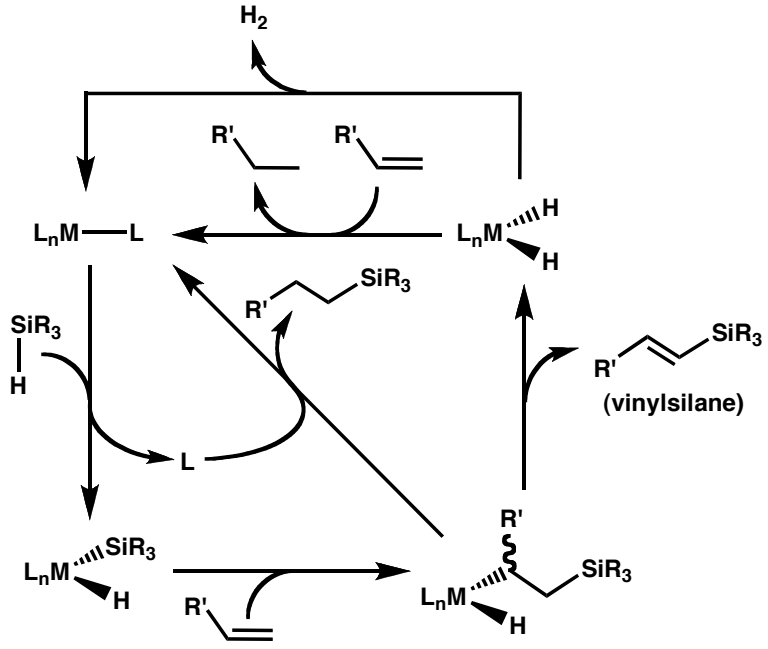

M–H bond) occurs. From this intermediate, one of two scenarios is possible. In the first case, reductive elimination of the silylalkyl and hydrido ligands occurs to give the anticipated alkylsilane product(s). On the other hand, β-hydride elimination from the silylalkyl group is likely in the event of coordinative unsaturation at the metal. In this case, the result is an unsaturated vinylsilane species, and the hydrogenated catalyst can either liberate hydrogen directly as a gaseous byproduct, or indirectly by hydrogenation of another equivalent of substrate olefin. This dehydrogenative (oxidative) silylation process is often observed as a side reaction occurring during many hydrosilylation processes. However, by altering catalyst properties, reaction conditions and substrate ratios, these silylation reactions can often be persuaded to selectively generate the vinylsilane products.[61] Vinylsilanes are attractive materials since the alkene group present in these compounds can be further functionalized by additional substrates.

1.5 Conclusions

The prospect of exploiting possible metal-metal cooperativity effects involving adjacent late metal atoms, in conjunction with hemilabile, bridging ligands to hold these metals in close proximity while allowing for some degree of coordinative unsaturation, has served as the driving force for work published in the following chapters. These concepts have led us to explore bis(*ortho*-phosphinoaniline) ligands as molecular scaffolds for binuclear complexes of rhodium and ruthenium. We have also developed a number of mononuclear analogues and compared their activities with the binuclear species in order to probe for metal-metal cooperativity effects. In addition, the possibility of generating non-labile phosphine-amido complexes by deprotonation of coordinated amines allowed a means of comparatively determining the effects of different *N*-donor groups while potentially enabling heterolytic substrate activation across the amido-metal bond.

1.6 References

1) Hunt, L. B.; Lever, F. M. *Platinum Metals Rev.* **1969**, *13*, 126 – 138.

2) Philpott, J. E. *Platinum Metals Rev.* **1971**, *15*, 52 – 57.

3) Jones, J. H. *Platinum Metals Rev.* **2000**, *44*, 94 – 105.

4) van Leeuwen, P. W. N. M.; Claver, C. Catalysis by Metal Complexes, *22,* "Rhodium Catalyzed Hydroformylation" Ed.; Kluwer Acad. Publ. **2000**, 1 – 279.

5) Crabtree, R. H. *The Organometallic Chemistry of the Transition Metals*, 4th edn., Wiley, New Jersey, **2005**, pp 165, 232 – 262.

6) Stephenson, T. A.; Wilkinson, G. *J. Inorg. Nucl. Chem.* **1966**, *28*, 945 – 956.

7) Seewald, O.; Flörke, U.; Henkel, G. *Acta Cryst.*, **2005**, *E61*, m1829 – m1830.

8) Eby, R. T.; Singleton, T. C. *Applied Industrial Catalysis*; Academic Press: London, 1983.

9) Hirose, K.; Keim, W. *J. Mol. Catal.* **1992**, *73*, 271 – 276.

10) Noyori, R.; Ohkuma, T. *Angew. Chem., Int. Ed.* **2001**, *40*, 40 – 73.

11) Ohkuma, T.; Koizumi, M.; Muñiz, K.; Hilt, G.; Kabuto, C.; Noyori, R. *J. Am. Chem. Soc.* **2002**, *124*, 6508 – 6509.

12) Sandoval, C. A.; Ohkuma, T.; Muñiz, K.; Noyori, R. *J. Am. Chem. Soc.* **2003**, *125*, 13490 – 13503.

13) Vineyard, B. D.; Knowles, W. S.; Sabacky, M. J.; Bachman, G. L.; Weinkauff, D. J. *J. Am. Chem. Soc.* **1977**, *99*, 5946 – 5952.

14) Kaminsky, W. *J. Chem. Soc., Dalton Trans.* **1998**, 1413 – 1418.

15) Ojima, I.; Tsai, C.-Y.; Tzamarioudaki, M.; Bonafoux, D. *Org. React.* **2000**, *56*, 1 – 354.

16) Barron, A. R. *J. Chem. Soc., Dalton Trans.* **1988**, 3047 – 3050.

17) Osborn, J. A.; Jardine, F. H.; Young, J. F.; Wilkinson, G. *J. Chem. Soc. (A)* **1966**, 1711 – 1732.

18) Takeuchi, R.; Yasue, H. *Organometallics* **1996**, *15*, 2098 – 2102.

19) Kakiuchi, F.; Nogami, K.; Chatani, N.; Seki, Y.; Murai, S. *Organometallics* **1993**, *12*, 4748 – 4750.

20) Schwab, P.; Grubbs, R. H.; Ziller, J. W. *J. Am. Chem. Soc.* **1996**, *118*, 100 – 110.

21) Zhang, J.; Gandelman, M.; Shimon, L. J. W.; Rozenberg, H.; Milstein, D. *Organometallics* **2004**, *23*, 4026 – 4033.

22) Beller, M.; Trauthwein, H.; Eichberger, M.; Breindl, C.; Müller, T. E.; Zapf, A. *J. Organomet. Chem.* **1998**, *566*, 277 – 285.

23) Elschenbroich, C. *Organometallics*, 3rd edn., Wiley, Weisbaden, **2005**, pp 670 – 672.

24) Schrock, R. R.; Osborn, J. A. *J. Am. Chem. Soc.* **1976**, *98*, 2134 – 2143.

25) Crabtree, R. *Acc. Chem. Res.* **1979**, *12*, 331 – 337.

26) Braunstein, P.; Naud, F. *Angew. Chem., Int. Ed.* **2001**, *40*, 680 – 699.

27) Rauchfuss, T. B.; Clements, J. L.; Agnew, S. F.; Roundhill, D. M. *Inorg. Chem.* **1977**, *16*, 775 – 778.

28) Jeffrey, J. C.; Rauchfuss, T. B. *Inorg. Chem.* **1979**, *18*, 2658 – 2666.

29) Braunstein, P. *J. Organomet. Chem.* **2004**, *689*, 3953 – 3967.

30) Ramirez, A.; Sun, X.; Collum, D. B. *J. Am. Chem. Soc.* **2006**, *128*, 10326 – 10336.

31) Vaska, L.; DiLuzio, J. W. *J. Am. Chem. Soc.* **1962**, *84*, 679 – 680.

32) Bertini, I.; Dapporto, P.; Fallani, G.; Sacconi, L. *Inorg. Chem.* **1971**, *10*, 1703 – 1707.

33) Yang, H.; Lugan, N.; Mathieu, R. *Organometallics* **1997**, *16*, 2089 – 2095.

34) Bader, A.; Lindner, E. *Coord. Chem. Rev.* **1991**, *108*, 27 – 110.

35) Baker, M. J.; Giles, M. F.; Orpen, A. G.; Taylor, M. J.; Watt, R. J. *J. Chem. Soc., Chem. Commun.* **1995**, 197 – 198.

36) Choualeb, A.; Lough, A. J.; Gusev, D. G. *Organometallics* **2007**, *26*, 5224 – 5229.

37) Bischoff, S.; Weigt, A.; Miessner, H.; Lücke, B. *Energy Fuels* **1996**, *10*, 520 – 523.

38) Angell, S. E.; Rogers, C. W.; Zhang, Y.; Wolf, M. O.; Jones Jr., W. E. *Coord. Chem. Rev.* **2006**, *250*, 1829 – 1841.

39) Hounjet, L. J.; Bierenstiel, M.; Ferguson, M. J.; McDonald, R.; Cowie, M.

Dalton Trans. **2009**, 4213 – 4226.

40) Fryzuk, M. D.; MacNeil, P. A.; Rettig, S. J. *Organometallics*, **1986**, *5*, 2469 – 2476.

41) Maire, P.; Büttner, T.; Breher, F.; Le Floch, P.; Grützmacher, H. *Angew. Chem., Int. Ed.* **2005**, *44*, 6318 – 6323.

42) Zweifel, T.; Naubron, J.-V.; Büttner, T.; Ott, T.; Grützmacher, H. *Angew. Chem., Int. Ed.* **2008**, *47*, 3245 – 3249.

43) Fryzuk, M. D.; MacNeil, P. A. *Organometallics*, **1983**, *2*, 682 – 684.

44) (a) Brady, R. C. (III); Pettit, R. *J. Am. Chem. Soc.* **1980**, *102*, 6181 – 6182; **1981**, *103*, 1287 – 1289. (b) Maitlis, P. M.; Long, H. C.; Quyoum, R.; Turner, M. L.; Wang, Z.-Q. *Chem. Commun.* **1996**, 1. (c) Maitlis, P. M.; Zanotti, V. *Chem. Commun.* **2009**, 1619 – 1634.

45) (a) Fischer, F.; Tropsch, H. *Brennst.-Chem.* **1926**, *7*, 97. (b) Fischer, F.; Tropsch, H. *Chem. Ber.* **1926**, *59*, 830.

46) Broussard, M. E.; Juma, B.; Train, S. G.; Peng, W.-J. Laneman, S. A.; Stanley, G. G. *Science* **1993**, *260*, 1784 – 1788.

47) Jones, N. D.; Meessen, P.; Smith, M. B.; Losehand, U.; Rettig, S. J.; Patrick, B. O.; James, B. R. *Can. J. Chem.* **2002**, *80*, 1600 – 1606.

48) Jones, N. D.; Foo, J. L; Patrick, B. O.; James, B. R. *Inorg. Chem.* **2004**, *43*, 4056 – 4063.

49) Jones, N. D.; James, B. R. *Adv. Synth. Catal.* **2002**, *344*, 1126 – 1134.

50) Dennett, J. N. L.; Bierenstiel, M.; Ferguson, M. J.; McDonald, R.; Cowie, M. *Inorg. Chem.* **2006**, *45*, 3705 – 3717.

51) Clapham, S. E.; Hadzovic, A. and Morris, R. H. *Coord. Chem. Rev.* **2004**, *248*, 2201 – 2237.

52) Halpern, J. *J. Organomet. Chem.* **1980**, *200*, 133 – 144.

53) Haack, K.-J.; Hashiguchi, S.; Fujii, A.; Ikariya, T.; Noyori, R. *Angew. Chem., Int. Ed. Engl.* **1997**, *36*, 285 – 288.

54) Sandoval, C. A.; Ohkuma, T.; Muñiz, K.; Noyori, R. *J. Am. Chem. Soc.* **2003**, *125*, 13490 – 13505.

55) Morris, R. H. *Chem. Soc. Rev.* **2009**, *38*, 2282 – 2291.

56) Harrod, J. F.; Chalk, A. J. *J. Am. Chem. Soc*. **1966**, *88*, 3491 – 3497.

57) Speier, J. L. *Adv. Organomet. Chem*. **1979**, *17*, 407 – 447.

58) (a) Lewis, L. N.; Lewis, N. *J. Am. Chem. Soc*. **1986**, *108*, 7228 – 7231.

59) (a) Karstedt, B. D. (General Electric) *US Patent* 3 715 334. (b) Hitchcock, P. B.; Lappert, M. F.; Warhurst, N. J. W. *Angew. Chem., Int. Ed. Engl*. **1991**, *30*, 438 – 440. (c) Stein, J.; Lewis, L. N.; Gao, Y.; Scott, R. A. *J. Am. Chem. Soc*. **1999**, *121*, 3693 – 3703.

60) Zhang, Z.; Sherlock, D.; West, R.; West, R. *Macromolecules* **2003**, *36*, 9176 – 9180.

61) Cipot, J.; McDonald, R.; Ferguson, M. J.; Schatte, G.; Stradiotto, M. *Organometallics*, **2007**, *26*, 594 – 608.

Chapter 2: Mono- and Binuclear Complexes of Rhodium Involving a New Series of Hemilabile *ortho*-Phosphinoaniline Ligands[i]

2.1 Introduction

Bi- and multidentate ligands occupy an important position in the chemistry of transition metals.[1-7] Not only do such groups find applications in mononuclear complexes, where they offer additional stability compared to related monodentate ligands, through the chelate effect,[8] they can also be used to bridge two or more metals in multinuclear complexes.[9-18] Multidentate ligands can also be extended to a series of "hybrid" ligands, capable of binding to the metal(s) through different donor atoms.[19-42] This not only introduces the flexibility of ligand fine-tuning, in which the metal(s) can be sterically and electronically "tuned" through the use of different combinations of donor sites within these hybrids, but also introduces the concept of hemilability,[19-38] in which one or more donor sites in the multidentate ligand bind more strongly to the metal(s) under study while other donor site(s) bind weakly. These labile donors are capable of stabilizing the complex in the absence of substrate, while being readily and reversibly displaced by the appropriate substrate. The resulting "incipient coordinative unsaturation" has obvious applications in catalysis,[20-27,35] in which the labile donor stabilizes the catalyst precursor prior to substrate coordination and assists in displacing the catalyst-modified substrate, regenerating the catalyst precursor, after the transformation is complete. In this context, ligands containing "soft" phosphorus and "hard" nitrogen donors have found many applications as hemilabile ligands in

[i] The work presented in this chapter has been previously reported. See: Hounjet, L. J.; Bierenstiel, M.; Ferguson, M. J.; McDonald, R.; Cowie, M. *Dalton Trans.* **2009**, 4213 – 4226.

the chemistry of low-valent, late transition-metal complexes,[20-24, 26-38] in which phosphorus binds strongly while nitrogen is more labile.

We have sought to combine two of the above themes through the use of diphosphine ligands having pendent amine groups, in which the diphosphine moiety binds effectively to and bridges a pair of late metals, holding them in close proximity, while the chelating amines function as labile groups. In earlier studies, we[43] and others[44-48] had used bis(di(*o*-*N*,*N*-dimethylanilinyl)phosphino)methane (dmapm = $Ar'_2PCH_2PAr'_2$; Ar' = *o*-$C_6H_4NMe_2$) as a bridging diphosphine ligand having chelating, hemilabile dimethylanilinyl groups. However, in our study we proposed that unfavorable steric repulsions involving the pairs of methyl substituents on the anilinyl groups had appeared to inhibit close approach of the adjacent metals, so we subsequently set out to synthesize the somewhat less bulky monomethylanilinyl analogue, $Ar_2PCH_2PAr_2$ (mapm; Ar = *o*-C_6H_4NHMe) in order to reduce the steric demand of the amine donors. In addition, we set out to prepare a series of monophosphine analogues of mapm in order to compare the reactivities of related mononuclear and binuclear diphosphine-bridged species, thereby gaining information on possible influences of adjacent metals in substrate activation and on the possibility of cooperative substrate activation by the adjacent metals. Such cooperative substrate activation has been elegantly demonstrated in a related dirhodium system,[16] that utilized a non-labile tetraphosphine ligand in which the central pair of phosphorus nuclei bridged the metals while the outer pair each chelated to a different metal.

A further aspect of interest in these monomethylanilinyl phosphines is the possibility of deprotonating the amine groups yielding amido functionalities. The reversible transformation of chelating amine to amido groups has generated enormous recent interest in the catalytic hydrogenation of polar substrates such as ketones.[49-51]

In this chapter we report the synthesis of a series of hybrid monomethylanilinyl phosphine ligands and the generation of a series of mononuclear and binuclear complexes of rhodium using these hybrid ligands. The steric influences of these monomethylanilinyl derivatives with regards to their lability and their structural influences are compared with the analogous species containing the dimethylanilinyl groups.

2.2 Experimental

2.2.1 General Comments

All solvents were deoxygenated, dried (using appropriate drying reagents) and distilled before use and stored under nitrogen. Reactions were performed under an argon atmosphere using standard Schlenk techniques. $RhCl_3 \cdot 3H_2O$, Ph_2PCl, $PhPCl_2$, PCl_3, $Cl_2PCH_2PCl_2$, were purchased from Strem Chemicals. *n*-BuLi and *t*-BuLi were purchased from Sigma-Aldrich. Dry carbon dioxide was purchased from Supelco. The compounds $[Rh(\mu\text{-}Cl)(COD)]_2$ (COD = 1,5-cyclooctadiene)[52] and $[Rh(\mu\text{-}Cl)(CO)_2]_2$[53] were prepared by the literature routes. The monophosphine ligands, bis(*o*-*N*,*N*-dimethylanilinyl)phenylphosphine ($PhPAr'_2$), tris(*o*-*N*,*N*-dimethylanilinyl)phosphine (PAr'_3),[54] and the diphosphine ligand, bis(di(*o*-*N*,*N*-dimethylanilinyl)phosphino)methane (dmapm),[44] were prepared as previously reported. *o*-Bromo-*N*,*N*-dimethylaniline was prepared from commercially available *o*-bromoaniline by exhaustive methylation with dimethylsulfate.[55] NMR spectra were recorded on Bruker AM-400, Varian Inova-400, -500 or Varian Unity-500 spectrometers operating at 400.0, 399.8 or 499.8 MHz, respectively, for ^1H, at 161.9, 161.8 or 202.3 MHz, respectively, for ^{31}P and at 100.6, 100.6 or 125.7 MHz, respectively, for ^{13}C nuclei. *J* values are given in Hz and overlapping, unresolved aromatic ^{13}C NMR signals, observed in the typical 80 – 120 ppm range, are not reported. Spectroscopic data for all metal complexes (**5** – **14**) are provided in Tables 2.1 and 2.2. Solution phase infrared

spectra (KBr cell) were recorded on either a FT-IR Bomem MB-100 spectrometer or a Nicolet Avatar 370 DTGS spectrometer. Elemental analyses were performed

Table 2.1. Infrared and $^{13}C\{^1H\}$ NMR Data for Rhodium Compounds

Compound	IR (cm^{-1})[a]	NMR[b] ($\delta(^{13}C\{^1H\})$)[c]
$[RhCl(CO)(Ph_2PAr)]$ (**5**)	1992 (s)	CO: 189.3 (dd, $^1J_{RhC}$ = 73 Hz, $^2J_{PC}$ = 18 Hz)[d] NMe: 44.1 (s)[d]
$[RhCl(CO)(PhPAr_2)]$ (**6**)	1996 (s)	CO: 188.9 (dd/br, $^1J_{RhC}$ = 55 Hz)[d] NMe: 43.9 (s/br), 30.2 (s/br)[d]
$[RhCl(CO)(PAr_3)]$ (**7**)	1994 (s)	CO: 189.6 (dd, $^1J_{RhC}$ = 73 Hz, $^2J_{PC}$ = 16 Hz)[d] NMe: 30.3 (s/br)[d]
$[RhCl(CO)(PhPAr'_2)]$ (**8**)	1987 (s)	CO: 189.1 (dd, $^1J_{RhC}$ = 74 Hz, $^2J_{PC}$ = 17 Hz)[d] NMe_2: 48.5 (s)[d]
$[RhCl(CO)(PAr'_3)]$ (**9**)	1988 (s)	CO: 190.1 (dd, $^1J_{RhC}$ = 76 Hz, $^2J_{PC}$ = 17 Hz)[d] NMe_2: 47.8 (s)[d]
$[Rh_2Cl_2(CO)_2(\mu\text{-mapm})]$ (**10**)	2000 (s)	CO: 185.3 (dd, $^1J_{RhC}$ = 71 Hz, $^2J_{PC}$ = 18 Hz)[d] NMe: 42.9 (s), 30.2 (s)[d] CH_2: 33.7 (t, $^1J_{PC}$ = 31 Hz)[d]
$[Rh_2Cl_2(CO)_2(\mu\text{-dmapm})]$ (**11**)	1999 (s)	CO: 187.6 (dd, $^1J_{RhC}$ = 80 Hz, $^2J_{PC}$ = 28 Hz)[e] NMe_2: 52.3 (s), 51.9 (s), 47.9 (s), 47.1 (s)[e] CH_2: 27.3 (t, $^1J_{PC}$ = 29 Hz)[e]
$[Rh_2(OTf)_2(CO)_2(\mu\text{-mapm})]$ (**12**)	2000 (s)	N/A (poorly soluble)
$[Rh_2I_2(CO)_2(\mu\text{-mapm})]$ (**13**)	2000 (s)	N/A (poorly soluble)
$[Rh_2(OAc)_2(CO)_2(\mu\text{-mapm})]$ (**14**)	1991 (s)[f]	N/A (slowly decomposes in CD_2Cl_2)

[a] IR abbreviations: s = strong, m = medium, w = weak. Only ν_{CO} signals given. CD_2Cl_2 solution; in units of cm^{-1}. [b] NMR abbreviations: s = singlet, d = doublet, t = triplet, m = multiplet, br = broad, dd = doublet of doublets. NMR data in CD_2Cl_2. [c] ^{13}C chemical shifts referenced to tetramethylsilane. Chemical shifts for aromatic groups not given. [d] NMR data at 27 °C. [e] NMR data at 0 °C. [f] THF solution.

by the Microanalytical Laboratory of the University of Alberta. Electrospray ionization mass spectra were run on a Micromass Zabspec spectrometer in the departmental MS facility. In all cases, the distribution of isotope peaks for the appropriate parent ion matched very closely that calculated from the formulation given. Spinworks version 2.5.5[56] was used for line-shape analyses and NMR spectral simulations. Conductivity measurements were carried out under inert conditions on 10^{-3} M solutions of $[Rh_2(OTf)_2(CO)_2(\mu\text{-mapm})]$ (**12**) and $[Rh_2(OAc)_2(CO)_2(\mu\text{-mapm})]$ (**14**) in dry nitromethane using a Yellow Springs Instrument Model 31 conductivity bridge. For these species the molar conductivities were determined as $\Lambda = 23$ and 12 $cm^2 \cdot \Omega^{-1} \cdot mol^{-1}$, respectively.

Table 2.2. $^{31}P\{^{1}H\}$ and ^{1}H NMR Data for Rhodium Compounds

Compound	NMR[a]	
	$\delta(^{31}P\{^{1}H\})$[b]	$\delta(^{1}H)$[c]
[RhCl(CO)(Ph_2PAr)] (**5**)	58.0 (d, $^{1}J_{RhP}$ = 169 Hz)[d]	NH: 5.57 (br, 1H)[d] NMe: 2.87 (d, $^{3}J_{HH}$ = 6.5 Hz, 3H)[d]
[RhCl(CO)($PhPAr_2$)] (**6**)	41.7 (d, $^{1}J_{RhP}$ = 156 Hz)[d]	NH: 5.73 (br, 2H)[d] NMe: 2.73 (br, 6H)[d] NH: 7.20 (3H),[i] 6.37 (br, 1H), 6.32 (br, 1H), 5.95 (br, 3H)[g] NMe: 2.88 (d, $^{3}J_{HH}$ = 5.9 Hz, 3H), 2.77 (d, $^{3}J_{HH}$ = 5.0 Hz, 3H), 2.62 (d, $^{3}J_{HH}$ = 5.7 Hz, 9H), 2.56 (d, $^{3}J_{HH}$ = 4.8 Hz, 9H)[g]
[RhCl(CO)(PAr_3)] (**7**)	27.9 (d, $^{1}J_{RhP}$ = 149 Hz)[d]	NH: 7.00 (1H),[i] 5.04 (br, 1H), 4.64 (br, 1H)[d] NMe: 2.79 (br, 9H)[d] NH: 7.38 (1H),[i] 5.23 (br, 1H), 4.36 (br, 1H)[e] NMe: 2.81 (d, $^{3}J_{HH}$ = 5.0 Hz, 3H), 2.71 (d, $^{3}J_{HH}$ = 4.9 Hz, 3H), 2.63 (d, $^{3}J_{HH}$ = 6.0 Hz, 3H)[e]
[RhCl(CO)($PhPAr'_2$)] (**8**)	49.7 (d, $^{1}J_{RhP}$ = 173 Hz)[d]	NMe_2: 2.75 (s, 12H)[d] NMe_2: 3.01 (s/br, 3H), 2.94 (s/br, 3H), 2.69 (s/br, 3H), 1.89 (s/br, 3H)[h]
[RhCl(CO)(PAr'_3)] (**9**)	37.8 (d, $^{1}J_{RhP}$ = 186 Hz)[d]	NMe_2: 2.69 (s, 18H)[d] NMe_2: 2.83 (s/br, 9H), 2.34 (s/br, 9H)[f]
[$Rh_2Cl_2(CO)_2$(μ-mapm)] (**10**)	23.3 (m, $^{1}J_{RhP}$ = 160 Hz)[d,j]	NH: 7.75 (2H), 6.94 (2H)[d,i] CH_2: 3.94 (m, 2H)[d] NMe: 3.17 (d, $^{3}J_{HH}$ = 6.0 Hz, 6H), 2.78 (d, $^{3}J_{HH}$ = 4.8 Hz, 6H)[d]
[$Rh_2Cl_2(CO)_2$(μ-dmapm)] (**11**)	41.0 (d, $^{1}J_{RhP}$ = 175 Hz)[d] 41.8 (m, $^{1}J_{RhP}$ = 179 Hz)[f,j]	CH_2: 4.59 (t/br, $^{2}J_{PH}$ = 12.4 Hz, 2H)[d] NMe_2: 3.70 (s/br, 6H), 2.97 (s/br, 6H), 2.73 (s/br, 6H), 2.53 (s/br, 6H)[d] CH_2: 4.59 (t, $^{2}J_{PH}$ = 11.6 Hz, 2H)[h] NMe_2: 3.68 (s, 6H), 2.86 (s, 6H), 2.70 (s, 6H), 2.27 (s, 6H)[h]
[$Rh_2(OTf)_2(CO)_2$(μ-mapm)] (**12**)	31.5 (m, $^{1}J_{RhP}$ = 176 Hz)[d,j]	NH: 7.64 (2H)[d,i], 6.62 (m/br, 2H)[d] CH_2: 3.97 (m, 2H)[d] NMe: 3.09 (d, $^{3}J_{HH}$ = 6.0 Hz, 6H), 2.85 (d, $^{3}J_{HH}$ = 5.0 Hz, 6H)[d]
[$Rh_2I_2(CO)_2$(μ-mapm)] (**13**)	20.3 (m, $^{1}J_{RhP}$ = 162 Hz)[d,j]	NH: 7.60 (2H), 6.62 (2H)[d,i] CH_2: 3.96 (m, 2H)[d] NMe: 3.25 (d, $^{3}J_{HH}$ = 6.0 Hz, 6H), 2.76 (d, $^{3}J_{HH}$ = 5.0 Hz, 6H)[d]
[$Rh_2(OAc)_2(CO)_2$(μ-mapm)] (**14**)	28.2 (m, $^{1}J_{RhP}$ = 155 Hz)[d,j]	NH: 8.91 (m/br, 2H), 8.12 (m/br, 2H)[d] CH_2: 3.81 (m, 2H)[d] NMe: 3.14 (d, $^{3}J_{HH}$ = 6.0 Hz, 6H), 2.78 (d, $^{3}J_{HH}$ = 4.8 Hz, 6H)[d]

[a] NMR abbreviations: s = singlet, d = doublet, t = triplet, m = multiplet, br = broad, dd = doublet of doublets. NMR data in CD_2Cl_2. [b] ^{31}P chemical shifts referenced to external 85% H_3PO_4. [c] ^{1}H chemical shifts referenced to tetramethylsilane. Chemical shifts for aromatic groups not given. [d] NMR data at 27 °C. [e] NMR data at –20 °C. [f] NMR data at –40 °C. [g] NMR data at –60 °C. [h] NMR data at –80 °C. [i] Multiplicities of NH signals could not be determined (due to overlapping aromatic signals); chemical shifts determined by GCOSY. [j] 2nd order effects complicate observed signal pattern.

2.2.2 Preparation of *P*,*N*-Ligands

(a) Diphenyl(*o*-*N*-methylanilinyl)phosphine, Ph_2PAr (1). In a 200 mL Schlenk flask under anhydrous conditions and argon atmosphere, *N*-methylaniline (1.73 mL, 15.9 mmol) was dissolved in 30 mL of freshly distilled, dry THF and cooled to –78 °C (acetone/dry ice bath). *n*-BuLi (2.5 M in hexanes, 6.3 mL, 16 mmol) was added dropwise via syringe resulting in immediate slow gas evolution and formation of a white precipitate. The reaction mixture was allowed to warm to ambient temperature (approx 45 min) after which carbon dioxide was passed through the reaction mixture via a syringe needle attachment at a moderate rate (approx 0.5 mL/s) for 15 min resulting in a clear, light yellow solution. The solution was allowed to stir for 15 min before cooling to –78 °C. *t*-BuLi (1.7 M in THF, 11 mL, 19 mmol) was added dropwise via syringe producing a white precipitate in a bright yellow-orange solution. The reaction mixture was stirred at –78 °C for 5 min, allowed to warm to –35 °C (acetonitrile/dry ice bath) and stirred for 1 h to generate the dilithiated intermediate. Chlorodiphenylphosphine (2.85 mL, 15.9 mmol) in 15 mL of dry THF was added dropwise via syringe. The cooling bath was removed and the reaction mixture was allowed to warm to ambient temperature. Aqueous hydrochloric acid (2 M, 15 mL) was added carefully to quench the reaction releasing carbon dioxide. After cessation of effervescence, the solution was neutralized with a 30% (w/w) KOH/H_2O solution, 50 mL of water was added and the aqueous layer was extracted with 3 x 50 mL of Et_2O. The combined organic layers were then washed with 100 mL of water, dried over anhydrous Na_2SO_4, filtered and the solvent was removed *in vacuo*. The *ortho*-phosphinoaniline was recrystallized from approx 50 mL of boiling ethanol (2.78 g, 60.1%) yielding a white, crystalline product (Found: C, 78.11; H, 6.30; N, 4.81%. Calcd for $C_{19}H_{18}NP$: C, 78.33; H, 6.23; N, 4.81%); δ_H(400 MHz; CD_2Cl_2; Me_4Si) 2.84 (3H, s/br, CH_3), 4.86 (1H, m/br, NH), 6.65 (2H, m, H_{Ar}), 6.79 (1H, m, H_{Ar}), 7.33 (11H, m, H_{Ar}). δ_C(101 MHz; CD_2Cl_2; Me_4Si) 30.8 (1C, s, CH_3). δ_P(162 MHz; CD_2Cl_2; H_3PO_4) –21.8 (s). HRMS (EI, 70 eV). Found: *m/z* 291.11697 for $[M]^+$. Calcd for $C_{19}H_{18}NP$: *m/z* 291.11768.

(b) Di(*o*-*N*-methylanilinyl)phenylphosphine, $PhPAr_2$ (2). The dilithiated intermediate was prepared from *N*-methylaniline (2.10 mL, 19.3 mmol) as described in part (a). Dichlorophenylphosphine (1.31 mL, 9.65 mmol) was added dropwise via syringe and the mixture was allowed to slowly warm to ambient temperature. The resulting solution was then acidified, neutralized, extracted, dried and filtered as described in part (a). Solvent was removed *in vacuo* and the *ortho*-phosphinoaniline was cleanly precipitated from approx 50 mL of boiling ethanol (1.40 g, 45.4%) yielding a white powder (Found: C, 74.64; H, 6.49; N, 8.66%. Calcd for $C_{20}H_{21}N_2P$: C, 74.98; H, 6.61; N, 8.74%); δ_H(400 MHz; CD_2Cl_2; Me_4Si) 2.85 (6H, s/br, CH_3), 4.71 (2H, m/br, NH), 6.67 (4H, m, H_{Ar}), 6.82 (2H, m, H_{Ar}), 7.37 (7H, m, H_{Ar}). δ_C(101 MHz; CD_2Cl_2; Me_4Si) 30.9 (2C, s, CH_3). δ_P(162 MHz; CD_2Cl_2; H_3PO_4) –38.0 (s). HRMS (EI, 70 eV). Found: *m*/*z* 320.14380 for $[M]^+$. Calcd for $C_{20}H_{21}N_2P$: *m*/*z* 320.14423.

(c) Tri(*o*-*N*-methylanilinyl)phosphine, PAr_3 (3). The dilithiated intermediate was prepared from *N*-methylaniline (2.10 mL, 19.3 mmol) as described in part (a). Trichlorophosphine (0.56 mL, 6.4 mmol) was added dropwise via syringe and the mixture was allowed to slowly warm to ambient temperature. The resulting solution was then acidified, neutralized, extracted, dried and filtered as described in part (a). Solvent was removed *in vacuo* and the *ortho*-phosphinoaniline was precipitated from approx 50 mL of boiling ethanol (0.436 g, 19.4%) yielding an off-white powder; δ_H(400 MHz; CD_2Cl_2; Me_4Si) 2.85 (9H, d/br, $^3J_{HH}$ = 5.0 Hz, CH_3), 4.57 (3H, m/br, NH), 6.69 (6H, m, H_{Ar}), 6.82 (3H, m, H_{Ar}), 7.34 (3H, m, H_{Ar}). δ_C(101 MHz; CD_2Cl_2; Me_4Si) 30.8 (3C, s, CH_3). δ_P(162 MHz; CD_2Cl_2; H_3PO_4) –53.6 (s). HRMS (EI, 70 eV). Found: *m*/*z* 349.17050 for $[M]^+$. Calcd for $C_{21}H_{24}N_3P$: *m*/*z* 349.17078.

(d) Bis(di(*o*-*N*-methylanilinyl)phosphino)methane, mapm (4). The dilithiated intermediate was prepared from *N*-methylaniline (1.75 mL, 16.2 mmol) as described in part (a). In a 25 mL Schlenk flask bis(dichlorophosphino)methane (0.53 mL, 4.0 mmol) was dissolved in 2 mL of freshly distilled, dry THF. The

diphosphine solution was added dropwise over 5 min to the reaction mixture via cannula and the mixture was allowed to slowly warm to ambient temperature. The resulting solution was then acidified, neutralized, extracted, dried and filtered as described in part (a). Solvent was removed *in vacuo* and the *ortho*-phosphinoaniline was cleanly precipitated from approx 20 mL of boiling ethanol (0.378 g, 18.9%) yielding an off-white powder (Found: C, 69.19; H, 6.80; N, 10.76%. Calcd for $C_{29}H_{34}N_4P_2$: C, 69.59; H, 6.85; N, 11.19%); δ_H(400 MHz; CD_2Cl_2; Me_4Si) 2.74 (2H, m, CH_2), 2.77 (12H, d, $^3J_{HH}$ = 4.8 Hz, CH_3), 4.62 (4H, m/br, NH), 6.58 (4H, m, H_{Ar}), 6.69 (4H, m, H_{Ar}), 7.24 (8H, m, H_{Ar}). δ_C(100 MHz; CD_2Cl_2; Me_4Si) 21.7 (1C, t, $^1J_{PC}$ = 16 Hz, CH_2), 31.1 (4C, s, CH_3). δ_P(162 MHz; CD_2Cl_2; H_3PO_4) –60.9 (s). HRMS (ESI): *m*/*z* 501.23282 [M^+ + H]. Calcd for $C_{29}H_{35}N_4P_2$: *m*/*z* 501.23315.

2.2.3 Preparation of Metal Complexes

(a) Chlorocarbonyl(diphenyl(*o*-*N*-methylanilinyl)phosphine)rhodium(I), [RhCl(CO)(Ph_2PAr)] (5). In a 50 mL Schlenk flask under anhydrous conditions and argon atmosphere, $[Rh(\mu\text{-}Cl)(COD)]_2$ (200 mg, 0.406 mmol) and Ph_2PAr (236 mg, 0.811 mmol) were dissolved in dichloromethane (10 mL) at ambient temperature. Carbon monoxide was passed through the solution for 10 min at an approximate rate of 0.5 mL/s and the reaction mixture was stirred for 18 h at ambient temperature. The solvent was reduced to approximately 2 mL under vacuum and a yellow solid precipitated upon addition of 20 mL of dry *n*-pentane. The yellow solid was filtered, washed with 10 mL of *n*-pentane and dried *in vacuo* (334 mg, 90.4%). Single crystals suitable for X-ray crystallographic analysis were obtained by dissolving the complex, under argon atmosphere, in a minimum volume of CH_2Cl_2 and layering the solution with anhydrous *n*-pentane in an NMR tube (Found: C, 50.80; H, 3.71; N, 2.96; Cl, 10.63%. Calcd for $[C_{20}H_{18}ClNOPRh]\cdot 0.25CH_2Cl_2$: C, 50.78; H, 3.89; N, 2.92; Cl, 11.10%).

(b) Chlorocarbonyl(di(*o*-*N*-methylanilinyl)phenylphosphine)rhodium(I), [RhCl(CO)(PhPAr$_2$)] (6). The compound was prepared as described in part (a) using [Rh(μ-Cl)(COD)]$_2$ (187 mg, 0.383 mmol) and PhPAr$_2$ (245 mg, 0.765 mmol) and isolated as a yellow solid (305 mg, 81.9%). Single crystals suitable for X-ray crystallographic analysis were obtained by dissolving the complex, under argon atmosphere, in a minimum volume of CH_2Cl_2 and layering the solution with anhydrous *n*-pentane in an NMR tube (Found: C, 48.82; H, 4.08; N, 5.38%. Calcd for $[C_{21}H_{21}ClN_2OPRh]\cdot 0.5CH_2Cl_2$: C, 48.80; H, 4.19; N, 5.29%).

(c) Chlorocarbonyl(tri(*o*-*N*-methylanilinyl)phosphine)rhodium(I), [RhCl(CO)(PAr$_3$)] (7). *Method a*. The compound was prepared as described in part (a) using [Rh(μ-Cl)(COD)]$_2$ (174 mg, 0.352 mmol) and PAr$_3$ (246 mg, 0.704 mmol) and isolated as a yellow solid (348 mg, 95.8%). Single crystals suitable for X-ray crystallographic analysis were obtained by dissolving the complex, under argon atmosphere, in a minimum volume of CH_2Cl_2 and layering the solution with anhydrous *n*-pentane in an NMR tube. *Method b*. In a 50 mL Schlenk flask under anhydrous conditions and argon atmosphere, [Rh(μ-Cl)(CO)$_2$]$_2$ (27 mg, 68 μmol) and PAr$_3$ (48 mg, 0.14 mmol) were dissolved in dry THF (5 mL) at ambient temperature. The yellow solution was stirred for 5 min then 10 mL of dry *n*-pentane were added and the resulting yellow precipitate was allowed to settle before removing the supernatant via cannula. The compound was then dried *in vacuo* (61 mg, 86%) producing a yellow solid (Found: C, 51.05; H, 4.83; N, 7.83%. Calcd for $[C_{22}H_{24}ClN_3OPRh]$: C, 51.23; H, 4.69; N, 8.15%).

(d) Chlorocarbonyl(bis(*o*-*N*,*N*-dimethylanilinyl)phenylphosphine)rhodium(I), [RhCl(CO)(PhPAr'$_2$)] (8). The compound was prepared as described in part (a) using [Rh(μ-Cl)(COD)]$_2$ (200 mg, 0.406 mmol) and PhPAr'$_2$ (282 mg, 0.812 mmol) and isolated as a yellow solid (366 mg, 87.5%). Single crystals suitable for X-ray crystallographic analysis were obtained by dissolving the complex, under argon atmosphere, in a minimum volume of CH_2Cl_2 and layering the solution with

anhydrous *n*-pentane in an NMR tube (Found: C, 53.49; H, 4.92; N, 5.48%. Calcd for $[C_{21}H_{20}ClN_2OPRh]$: C, 53.66; H, 4.89; N, 5.44%).

(e) Chlorocarbonyl(tris(*o*-*N*,*N*-dimethylanilinyl)phosphine)rhodium(I), [RhCl(CO)(PAr'$_3$)] (9). The compound was prepared as described in part (a) using $[Rh(\mu\text{-}Cl)(COD)]_2$ (58 mg, 0.13 mmol) and PAr'$_3$ (92 mg, 0.24 mmol) and isolated as a yellow solid (101 mg, 76.6%). Single crystals suitable for X-ray crystallographic analysis were obtained by dissolving the complex, under argon atmosphere, in a minimum volume of CH_2Cl_2 and layering the solution with anhydrous *n*-pentane in an NMR tube (Found: C, 52.81; H, 5.31; N, 7.32; Cl, 7.43%. Calcd for $[C_{25}H_{30}ClN_3OPRh]\cdot 0.11CH_2Cl_2$: C, 53.20; H, 5.37; N, 7.41; Cl, 7.57%). Although the crystal structure indicates no methylene chloride content, a microcrystalline sample was analyzed here. Chloride analysis and ^{1}H NMR analysis in $CDCl_3$ (both obtained at approximately the same time) were used to determine methylene chloride.

(f) Dichlorodicarbonyl(μ-*P*,*N*,*P*',*N*'-bis(di(*o*-*N*-methylanilinyl)phosphino)-methane)dirhodium(I,I), [Rh$_2$Cl$_2$(CO)$_2$(μ-mapm)] (10). In a 50 mL Schlenk flask under anhydrous conditions and argon atmosphere, $[Rh(\mu\text{-}Cl)(CO)_2]_2$ (77 mg, 0.20 mmol) and mapm (103 mg, 0.206 mmol) were dissolved in THF (15 mL) by stirring at ambient temperature. Solvent was slowly removed from the bright red-orange solution by heating to 40 °C under a steady flow of argon. Dichloromethane (3 mL) was added to the resultant orange solids yielding a red solution with a bright yellow precipitate. The precipitate was isolated by Schlenk filtration, washed with three times with 1 mL aliquots of dichloromethane and dried *in vacuo* (118 mg, 71%). Single crystals suitable for X-ray crystallographic analysis were obtained by dissolving the complex, under argon atmosphere, in a minimum volume of CH_2Cl_2 and layering the solution with anhydrous Et_2O in an NMR tube (Found: C, 42.60; H, 3.96; N, 6.15; Cl, 13.67%. Calcd for $[C_{31}H_{34}Cl_2N_4O_2P_2Rh_2]\cdot 0.75CH_2Cl_2$: C, 42.51; H, 3.99; N, 6.25; Cl, 13.68%).

(g) Dichlorodicarbonyl(μ-*P*,*N*,*P*',*N*'-bis(di(*o*-*N*,*N*-dimethylanilinyl)-phosphino)methane)dirhodium(I,I), [$Rh_2Cl_2(CO)_2$(μ-dmapm)] (11). In a 100 mL Schlenk flask under anhydrous conditions and argon atmosphere, [Rh(μ-Cl)$(CO)_2]_2$ (149 mg, 0.383 mmol) and dmapm (227 mg, 0.408 mmol) were dissolved in 10 mL of dichloromethane at ambient temperature and stirred. Stirring was stopped after 30 min and a light argon stream was left blowing over the saturated red-orange solution for 18 h producing cube-shaped, orange-yellow crystals. The crystals were then washed with 1 mL of dry dichloromethane and dried *in vacuo* (278 mg, 81.5%). Single crystals suitable for X-ray crystallographic analysis were obtained by dissolving the complex, under argon atmosphere, in a minimum volume of CH_2Cl_2 and layering the solution with anhydrous *n*-pentane in an NMR tube (Found: C, 47.35; H, 4.89; N, 6.37%. Calcd for [$C_{35}H_{42}Cl_2N_4O_2P_2Rh_2$]: C, 47.27; H, 4.76; N, 6.30%).

(h) Bis(trifluoromethanesulfonato)dicarbonyl(μ-*P*,*N*,*P*',*N*'-bis(di(*o*-*N*-methyl-anilinyl)phosphino)methane)dirhodium(I,I), [$Rh_2(OTf)_2(CO)_2$(μ-mapm)] (12). In a 25 mL Schlenk tube under anhydrous conditions and argon atmosphere, [$Rh_2Cl_2(CO)_2$(μ-mapm)] (51 mg, 61 μmol) and AgOTf (34 mg, 130 μmol) were dissolved in 5 mL of dichloromethane at ambient temperature and stirred for 12 h in the dark. The resultant orange-brown slurry was then left unstirred and the precipitate was allowed to settle before filtering the orange solution through Celite® into a 50 mL Schlenk flask. Solvent was removed *in vacuo* and the complex was washed with 1 mL of dichloromethane before drying *in vacuo* (43 mg, 66%) producing an orange solid (Found: C, 37.34; H, 3.56; N, 5.63%. Calcd for [$C_{33}H_{34}F_6N_4O_8P_2Rh_2S_2$]: C, 37.37; H, 3.23; N, 5.28%).

(i) Diiododicarbonyl(μ-*P*,*N*,*P*',*N*'-bis(di(*o*-*N*-methylanilinyl)phosphino)-methane)dirhodium(I,I), [$Rh_2I_2(CO)_2$(μ-mapm)] (13). In a 100 mL Schlenk flask under anhydrous conditions and argon atmosphere, [$Rh_2Cl_2(CO)_2$(μ-mapm)] (106 mg, 0.127 mmol) was dissolved in 10 mL of dichloromethane at ambient temperature and stirred. Under similar conditions, KI (207 mg, 1.25 mmol) was

dissolved in 8 mL of methanol at ambient temperature. The KI solution was transferred to the solution of $[Rh_2Cl_2(CO)_2(\mu\text{-mapm})]$ via cannula and the resultant orange solution was stirred at ambient temperature for 1 h producing an orange-brown slurry. Solvents were removed *in vacuo* yielding a brown solid. Water (40 mL) was added with stirring and the product was extracted with 3 x 5 mL of dichloromethane into a 50 mL Schlenk flask. The solution was stirred vigorously while adding 15 mL of Et_2O followed by 10 mL of *n*-pentane producing a yellow precipitate which was allowed to settle before the supernatant was decanted. The complex was then dried under a brisk flow of argon and dried further *in vacuo* (85 mg, 66%) producing a yellow solid (Found: C, 36.38; H, 3.43; N, 5.15%. Calcd for $[C_{31}H_{34}I_2N_4O_2P_2Rh_2]$: C, 36.64; H, 3.37; N, 5.5%).

(j) Diacetatodicarbonyl(μ-*P*,*N*,*P*',*N*'-bis(di(*o*-*N*-methylanilinyl)phosphino)-methane)dirhodium(I,I), $[Rh_2(OAc)_2(CO)_2(\mu\text{-mapm})]$ (14). In a 50 mL Schlenk flask under anhydrous conditions and argon atmosphere, 25 mL of dry THF was added to $[Rh_2Cl_2(CO)_2(\mu\text{-mapm})]$ (161 mg, 0.193 mmol) and KOAc (186 mg, 1.90 mmol). The resulting dark red slurry was stirred for 18 h then filtered through Celite®. The solvent volume was reduced to approx 2 mL *in vacuo* then dry *n*-pentane was added and the resultant yellow-brown slurry was stirred for 5 minutes. The precipitate was allowed to settle and the supernatant was removed via cannula. The complex was then dried *in vacuo* (145 mg, 78.8%) producing a dark yellow-green solid (Found: C, 47.57; H, 4.76; N, 6.01%. Calcd for $[C_{35}H_{40}N_4O_6P_2Rh_2]$: C, 47.74; H, 4.58; N, 6.36%). Single crystals suitable for X-ray crystallographic analysis were obtained from a saturated 1 : 1 THF/*n*-pentane solution under argon atmosphere.

2.2.4 X-Ray Structure Determinations

(a) General. Data for compounds **5**, **6**, **7**, **9** and **11** were collected using a Bruker SMART 1000 CCD detector/PLATFORM diffractometer[57] using Mo Kα radiation, with the crystals cooled to –80 °C. Data for compound **14** were collected using a Bruker APEX II CCD detector/D8 diffractometer[57] using Mo

Kα radiation, with the crystal cooled to –80 °C. The data were corrected for absorption through use of a multi-scan model (*SADABS* [**5**, **9**, **10**, **11**, **14**] or *TWINABS* [**6**]) or through Gaussian integration from indexing of the crystal faces (**7**). Structures were solved using the direct methods programs *SHELXS–97*[58] (**5**, **7**, **9**, **10**, **11**) and *SIR97*[59] (**14**) or using the Patterson search/structure expansion facilities within the *DIRDIF-99*[60] program system (**6**). Refinements were completed using the program *SHELXL-97*.[58] Hydrogen atoms were assigned positions based on the sp^2 or sp^3 hybridization geometries of their attached carbon or nitrogen atoms, and were given thermal parameters 20% greater than those of their parent atoms. Crystallographic experimental details are provided in Table 2.3 for compounds **5** – **7** and **9** and Table 2.4 for compounds **10**, **11** and **14**. See Appendix III for information about accessing additional crystallographic data.

Table 2.3. Crystallographic Experimental Details for **5** – **7** and **9**

Compound	**5**·0.25 CH_2Cl_2	**6**·0.5 CH_2Cl_2	**7**	**9**
Formula	$RhCl_{1.5}PONC_{20.25}H_{18.5}$	$RhCl_2PON_2C_{21.5}H_{22}$	$RhClPON_3C_{22}H_{24}$	$RhClPON_3C_{25}H_{30}$
Formula Weight	478.92	529.19	515.77	557.85
Crystal Dimensions (mm)	0.43 × 0.33 × 0.09	0.50 × 0.34 × 0.17	0.43 × 0.41 × 0.26	0.44 × 0.12 × 0.12
Crystal System	monoclinic	triclinic	triclinic	monoclinic
Space Group	$P2_1/n^a$	$P\bar{1}$ (No. 2)	$P\bar{1}$ (No. 2)	$P2_1/n^a$
a (Å)	10.2776 (8)	12.768 (2)	9.3726 (8)	9.3735 (9)
b (Å)	34.571 (3)	13.306 (2)	11.3968 (10)	15.9907 (15)
c (Å)	11.5554 (9)	14.389 (2)	11.4388 (10)	17.1786 (16)
α (deg)		84.988 (2)	85.0063 (12)	
β (deg)	103.2770 (10)	76.837 (2)	77.9072 (12)	100.0340 (10)
γ (deg)		74.965 (2)	72.8739 (11)	
V (Å^3)	3996.0 (5)	2297.7 (6)	1141.36 (17)	2535.5 (4)
Z	8	4	2	4
ρ_{calcd} (g cm^{-3})	1.592	1.530	1.501	1.461
μ (mm^{-1})	1.144	1.060	0.953	0.864
$2\theta_{max}$ (deg)	52.78	55.18	54.90	52.78
Total Data Collected	30586 (–12 ≤ h ≤ 12, –43 ≤ k ≤ 43, –14 ≤ l ≤ 14)	17407 (–15 ≤ h ≤ 16, –17 ≤ k ≤ 17, 0 ≤ l ≤ 18)	10067 (–12 ≤ h ≤ 12, –14 ≤ k ≤ 14, –14 ≤ l ≤ 14)	18416 (–11 ≤ h ≤ 11, –19 ≤ k ≤ 20, –21 ≤ l ≤ 21)
Independent Reflections (R_{int})	8169 (0.0275)	17407 (0.0000)	5172 (0.0119)	5195 (0.0304)
Observed Reflns [$I \geq 2\sigma(I)$]	7347	12537	4964	4574
Restraints/ Parameters	0 / 451	0 / 519	0 / 264	0 / 289
Goodness-of-Fit (All Data)	1.137	0.971	1.104	1.052
R_1 [$I \geq 2\sigma(I)$]	0.0307	0.0400	0.0206	0.0247
wR_2 [All Data]	0.0746	0.0956	0.0576	0.0696
Largest Diff. Peak, Hole (e Å^{-3})	0.879, –0.449	1.143, –0.800	0.484, –0.589	0.691, –0.317

[a] An alternate setting of $P2_1/c$ (No. 14).

Table 2.4. Crystallographic Experimental Details for **10**, **11** and **14**

Compound	**10·0.75 CH_2Cl_2**	**11**	**14·C_4H_8O**
Formula	$Rh_2Cl_{3.5}P_2O_2N_4C_{31.75}H_{35.5}$	$Rh_2Cl_2P_2O_2N_4C_{35}H_{42}$	$Rh_2P_2O_7N_4C_{39}H_{48}$
Formula Weight	896.98	889.39	952.57
Crystal Dimensions (mm)	0.33 x 0.21 x 0.09	0.38 × 0.38 × 0.16	0.53 x 0.34 x 0.26
Crystal System	monoclinic	orthorhombic	monoclinic
Space Group	$P2_1/n^a$	$P2_12_12_1$ (No. 19)	$P2_1/n^a$
a (Å)	11.6270 (8)	17.363 (3)	11.2965 (5)
b (Å)	18.1593 (12)	20.180 (3)	25.9075 (11)
c (Å)	17.4024 (12)	20.910 (3)	14.7517 (6)
β (deg)	104.6430 (11)		108.5840 (10)
V (Å^3)	3555.0 (4)	7326.5 (18)	4092.2 (3)
Z	4	8	4
ρ_{calcd} (g cm^{-3})	1.676	1.613	1.546
μ (mm^{-1})	1.317	1.171	0.937
$2\theta_{max}$ (deg)	52.80	55.20	55.00
Total Data Collected	25488 ($-14 \le h \le 14$, $-22 \le k \le 22$, $-21 \le l \le 21$)	62099 ($-22 \le h \le 22$, $-26 \le k \le 26$, $-26 \le l \le 27$)	35647 ($-14 \le h \le 14$, $-33 \le k \le 33$, $-19 \le l \le 19$)
Independent Reflections (R_{int})	7269 (0.0394)	16892 (0.0826)	9382 (0.0165)
Observed Reflections [$I \ge 2\sigma(I)$]	5696	14226	8686
Restraints/ Parameters	0 / 388	0 / 847	0 / 493
Flack Absolute Parameter		–0.03(2)	
Goodness-of-Fit (All Data)	1.036	1.053	1.050
R_1 [$I \ge 2\sigma(I)$]	0.0355	0.0424	0.0227
wR_2 [All Data]	0.0871	0.0980	0.0598
Largest Difference Peak, Hole (e Å^{-3})	0.670, –0.603	1.516, –0.778	0.723, –0.365

[a] An alternate setting of $P2_1/c$ (No. 14).

(b) Special Refinement Conditions. (i) Compound **5**: Attempts to refine peaks of residual electron density as solvent dichloromethane carbon or chlorine atoms were unsuccessful. The data were corrected for disordered electron density through use of the *SQUEEZE* procedure as implemented in *PLATON*.[61] A total solvent-accessible void volume of 237.7 Å^3 with a total electron count of 83 (consistent with two molecules of solvent dichloromethane, or 0.25 molecules per formula unit of the complex molecule) was found in the unit cell. (ii) Compound **6**: The crystal used for data collection was found to display non-merohedral twinning. Both components of the twin were indexed with the program *CELL_NOW*. The second twin component can be related to the first component by 180° rotation about the [$-1/4$ 1 0] axis in real space and about the [0 1 0] axis in

reciprocal space. Integrated intensities for the reflections from the two components were written into a *SHELXL-97* HKLF 5 reflection file with the data integration program *SAINT* (version 7.06A), using all reflection data (exactly overlapped, partially overlapped and non-overlapped). (iii) Compound **10**: The disordered dichloromethane electron density was treated in the same manner as for **5**. A total solvent-accessible void volume of 445.8 $Å^3$ with a total electron count of 125 (consistent with three molecules of solvent dichloromethane, or 0.75 molecules per formula unit of the complex molecule) was found in the unit cell.

2.3 Results and Discussion

2.3.1 *P,N*-Ligands

The simple, five-step, one-pot syntheses of the targeted (*o*-*N*-methylanilinyl)phosphine compounds, **1** – **4**, as illustrated in Scheme 2.1, were

Scheme 2.1. Synthesis of Ligands **1** – **4**

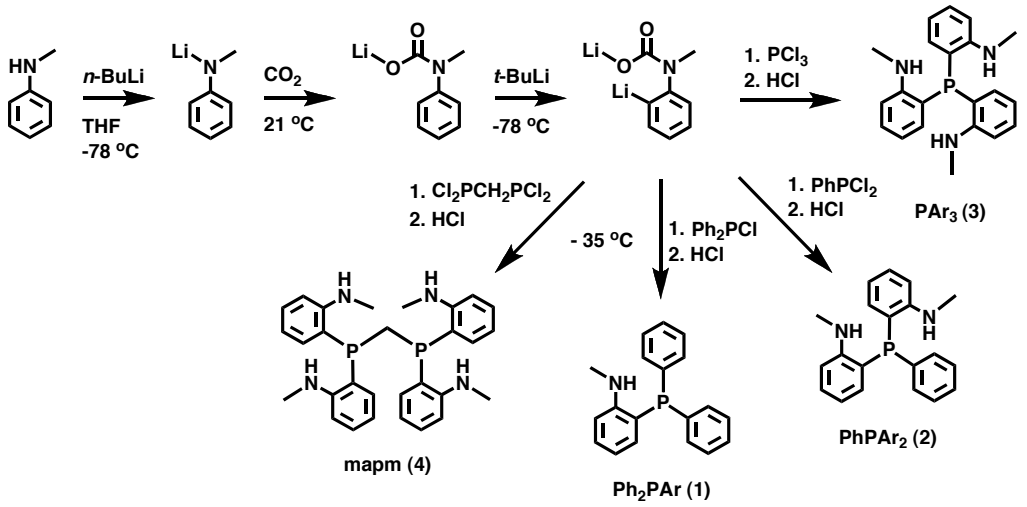

carried out using the method reported by Budzelaar *et al*. for the synthesis of diphenyl(*o*-*N*-methylanilinyl)phosphine[62] (**1**), which was in turn based on the methodology of Katritzky.[63] Synthetic versatility is achieved using the commercially available phosphorus synthons, chlorodiphenylphosphine (Ph_2PCl), dichlorophenylphosphine ($PhPCl_2$), trichlorophosphine (PCl_3) and

bis(dichlorophosphino)methane ($Cl_2PCH_2PCl_2$) in conjunction with the nitrogen-containing precursor, *N*-methylaniline. None of the prepared *P*,*N*-ligands is sensitive to air or water and all are readily soluble in ether, enabling their purification by standard ether/aqueous extraction. The toxic and odorous byproducts of the hydrolysis of chlorophosphines are typically water-soluble and are removed during the aqueous work-up along with any unreacted lithium reagents. In general, these ligands are thermally stable, white solids and can be purified by recrystallization from a minimal amount of boiling ethanol. We suggest that increased steric congestion at phosphorus after each subsequent *ortho*-arylation of the phosphine tends to hinder production of the more heavily aminated *P*,*N*-ligands as is illustrated by the lower yields of these targets.

The challenge of synthesizing (*o*-*N*-methylanilinyl)phosphines can be attributed to the reactivity of the 2° amino group of *N*-alkylanilines[64] that, under basic nucleophilic conditions, leads to unwanted side reactions, thereby necessitating its protection (with CO_2 to afford the *O*-lithiocarbamate) prior to *ortho*-functionalization of the arene. *o*-Metallation to afford the dilithiated intermediate is problematic and rigorous exclusion of air and moisture is required. In this step it is necessary to use the more basic *t*-BuLi as the *o*-metallating agent since *n*-BuLi failed to react with the *O*-lithiocarbamate precursor. For example, in attempts to use *n*-BuLi as the *o*-metallating agent for the preparation of compound **4**, bis(di-*n*-butylphosphino)methane was instead isolated in quantitative yield, resulting from reaction of the precursor, bis(dichlorophosphino)methane with *n*-BuLi that had failed to react in the *o*-metallation step. Subsequently, Lee and co-workers have reported that addition of 1 equiv of THF in diethyl ether significantly enhanced product yields for syntheses involving the *o*-metallation of tetrahydroquinoline[65] derivatives with *t*-BuLi. We have not used this methodology to determine the effect of adding stoichiometric THF on product yields of (*o*-*N*-methylanilinyl)phosphines. ^{1}H NMR spectra of the ligands (Figure 2.1) exhibit broad NH signals (due to quadrupolar broadening by nitrogen) between δ_H 4.6

and 4.9 with the general trend that greater shielding of the NH protons occurs in the more heavily aminated phosphines. The ^{1}H NMR signals of the NMe protons

Figure 2.1. ^{1}H NMR Spectra of Ligands **1** – **4**

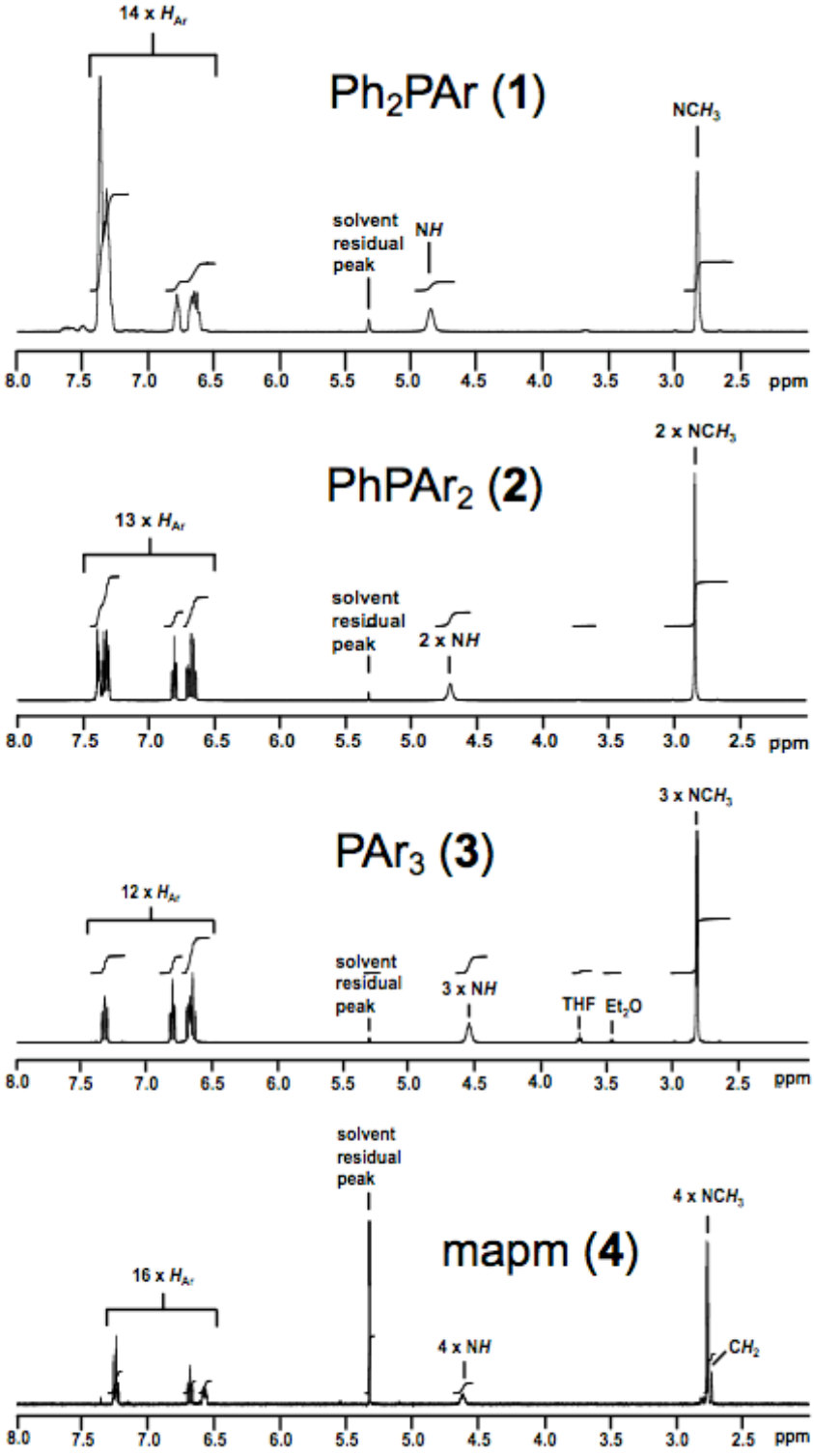

at *ca.* δ_H 2.8 appear either as broad singlets or as doublets at ambient temperature, the latter situation arising from observable, vicinal coupling to the NH protons ($^3J_{HH}$ = *ca.* 5 Hz). $^{31}P\{^1H\}$ NMR signals within the series of monophosphines show a significant upfield shift of the singlet resonances (from δ_P –21.8 to –53.6) as the number of amino substituents increases (from one to three) whereas the diphosphine, mapm (**4**), exhibits an even higher-field signal at δ_P –60.9.

2.3.2 Mononuclear Complexes

Mononuclear rhodium complexes were readily prepared by the reaction of the above monophosphine *P*,*N*-ligands (**1** – **3**) with $[Rh(\mu\text{-}Cl)(COD)]_2$ at ambient temperature under strictly inert conditions in dichloromethane, before passing carbon monoxide through the reaction mixtures (Scheme 2.2). The complexes

Scheme 2.2. Synthesis of Mononuclear Rhodium Compounds **5** – **7**

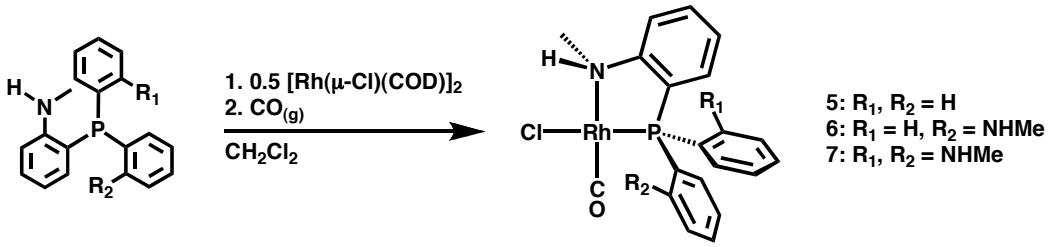

were then precipitated by addition of *n*-pentane and were obtained in moderate to high yields. A more direct route using $[RhCl(CO)_2]_2$ as a starting material had previously been exploited by Roundhill *et al*. to prepare the *N*,*N*-dimethylanilinyl compound, [RhCl(CO)(Ph_2PAr')],[66] and we have also used this methodology to prepare [RhCl(CO)(PAr_3)] (**7**). The monophosphines, $PhPAr'_2$ and PAr'_3, first prepared by Venanzi and coworkers[54] have also been used to prepare the *N*,*N*-dimethyl analogues of **6** and **7**, [RhCl(CO)($PhPAr'_2$)] (**8**) and [RhCl(CO)(PAr'_3)] (**9**), respectively. At 27 °C the ^1H NMR signal for NMe protons of [RhCl(CO)(Ph_2PAr)] (**5**) appears as a fully resolved doublet with $^3J_{HH}$ = 6.5 Hz. The complexes, [RhCl(CO)($PhPAr_2$)] (**6**), [RhCl(CO)(PAr_3)] (**7**), [RhCl(CO)($PhPAr'_2$)] (**8**) and [RhCl(CO)(PAr'_3)] (**9**), which contain coordinated and pendent amine groups (*vide infra*), all display only a single ^1H NMR

resonance for *N*-methyl protons at ambient temperature indicating the rapid exchange of these coordinated and pendent groups – a feature indicative of the (Type II) hemilabile nature of these complexes.[21] Within the series of compounds, **5** – **9**, the greater the number of anilinyl substituents on the phosphine, the greater the shielding of the ^{31}P nuclei and the greater the $^{1}J_{RhP}$ (Table 2.2).

In order to determine how the degree of *N*-methyl substitution affects the lability of the anilinyl groups we carried out variable temperature NMR experiments on the related dimethyl- and monomethylanilinyl complexes, [RhCl(CO)(PhPAr'$_2$)] (**8**; Ar' = $C_6H_4NMe_2$) and [RhCl(CO)(PhPAr$_2$)] (**6**; Ar = C_6H_4NHMe), respectively. Variable temperature ^{1}H NMR analysis of [RhCl(CO)(PhPAr'$_2$)] (**8**, Figure 2.2) reveals significant broadening of the single

Figure 2.2. ^{1}H NMR Spectra of [RhCl(CO)(Ph$_2$PAr')] (**8**)

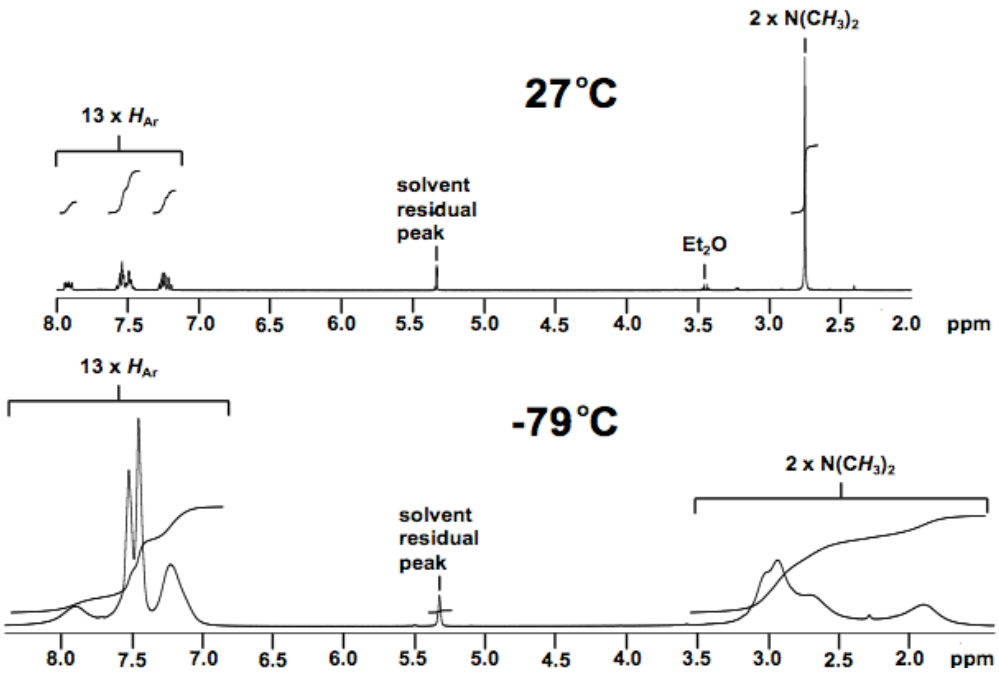

resonance representing all *N*-methyl protons upon cooling to –20 °C and at –71 °C (not shown) three distinct signals are evident, in a 1 : 1 : 2 intensity ratio – two for the diastereotopic methyl groups of the coordinated amine, and one for both methyl groups of the pendent amine (Scheme 2.3) – indicating that amine exchange at rhodium is slow on the NMR timescale at that temperature. Upon

further cooling to –79 °C, four broad *N*-methyl proton resonances are observed in the spectrum suggesting that lone pair inversion of the pendent amine has slowed to allow the resolution of the two chemically unique environments at this nitrogen.

Scheme 2.3. Enantiomerization of [RhCl(CO)(PhPAr'$_2$)] (**8**)

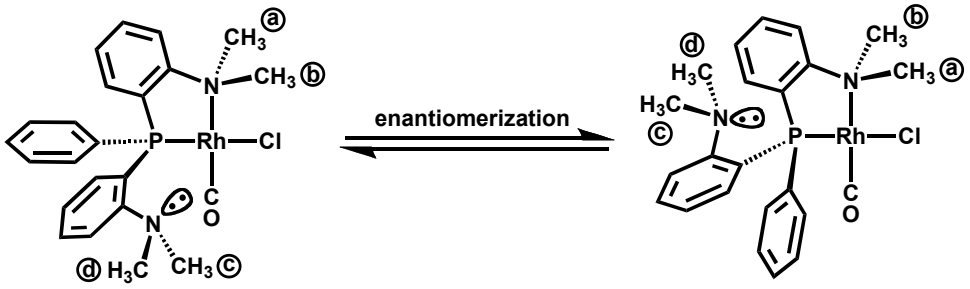

The variable temperature ^{1}H NMR spectroscopic study of [RhCl(CO)(PhPAr$_2$)] (**6**) has proven to be more complicated than that of its dimethylated counterpart (**8**), as it is immediately apparent from Scheme 2.4 that any particular coordination geometry of the complex possesses two stereogenic centers (one at phosphorus, the other at the coordinated amine) giving rise to four

Scheme 2.4. Possible Isomerization Mechanisms of [RhCl(CO)(PhPAr$_2$)] (**6**). Four kinetically independent mechanisms of amine donor exchange at rhodium are shown.

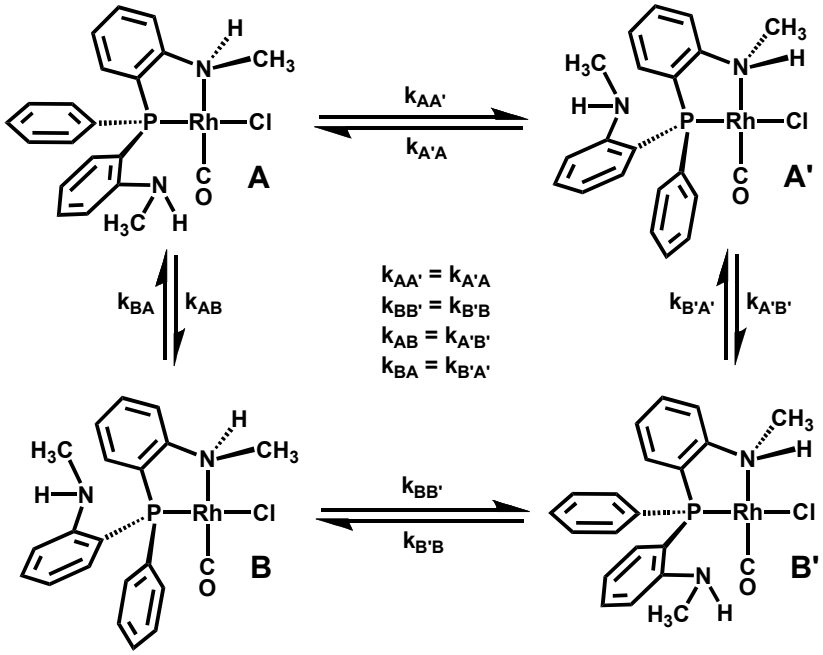

stereoisomers existing as two diastereomeric pairs of enantiomers (**A**/**A**' and **B**/**B**'). The ^{1}H NMR spectrum of [RhCl(CO)(PhPAr$_2$)] (**6**) at 27 °C (Figure 2.3)

Figure 2.3. ^{1}H NMR Spectra of [RhCl(CO)(PhPAr$_2$)] (**6**)

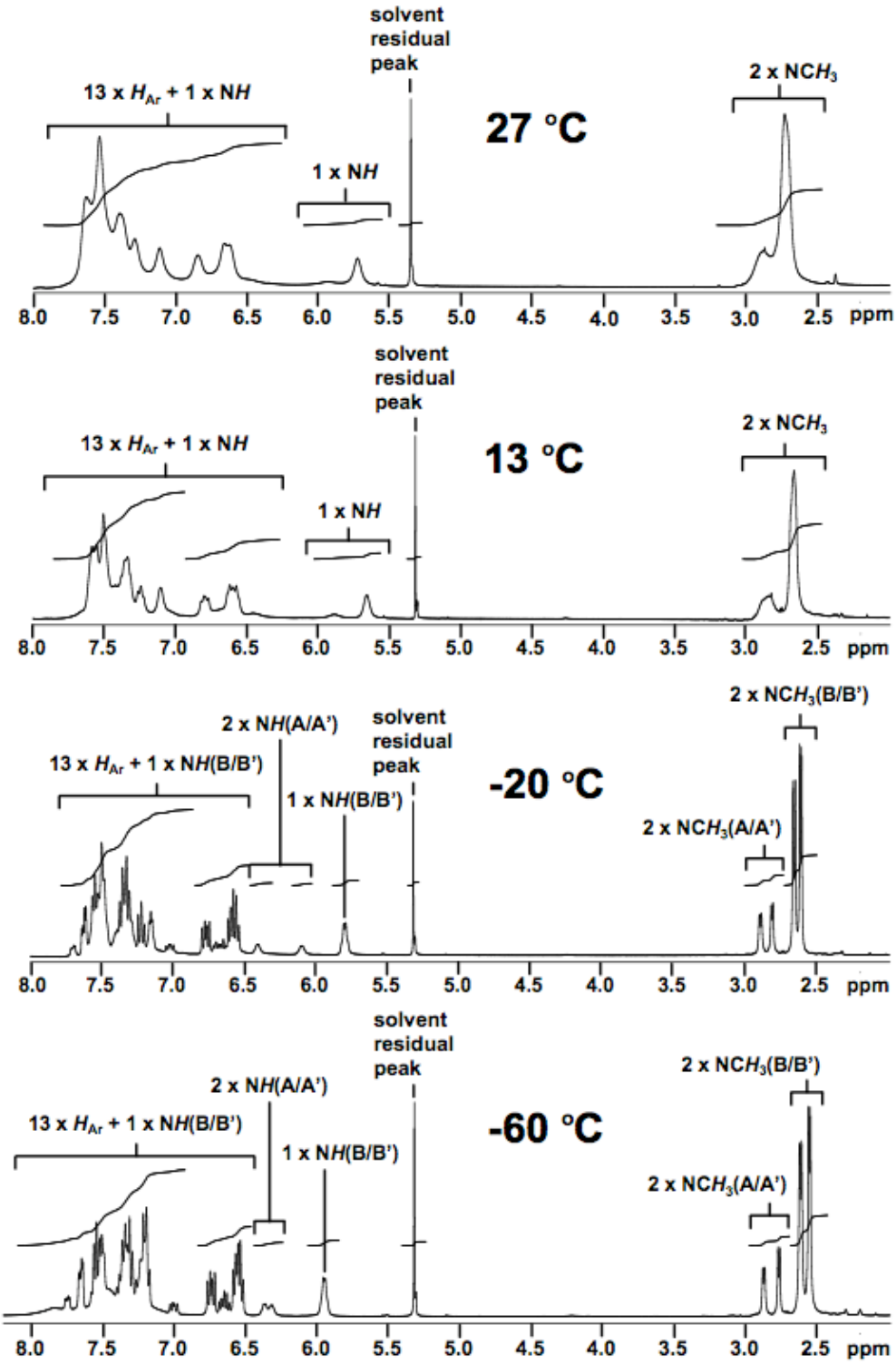

reveals two broad, nearly coalescing signals representing two diastereomeric pairs of enantiomers the intensity ratio of which is approximately 3 : 1 suggesting a thermodynamic preference for one pair of rapidly interconverting enantiomers over the other. The relative concentrations of the diastereomers which, in turn, provide a measure of the equilibrium constant for the diastereoisomerization via amine-donor exchange, only vary from 2.80 respectively at 13 °C, to 3.20 respectively at –60 °C and values of K for the diastereoisomerization at the temperatures 13, –20 and –60 °C were used to calculate ΔG for this process (Equation 2.1) of 2.3 ± 0.5 kJ/mol at 95% confidence. We assume that the major

$$\Delta G_{diaster} = -RT \ln(K_{diaster}) \qquad (2.1)$$

diastereoisomeric pair corresponds to the pair of enantiomers **B**/**B'**, on the basis of steric considerations in which the methyl group on the coordinated anilinyl moiety avoids the larger pendent anilinyl substituent in favor of the smaller phenyl group. This is also the structure found in the solid state for **6** (*vide infra*). Cooling to 13 °C results in the resolution of the two different *N*-methyl signals (for the coordinated and pendent amines) of the major enantiomeric pair into two doublets indicating the coalescence point for this enantiomerization. At 10 °C the *N*-methyl signal for the minor enantiomeric pair begins to split into two more doublets indicating the coalescence point for the enantiomerization of the minor stereoisomers (proposed to result from **A** ≒ **A'**, Scheme 2.4).

Line-shape analyses for the methyl resonances of [RhCl(CO)($PhPAr_2$)] (**6**) and [RhCl(CO)($PhPAr'_2$)] (**8**) were undertaken to compare the rates of exchange processes within these compounds along with the corresponding values of $\Delta G^{\ddagger}$, calculated using Equation 2.2.[67] For compound **6**, the rate of enantiomerization for

$$k = (k_B T)/h \exp[-\Delta G^{\ddagger}/(RT)] \qquad (2.2)$$

the major stereoisomers (presumably $k_{BB'} = k_{B'B}$) was determined as 17 s^{-1} at 286 K and this value was used to calculate $\Delta G^{\ddagger}$ (286K) = 63.2 kJ•mol^{-1}. Similarly, the rate of enantiomerization for the minor stereoisomers (presumably $k_{AA'} = k_{A'A}$)

was determined as 25 s^{-1} at 283 K and this value was used to calculate $\Delta G^{\ddagger}$ (283K) = 61.6 kJ•mol^{-1}. Exchange parameters for the enantiomerization of the *N*,*N*-dimethyl analogue, **8**, were also obtained: k(194 K) = 274 s^{-1}, $\Delta G^{\ddagger}$ (194K) = 38.4 kJ•mol^{-1}. A comparison of the $\Delta G^{\ddagger}$ values for compounds **6** and **8** indicates that, despite its stronger Lewis basicity, the *N*,*N*-dimethylanilinyl group of **8** renders the complex much more labile than its monomethylated counterpart, **6**. This labilization of the dimethylanilinyl donor can be rationalized on the basis of the more severe steric repulsion involving the more highly substituted anilinyl groups (*vide infra*).

The ^{1}H NMR spectrum of [RhCl(CO)(PAr_3)] (**7**) at –20 °C displays three well resolved doublets representing all mutually non-equivalent *N*-methyl groups, while at 27 °C, a rapid three-site exchange process results only in a broad singlet. The ^{1}H NMR spectrum of [RhCl(CO)(PAr'_3)] (**9**) exhibits only one signal for all methyl protons at room temperature but interestingly, at –80 °C only two methyl signals are observed, each integrating as 9 protons (see Figure 2.4). The

Figure 2.4. ^{1}H NMR Spectra of [RhCl(CO)(PAr'_3)] (**9**)

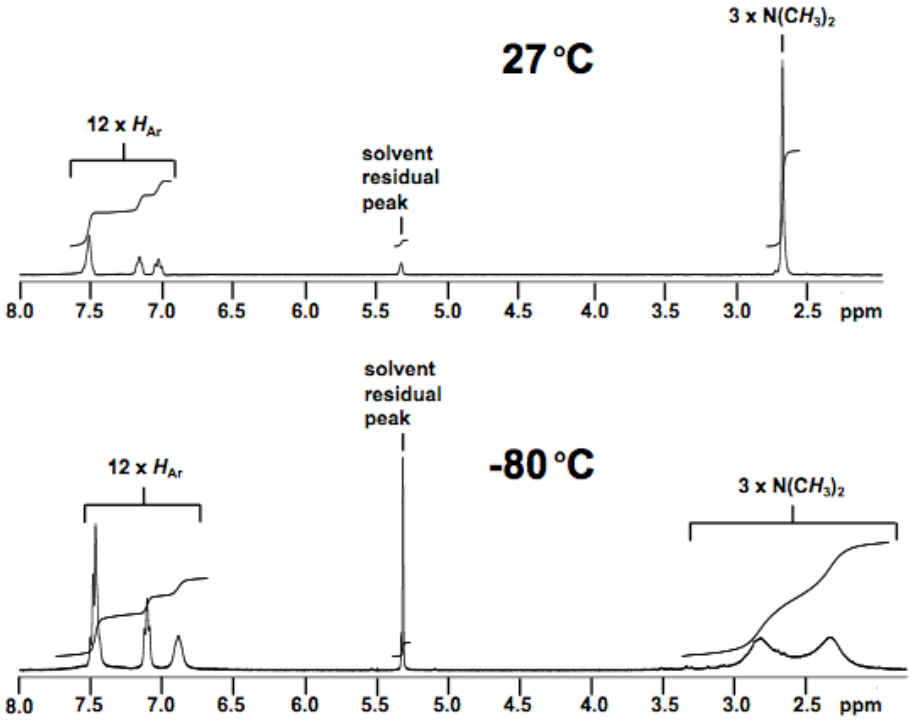

appearance of two equal-intensity methyl resonances in the low temperature spectrum of **9** can be rationalized by the geometry of the PAr'_3 ligand of **9** in the solid state (*vide infra*) in which the pendent amine groups each have methyl groups in clearly different environments. It appears that rapid exchange of the amine donors at rhodium by rotation about the Rh-P bond, even at –80 °C, occurs in a propeller-like manner, resulting in two chemically distinct average methyl environments in solution.

In order to compare the structural differences between the monomethyl- and dimethylanilinyl analogues the single-crystal X-ray structures of the three mononuclear [RhCl(CO)(L)] complexes (L = Ph_2PAr (**5**), $PhPAr_2$ (**6**), PAr_3 (**7**); Ar = *o*-C_6H_4NHMe) have been carried out and are compared to the previously reported dimethylanilinyl complex, [RhCl(CO)(Ph_2PAr')] (Ar' = *o*-$C_6H_4NMe_2$).[68] In addition, we have determined the structure of the compound [RhCl(CO)(PAr'_3)] (**9**) as a further comparison. The ORTEP diagrams of compounds **5**, **6**, **7** and **9** are shown in Figure 2.5 and a comparison of their structural parameters, along with those of [RhCl(CO)(Ph_2PAr')] is given in Table 2.5. All compounds have the expected square-planar geometry at rhodium in

Table 2.5. Selected Structural Parameters for Mononuclear Compounds

	[RhCl(CO) (Ph_2PAr)] (5)	**[RhCl(CO) ($PhPAr_2$)] (6)**	**[RhCl(CO) (PAr_3)] (7)**	**[RhCl(CO) (Ph_2PAr')]**[67]	**[RhCl(CO) (PAr'_3)] (9)**
Atoms	Bond Lengths (Å)[a]	Bond Lengths (Å)[a]	Bond Lengths (Å)	Bond Lengths (Å)	Bond Lengths (Å)
Rh-P	2.1933(7), 2.1909(7)	2.2150(8), 2.2035(8)	2.2199(4)	2.1947(6)[b]	2.2019(6)
Rh-N(1)	2.129(2), 2.140(2)	2.131(2), 2.139(2)	2.1368(13)	2.1865(2)	2.1883(18)
Rh-C(1)	1.819(3), 1.809(3)	1.825(3), 1.819(3)	1.8160(17)	1.807(2)	1.801(3)
Rh-Cl	2.3936(7), 2.3757(7)	2.3786(8), 2.3797(8)	2.3787(4)	2.3867(7)	2.3941(6)
Atoms	Angles (°)	Angles (°)	Angles (°)	Angles (°)	Angles (°)
P-Rh-N(1)	83.49(6), 83.24(7)	83.28(6), 82.83(7)	84.05(4)	85.03(5)	84.62(5)
Cl-Rh-N(1)	86.69(6), 89.11(7)	88.13(6), 87.16(7)	88.16(4)	91.11(5)	92.17(5)
Cl-Rh-C(1)	98.04(9), 95.36(10)	92.87(9), 96.06(10)	93.16(5)	92.62(7)	90.08(7)
P-Rh-C(1)	91.83(9), 92.65(10)	95.71(9), 94.07(10)	95.00(6)	91.24(7)	93.86(8)

[a] Two crystallographically independent molecules. [b] Correct bond lengths and angles for [RhCl(CO)(Ph_2PAr')] obtained from Table 5 within reference 68.

which the carbonyl ligand is opposite the weaker *trans*-directing amine group while the chloro ligand is opposite the phosphine moiety, having the greater *trans* effect. All five compounds also have quite comparable structural parameters in which the bond lengths and angles are as expected. Certainly, within the series of

monomethylanilinyl complexes (**5** – **7**) all related parameters are closely comparable, indicating that the incorporation of additional *N*-methylanilinyl

Figure 2.5. ORTEP Diagrams of Compounds **5** – **7** and **9**. Only one of two crystallographically independent molecules of [RhCl(CO)(Ph_2PAr)] (**5**), one of two crystallographically independent molecules of [RhCl(CO)($PhPAr_2$)] (**6**), [RhCl(CO)(PAr_3)] (**7**) and [RhCl(CO)(PAr'_3)] (**9**) are shown. Gaussian ellipsoids for all non-hydrogen atoms are depicted at the 20% probability level. Hydrogens are shown artificially small, except for aryl hydrogens which are omitted.

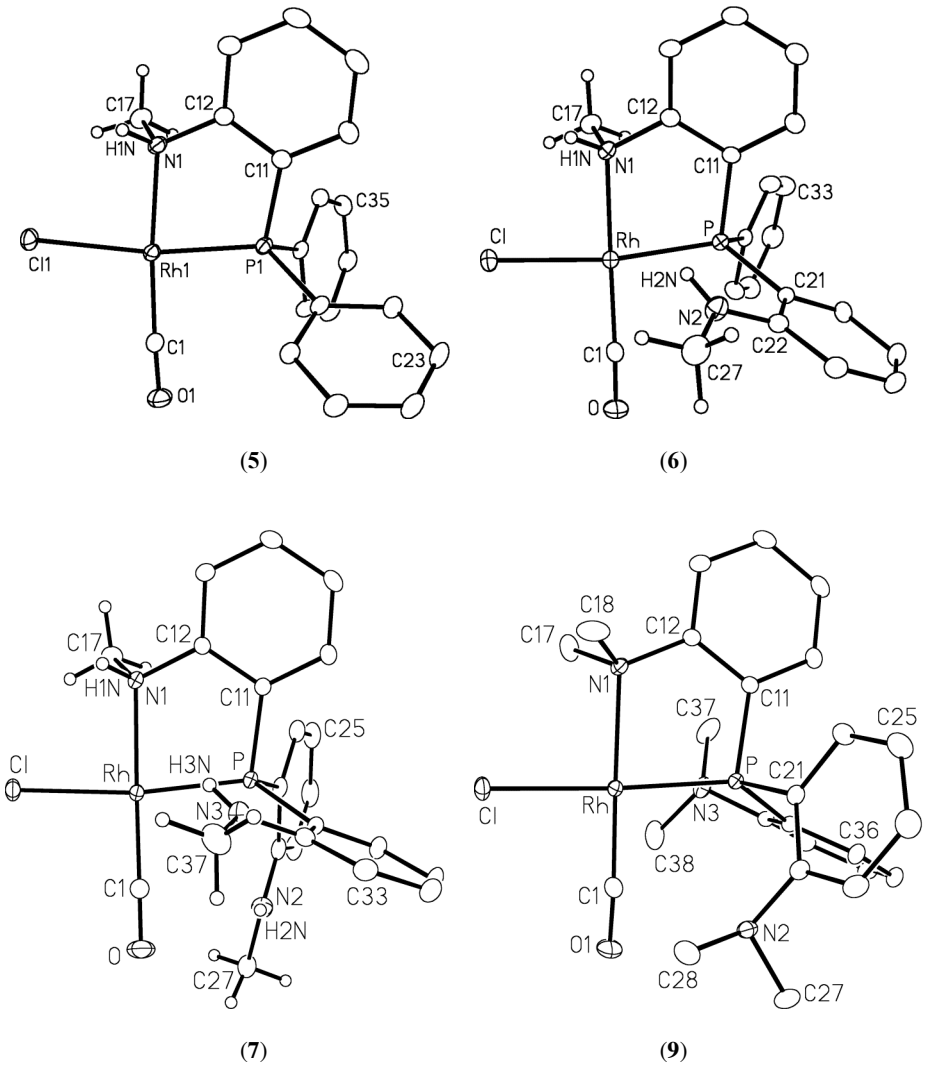

groups (Ph_2PAr *vs.* $PhPAr_2$ *vs.* PAr_3) has no obvious structural influence on the metal coordination geometries, although minor differences in the orientations of the aryl groups are observed between the three complexes. Similarly, within the pair of dimethylanilinyl compounds the structural parameters are closely comparable. However, a comparison of the monomethyl- and dimethylanilinyl compounds shows significant differences between the two classes. A visual

comparison of the two trisubstituted species **7** and **9**, shown in Figure 2.5, indicates that the most significant differences between the monomethyl- and dimethylanilinyl analogues relate to the coordinated amine groups. An analysis of Table 2.5 shows that in the case of the dimethylanilinyl-containing compounds, [RhCl(CO)(Ph_2PAr')] and **9**, the Rh–N distance (2.1947(6), 2.2019(6) Å, respectively) is greater than that for the three monomethylanilinyl-containing species (*av*. 2.135(5) Å). This lengthening for the dimethylated compounds is also accompanied by a slight widening of the N–Rh–Cl angle, which is greater than 90° for the dimethylanilinyl compounds and less than 90° for the monomethylanilinyl analogues. Both differences appear to result from the greater steric crowding in the dimethylamines which weakens the Rh–N bond and gives rise to greater repulsions involving the adjacent chloro ligand. These structural comparisons are consistent with the significantly greater lability of the dimethylanilinyl species as discussed above for compounds **6** and **8**.

We had initially intended to compare the above monophosphine complexes with the mononuclear diphosphine equivalent, [RhCl(CO)(*P*,*N*-mapm)], for which we had assumed a phosphine binding mode, analogous to compounds **5** – **9**, would be observed in which the diphosphine ligand is bound to Rh via one phosphorus and an adjacent amine, while the other end of the diphosphine remained uncoordinated and pendent. The related complex, [RhCl(CO)(*P*,*N*-dmapm)], was previously shown to have this structure type.[43] However, all attempts to prepare this mononuclear mapm analogue gave the binuclear diphosphine-bridged species, [$Rh_2Cl_2(CO)_2$(μ-mapm)] (*vide infra*), as the major product accompanied by minor amounts of uncharacterized side products. None of these side products displayed spectra characteristic of our targeted mononuclear species. It appears that the greater steric accessibility of the mapm ligand favors the formation of the bimetallic complexes over the mononuclear pendent complexes.

2.3.3 Binuclear Complexes

The binuclear mapm-bridged complex, $[Rh_2Cl_2(CO)_2(\mu\text{-mapm})]$ (**10**; mapm = $Ar_2PCH_2PAr_2$) was prepared, as alluded to above, by adding dichloromethane to a flask containing $[Rh(\mu\text{-}Cl)(CO)_2]_2$ and mapm (**4**) at ambient temperature; the dmapm analogue, $[Rh_2Cl_2(CO)_2(\mu\text{-dmapm})]$ (**11**; dmapm = $Ar'_2PCH_2PAr'_2$) was prepared by a similar procedure (Scheme 2.5). Compound **11** had been previously

Scheme 2.5. Synthesis of Binuclear Rhodium Compounds **10** and **11**

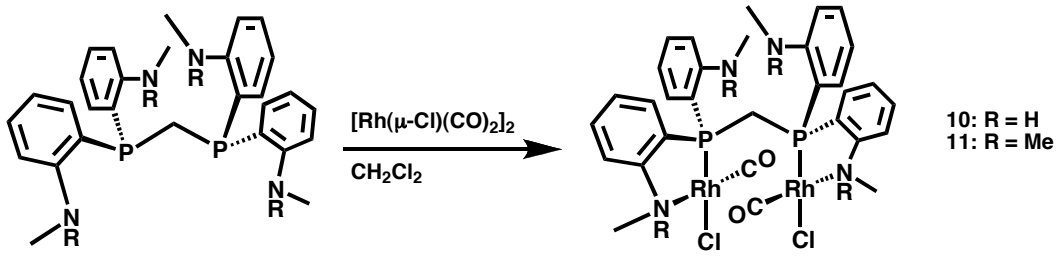

reported[69] but had not been structurally characterized. We were interested in establishing the structural differences that would result from substituting the amine hydrogen in **10** by a methyl group, and were also interested in whether such a substitution would influence the lability of the coordinated amine groups. Both compounds display a single carbonyl stretch in the IR spectrum at around 2000 cm^{-1}, characteristic of Rh(I), and also show a doublet of doublets for the pair of carbonyls in the $^{13}C\{^1H\}$ NMR spectra at near δ_C 186, displaying typical one-bond coupling to Rh and two-bond coupling to P (see Table 2.1). At ambient temperature the ^1H NMR spectrum of **11** (see Figure 2.6) shows a well resolved broad triplet resonance at δ_H 4.59 ($^2J_{PH}$ = 12.4 Hz) for the methylene group of the dmapm ligand, but shows only very broad, unresolved resonances for the methyl groups between approximately δ_H 2.2 and 3.7 and for the aromatic protons. Upon cooling to –80 °C the methyl resonances appear as sharp singlets at δ_H 3.68, 2.86, 2.70 and 2.27, each integrating as six protons while the signal for the methylene protons also sharpens significantly. This temperature dependence suggests fluxionality, presumably involving the sequential exchange of dimethylanilinyl groups at each Rh via a transient C_s-symmetric intermediate that renders the methylene hydrogens inequivalent. The ^1H NMR temperature dependence is

paralleled by differences in the ^{31}P NMR spectra in which the diphosphine appears as a broad doublet at δ_P 41.0 ($^1J_{RhP}$ = 173 Hz) at ambient temperature but

Figure 2.6. ^1H NMR Spectra of $[Rh_2Cl_2(CO)_2(\mu\text{-dmapm})]$ (**11**)

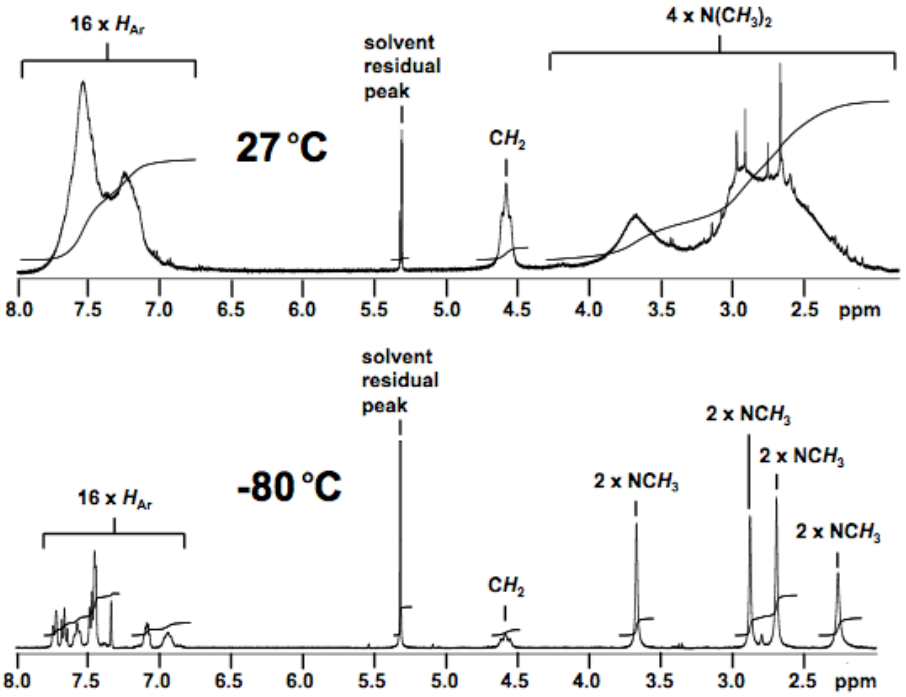

sharpens to a well resolved multiplet characteristic of an AA'XX' spin system at –80 °C. In contrast, the resonances in the ^1H and the $^{31}P\{^1H\}$ NMR spectra of the mapm analogue (**10**) are sharp and well resolved, showing no evidence of fluxionality over the full temperature range between 25 °C and –80 °C. In the ^1H NMR spectrum (Figure 2.7) the amine hydrogens overlap two aromatic proton resonances at δ_H 7.75 and 6.94 (as is indicated by the GCOSY NMR plot in

Figure 2.7. ^1H NMR Spectrum of $[Rh_2Cl_2(CO)_2(\mu\text{-mapm})]$ (**10**)

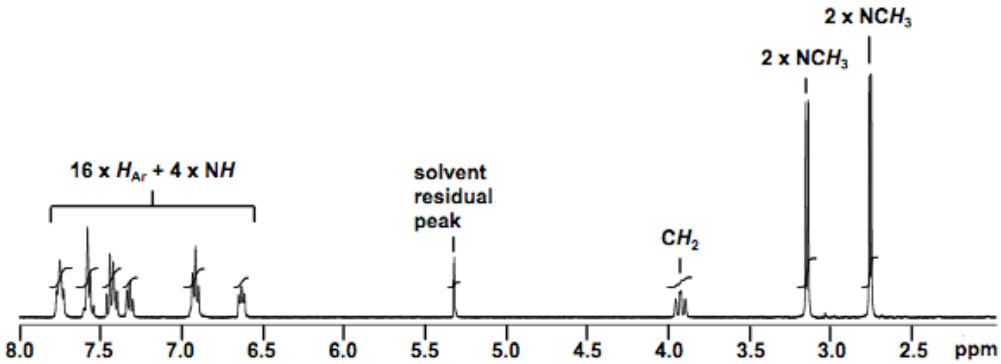

Figure 2.8, which shows strong correlations to *N*-methyl resonances) while the methylene group of the bridging mapm ligand appears as a multiplet at δ_H 3.94.

Figure 2.8. GCOSY Plot of $[Rh_2Cl_2(CO)_2(\mu\text{-mapm})$ (**10**)

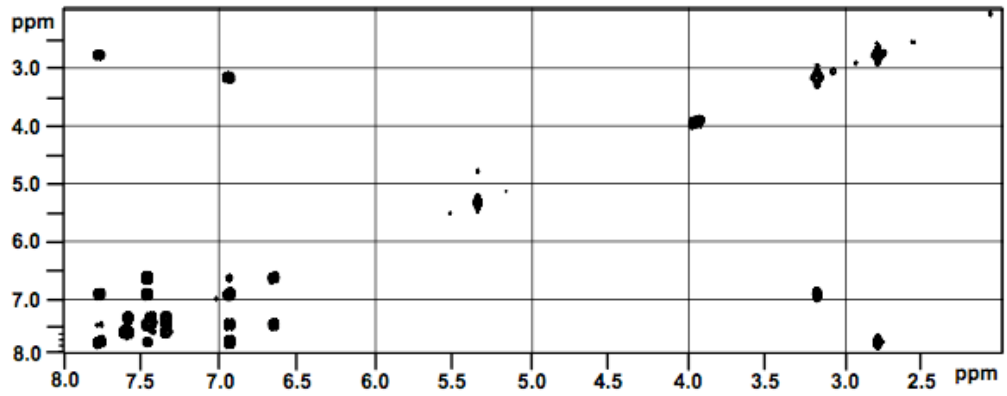

The *N*-methyl groups appear as two sharp doublets at δ_H 3.17 and 2.78. The downfield NH signal of the (presumably) coordinated amine (δ_H 7.75) exhibits a strong GCOSY correlation to the more upfield NMe signal (δ_H 2.78) while the more upfield NH signal (δ_H 6.94) shows similar correlation to the more downfield NMe signal (δ_H 3.17) providing a means for the assignment of coordinated and pendent NMe signals. In the $^{31}P\{^1H\}$ NMR spectrum a well resolved multiplet, resembling the low-temperature resonance for **11** appears at δ_P 23.3. The observed and simulated[56] $^{31}P\{^1H\}$ NMR spectra, assuming an AA'XX' spin system, for compounds **10** and **11** are given in Figure 2.9. All derived parameters (**10** : $^1J_{RhP}$ =

Figure 2.9. $^{31}P\{^1H\}$ NMR Spectra of Compounds **10** (Calculated (**A**) and Observed (**B**) at 27 °C) and **11** (Calculated (**C**) and Observed (**D**) at –40 °C)

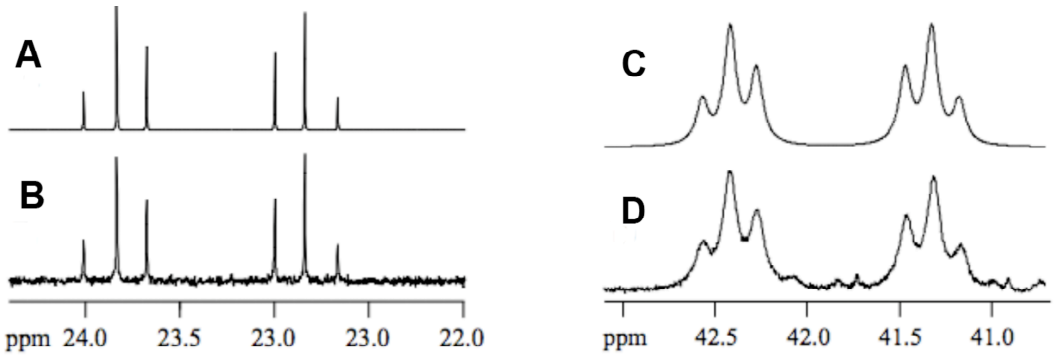

157 Hz ,$^2J_{PP}$ = 53.6 Hz, $^3J_{RhP}$ = 3.2 Hz, $^2J_{RhRh}$ = –0.05 Hz; **11** : $^1J_{RhP}$ = 175.6 Hz, $^2J_{PP}$ = 46.1 Hz, $^3J_{RhP}$ = 2.7 Hz, $^2J_{RhRh}$ = –0.05 Hz) are consistent with those reported for

the related diphosphine-bridged species $[Rh_2(\mu\text{-}Cl)(COD)_2(\mu\text{-}dppm)][BF_4]$ (dppm = $Ph_2PCH_2PPh_2$).[70] As noted for the monophosphine compounds, substitution of the amine hydrogen in **10** by a methyl group to give **11** substantially labilizes this coordinated amine, again probably due to steric repulsions between this larger tertiary amine and other ligands on Rh. Although exchange between the free and coordinated aniline groups in **11** is facile at ambient temperature, there is no evidence of fluxionality at this temperature for **10**.

In order to gain a better understanding of the influence of the additional *N*-methyl substituent we have carried out the X-ray structure determination of compounds **10** and **11** and both structures are shown in Figure 2.10 with a

Figure 2.10. ORTEP Diagrams of $[Rh_2Cl_2(CO)_2(\mu\text{-mapm})]$ (**10**, left) and $[Rh_2Cl_2(CO)_2(\mu\text{-dmapm})]$ (**11**, right). Thermal ellipsoids as in Figure 2.5.

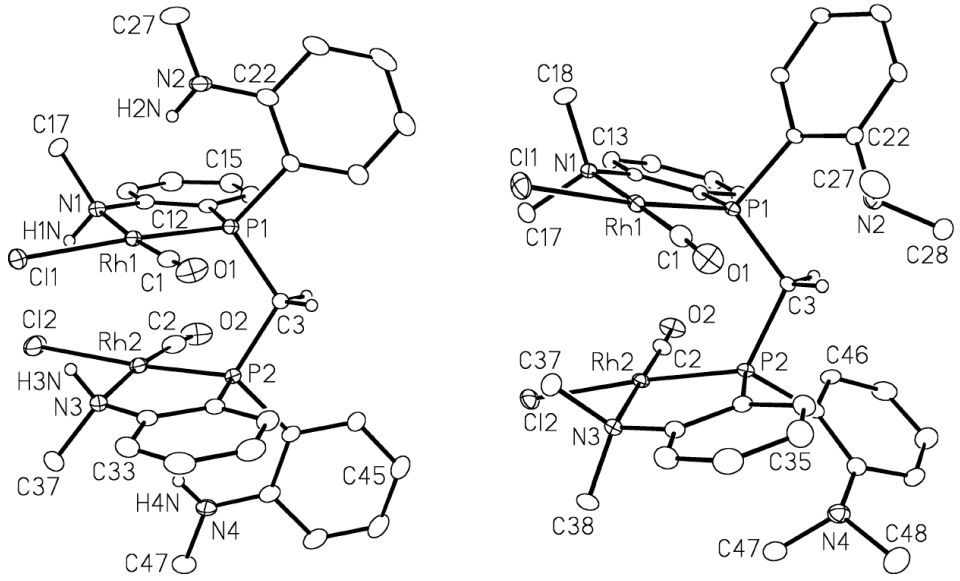

summary of metrical parameters given in Table 2.6. Both structures are similar in having a face-to-face arrangement of the two Rh square planes that are bridged by the diphosphine unit of mapm or dmapm and both square planes are also staggered with respect to each other by approximately 40° (**10**) and 44° (**11**), allowing the ligands on one metal to avoid those on the other. Furthermore, in both cases the coordinated aniline group on one metal occupies one side of the approximate Rh_2P_2 plane while that on the other metal coordinates to the opposite

face such that both complexes are C_2-symmetric. In addition, a slight lengthening of the Rh–Cl bonds is observed in **11** (*av*. 2.404 Å) compared to **10** (*av*. 2.387 Å)

Table 2.6. Selected Structural Parameters for Compounds **10** and **11**

	[$Rh_2Cl_2(CO)_2$(μ-mapm)] (10)	**[$Rh_2Cl_2(CO)_2$(μ-dmapm)] (11)**
Atoms	Distances (Å)	Distances (Å)
Rh(1)-Rh(2)	3.4500(4)	4.1211(7), 4.3185(6)[a]
Rh(1)-Cl(1)	2.3810(9)	2.398(1), 2.412(1)
Rh(2)-Cl(2)	2.393(1)	2.396(1), 2.409(1)
Rh(1)-N(1)	2.140(3)	2.181(4), 2.217(4)
Rh(2)-N(3)	2.162(3)	2.200(4), 2.202(4)
Cl(1)-H3N	2.51	–
Cl(2)-H1N	2.51	–
Atoms	Angles (deg)	Angles (deg)
Rh(1)-P(1)-C(3)	116.2(1)	124.8(2), 120.1(2)
Rh(2)-P(2)-C(3)	116.6(1)	122.3(2), 122.8(2)
P(1)-C(3)-P(2)	114.0(2)	118.0(2), 122.0(3)

[a] Two crystallographically independent molecules.

also probably due to repulsions involving the more bulky dimethylaniline groups. Again, as for the monophosphine analogues discussed above, the Rh–N distances are longer for the dimethylanilinyl complex **11** (2.181(4) – 2.217(4) Å) compared to the monomethylanilinyl species **10** (2.140(3), 2.162(3) Å) – a consequence of steric crowding in the former. However, the major differences between compounds **10** and **11** become obvious on visual comparison of the two in Figure 2.10 which demonstrates that the two Rh square planes in **11** are significantly tilted resulting in a much larger Rh–Rh separation (4.1211(7), 4.3185(6) Å for the two independent molecules) than in **10** (3.4500(4) Å). This tilt of the Rh square planes in **11** is evident in the dihedral angle between these planes of 27.78(5)° and 24.5(1)° in the two independent molecules, whereas the Rh planes in **10** are close to parallel (dihedral angle = 2.93(8)°). The opening up of the cavity between the two Rh square planes in **11** clearly results from repulsion between the chloro ligand on one metal and one methyl of the coordinated dimethylanilinyl group on the adjacent metal, leading to close contacts between Cl(1) and the methyl hydrogens on C(37) of *ca*. 2.94 Å and between Cl(2) and the C(17) methyl group of *ca*. 2.92 Å. Both separations are slightly less than a normal van der Waals separation of 3.00 Å[71] and indicate that these groups are close to their minimum separation. An additional consequence of the above repulsions is the slight bending of the Cl ligands away from these contacts (P(1)–Rh(1)–Cl(1) =

174.51(6)°, 175.79(5)°; P(2)–Rh(2)–Cl(2) = 175.62(5)°, 176.26(5)°). Furthermore, the repulsions that force the Rh planes apart in **11** give rise to significantly enlarged Rh–P–C(3) (*av*. 122.5°) and P(1)–C(3)–P(2) (*av*. 120.0°) angles compared to those in **10** (116.4° and 114.0°, respectively).

In contrast, the contacts between the chloro ligands in **10** and the amino hydrogens, associated with the adjacent metal (Cl(1)–HN(3) and Cl(2)–HN(1)), at 2.51 Å, are much shorter than a normal van der Waals separation[71] and indicate the presence of a reasonably strong hydrogen bond that actually appears to be pulling the metal coordination planes together. This attraction is further manifested in a slight bending of the chlorine ligands towards the amine to which it is hydrogen bonded (P(1)–Rh(1)–Cl(1) = 171.19(4)°; P(2)–Rh(2)–Cl(2) = 171.10(4)°). Interestingly, the pendent methylanilinyl groups in **10** are oriented such that the amino hydrogens are aimed towards the adjacent metals above and below the vacant coordination sites on the outsides of the face-to-face dimer. However, these Rh(1)–HN(2) and Rh(2)–HN(4) contacts (2.59 and 2.57 Å, respectively) appear to be normal and do not suggest an attractive interaction between these hydrogens and the metals. As a consequence, the Rh(1)–P(1)–C(21) and Rh(2)–P(2)–C(41) angles (123.8(1)° and 122.8(1)°) are much larger than the other angles at phosphorus which range from 102.8(1)° to 105.8(2)°, suggesting that the above Rh–H contacts are repulsive, forcing the anilinyl groups away from the metals slightly. Certainly, the downfield shift in the ^{1}H NMR spectrum of these amine hydrogens (δ_H 6.94) argues against an agostic interaction in solution, for which we would expect an upfield shift. Nevertheless, the Rh-H contacts observed is the solid state cannot be too unfavorable, given the orientation of the pendent methylanilinyl groups which project the amine hydrogens into the vicinities of the two metals, rather than away from them as observed for the dimethylanilinyl groups in **11**.

The apparent lack of amine lability in complex **10** prompted our attempts to prepare a species with inherently lower coordinative saturation at the bimetallic

core. Specifically, a cationic, chloro-bridged complex similar to $[Rh_2(COD)_2(\mu\text{-}Cl)(\mu\text{-}dppm)][BF_4]$[70] was targeted in which the remaining chloride was bridging and could serve as a source of coordinative unsaturation. The targeted complex, $[Rh_2(\mu\text{-}Cl)(CO)_2(\mu\text{-}mapm)]^+$, involving mapm as the bridging diphosphine, was selected due to the proximity of the Rh centers of the parent complex **10** relative to the dmapm analogue, **11**. Unfortunately, reaction of **10** with a variety of silver salts, including $AgBF_4$, $AgPF_6$ and AgOTf, failed to yield the monochloride. Reactions of **10** with $AgBF_4$ and $AgPF_6$ under a variety of conditions and solvent systems routinely resulted in multiple decomposition products, while reaction of **10** with AgOTf yielded the symmetric disubstituted species, $[Rh_2(OTf)_2(CO)_2(\mu\text{-}mapm)]$ (**12**) (Scheme 2.6). The molar conductivity of **12** in CH_3NO_2 was

Scheme 2.6. Chloride Replacement Reactions of $[Rh_2Cl_2(CO)_2(\mu\text{-}mapm)]$ (**10**)

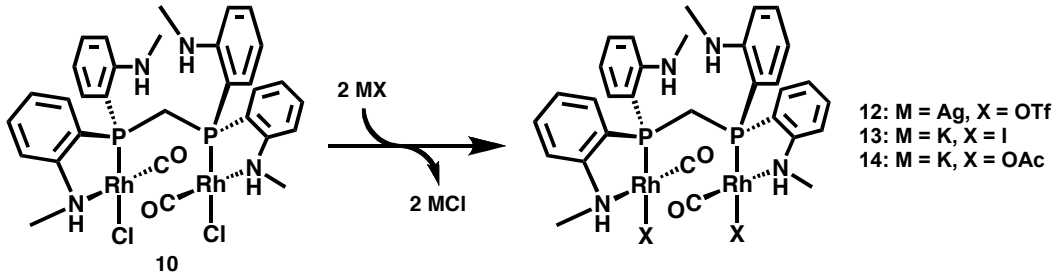

determined to be 23 $cm^2 \cdot \Omega^{-1} \cdot mol^{-1}$ suggesting some degree of triflate dissociation. Additionally, $^{19}F\{^1H\}$ NMR spectroscopy of **12** at 27 °C reveals two broad coalescing signals suggesting two chemically distinct fluorine environments by a possible exchange of inner- and outer-sphere triflate moieties. $^{31}P\{^1H\}$ NMR spectroscopy of **12** shows a downfield shift (relative to the parent complex, **10**) of the multiplet resonance (δ_P 31.5, $^1J_{RhP}$ = 176 Hz) and the ^1H NMR spectrum of **12** is similar to that of **10**. In spite of some degree of apparent triflate ion dissociation, we were unable to isolate the presumed cationic monotriflate species. Expecting that exchange of the chloro substituents of **10** for the larger iodide ions could favor formation of an iodide-bridged species, we synthesized $[Rh_2I_2(CO)_2(\mu\text{-}mapm)]$ (**13**, Scheme 2.6) through reaction of **10** with a five-fold excess of KI in dichloromethane / methanol. However, subsequent reactions of **13** with $AgBF_4$, $AgPF_6$ and AgOTf yielded either decomposition in the first two

cases or the bis-triflato species **12**, as was observed for **10**. Although the targeted, cationic, halogeno-bridged complexes could not be prepared, the weakly coordinating sulfonate ligands of **12** appear to be labile as suggested by the molar conductivity and the observation of both free and coordinated triflate ions in solution. The $^{31}P\{^{1}H\}$ NMR spectrum of **13**, although similar to **10**, shows a slight upfield shift of the multiplet resonance to δ_P 20.3 with $^{1}J_{RhP}$ = 162 Hz. As expected, the ambient temperature ^{1}H NMR spectrum of **13** is very similar to that of **10**. Unfortunately, $^{13}C\{^{1}H\}$ spectra for complexes **12** and **13** could not be obtained due to their poor solubilities in a variety of solvents.

The acetato complex, $[Rh_2(OAc)_2(CO)_2(\mu\text{-mapm})]$ (**14**), could also be prepared by reaction of **10** with KOAc in THF. The low molar conductivity of **14** (12 $cm^2 \cdot \Omega^{-1} \cdot mol^{-1}$ in CH_3NO_2) suggests little acetate ion dissociation, and may result from minor amounts of salt impurities. Interestingly, compound **14** exhibits strong solvatochroic tendencies, transforming from a deep red solution to a dark yellow-green powdery solid upon removal of solvent *in vacuo*. Furthermore, the ^{1}H NMR spectrum of this complex (Figure 2.11) exhibits highly deshielded NH

Figure 2.11. ^{1}H NMR Spectrum of $[Rh_2(OAc)_2(CO)_2(\mu\text{-mapm})]$ (**14**)

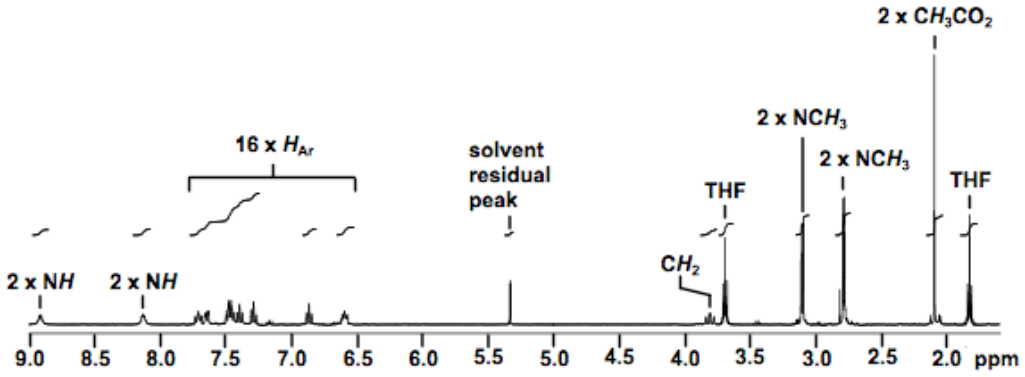

protons at δ_H 8.91 and 8.12 which were identified by their strong correlations to NMe protons via GCOSY analysis. $^{31}P\{^{1}H\}$ NMR data show the expected multiplet at δ_P 28.2 with $^{1}J_{RhP}$ = 155 Hz. $^{13}C\{^{1}H\}$ NMR data could not be obtained from CD_2Cl_2 due to decomposition to multiple products in solution over a 24 h period. Interestingly, one of these multiple decomposition products has been

identified as $[Rh_2Cl_2(CO)_2(\mu\text{-mapm})]$ via ^{31}P NMR spectroscopy. It was also noticed that **14** is quite hygroscopic, and the incorporation of water was made evident spectroscopically along with concomitant decomposition to numerous unidentified species.

The structure of **14** has been determined crystallographically, and an ORTEP diagram of this species is shown in Figure 2.12. As is obvious from a

Figure 2.12. ORTEP Diagram of $[Rh_2(OAc)_2(CO)_2(\mu\text{-mapm})]$ (**14**). Thermal ellipsoids as in Figure 2.5.

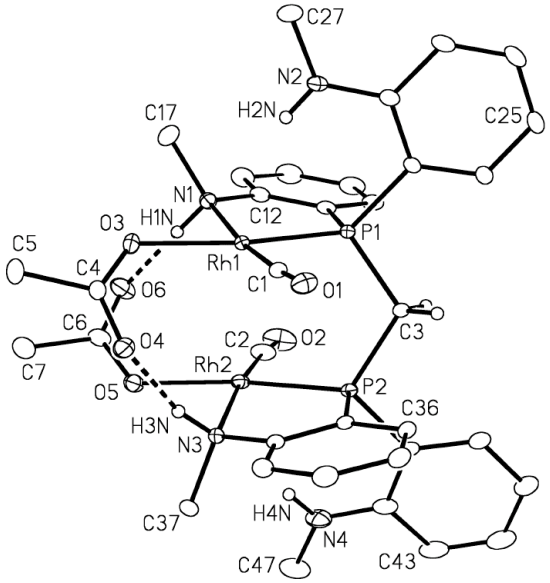

comparison of Figures 2.10 and 2.12, compounds **10** and **14** have closely related structures. Again, the hydrogen atoms of the coordinated amine are hydrogen bonded to the anionic ligand (in this case acetate) on the adjacent metal as demonstrated by the close O–H contacts (O(4)–H(3N) = 1.94 Å; O(6)–H(1N) = 1.84 Å). In spite of the larger acetate compared to chloro ligand, the Rh(1)–Rh(2) separation in **14** (3.2227(2) Å) is actually less than in **10** (3.4500(4) Å). This mutual approach of both metals results in a slight pyramidalization of both square planes, as shown in Figure 2.12, with the metals being 0.08 Å and 0.07 Å out of the planes defined by the four attached ligands. This distortion appears not to result from any mutual attraction of the metals, but instead appears to result from repulsion due to pendent amine hydrogens above and below the pair of almost-parallel square planes. We had noted for compound **10** that these contacts (~2.58

Å) were probably repulsive; in **14** the Rh–HN contacts (~2.50 Å) are even shorter and in this case leads to a significant deviation of the metals from their respective planes. Again, the very downfield chemical shifts of these protons (δ_H 8.91, 8.12) argues against any type of agostic interaction in solution, for which we would expect a significant upfield shift.

2.4 Conclusions

A number of *P*,*N*-ligated, mono- and binuclear complexes of rhodium have been synthesized and fully characterized. The complexes [RhCl(CO)($PhPAr_2$)] (**6**), [RhCl(CO)(PAr_3)] (**7**), [RhCl(CO)($PhPAr'_2$)] (**8**), [RhCl(CO)(PAr'_3)] (**9**) and [$Rh_2Cl_2(CO)_2$(μ-dmapm)] (**11**) are shown by NMR to display fluxional behaviour consistent with the hemilabile nature of these systems. The more highly substituted dimethylanilinyl ligands are found to be more labile than the monomethyl analogues. X-ray structural comparisons of related dimethyl- and monomethylanilinyl species show greater steric repulsions and concomitant weaker Rh-amine interactions for the former, offering a rationalization for the greater lability of the NMe_2-substituted ligands. The *N*-methylamino-tethered, binuclear complex, [$Rh_2Cl_2(CO)_2$(μ-mapm)] (**10**), has a greatly reduced interatomic Rh···Rh separation than its *N*,*N*-dimethylated counterpart, [$Rh_2Cl_2(CO)_2$(μ-dmapm)] (**11**), owing to greater steric repulsions between the two Rh coordination planes in the latter case. While the mapm-bridged binuclear complex is expected to have greater potential for bimetallic cooperativity owing to significantly closer approach of the metals, it may be that the lower steric bulk of the monomethylanilinyl group, which allows this closer approach, may actually work to the detriment of the system, owing to the lower lability of these groups. What affects the two competing influences will have must await subsequent reactivity studies.

Our failure to prepare cationic, halide-bridged species probably results from the strain inherent in such a product in which the halide bridge would be required to lie opposite both ends of the bridging diphosphine. In addition, the staggered arrangement of the Rh coordination planes in the dichloro precursor (**10**) appears necessary in order to minimize unfavorable contacts between these planes. Replacement of one chloride ligand by a bridging arrangement of the remaining chloride would force an eclipsed conformation of the planes leading to a closer and less favorable approach of the anilinyl and carbonyl groups on adjacent metals. Nevertheless, it should still be possible to achieve an anion-bridged structure through the use of bidentate groups such as acetates, which should give rise to less strain while maintaining more favorable contacts between the planes, although we have until now failed to isolate such species in this chemistry.

The chemistries of the mapm-bridged species **10**, **12** – **14** have yet to be investigated in order to determine whether ligand hemilability and effects of metal-metal cooperativity will play a role. Furthermore, the potential of using the acetate moieties in **14** as an internal base for deprotonation of one or more of the amine groups to generate catalytically active amido-rhodium species[51] is an immediate goal of these studies.

2.5 References

(1) Sargeson, A. M. *Pure Appl. Chem.*, **1984**, *56*, 1603–1619.

(2) Archibald, S. J. *Annu. Rep. Prog. Chem., Sect. A.*, **2007**, *103*, 264–286.

(3) Edelmann, F. T. *Angew. Chem., Int. Ed.*, **2001**, *40*, 1656–1660.

(4) Albrecht, M.; van Koten, G. *Angew. Chem., Int. Ed.*, **2001**, *40*, 3750–3781.

(5) Taqui. Khan, M. M.; Martell, A. E. *Inorg. Chem.*, **1974**, *13*, 2961–2966.

(6) Bessel, C. A.; Aggarwal, P.; Marschilok, A. C.; Takeuchi, K. J. *Chem. Rev.*, **2001**, *101*, 1031–1066.

(7) Hierso, J.–C.; Smaliy, R.; Amardeil, R.; Meunier, P. *Chem. Soc. Rev.*, **2007**, *36*, 1754–1769.

(8) Huheey, J. E.; Keiter, E. A.; Keiter, R. L. *Inorganic Chemistry: Principles of Structure and Reactivity*, 4th edn., HarperCollins, New York, **1993**, pp 522–524.

(9) Puddephatt, R. J. *Chem. Soc. Rev.*, **1983**, *12*, 99–127.

(10) Chaudret, B.; Delavaux, B.; Poilblanc, R. *Coord. Chem. Rev.*, **1988**, *86*, 191–243.

(11) Balch, A. L.; Fossett, L. A.; Guimerans, R. R.; Olmstead, M. M. *Organometallics*, **1985**, *4*, 781–788.

(12) Andrieu, J.; Braunstein, P.; Tiripicchio, A.; Ugozzoli, F. *Inorg. Chem.*, **1996**, *35*, 5975–5985.

(13) Ronson, T. K.; Adams, H.; Ward, M. D. *Inorg. Chim. Acta*, **2005**, *358*, 1943–1954.

(14) Jalil, M. A.; Fujinami, S.; Honjo, T.; Nishikawa, H. *Polyhedron,* **2001**, *20*, 1071–1078.

(15) Mashima, K.; Kaneda, Y.; Fukumoto, A.; Tanaka, M.; Tani, K.; Nakano, H.; Nakamura, A. *Inorg. Chim. Acta*, **1998**, *270*, 459–466.

(16) Broussard, M. E.; Juma, B.; Train, S. G.; Peng, W.–J.; Laneman, S. A.; Stanley, G. G. *Science*, **1993**, *260*, 1784–1788.

(17) Farr, J. P.; Olmstead, M. M.; Hunt, C. H.; Balch, A. L. *Inorg. Chem.,* **1981**, *20*, 1182–1187.

(18) Wood, F. E.; Hvoslef, J.; Hope, H.; Balch, A. L. *Inorg. Chem.*, **1984**, *23*, 4309–4315.

(19) Jeffrey, J. C.; Rauchfuss, T. B. *Inorg. Chem.*, **1979**, *18*, 2658–2666.

(20) Slone, C. S.; Weinberger, D. A.; Mirkin, C. A. *Prog. Inorg. Chem.*, **1999**, *48*, 233–350.

(21) Braunstein, P.; Naud, F. *Angew. Chem., Int. Ed.*, **2001**, *40*, 680–699.

(22) Espinet, P.; Soulantica, K. *Coord. Chem. Rev.*, **1999**, *193–195*, 499–556.

(23) Braunstein, P. *J. Organomet. Chem.*, **2004**, *689*, 3953–3967.

(24) Andrieu, J.; Camus, J.–M.; Richard, P.; Poli, R.; Gonsalvi, L.; Vizza F.;

Peruzzini, M. *Eur. J. Inorg. Chem.*, **2006**, 51–61.

(25) Bader, A.; Lindner, E. *Coord. Chem. Rev.*, **1991**, *108*, 27–110.

(26) Yang, H.; Alvarez-Gressier, M.; Lugan, N.; Mathieu, R. *Organometallics*, **1997**, *16*, 1401–1409.

(27) Speiser, F.; Braunstein, P.; Saussine, L. *Organometallics*, **2004**, *23*, 2625–2632.

(28) Bassetti, M. *Eur. J. Inorg. Chem.*, **2006**, 4473–4482.

(29) Yang, H.; Lugan, N.; Mathieu, R. *Organometallics*, **1997**, *16*, 2089–2095.

(30) Fernández-Galán, R.; Jalón, F. A.; Manzano, B. R.; Rodríguez-de la Fuente, J. *Organometallics*, **1997**, *16*, 3758–3768.

(31) Anderson, M. P.; Casalnuovo, A. L.;. Johnson, B. J; Mattson, B. M.; Mueting, A. M.; Pignolet, L. H. *Inorg. Chem.*, **1988**, *27*, 1649–1658.

(32) Jeffrey, J. C.; Rauchfuss, T. B.; Tucker, P. A. *Inorg. Chem.*, **1980**, *19*, 3306–3315.

(33) Bertini, I.; Dapporto, P.; Fallani, G.; Sacconi, L. *Inorg. Chem.*, **1971**, *10*, 1703–1707.

(34) Del Zotto, A.; Nardin, G.; Rigo, P. *J. Chem. Soc., Dalton Trans.*, **1995**, 3343–3351.

(35) Baker, K. V.; Brown, J. M.; Cooley, N. A.; Hughes, G. D.; Taylor, R. J. *J. Organomet. Chem.*, **1989**, *370*, 397–406.

(36) Tani, K.; Yabuta, M.; Nakamura, S.; Yamagata, T. *J. Chem. Soc., Dalton Trans.*, **1993**, 2781–2789.

(37) Habib, M.; Trujillo, H.; Alexander, C. A.; Storhoff, B. N. *Inorg. Chem.,* **1985**, *24*, 2344–2349.

(38) Farr, J. P.; Wood, F. E.; Balch, A. L. *Inorg. Chem.*, **1983**, *22*, 3387–3393.

(39) Aluri, B. R.; Kindermann, M. K.; Jones, P. G.; Dix, I.; Heinicke, J. *Inorg. Chem.*, **2008**, *47*, 6900–6912.

(40) Whited, M. T.; Rivard, E.; Peters, J. C. *Chem. Commun.*, **2006**, 1613–1615.

(41) Fryzuk, M. D.; MacNeil, P. A. *J. Am. Chem. Soc.*, **1981**, *103*, 3592–3593.

(42) Soulivong, D.; Wieser, C.; Marcellin, M.; Matt, D.; Harriman, A.; Toupet, L. *J. Chem. Soc., Dalton Trans.*, **1997**, 2257–2262.

(43) Dennett, J. N. L.; Bierenstiel, M.; Ferguson, M. J.; McDonald, R.; Cowie, M. *Inorg. Chem.*, 2006, **45**, 3705–3717.

(44) Jones, N. D.; Meessen, P.; Smith, M. B.; Losehand, U.; Rettig, S. J.; Patrick, B. O.; James, B. R. *Can. J. Chem.*, **2002**, *80*, 1600–1606.

(45) Jones, N. D.; James, B. R. *Adv. Synth. Catal.*, **2002**, *344*, 1126–1134.

(46) Foo, S. J. L.; Jones, N. D.; Patrick, B. O.; James, B. R. *Chem. Commun.*, **2003**, 988–989.

(47) Jones, N. D.; Foo, S. J. L.; Patrick, B. O.; James, B. R. *Inorg. Chem.*, **2004**, *43*, 4056–4063.

(48) Jones, N. D.; Meessen, P.; Losehand, U.; Patrick, B. O.; James, B. R. *Inorg. Chem.*, **2005**, *44*, 3290–3298.

(49) Clapham, S. E.; Hadzovic, A.; Morris, R. H. *Coord. Chem. Rev.*, **2004**, *248*, 2201–2237.

(50) Noyori, R. *Angew. Chem., Int. Ed.*, **2002**, *41*, 2008–2022.

(51) Maire, P.; Büttner, T.; Breher, F.; Le Floch, P.; Grützmacher, H. *Angew. Chem., Int. Ed.*, **2005**, *44*, 6318–6323.

(52) Giordano, G.; Crabrtree, R. H. *Inorg. Synth.*, **1979**, *19*, 218–220.

(53) McCleverty, J. A.; Wilkinson, G.; Lipson, L. G.; Maddox, M. L.; Kaesz, H. D. *Inorg. Synth.*, **1990**, *28*, 84–86.

(54) Fritz, H. P.; Gordon, I. R.; Schwarzhans, K. E.; Venanzi, L. M. *J. Chem. Soc.*, **1965**, 5210–5216.

(55) Gilman, H.; Banner, I. *J. Am. Chem. Soc.*, **1940**, *62*, 344–345.

(56) Spectral simulations were carried out using Spinworks v. 2.5.5 (Kirk Marat, University of Manitoba, 2006/11/29).

(57) Programs for diffractometer operation, unit cell indexing, data collection, data reduction and absorption correction were those supplied by Bruker.

(58) Sheldrick, G. M. *Acta Crystallogr.*, **2008**, *A64*, 112–122.

(59) Altomare, A.; Burla, M. C.; Camalli, M.; Cascarano, G. L.; Giacovazzo, C.; Guagliardi, A.; Moliterni, A. G. G.; Polidori, G.; Spagna, R. *J. Appl. Cryst.*, **1999**, *32*, 115–119.

(60) Beurskens, P. T.; Beurskens, G.; de Gelder, R.; Garcia-Granda, S.; Israel, R.;

Gould, R. O.; Smits, J. M. M. (**1999**). The *DIRDIF-99* program system. Crystallography Laboratory, University of Nijmegen, The Netherlands.

(61) van der Sluis, P.; Spek, A. L. *Acta Crystallogr.*, **1990**, *A46*, 194–201; Spek, A.L. *Acta Crystallogr.*, **1990**, *A46*, C34. *PLATON* - a multipurpose crystallographic tool. Utrecht University, Utrecht, The Netherlands.

(62) van Oort, A. B.; Budzelaar, P. H. M.; Frijns, J. H. G.; Orpen, A. G. *J. Organomet. Chem.*, **1990**, *396*, 33–47.

(63) Katritzky, A. R.; Fan, W.–Q.; Akutagawa, K. *Tetrahedron*, **1986**, *42*, 4027–4034.

(64) Wu, C. J.; Lee, S. H.; Yu, S. T.; Na, S. J.; Yun, H.; Lee, B. Y. *Organometallics*, **2008**, *27*, 3907–3917.

(65) Wu, C. J.; Lee, S. H.; Yun, H.; Lee, B. Y. *Organometallics*, **2007**, *26*, 6685–6687.

(66) Rauchfuss, T. B.; Roundhill, D. M. *J. Am. Chem. Soc.*, **1974**, *96*, 3098–3105.

(67) Bain, A. D. *Prog. Nucl. Magn. Reson. Spectrosc.*, **2003**, *43*, 63–103.

(68) Suomalainen, P.; Jääskeläinen, S.; Haukka, M.; Laitinen, R. H.; Pursiainen, J.; Pakkanen, T. A. *Eur. J. Inorg. Chem.*, **2000**, 2607–2613.

(69) N. D. Jones, PhD. Thesis, University of British Columbia, **2001**.

(70) Lorenzini, F.; Hindle, K. T.; Craythorne, S. J.; Crozier, A. R.; Marchetti, F.; Martin, C. J.; Marr, P. C.; Marr, A. C. *Organometallics*, **2006**, *25*, 3912–3919.

(71) Zefirov, Y. V.; Zorkii, P. M. *Russ. Chem. Rev.*, **1989**, *58*, 421–440.

Chapter 3: Coordinatively Diverse *ortho*-Phosphinoaniline Complexes of Ruthenium and Isolation of a Putative Intermediate in Ketone Transfer Hydrogenation Catalysis[i]

3.1 Introduction

Hybrid ligands, which contain more than one type of donor functionality, have attracted much recent interest.[1-5] The incorporation of two or more different donor groups can result in coordinatively diverse complexes due to the steric and electronic asymmetries[6] that are introduced by the mixed-donor ligands upon coordination. Furthermore, when the differing donor atoms are electronically diverse hard and soft combinations, the additional aspect of hemilability[7] can come into play. *P*,*N*-Ligands bearing soft phosphine and hard amine donors can provide a unique electronic environment for the metal center, in which the weakly π-acidic character of the phosphine is coupled with the σ-donor character of the amine.[5,6] The hybrid electronic characteristics of ruthenium *P*,*N*-complexes have been exemplified by their highly variable stereochemistries[8-13] and such complexes have found many applications as catalysts for (transfer) hydrogenation,[11-16] hydroformylation,[17,18] hydrosilylation[19,20] and terminal alkyne homocoupling[21] reactions.

Hybrid *P*,*N*-chelate complexes which exhibit hemilability are of particular interest in homogeneous catalysis by low-valent, late-metal complexes[12,14] in which the labile amine can be readily displaced by the catalytic substrate and,

[i] The work presented in this chapter has been previously reported. See: Hounjet, L. J.; Bierenstiel, M.; Ferguson, M. J.; McDonald, R.; Cowie, M. *Inorg. Chem.* **2010**, *49,* 4288 – 4300.

after completion of the metal-mediated transformation, can facilitate decomplexation of the modified substrate by recoordination, thereby stabilizing the catalyst. Recently, we demonstrated how the rate of hemilabile, internal ligand exchange processes within *ortho*-phosphinoaniline complexes of rhodium(I) can be varied by exploiting steric requirements of the amines via the degree of *N*-methyl substitution.[22]

In the current study, we illustrate how the degree of *N*-methylation and the number of available phosphine and amine donors substantially diversifies the coordination behaviour of these ligands at ruthenium, but surprisingly, does not give rise to observable hemilability in the compounds studied. A further motivation for the study of incompletely substituted amines as donors to ruthenium stems from the well-documented "N-H effect,"[23] in which the amine can be deprotonated by the addition of an external base to generate amido-ruthenium complexes, many of which function as catalytic intermediates for the (transfer) hydrogenation of polar substrates, particularly ketones.[23,24] Recently, Stradiotto *et al.* reported efficient "non-N-H" iridium-based transfer hydrogenation catalysts bearing an *o*-*N*,*N*-dimethylanilinylphosphine ligand,[25] while Pelagatti *et al.* also demonstrated transfer hydrogenation using the same ligand within a ruthenium complex.[16] Ruthenium complexes possessing other types of NMe_2-containing donor ligands, have also been shown to act as catalysts for ketone transfer hydrogenation reactions.[26,27] Such examples serve to illustrate the catalytic utility of completely *N*-substituted *ortho*-phosphinoaniline complexes. Interestingly, *P*,*N*-ligated ruthenium(II)-arene complexes have also received attention as selective anticancer agents.[28]

3.2 Experimental

3.2.1 General Comments

All solvents were deoxygenated, dried (using appropriate drying agents) distilled before use, and stored under nitrogen. All reactions were performed under an argon atmosphere using standard Schlenk techniques. The reagents, $[Ru_3(CO)_{12}]$, $[RuCl(\mu\text{-}Cl)(\eta^6\text{-}p\text{-cymene})]_2$ (**1**) and triethylamine were purchased from Strem Chemicals. Isopropanol (> 99%, distilled over Mg turnings and stored under argon), acetophenone (99%, deoxygenated and stored under argon over 5 Å molecular sieves) and potassium *tert*-butoxide (resublimed and stored under argon) used for transfer hydrogenation catalysis, were purchased from Aldrich. Ethylene was purchased from Matheson Tri-Gas. Diphenyl(*o*-*N*,*N*-dimethylanilinyl)phosphine (Ph_2PAr'),[29] bis(di(*o*-*N*,*N*-dimethylanilinyl)-phosphino)methane (dmapm),[30] diphenyl(*o*-*N*-methylanilinyl)phosphine (Ph_2PAr)[22] and bis(di(*o*-*N*-methylanilinyl)phosphino)methane (mapm)[22] were prepared as previously reported. NMR spectra were recorded on Varian Inova-400, -500 or Varian Unity-500 spectrometers operating at 399.8, 498.1 or 499.8 MHz, respectively, for ^1H, at 161.8, 201.6 or 202.3 MHz, respectively, for ^{31}P and at 100.6, 125.3 or 125.7 MHz, respectively, for ^{13}C nuclei. Coupling constants are given in Hz and overlapping or unresolved aromatic ^1H signals, observed in the typical 6 – 8 ppm range, and $^{13}C\{^1H\}$ signals, found between 80 – 120 ppm, respectively, are not reported. Spectroscopic data for all metal complexes (**2a** - **c**, **3b**, **4**, **5**, **6a**, **6b** and **7**) are provided in Table 3.1. Solution phase infrared spectra (KBr cell) were recorded on a FT-IR Bomem MB-100 spectrometer. Elemental analyses were performed by the Microanalytical Laboratory of the University of Alberta. Electrospray ionization mass spectra were run on a Micromass Zabspec spectrometer in the departmental MS facility. In all cases, the distribution of isotope peaks for the appropriate parent ion matched very closely that calculated from the formulation given. Conductivity measurements were carried out under inert conditions on 10^{-3} M solutions of $[RuCl_2(\eta^6\text{-}p\text{-cymene})(P\text{-}Ph_2PAr)]$ (**2a**), $[RuCl(\eta^6\text{-}p\text{-cymene})(P,N\text{-}Ph_2PAr)]Cl$ (**2b**), $[RuCl(\eta^6\text{-}p\text{-cymene})(P,N\text{-}Ph_2PAr^-)]$

Table 3.1. $^{31}P\{^{1}H\}$, ^{1}H and $^{13}C\{^{1}H\}$ NMR Data for Ruthenium Compounds[a]

Compound	$\delta(^{31}P\{^{1}H\})$[b]	$\delta(^{1}H)$[c]	$\delta(^{13}C\{^{1}H\})$[c]
[$RuCl_2(\eta^6$-*p*-cymene)(*P*-Ph_2PAr)] (**2a**)	28.2 (s)	N*H*: 5.47 (q/br, $^3J_{HH}$ = 5.0 Hz, 1H) C*H*$(CH_3)_2$: 3.08 (sept, $^3J_{HH}$ = 7.0 Hz, 1H) NC*H*$_3$: 2.81 (d, $^3J_{HH}$ = 5.0 Hz, 3H) ArC*H*$_3$: 1.84 (s, 3H) CH(C*H*$_3)_2$: 1.39 (d, $^3J_{HH}$ = 7.0 Hz, 6H)	*C*H$(CH_3)_2$: 30.9 (s) N*C*H$_3$: 30.3 (s) CH(*C*H$_3)_2$: 22.0 (s/br) Ar*C*H$_3$: 18.1 (s) CH(*C*H$_3)_2$: 24.3 (s), 19.6 (s)[g]
[RuCl(η^6-*p*-cymene)(*P*,*N*-Ph_2PAr)]Cl (**2b**)	53.4 (s)	N*H*: 10.8 (m/br, 1H) NC*H*$_3$: 3.52 (d, $^3J_{HH}$ = 4.4 Hz, 3H) C*H*$(CH_3)_2$: 2.91(sept, $^3J_{HH}$ = 7.0 Hz, 1H) ArC*H*$_3$: 1.36 (s, 3H) CH(C*H*$_3)_2$: 1.33 (d, $^3J_{HH}$ = 7.0 Hz, 3H), 1.31 (d, $^3J_{HH}$ = 7.0 Hz)	N*C*H$_3$: 76.7 (s) *C*H$(CH_3)_2$: 31.5 (s) CH(*C*H$_3)_2$: 22.7 (s), 20.5 (s) Ar*C*H$_3$: 15.6 (s)
[RuCl(η^6-*p*-cymene)(*P*,*N*-Ph_2PAr^-)] (**2c**)	59.3 (s)	NC*H*$_3$: 3.52 (s, 3H) C*H*$(CH_3)_2$: 2.39 (sept, $^3J_{HH}$ = 6.8 Hz, 1H) ArC*H*$_3$: 2.09 (s, 3H) CH(C*H*$_3)_2$: 1.14 (s/br, 3H), 0.99 (s/br, 3H)	N*C*H$_3$: 48.6 (s) *C*H$(CH_3)_2$: 31.2 (s) CH(*C*H$_3)_2$: 22.4 (s) Ar*C*H$_3$: 18.3 (s)
[RuCl(η^6-*p*-cymene)(*P*,*N*-Ph_2PAr')]Cl (**3b**)	47.5 (s)	N(C*H*$_3)_2$: 4.04 (s, 3H), 3.50 (s, 3H) C*H*$(CH_3)_2$: 2.87 (sept, $^3J_{HH}$ = 7.0 Hz, 1H) ArC*H*$_3$: 1.36 (s, 3H) CH(C*H*$_3)_2$: 1.35 (d, $^3J_{HH}$ = 7.0 Hz, 3H), 1.26 (d, $^3J_{HH}$ = 7.0 Hz, 3H)	N(*C*H$_3)_2$: 65.2 (s), 58.4 (s) *C*H$(CH_3)_2$: 31.7 (s) CH(*C*H$_3)_2$: 22.3 (s), 20.7 (s) Ar*C*H$_3$: 15.5 (s)
[RuCl(η^6-*p*-cymene)(*P*,*P'*-dmapm)]Cl (**4**)	–1.5 (s)[d] 1.5 (d/br, $^2J_{PP}$ = 56 Hz)[e], –15.4 (d/br, $^2J_{PP}$ = 56 Hz)[e]	C*H*$_2$: 5.09 (m/br, 1H)[e], 4.54 (m/br, 1H)[e] C*H*$(CH_3)_2$: 2.77 (m/br, 1H)[e] N(C*H*$_3)_2$: 2.16 (br, 24H)[e] ArC*H*$_3$: 1.46 (s/br, 3H)[e] CH(C*H*$_3)_2$: 1.35 (s/br, 3H)[e], 1.05 (s/br, 3H)[e]	N/A
[$RuCl_2$(*P*,*P'*,*N*,*N'*-mapm)] (**5**)	17.1 (d, $^2J_{PP}$ = 90 Hz)[e], 8.4 (d, $^2J_{PP}$ = 90 Hz)[e] 13.7 (s)[f]	N*H*: 6.61 (q/br, $^3J_{HH}$ = 4.8 Hz, 2H)[f], 6.01 (q/br, $^3J_{HH}$ = 6.0 Hz, 2H)[f] C*H*$_2$: 4.77 (t, $^2J_{PH}$ = 11.6 Hz, 2H)[f] NC*H*$_3$: 3.06 (d, $^3J_{HH}$ = 6.4 Hz, 6H)[f], 2.66 (d, $^3J_{HH}$ = 4.8 Hz, 6H)[f]	*C*H$_2$: 55.9 (t, $^1J_{PC}$ = 25 Hz)[f] N*C*H$_3$: 47.8 (s)[f], 30.6 (s)[f]
[$Ru(CO)_4$(*P*-mapm)] (**6a**)	15.1 (d, $^2J_{PP}$ = 115 Hz), –66.0 (d, $^2J_{PP}$ = 115 Hz)	N*H*: 4.65 (q/br, $^3J_{HH}$ = 5.0 Hz, 2H), 4.19 (q/br, $^3J_{HH}$ = 5.0 Hz, 2H) C*H*$_2$: 3.53 (dd, $^2J_{PH}$ = 9.0 Hz, $^2J_{PH}$ = 3.2 Hz, 2H) NC*H*$_3$: 2.74 (d, $^3J_{HH}$ = 5.0 Hz, 6H), 2.54 (d, $^3J_{HH}$ = 5.0 Hz, 6H)	N/A
[$Ru(CO)_3$(*P*,*P'*-mapm)] (**6b**)	–41.3 (s) –42.0 (s/br)[g], –46.5 (s/br)[g]	N*H*: 4.95 (q/br, $^3J_{HH}$ = 5.2 Hz, 4H) C*H*$_2$: 4.89 (t, $^2J_{PH}$ = 10.0 Hz, 2H) NC*H*$_3$: 2.59 (d, $^3J_{HH}$ = 5.2 Hz, 12H)	*C*O: 209.4 (t, $^2J_{PC}$ = 13 Hz) *C*H$_2$: 42.0 (t, $^1J_{PC}$ = 27 Hz) N*C*H$_3$: 30.3 (s)
[$Ru_3(CO)_{10}$(μ-*P*,*P'*-mapm)] (**7**)	2.2 (s)	C*H*$_2$: 4.76 (t, $^2J_{PH}$ = 4.4 Hz, 2H) N*H*: 3.94 (q/br, $^3J_{HH}$ = 2.5 Hz, 4H) NC*H*$_3$: 2.60 (d/br, $^3J_{HH}$ = 2.5 Hz, 12H)	*C*O: 210.9 (s) *C*H$_2$: 45.2 (t, $^1J_{PC}$ = 29 Hz) N*C*H$_3$: 30.5 (s)

[a] NMR abbreviations: s = singlet, d = doublet, t = triplet, q = quartet, sept = septet, br = broad, dd = doublet of doublets. All NMR data recorded at 27°C in CD_2Cl_2 unless otherwise indicated. [b] ^{31}P chemical shifts referenced to external 85% H_3PO_4. [c] ^{1}H and ^{13}C chemical shifts referenced to external tetramethylsilane. Chemical shifts for aryl groups not given. [d] C_s-symmetric species. [e] C_1-symmetric species. [f] C_2-symmetric species. [g] NMR data at –80°C.

(**2c**), [RuCl(η^6-*p*-cymene)(*P*,*N*-Ph_2PAr')]Cl (**3b**), [RuCl(η^6-*p*-cymene)(*P*,*P'*-dmapm)]Cl (**4**) and [$RuCl_2$(*P*,*P'*,*N*,*N'*-mapm)] (**5**) in dry nitromethane using a Yellow Springs Instrument Model 31 conductivity bridge. For these species the molar conductivities were determined as Λ = 6, 59, 23, 79, 62 and 7 $cm^2\ \Omega^{-1}\ mol^{-1}$, respectively.

3.2.2 Preparation of Metal Complexes

(a) Dichloro(η^6-*p*-cymene)(diphenyl(*o*-*N*-methylanilinyl)phosphine)-ruthenium(II), [$RuCl_2$(η^6-*p*-cymene)(*P*-Ph_2PAr)] (2a). *Method i.* In a 50 mL Schlenk flask under anhydrous conditions and argon atmosphere, [RuCl(μ-Cl)(η^6-*p*-cymene)]$_2$ (**1**) (109 mg, 178 μmol) and Ph_2PAr (104 mg, 356 μmol) were dissolved in 15 mL of benzene at ambient temperature. The resulting red solution was stirred at ambient temperature for 30 min and a bright red precipitate formed. The solvent was then removed *in vacuo*, and the red solid was washed with 15 mL of *n*-pentane. The solid was then dried *in vacuo* producing an orange-red powder (219 mg, 91% yield, found: C, 62.24; H, 6.10; N, 2.04%. Calc for $[C_{29}H_{32}Cl_2NPRu]\cdot C_6H_6$: C, 62.22; H, 5.67; N, 2.07%). Although the crystal structure determination indicated no solvent inclusion, the sample used for elemental analysis was non-crystalline and ^{1}H NMR analysis of this sample in CD_2Cl_2 (obtained at approximately the same time as the elemental analysis) verified the benzene content. Single crystals suitable for X-ray crystallographic analysis were obtained by dissolving the complex, under argon atmosphere, in a minimum volume of benzene and layering the solution with anhydrous *n*-pentane in an NMR tube. HRMS (ESI): *m*/*z* 598.0760 $[M + H]^+$. Calc for $C_{29}H_{33}Cl_2NPRu$: *m*/*z* 598.0766. *Method ii.* Using dichloromethane rather than benzene, the product did not spontaneously precipitate, but was obtained in excellent yield by precipitation with ether and subsequent workup. However, satisfactory elemental analyses and X-ray quality single crystals could not be obtained owing to facile solvent loss.

(b) Dichloro(η^6-*p*-cymene)(diphenyl(*o*-*N*-methylanilinyl)phosphine)-ruthenium(II), [RuCl(η^6-*p*-cymene)(*P*,*N*-Ph_2PAr)]Cl (2b). In a 50 mL three-necked, round-bottom flask with an attached reflux condenser under anhydrous conditions and argon atmosphere, $[RuCl(\mu\text{-}Cl)(\eta^6\text{-}p\text{-cymene})]_2$ (**1**) (224 mg, 365 μmol) and Ph_2PAr (213 mg, 731 μmol) were stirred in 10 mL of refluxing methanol (at 70 °C) for 2 hours over which time the dark red slurry turned to a bright orange solution. The solvent was removed *in vacuo* and the viscous residue was dissolved in 5 mL of tetrahydrofuran. After the addition of 15 mL of diethyl ether, a yellow precipitate formed which was then separated from the supernatant by filtration and dried *in vacuo* producing a yellow powder (380 mg, 87% yield, found: C, 58.09; H, 5.71; N, 2.12. Calc for $[C_{29}H_{32}Cl_2NPRu]$: C, 58.29; 5.40; 2.34%). Although the crystal structure indicates tetrahydrofuran inclusion, a non-crystalline sample was analyzed here. ^1H NMR analysis in CD_2Cl_2 (obtained at approximately the same time as the elemental analysis) was used to verify solvent content. Single crystals suitable for X-ray crystallographic analysis were obtained by slow evaporation from a 1:1 solution of tetrahydrofuran and diethyl ether. HRMS (ESI): *m*/*z* 562.0993 $[M]^+$. Calc for $C_{29}H_{32}ClNPRu$: *m*/*z* 562.0999.

(c) Dichloro(η^6-*p*-cymene)(diphenyl(*o*-*N*-methylanilido)phosphine)-ruthenium(II), [RuCl(η^6-*p*-cymene)(*P*,*N*-Ph_2PAr^-)] (2c). In a 50 mL Schlenk flask under anhydrous conditions and argon atmosphere, 10 mL of benzene was added to compound **2b** (381 mg, 638 μmol) resulting in yellow slurry. A ten-fold excess of triethylamine (0.89 mL, 6.4 mmol) was added to the slurry while stirring, resulting in an opaque, black-red mixture, to which was then added 10 mL of deoxygenated water. After stirring the mixture for 5 min, the layers were allowed to separate and the organic layer was transferred to a 50 mL Schlenk tube via cannula under argon. The solvent and residual triethylamine were removed *in vacuo*, then 5 mL of tetrahydrofuran was added to the dark residue followed by 30 mL of diethyl ether which resulted in the formation of a precipitate from the dark solution. The solid was collected by filtration, washed with 15 mL of *n*-pentane and dried *in vacuo* producing chocolate-coloured micro-crystals (256 mg, 72%

yield, found: C, 61.98; H, 5.60; N, 2.43. Calc for [$C_{29}H_{31}ClNPRu$]: C, 62.08; H, 5.57; N, 2.50%. Single crystals suitable for X-ray crystallographic analysis were obtained dissolving the complex, under argon atmosphere, in a minimum volume of tetrahydrofuran and layering the solution with anhydrous *n*-pentane in a Schlenk tube. HRMS (ESI): *m*/*z* 526.1227 $[M - Cl]^+$. Calc for $C_{29}H_{31}NPRu$: *m*/*z* 526.1232.

(d) Dichloro(η^6-*p*-cymene)(diphenyl(*o*-*N*,*N*-dimethylanilinyl)phosphine)-ruthenium(II), [RuCl(η^6-*p*-cymene)(*P*,*N*-Ph_2PAr')]Cl (3b). The orange powder was prepared in a manner similar to that of part (**a**, *Method ii*) using [RuCl(μ-Cl)(η^6-*p*-cymene)]$_2$ (**1**) (104 mg, 169 μmol) and Ph_2PAr' (104 mg, 339 μmol) and was isolated as an orange powder (200 mg, 96% yield, found: C, 55.37; H, 5.54; N, 2.22. Calc for [$C_{30}H_{34}Cl_2NPRu$]·$2H_2O$: C, 55.64; H, 5.91; N, 2.16%). Although the crystal structure indicates 1 equiv of H_2O and 2 equiv CH_2Cl_2 per formula unit, a non-crystalline sample was analyzed here which was exposed to air before analysis. ^1H NMR analysis in $CDCl_3$ (obtained at approximately the same time as the elemental analysis) was used to verify water and dichloromethane content. HRMS (ESI) found: *m*/*z* 576.1158 for $[M]^+$. Calc for [$C_{30}H_{34}ClNPRu$]: *m*/*z* 576.1155. Single crystals suitable for X-ray crystallographic analysis were obtained by slow evaporation from a saturated dichloromethane solution.

(e) Dichloro(η^6-*p*-cymene)(bis(di(*o*-*N*,*N*-dimethylanilinyl)phosphino)-methane)ruthenium(II), [RuCl(η^6-*p*-cymene)(*P*,*P'*-dmapm)]Cl (4). In a 50 mL Schlenk flask under anhydrous conditions and argon atmosphere, [RuCl(μ-Cl)(η^6-*p*-cymene)]$_2$ (**1**) (52 mg, 85 μmol) and dmapm (94 mg, 169 μmol) were dissolved in 10 mL dichloromethane at ambient temperature. The initially red solution was stirred at ambient temperature for 10 min until it had turned orange in colour. The solvent volume was reduced to approximately 1 mL *in vacuo* and 10 mL of *n*-pentane was added with stirring resulting in an immiscible, red oil which was allowed to settle from the yellow solution. The supernatant was removed via syringe and the oily residue was dried *in vacuo* producing an orange powder (115

mg, 79% yield). HRMS (ESI) found: *m/z* 827.2724 for $[M]^+$. Calc for $[C_{43}H_{56}ClN_4P_2Ru]$: *m/z* 827.2707. Single crystals suitable for X-ray crystallographic analysis were obtained by dissolving the complex, under argon atmosphere, in a minimum volume of CH_2Cl_2 and layering the solution with anhydrous *n*-pentane in an NMR tube.

(f) Dichloro(bis(di(*o*-*N*-methylanilinyl)phosphino)methane)ruthenium(II), [$RuCl_2$(*P,P',N,N'*-mapm)] (5). In a 50 mL Schlenk flask under anhydrous conditions and argon atmosphere, $[RuCl(\mu\text{-}Cl)(\eta^6\text{-}p\text{-cymene})]_2$ (**1**) (105 mg, 194 μmol) and mapm (194 mg, 388 μmol) were cooled to –78 ºC (acetone/dry ice bath) and 10 mL of dichloromethane was added. The red-orange slurry was stirred for 5 min before warming to ambient temperature over 15 min. The solvent volume was reduced to approximately 1 mL *in vacuo* then 10 mL of *n*-pentane was added to the solution, with stirring, resulting in an orange-yellow precipitate. The solution was filtered under argon and the solids were washed with 10 mL of *n*-pentane then dried *in vacuo*. The solid was dissolved in 5 mL of dichloromethane and the solution was layered with 15 mL of *n*-pentane and left unstirred for 3 hours producing orange-yellow crystals suitable for X-ray crystallographic analysis (282 mg, 95% yield, found: C, 49.78; H, 5.08; N, 7.48%. Calc for $[C_{29}H_{34}Cl_2N_4P_2Ru]\bullet 0.5CH_2Cl_2$: C, 49.55; H, 4.93; N, 7.84%). HRMS (ESI) found: *m/z* 637.0985 for $[M - Cl]^+$. Calc for $[C_{29}H_{34}ClN_4P_2Ru]$: *m/z* 637.0985.

(g) Tricarbonyl(bis(di(*o*-*N*-methylanilinyl)phosphino)methane)ruthenium(0), [$Ru(CO)_3$(*P,P'*-mapm)] (6b). A 100 mL hexane solution of $[Ru(CO)_4(\eta^2\text{-}C_2H_4)]$ was prepared photolytically with the use of $[Ru_3(CO)_{12}]$ (42 mg, 66 μmol) and an ethylene purge.[31] Under anhydrous conditions and argon atmosphere, the solution was transferred, via cannula, to a prepared 250 mL Schlenk flask containing mapm (90 mg, 180 μmol). The pale-yellow slurry was stirred for 5 min then 10 mL of dichloromethane was added. The resulting solution was stirred for 2 h, eventually turning orange in colour, and was left exposed to ambient light

overnight. Solvents were removed *in vacuo* and the resulting orange solid was then washed with 10 mL of *n*-pentane. The product was then dried *in vacuo* and isolated as an orange powder (110 mg, 89% yield, found: C, 55.71; H, 5.12; N, 7.80%. Calc for $[C_{32}H_{34}N_4O_3P_2Ru]$: C, 56.06; H, 5.00; N, 8.17%). IR (CH_2Cl_2 solution cell): ν_{CO} 2004 (s), 1932 (s) and 1912 (s) cm^{-1}. HRMS (ESI) found: *m/z* 687.1220 for $[M + H]^+$. Calc for $[C_{32}H_{35}N_4O_3P_2Ru]$: *m/z* 687.1222. Single crystals suitable for X-ray crystallographic analysis were obtained by dissolving the complex, under argon atmosphere, in a minimum volume of CH_2Cl_2 and layering the solution with anhydrous *n*-pentane in an NMR tube.

(h) Decacarbonyl(bis(di(*o*-*N*-methylanilinyl)phosphino)methane)-triruthenium(0,0,0), $[Ru_3(CO)_{10}(\mu$-*P,P'*-mapm)] (7). *Method i.* A 125 mL *n*-pentane solution of $[Ru(CO)_4(\eta^2$-$C_2H_4)]$ was prepared photolytically with the use of $[Ru_3(CO)_{12}]$ (48 mg, 75 μmol) and an ethylene purge.[31] Meanwhile, a solution of mapm (52 mg, 104 μmol) in 5 mL of dichloromethane was prepared under argon atmosphere. In complete darkness, the mapm solution was then transferred to the solution of $[Ru(CO)_4(\eta^2$-$C_2H_4)]$ by cannula and the resulting solution was heated to 50°C with a water bath while stirring under a brisk flow of argon to remove the solvents. The red solid residue was then dissolved, in the dark, in 20 mL of dichloromethane and stirred for 5 h under a very slight flow of argon. The solvent volume was then reduced to approximately 5 mL *in vacuo* and 25 mL of *n*-pentane was added resulting in the formation of a yellow precipitate in a bright red solution. The precipitate was allowed to settle and the red supernatant was removed by cannula. The remaining solid was then dried *in* vacuo and isolated as an orange-red powder (34 mg, 42% yield, found: C, 43.86; H, 3.79; N, 4.34%. Calc for $[C_{39}H_{34}N_4O_{10}P_2Ru_3]\cdot 0.5C_5H_{12}\cdot 0.5CH_2Cl_2$: C, 43.40; H, 3.56; N, 4.82%). IR (CH_2Cl_2 solution cell): ν_{CO} 2079 (m), 2060 (m), 2020 (sh), 2008 (s), 1996 (sh) and 1955 (m) cm^{-1}. Single crystals suitable for X-ray crystallographic analysis were obtained by dissolving the complex, under argon atmosphere, in a minimum volume of CH_2Cl_2 and layering the solution with anhydrous *n*-pentane in an NMR tube. *Method ii.* In a 100 mL Schlenk tube under anhydrous conditions and argon

atmosphere, [$Ru_3(CO)_{12}$] (133 mg, 208 μmol) and mapm (104 mg, 208 μmol) were dissolved in 25 mL of tetrahydrofuran by stirring the mixture for 10 min at ambient temperature. The initially orange solution was then stirred for 24 h under a very slight flow of argon, eventually turning bright red in colour. The solvent volume was reduced to approximately 5 mL *in vacuo* and the solution was then left unstirred and layered with 40 mL of *n*-pentane. After 3 h an orange precipitate had developed and the supernatant was removed by cannula transfer. The product was then dried *in vacuo* and isolated as an orange-red powder (151 mg, 67% yield).

3.2.3 X-Ray Structure Determinations

(a) General. Crystals were grown via slow diffusion of *n*-pentane into a benzene (**2a**) or CH_2Cl_2 (**2c**, **3b**, **4**, **5**, **6b**, **7**) solution of the compound, or diffusion of ether into a THF solution (**2b**) of the compound. Data were collected using either a Bruker APEX-II CCD detector/D8 diffractometer[32] with the crystals cooled to –100 °C (**2a**, **2b**, **2c**, **4**, **7**) or a Bruker SMART 1000 CCD detector/PLATFORM diffractometer with the crystals cooled to –80 °C (**3b**, **5**, **6b**); all data were collected using Mo Kα radiation (λ = 0.71073 Å). The data were corrected for absorption through Gaussian integration from indexing of the crystal faces (**2a**, **2b**, **2c**, **3b**, **7**) or through use of a multi-scan model (*SADABS*[32]) (**4**, **5**, **6b**). Structures were solved using Patterson search/structure expansion (*DIRDIF-2008*[33]) (**2a**), direct methods (*SHELXS–97*[34]) (**2b**, **2c**, **3b**, **6b**, **7**), or direct methods/structure expansion (*SIR97*[35]) (**4**, **5**). Refinements were completed using the program *SHELXL-97*.[34] Hydrogen atoms were assigned positions based on the sp^2 or sp^3 hybridization geometries of their attached carbon or nitrogen atoms, and were given thermal parameters 20% greater than those of their parent atoms. Crystallographic experimental details for the mono- and diphosphinoaniline complexes can be found in Tables 3.2 and 3.3, respectively. See Appendix III for information about accessing additional crystallographic data.

(b) Special Refinement Conditions. (i) **3b**: Distances involving hydrogens of the solvent water molecules were assigned fixed idealized values during refinement

(d(O–H) = 0.85 Å; d(H···H) = 1.39 Å). (ii) **5**: The Cl–C distances within the solvent CH_2Cl_2 molecule were restrained to be equal (within 0.03 Å) during refinement. (iii) **7**: Distances within the disordered solvent *n*-pentane and CH_2Cl_2 molecules were subject to the following restraints during refinement: $d(C–C)_{n\text{-pentane}}$ = 1.53(1) Å; $d_{1,3}(C\cdots C)_{n\text{-pentane}}$ = 2.50(1) Å; $d(Cl–C)_{dichloromethane}$ = 1.80(1); $d(Cl\cdots Cl)_{dichloromethane}$ = 2.87(1) Å.

Table 3.2. Crystallographic Experimental Details for **2a – c** and **3b**

Compound	**2a**	**2b**·C_4H_8O	**2c**	**3b**·$2CH_2Cl_2$,H_2O
Formula	$C_{29}H_{32}Cl_2NPRu$	$C_{33}H_{40}Cl_2NOPRu$	$C_{29}H_{31}ClNPRu$	$C_{32}H_{40}Cl_6NOPRu$
Formula Weight	597.50	669.60	561.04	799.39
Crystal Dimensions (mm)	0.67 × 0.31 × 0.19	0.51 × 0.22 × 0.08	0.35 × 0.15 × 0.15	0.48 × 0.28 × 0.22
Crystal System	monoclinic	monoclinic	monoclinic	triclinic
Space Group	$P2_1/c$ (No. 14)	$P2_1/c$ (No. 14)	$P2_1/c$ (No. 14)	$P\bar{1}$ (No. 2)
a (Å)	7.9672 (4)	15.6106 (13)	8.9830 (4)	10.5904 (7)
b (Å)	18.0587 (9)	11.3767 (9)	15.4775 (6)	14.7948 (9)
c (Å)	18.2121 (9)	18.0365 (15)	18.5190 (8)	22.9421 (14)
α (deg)				96.8793 (9)
β (deg)	99.7796 (6)	100.2180 (10)	100.5820 (10)	95.4204 (9)
γ (deg)				96.1720 (9)
V (Å^3)	2582.2 (2)	3152.4 (4)	2530.99 (19)	3527.0 (4)
Z	4	4	4	4
ρ_{calcd} (g cm^{-3})	1.537	1.411	1.472	1.505
μ (mm^{-1})	0.895	0.744	0.806	0.971
$2\theta_{max}$ (deg)	57.28	55.08	55.08	52.76
Total Data Collected	23042 (–10 ≤ h ≤ 10, –23 ≤ k ≤ 24, –24 ≤ l ≤ 24)	27171 (–20 ≤ h ≤ 20, –14 ≤ k ≤ 14, –23 ≤ l ≤ 23)	21963 (–11 ≤ h ≤ 11, –20 ≤ k ≤ 19, –24 ≤ l ≤ 24)	28025 (–13 ≤ h ≤ 13, –18 ≤ k ≤ 18, –28 ≤ l ≤ 28)
Independent Reflections (R_{int})	6309 (0.0108)	7228 (0.0416)	5836 (0.0189)	14380 (0.0213)
Observed Reflections [$I \geq 2\sigma(I)$]	6028	5979	5341	12471
Restraints/ Parameters	0 / 309	0 / 354	0 / 300	6[a] / 771
Flack Absolute Parameter				
Goodness-of-Fit (All Data)[b]	1.045	1.063	1.121	1.070
R_1 [$I \geq 2\sigma(I)$][c]	0.0198	0.0350	0.0286	0.0332
wR_2 [All Data][d]	0.0535	0.0897	0.0733	0.0940
Largest Difference Peak, Hole (e Å^{-3})	0.488, –0.378	0.828, –0.602	0.649, –0.457	2.119, –1.094

[a] Distances involving hydrogens of the solvent water molecules were assigned idealized values during refinement (d(O–H) = 0.85 Å; d(H···H) = 1.39 Å). [b] $S = [\Sigma w(F_o^2 - F_c^2)^2/(n-p)]^{1/2}$ where n = number of data; p = number of parameters varied; $w = [\sigma^2(F_o^2) + (a_0P)^2 + a_1P]^{-1}$ where $P = [\text{Max}(F_o^2, 0) + 2F_c^2]/3$, and a_0 and a_1 are optimized by the refinement program; for **2a**, a_0 = 0.0289, a_1 = 1.3642; for **2b**, a_0 = 0.0410, a_1 = 2.4231; for **2c**, a_0 = 0.0303, a_1 = 2.3504; for **3b**, a_0 = 0.0443, a_1 = 3.7038; for **4**, a_0 = 0.0326, a_1 = 1.9568; for **5**, a_0 = 0.0350, a_1 = 4.3573; for **6b**, a_0 = 0.0346, a_1 = 0.0654; for **7**, a_0 = 0.0459, a_1 = 5.1261. [c] $R_1 = \Sigma||F_o| - |F_c||/\Sigma|F_o|$. [d] $wR_2 = [\Sigma w(F_o^2 - F_c^2)^2/\Sigma w(F_o^4)]^{1/2}$.

Table 3.3. Crystallographic Experimental Details for **4**, **5**, **6b** and **7**

Compound	**4**	**5**·0.5CH_2Cl_2	**6b**	**7**·0.5C_5H_{12},0.5CH_2Cl_2
Formula	$C_{43}H_{56}Cl_2N_4P_2Ru$	$C_{29.5}H_{35}Cl_3N_4P_2Ru$	$C_{32}H_{34}N_4O_3P_2Ru$	$C_{42}H_{41}ClN_4O_{10}P_2Ru_3$
Formula Weight	862.83	714.98	685.64	1162.39
Crystal Dimensions (mm)	0.32 × 0.28 × 0.14	0.54 × 0.15 × 0.13	0.44 × 0.30 × 0.08	0.38 × 0.16 × 0.12
Crystal System	orthorhombic	orthorhombic	monoclinic	monoclinic
Space Group	*Pca*2$_1$ (No. 29)	*Pbca* (No. 61)	*P*2$_1$ (No. 4)	*P*2$_1$/*n*[a]
a (Å)	36.0666 (14)	16.7298 (14)	11.2706 (12)	17.7363 (5)
b (Å)	10.3284 (4)	16.5689 (14)	12.7184 (14)	12.7680 (3)
c (Å)	22.7085 (9)	22.2494 (19)	11.9508 (13)	21.6124 (6)
α (deg)				
β (deg)			116.9570 (10)	94.7770 (3)
γ (deg)				
V (Å^3)	8459.2 (6)	6167.4 (9)	1526.9 (3)	4877.3 (2)
Z	8	8	2	4
ρ_{calcd} (g cm^{-3})	1.355	1.540	1.491	1.583
μ (mm^{-1})	0.608	0.899	0.658	1.093
$2\theta_{max}$ (deg)	54.96	55.06	55.00	54.96
Total Data Collected	71812 (–46 ≤ *h* ≤ 46, –13 ≤ *k* ≤ 13, –29 ≤ *l* ≤ 29)	51801 (–21 ≤ *h* ≤ 21, –21 ≤ *k* ≤ 21, –28 ≤ *l* ≤ 28)	13494 (–14 ≤ *h* ≤ 14, –16 ≤ *k* ≤ 16, –15 ≤ *l* ≤ 15)	42128 (–23 ≤ *h* ≤ 22, –16 ≤ *k* ≤ 16, –28 ≤ *l* ≤ 28)
Independent Reflections (R_{int})	19378 (0.0401)	7096 (0.0346)	6972 (0.0175)	11166 (0.0214)
Observed Reflections [$I \geq 2\sigma(I)$]	17974	6185	6728	9664
Restraints/ Parameters	0 / 939	1[b] / 391	0 / 383	20[c] / 579
Flack Absolute Parameter	0.298(12)		–0.005(16)	
Goodness-of-Fit (All Data)[d]	1.022	1.090	1.097	1.051
R_1 [$I \geq 2\sigma(I)$][e]	0.0276	0.0299	0.0239	0.0279
wR_2 [All Data][f]	0.0647	0.0742	0.0601	0.0860
Largest Difference Peak, Hole (e Å^{-3})	0.970, –0.449	0.672, –0.400	0.536, –0.320	1.186 and –0.931

[a] An alternate setting of *P*2$_1$/*c* (No. 14). [b] The Cl–C distances within the solvent dichloromethane molecule were restrained to be equal (within 0.03 Å) during refinement. [c] Distances within the disordered solvent *n*-pentane and CH_2Cl_2 molecules were subject to the following restraints during refinement: $d(C–C)_{n\text{-pentane}}$ = 1.53(1) Å; $d_{1,3}$ $(C\cdots C)_{n\text{-pentane}}$ = 2.50(1) Å; $d(Cl–C)_{dichloromethane}$ = 1.80(1); $d(Cl\cdots Cl)_{dichloromethane}$ = 2.87(1) Å. [d] $S = [\Sigma w(F_o^2 - F_c^2)^2/(n-p)]^{1/2}$ where *n* = number of data; *p* = number of parameters varied; $w = [\sigma^2(F_o^2) + (a_0P)^2 + a_1P]^{-1}$ where $P = [\text{Max}(F_o^2, 0) + 2F_c^2]/3$, and a_0 and a_1 are optimized by the refinement program; for **4**, a_0 = 0.0326, a_1 = 1.9568; for **5**, a_0 = 0.0350, a_1 = 4.3573; for **6b**, a_0 = 0.0346, a_1 = 0.0654; for **7**, a_0 = 0.0459, a_1 = 5.1261. [e] $R_1 = \Sigma||F_o| - |F_c||/\Sigma|F_o|$. [f] $wR_2 = [\Sigma w(F_o^2 - F_c^2)^2/\Sigma w(F_o^4)]^{1/2}$.

3.2.4 Ketone Transfer Hydrogenation Catalysis

In a 50 mL three-necked, round-bottom flask with an attached reflux condenser under anhydrous conditions and argon atmosphere, [RuCl(η^6-*p*-cymene)(*P*,*N*-Ph_2PAr^-)] (**2c**, 10.0 mg, 17.8 μmol) was dissolved in isopropanol (*i*-PrOH, 13.6 mL, 178 mmol). The mixture was heated to 90 °C for 1.0 min while stirring which resulted in an orange-brown solution. Acetophenone (2.08 mL, 17.8 mmol)

was then added to the refluxing mixture followed immediately by solid potassium *tert*-butoxide (*t*-BuOK, 8.0 mg, 71 μmol), which was added to the reaction flask under a light stream of argon (t_{rxn} = 0 min) and resulted in darkening to a red-brown solution. The molar composition of the reaction mixture at this point was [Ru] : *t*-BuOK : acetophenone : *i*-PrOH = 1 : 4 : 1,000 : 10,000. Aliquots were withdrawn at t_{rxn} = 0, 5, 60 and 120 min which were immediately filtered through columns containing 2 cm of acidic alumina atop 2 cm of Florisil (to remove catalyst) and collected in vials which were quickly capped. Each sample was analyzed by ^{1}H NMR analysis ($CDCl_3$) within 10 min of its withdrawal from the reaction mixture. GC-EI-MS analysis was carried out on the filtered samples after 10-fold volumetric dilution with dichloromethane. Conversion percentages, turnover numbers and frequencies determined from acetophenone and 1-phenylethanol signals in both ^{1}H NMR and GC-EI-MS analyses were mutually consistent.

3.3 Results and Discussion

3.3.1 Monophosphinoaniline Complexes

(a) Diphenyl(*o*-*N*-methylanilinyl)phosphine. The monophosphinoaniline ligand, Ph_2PAr (Ar = *o*-C_6H_4NHMe) reacts with 0.5 equiv of $[RuCl(\mu\text{-}Cl)(\eta^6\text{-}p\text{-cymene})]_2$ (**1**), under mild conditions in dichloromethane to produce the neutral complex, $[RuCl_2(\eta^6\text{-}p\text{-cymene})(P\text{-}Ph_2PAr)]$ (**2a**), in which the chloro-bridged dimer has been cleaved by coordination of the phosphine donor while the amine functionality remains uncoordinated and pendent (Scheme 3.1). The $^{31}P\{^1H\}$ NMR spectrum of **2a** displays the expected singlet at δ_P 28.2 while the ^{1}H NMR spectrum (Figure 3.1) shows a doublet at δ_H 2.81, representing the NMe protons having $^3J_{HH}$ = 5.0 Hz due to coupling with the amine hydrogen (δ_H 5.47, q/br). The phosphorus chemical shift of **2a** is similar to that of the non-*N*-methylated analogue, $[RuCl_2(\eta^6\text{-}p\text{-cymene})(P\text{-}Ph_2PC_6H_4NH_2)]$ (δ 28.9), reported by Pelagatti

et al.[16] Moreover, the *N*-methyl signal of **2a** has a chemical shift similar to that of the free Ph_2PAr ligand (δ_H 2.84) suggesting that the amine is not coordinated. The

Scheme 3.1. Synthesis of Monophosphinoaniline Compounds **2a** – **c**

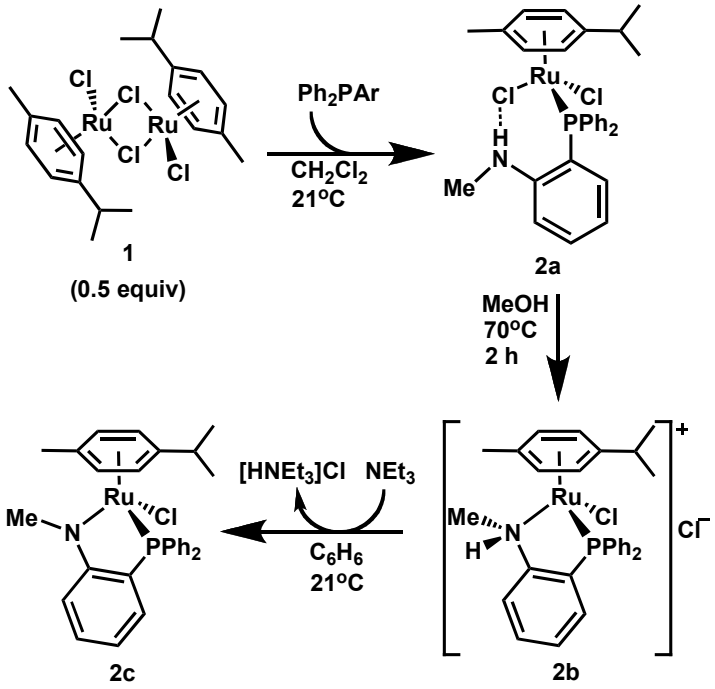

methyl protons of the isopropyl group of **2a** are all represented by a doublet at δ_H 1.39, displaying vicinal coupling with the adjacent methine proton ($^3J_{HH}$ = 7.0

Figure 3.1. ^{1}H NMR Spectrum of [$RuCl_2$(η^6-*p*-cymene)(*P*-Ph_2PAr)] (**2a**).

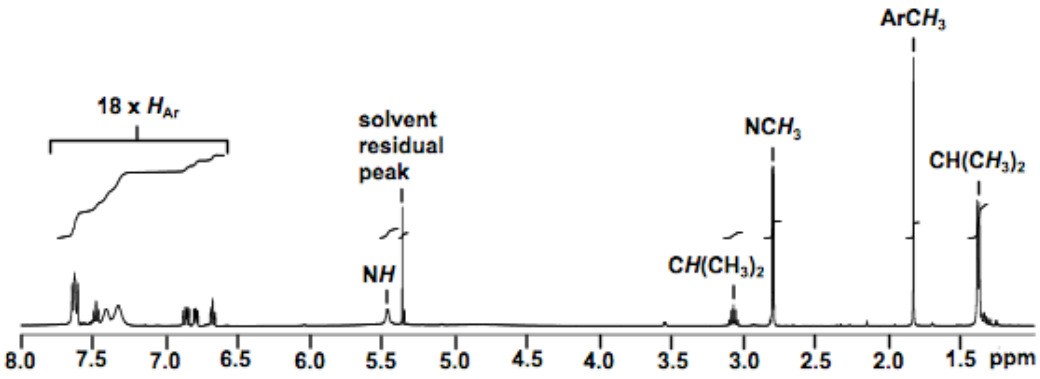

Hz). The $^{13}C\{^1H\}$ NMR spectrum of **2a** shows signals for the aliphatic carbons, which were identified between δ_C 30.9 and 18.1 by gradient heteronuclear single quantum coherence (GHSQC) analysis (see Figure 3.2).

Figure 3.2. GHSQC Plot of [$RuCl_2$(η^6-*p*-cymene)(*P*-Ph_2PAr)] (**2a**)

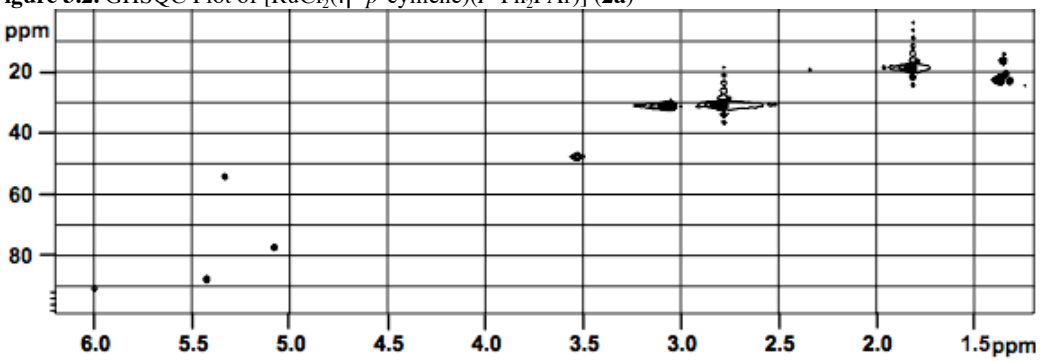

The solid state structure of complex **2a** (Figure 3.3, top-left) displays a hydrogen bond between one of the inner-sphere chlorides and the pendent amine hydrogen, for which the resulting H(N1)–Cl(1) distance of 2.43 Å is significantly shorter

Figure 3.3. ORTEP Diagrams of Compounds **2a** – **c**. [$RuCl_2$(η^6-*p*-cymene)(*P*-Ph_2PAr)] (**2a**, top left), [RuCl(η^6-*p*-cymene)(*P*,*N*-Ph_2PAr)]Cl (**2b**, top right) and [RuCl(η^6-*p*-cymene)(*P*,*N*-Ph_2PAr^-)] (**2c**, bottom) are shown. Gaussian ellipsoids for all non-hydrogen atoms are depicted at the 20% probability level. Hydrogen atoms, where included, are shown artificially small.

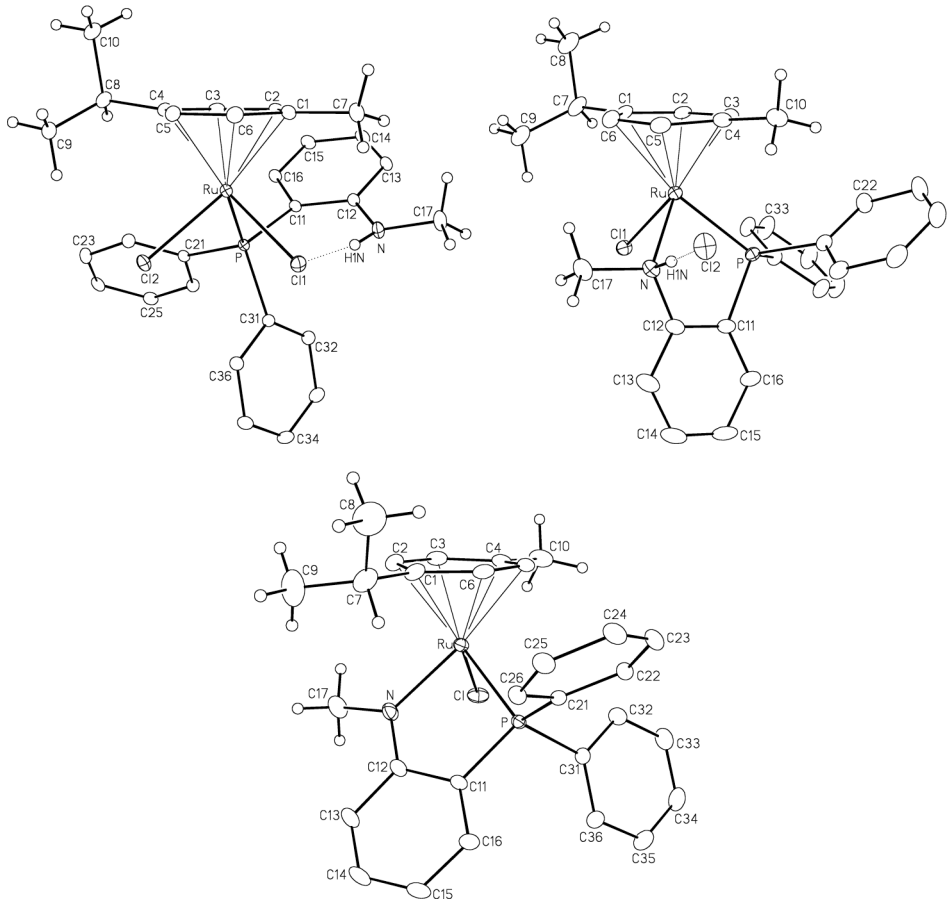

than a normal van der Waals separation of 3.05 Å.[36] An analysis of the structural parameters within complex **2a** (Table 3.4) reveals that the Ru–Cl(1) bond is

Table 3.4. Selected Structural Parameters for Compounds **2a** – **c** and **3b**

	[$RuCl_2(\eta^6$-*p*-cymene)-(*P*-Ph_2PAr)] (2a)	**[$RuCl(\eta^6$-*p*-cymene)(*P*,*N*-Ph_2PAr)]Cl (2b)**	**[$RuCl(\eta^6$-*p*-cymene)(*P*,*N*-Ph_2PAr^-)] (2c)**	**[$RuCl(\eta^6$-*p*-cymene)(*P*,*N*-Ph_2PAr')]Cl (3b)**
Atoms	Distances / Å	Distances / Å	Distances / Å	Distances / Å
Ru–P	2.3633(3)	2.2899(7)	2.2925(6)	2.3059(7), 2.3005(7)[a]
Ru–Cl(1)	2.4258(4)	2.3947(6)	2.4050(6)	2.3944(6), 2.3982(6)
Ru–Cl(2)	2.4035(3)	–	–	–
Cl(1)–H1N	2.43	2.16	–	–
Ru–N	–	2.172(2)	2.0861(19)	2.199(2), 2.209(2)
Atoms	Angles / °	Angles / °	Angles / °	Angles / °
Cl(1)–Ru–P	87.262(12)	85.58(2)	90.48(2)	84.27(2), 83.34(2)
Cl(2)–Ru–P	89.887(12)	–	–	–
Cl(1)–Ru–Cl(2)	86.271(12)	–	–	–
Cl(1)–Ru–N	–	83.32(6)	83.86(6)	83.73(6), 83.56(6)
Cl(2)–Ru–N	–	–	–	–
P–Ru–N	–	80.58(6)	80.41(6)	81.27(6), 81.92(6)

[a] Two crystallographically independent molecules.

slightly longer than Ru–Cl(2) (2.4258(8) *vs.* 2.4035(3) Å) presumably due to its interaction with the pendent amine hydrogen. The previously reported structure of the non-*N*-methylated analogue of **2a**, $[RuCl_2(\eta^6$-*p*-cymene)(*P*-$Ph_2P(o$-$C_6H_4NH_2)]$, also shows a similar hydrogen bond.[16]

Interestingly, while the *N*-methyl, methine and aryl-methyl carbon resonances of **2a** appear as sharp singlets, the signals for the methyl carbons of the isopropyl group (δ_C 22.0), as well as some aromatic carbon signals, are broad (see Figure 3.4). Such broadening suggests fluxionality that we propose results from the intramolecular hydrogen bond involving the amine hydrogen and a chloro ligand being weak enough to allow for facile enantiomerization via movement from one chloro ligand to the other, yet strong enough to render some carbon environments pseudo-diastereotopic on the NMR timescale. A $^{13}C\{^1H\}$ NMR spectroscopic analysis carried out at –80 °C supports this hypothesis as two sharp signals representing the isopropyl methyl carbons are now observed at this temperature at δ_C 24.3 and 19.6. The molar conductivity of **2a** is Λ = 6 $cm^2\ \Omega^{-1}\ mol^{-1}$, consistent with a non-conducting complex.

Figure 3.4. $^{13}C\{^{1}H\}$ NMR Spectra of [$RuCl_2(\eta^6$-*p*-cymene)(*P*-Ph_2PAr)] (**2a**)

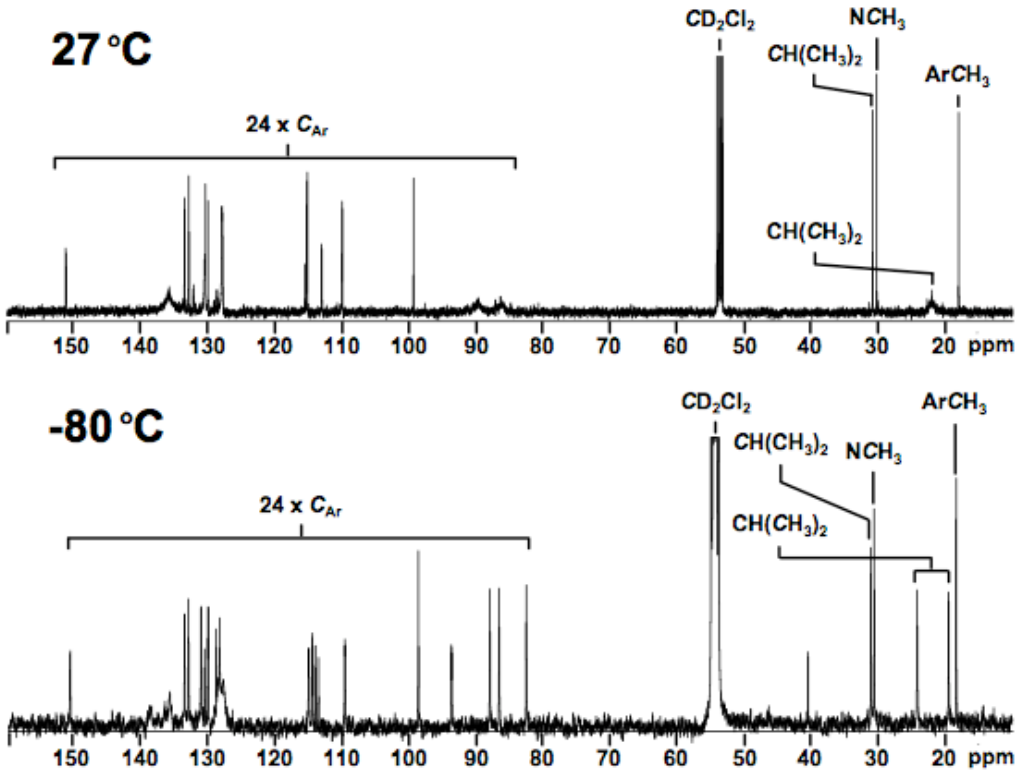

While **2a** is indefinitely stable in dichloromethane solution, the compound can be converted to the cationic *P*,*N*-chelated isomer, [RuCl(η^6-*p*-cymene)(*P*,*N*-Ph_2PAr)]Cl (**2b**) in refluxing methanol within hours (Scheme 3.1). Faraone *et al.* have shown that protic solvents kinetically enhance amine coordination in a similar complex by providing strong hydrogen bond donors to facilitate the dissociation of a chloro ligand.[37] Although the solid-state structure of **2a** (*vide supra*) clearly depicts a hydrogen bond between the pendent amine hydrogen and a chloro ligand, it appears that, rather than promoting chloride ion dissociation, this intramolecular hydrogen bond actually appears to stabilize the monodentate complex against chelation of the amine by orienting the lone pair on nitrogen away from the metal. Once formed, the chelate complex **2b** is never observed to revert back to **2a**. Chelation in **2b** results in a significant downfield shift of the ^{31}P resonance to δ_P 53.4 due to the effect of the five-membered ring[38] as also reported for the non-*N*-methylated analogue.[16] The ^{1}H NMR spectrum (Figure 3.5) shows a broad signal at δ_H 10.8 representing the deshielded amine hydrogen which

becomes quite acidic upon coordination of the amine to the cationic ruthenium center; the doublet *N*-methyl proton resonance found at δ_H 3.52 (with $^3J_{HH}$ = 4.4

Figure 3.5. ^{1}H NMR Spectrum of [RuCl(η^6-*p*-cymene)(*P*,*N*-Ph_2PAr)]Cl (**2b**)

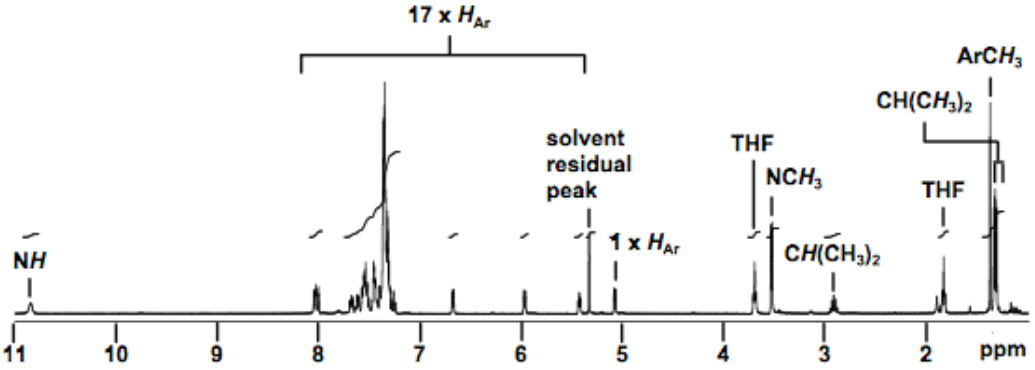

Hz) is also shifted downfield from that of **2a**. The chirality of **2b** is made evident by two distinct signals representing diastereotopic methyl groups of the isopropyl moiety at δ_H 1.33 and 1.31 each of which appears as a doublet due to vicinal coupling ($^3J_{HH}$ = 7.0 Hz) with the methine hydrogen. The $^{13}C\{^1H\}$ NMR spectrum of **2b** shows a strongly deshielded *N*-methyl carbon resonance at δ_C 76.7 because of its geminal relationship to the formally cationic ruthenium center. The molar conductivity of **2b** is Λ = 59 cm^2 Ω^{-1} mol^{-1}, consistent with a 1:1 electrolyte.

The X-ray structure of **2b** (Figure 3.3, top-right) shows a strong hydrogen bond between the outer-sphere chloride anion (Cl(2)) and the coordinated amine hydrogen (H(1N); 2.16 Å), which is consistent with the extensive deshielding of this proton observed spectroscopically, while also clearly illustrating the diastereotopicity of the isopropyl methyl groups of the *p*-cymene ligand, consistent with the observation of two distinct signals for these groups in both the ^{1}H and $^{13}C\{^1H\}$ NMR spectra.

The acidic amine hydrogen of **2b** is readily deprotonated to give the corresponding amido complex, [RuCl(η^6-*p*-cymene)(*P*,*N*-Ph_2PAr^-)] (**2c**, Ar^- = *o*-$C_6H_4NMe^-$; Scheme 3.1). Addition of ten equiv of triethylamine to a slurry of **2b** in benzene resulted in immediate darkening to an opaque, black-red mixture from

which the triethylammonium chloride byproduct was easily removed by aqueous extraction, yielding **2c** as a brown, micro-crystalline solid. Spectroscopic analysis of **2c** shows the phosphorus resonance at δ_P 59.3, which is shifted even further downfield from that of **2b**. Interestingly, the ^{1}H NMR spectrum of **2c** in CD_2Cl_2 (Figure 3.6) shows broad signals at ambient temperature and, notably, the proton

Figure 3.6. ^{1}H NMR Spectrum of [RuCl(η^6-*p*-cymene)(*P*,*N*-Ph_2PAr^-)] (**2c**)

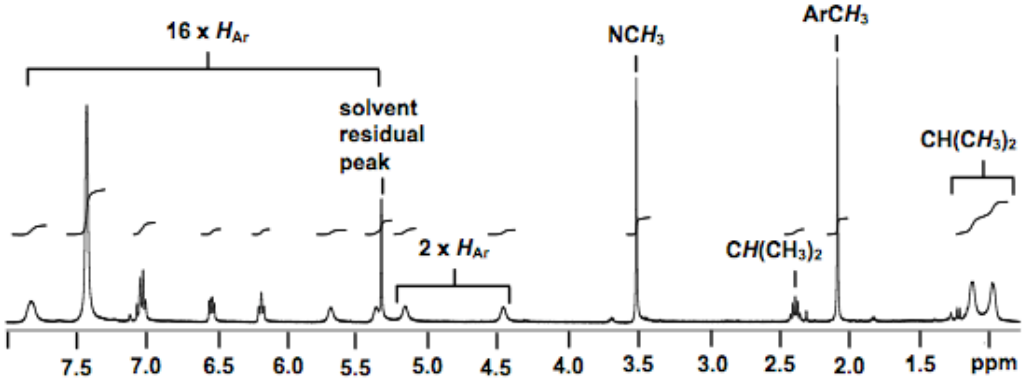

signals for the two diastereotopic isopropyl methyl groups of the *p*-cymene unit coalesce at 40 °C. Such fluxional behaviour implies that a rapid enantiomerization process is occurring in solution, presumably by chloride ion dissociation to generate the cationic, coordinatively unsaturated intermediate, [Ru(η^6-*p*-cymene)(*P*,*N*-Ph_2PAr^-)]Cl (**2d**, Scheme 3.2), followed by recoordination of the

Scheme 3.2. Enantiomerization of Compound **2c** via Intermediate **2d**

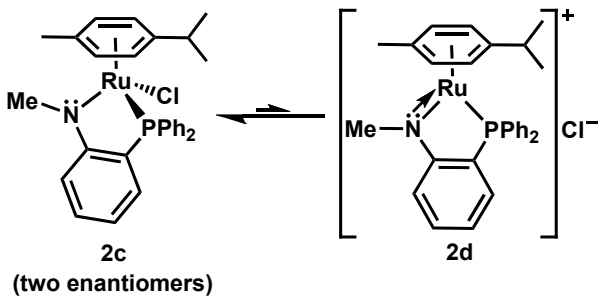

chloride ion on the opposite face of the chelate ring, resulting in stereo-inversion at ruthenium. A fluxional process involving stereoinversion at nitrogen seems less likely since such a mechanism would involve two diastereoisomers which should produce two signals in the $^{31}P\{^1H\}$ NMR spectrum. Futhermore, the X-ray structure of **2c**, discussed below, reveals nearly perfect planarity of the amido

nitrogen, suggesting that lone pair inversion is not a likely cause for the observed fluxionality. The conductivity of complex **2c** (Λ = 23 cm^2 $\Omega^{-1}mol^{-1}$) is intermediate between that of a neutral species and a 1:1 electrolyte, supporting the equilibrium shown in Scheme 3.2. Pellagatti reports a computationally determined energy difference between two species, that are structurally analogous to **2c** and **2d**, of only ΔG = 2.9 kcal/mol, with the cationic, coordinatively unsaturated complex (similar to **2d**) being less stable.[16] Our variable temperature NMR analysis of **2c** indicates that its enantiomerization, at the coalescence temperature of the proton signals for the methyl groups of the isopropyl moiety (T_{coal} = 40 °C), occurs with a rate constant of k_{coal} = 95 s^{-1}, corresponding to an energy barrier of $\Delta G^{\ddagger}$ (313 K) = 15 kcal/mol.[39]

A representation of the amido complex **2c** is shown in Figure 3.3 (bottom), confirming the spectroscopic characterization of this species. The three structures depicted in Figure 3.3 clearly illustrate the transition of the complex with the Ph_2PAr ligand in a monodentate, *P*-bound coordination mode (**2a**), to the *P*,*N*-chelate (**2b**), to the amido species (**2c**). The η^6-*p*-cymene unit appears normal in all of the monophosphinoaniline complexes with relatively small deviations in Ru–C_{arene} bond lengths. Compound **2c** has a significantly shorter Ru–N bond length (2.086(2) Å) than that of **2b** (2.172(2) Å) owing presumably to both the decreased steric demand of the deprotonated donor and greater basicity of the formally anionic amido nitrogen in **2c** which strengthens the Ru–N bond. The three atoms bound to the amido nitrogen atom of **2c** (Ru, C(17), C(12)) are arranged in an approximate trigonal plane as is evident from the sum of the three angles about nitrogen (358.0°) and can be compared to the sum of the same three angles (341.0°) in **2b** containing the pyramidal nitrogen. The planarity of the amido group illustrates the strong sp^2 character of the nitrogen atom suggesting some degree of π-donation to ruthenium which could also be reflected in the short Ru–N bond (*vide supra*).

(b) Diphenyl(*o*-*N*,*N*-dimethylanilinyl)phosphine. Pelagatti *et al*. have reported that reaction of the *N*,*N*-dimethyl analogue, Ph_2PAr', with 0.5 equiv of **1** initially results in the pendent, monodentate complex, $[RuCl_2(\eta^6\text{-}p\text{-cymene})(P\text{-}Ph_2PAr')]$ (**3a**) analogous to **2a**, which over time in dichloromethane converted to the *P*,*N*-chelated species, $[RuCl(\eta^6\text{-}p\text{-cymene})(P,N\text{-}Ph_2PAr')]Cl$ (**3b**),[16] in which the amine has replaced a chloro ligand at ruthenium to generate a cationic complex analogous to **2b** (see Scheme 3.3). In our hands, however, the intermediate **3a** was

Scheme 3.3. Synthesis of Monophosphinoaniline Compound **3b**

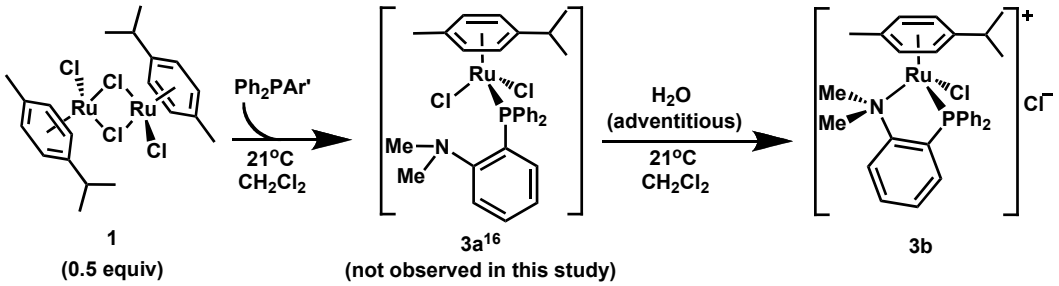

never observed. Despite our best efforts to exclude moisture from reaction mixtures, the hygroscopic intermediate **3a** readily sequesters adventitious water, as is observed by ^1H NMR spectroscopy, elemental analysis and X-ray crystallography of **3b** (which showed the presence of water in the unit cell), which appears to facilitate chelation by hydrogen-bonding assisted chloride ion abstraction.[16,37] Unfortunately very little characterization of the intermediate **3a** is given in the report of this compound beyond the $^{31}P\{^1H\}$ NMR chemical shift; the other spectroscopic data given for this compound[16] appear to be that of **3b**, as shown by comparison with our data. The apparent ease with which intermediate **3a** is able to undergo chelation under mild conditions contrasts the protic, forcing conditions necessary to promote chelation in **2a**. Presumably, the intramolecular hydrogen bond between the amine hydrogen and a chloro ligand in **2a** (Figure 3.1) renders the pendent amine more inert to chelation (*vide supra*), while the more nucleophilic *N*,*N*-dimethylanilinyl group of **3a** rapidly displaces a chloro ligand to generate the cationic, chelated product, **3b**.[37] Coordination of the *N*,*N*-dimethylanilinyl group is favored despite the increased steric bulk of this group compared with the *N*-methyl analogue.

The $^{31}P\{^{1}H\}$ NMR spectrum of **3b** shows a singlet at δ_P 47.5 (CD_2Cl_2) which is shifted significantly downfield from those of **2a** or **3a**[16] and is again consistent with the presence of a five-membered chelate ring.[38] The *P*,*N*-chelation mode of **3b** is demonstrated by ^{1}H NMR spectroscopy (see Figure 3.7), which

Figure 3.7. ^{1}H NMR Spectrum of [RuCl(η^6-*p*-cymene)(*P*,*N*-Ph_2PAr')]Cl (**3b**)

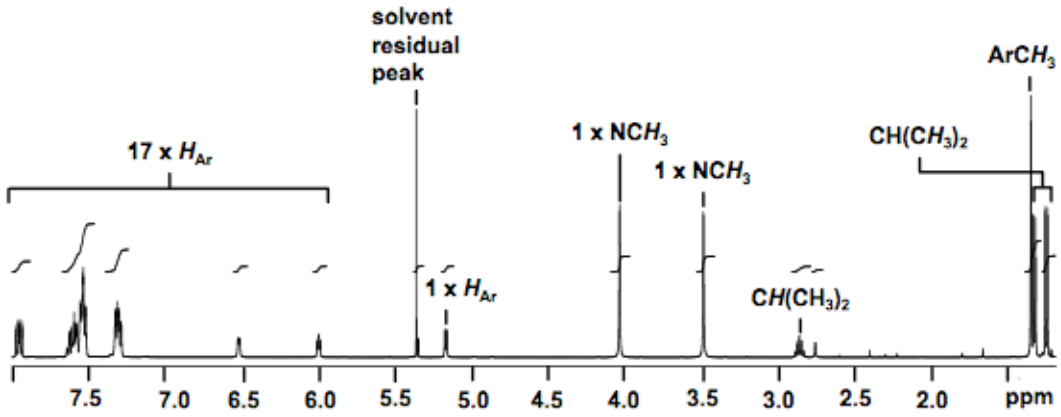

shows two distinct, relatively downfield singlets (δ_H 4.04 and 3.50) for the diastereotopic *N*-methyl groups – a result of the stereogenic center created at ruthenium upon coordination of the amine. The asymmetry of **3b** is also made evident by two distinct doublet resonances for the methyl protons of the *p*-cymene isopropyl group (δ_H 1.26 and 1.35, $^{3}J_{HH}$ = 7.0 Hz), as well as four chemically distinct aromatic *p*-cymene proton signals between δ_H 7.32 and 5.18, which were identified by gradient correlation spectroscopic (GCOSY) analysis. By contrast with **2a**, the $^{13}C\{^{1}H\}$ NMR spectrum of **3b** shows two sharp singlets for the methyl carbons of the isopropyl groups at δ_C 22.3 and 20.7 and relatively deshielded *N*-methyl resonances at δ_C 65.2 and 58.4, consistent with amine coordination to a formally cationic ruthenium center. The molar conductivity of **3b** is Λ = 79 $cm^2\ \Omega^{-1}\ mol^{-1}$, characteristic of a 1:1 electrolyte. The *p*-cymene ligands of the monophosphinoaniline complexes remain coordinated and are not displaced, even in the presence of an excess of the ligands Ph_2PAr and Ph_2PAr', respectively. This presumably reflects the strong binding affinity of the η^6-*p*-cymene ligand and is apparently not the result of any inherent instability of the

presumed products, $[RuCl_2(P,N\text{-}Ph_2PAr)_2]$ and $[RuCl_2(P,N\text{-}Ph_2PAr')_2]$, since a number of analogous species are known.[8,11,40,41]

The X-ray structural analysis of **3b** (ORTEP Figure 3.8) shows the Ru–Cl bond lengths (for the two independent molecules) of 2.3944(6) and 2.3982(6) Å,

Figure 3.8. ORTEP Diagram of $[RuCl(\eta^6\text{-}p\text{-cymene})(P,N\text{-}Ph_2PAr')]Cl$ (**3b**). Only one of two crystallographically independent molecules of $[RuCl(\eta^6\text{-}p\text{-cymene})(P,N\text{-}Ph_2PAr')]^+$ (cation of **3b**) is shown. Gaussian ellipsoids for all non-hydrogen atoms are depicted at the 20% probability level. Hydrogen atoms, where included, are shown artificially small.

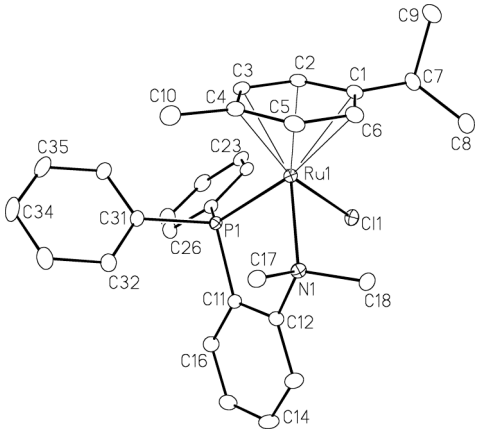

which are close to that of **2b** (2.3947(6) Å) and the non-hydrogen-bonded chloro ligand in **2a** (2.4035(3) Å). The Ru–P bond lengths in the chelated complexes **2b**, **2c** and **3b** (each ~2.30 Å) are shorter than that of the pendent complex **2a** (~2.36 Å) presumably due to restraints imposed by the chelate rings. The crystal structure of **3b** clearly shows the chemically distinct *N*-methyl groups of the coordinated amine. A comparison of the Ru–N bond lengths in the structural analogues **2b** and **3b** illustrates the steric effects of the additional *N*-methyl group on the length of the Ru–N bond as that of **2b** (2.172(2) Å) is shorter than that of **3b** (2.199(2) and 2.209(2) Å for the two independent molecules) despite the stronger σ-donor character of the *N*,*N*-dimethylanilinyl donor.

(c) Ketone Transfer Hydrogenation Catalysis. Compounds **2c** and **2d** are of interest since similar species were recently proposed as intermediates involved in efficient ketone transfer hydrogenation catalysis, likely operating by a mechanism involving the simultaneous transfer of protic and hydridic hydrogen atoms from

reagent alcohol to the coordinatively unsaturated amido complex (similar to **2d**) via an outer-sphere mechanism.[16] Herein we have verified that the amido species (**2c**) under basic conditions, is also an efficient catalyst for the transfer hydrogenation of acetophenone from isopropanol to produce 1-phenylethanol and acetone. Although this reaction has already been studied using the *N*,*N*-dimethyl complex, **3b**, as well as the non-*N*-methylated analogue, [RuCl(η^6-*p*-cymene)(*P*,*N*-$Ph_2P(o\text{-}C_6H_4NH_2)$)]Cl (**2e**), as catalysts,[16] we sought to compare the catalytic activity of the *N*-methylamido compound, **2c**, with those previously reported. Not surprisingly perhaps, Table 3.5 shows that under similar conditions

Table 3.5. Effects of *N*-Methyl Substitution on Transfer Hydrogenation

Entry	Complex	No. of *N*-Me Groups	t_{rxn} (min)	Conversion (%) [a]	TOF (h^{-1}) [b]
1[16]	**2e** [c]	0	5	37	4440
2[16]	**2e** [c]	0	60	≥ 98	≥ 980
3[16]	**2e** [d]	0	60	–	–
4	**2c** [e]	1	5	13	1560
5	**2c** [e]	1	60	34	340
6	**2c** [e]	1	120	46	230
7	**2c** [d]	1	60	–	–
8[16]	**3b** [c]	2	60	10	100

[a] Determined by CG analysis. [b] Turnover frequency determined at the corresponding reaction time (t_{rxn}) in column 4. [c] Reaction conditions: Temperature = 90 °C; Ru : KOH : acetophenone : *i*-PrOH = 1 : 4 : 1,000 : 128,000. [d] In the absence of base. [e] Reaction conditions: Temperature = 90 °C; Ru : *t*-BuOK : acetophenone : *i*-PrOH = 1 : 4 : 1,000 : 10,000.

the *N*-methylamido complex, **2c**, exhibits a catalytic activity intermediate between the more active non-*N*-methylated complex, **2e**, and the less active *N*,*N*-dimethyl complex, **3b**.[16]

In principle, compound **2c** could function as a transfer hydrogenation catalyst in the absence of base, via the Noyori bifunctional mechanism[23,24] whereby the amido species is converted into the catalytically active amine-hydride by H^+/H^- transfer from isopropanol. However, Entry 7 shows that **2c** is inactive as a catalyst in the absence of base. This suggests that an amido-hydride species, generated from **2c** via chloride replacement by isopropoxide followed by β-hydride elimination, may be the catalytically active species. However, this possibility remains to be tested. It should also be noted that a related NMe_2-containing complex, which cannot function by the bifunctional mechanism, has also been shown to require base, yet the derived hydride species was found to be

inactive as a catalyst.[26] Another possible mechanism that needs to be investigated is the Meerwein-Ponndorf-Verley-Oppenauer mechanism in which simultaneous coordination of both the alkoxide and ketone to the metal leads to direct transfer of the β-hydrogen on the alkoxide to the ketone without the formation of a hydrido complex.[23,42,43]

The *N*,*N*-dimethyl complex (**3b**) is believed to operate by an inner-sphere mechanism[16] since amine deprotonation to afford an amido species is not possible and hemilability of the Ph_2PAr' ligand (via displacement of the amine from ruthenium) seems more likely.[22] Although the amine complex, **2b**, itself was never tested as a transfer hydrogenation catalyst, it can be assumed that the addition of *t*-BuOK to reaction mixtures would immediately deprotonate **2b** to give the amido complex, **2c**, since even weakly basic triethylamine instantly deprotonates **2b**. In Chapter 4 the synthesis of the hydrido-amido complex, [RuH(η^6-*p*-cymene)(*P*,*N*-Ph_2PAr^-)] will be reported together with its efficacy as a ketone transfer hydrogenation catalyst.

3.3.2 Diphosphinoaniline Complexes

In addition to the monophosphinoanilines we were also interested in the analogous diphosphines, $Ar_2PCH_2PAr_2$ (Ar = *o*-C_6H_4NHMe; mapm) and $Ar'_2PCH_2PAr'_2$ (Ar' = *o*-$C_6H_4NMe_2$; dmapm) and the effects of *N*-methyl substitution on the coordination modes displayed by these ligands. Reaction of dmapm with 0.5 equiv of [RuCl(μ-Cl)(η^6-*p*-cymene)]$_2$ (**1**), shown in Scheme 3.4,

Scheme 3.4. Synthesis of Diphosphinoaniline Complexes **4** and **5**

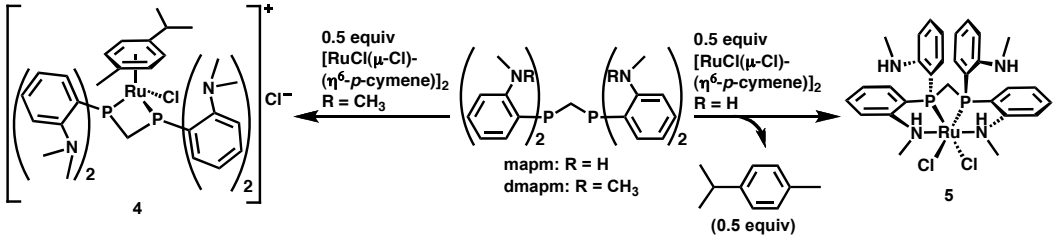

occurs much as observed earlier for the Ph_2PAr' ligand, in which an inner-sphere chloride is lost to allow dmapm to bind as a bidentate ligand, while the *p*-cymene

ligand remains bound to Ru. However, the product observed in the solid state, [RuCl(η^6-*p*-cymene)(*P*,*P'*-dmapm)]Cl (**4**), differs from **3** by displaying *P*,*P'*-chelation rather than the *P*,*N*-coordination mode observed in the monophosphine analogue.

Surprisingly, the $^{31}P\{^1H\}$ NMR spectrum of **4** actually shows two species in solution. The expected singlet of **4**, at δ_P –1.5, which is consistent with the structure shown for **4** in Scheme 3.4, and as determined in the X-ray structure analysis (*vide infra*), is in fact the minor species, while a species displaying two broad doublets, at δ_P 1.5 and –15.4 ($^2J_{PP}$ = 56 Hz), predominates in a 6 : 1 ratio. By comparison, the $^{31}P\{^1H\}$ NMR spectrum of the closely related dppm analogue displays only the expected singlet at δ_P 2.7 (in $CDCl_3$).[44] The mass spectrum of **4** shows only one predominant signal pattern consistent with that calculated for the formulation of the cation depicted in Scheme 3.4, supporting our hypothesis that the non-symmetrical species is an isomer of the symmetrical *P*,*P'*-chelate observed in the solid state.

A $^{31}P\{^1H\}$ spin saturation transfer (SST) experiment was carried out on a sample of **4** in CD_3NO_2 at 40 °C by irradiating the resonance at δ_P –15.4, resulting in a significant reduction in the intensity of the signals at δ_P 1.5 and –1.5 relative to an internal standard, indicating that all three phosphorus environments are undergoing chemical exchange at this temperature. We have considered a couple of structures that could give rise to an unsymmetrical species having two ^{31}P environments but neither seems possible. We have ruled out the possibility that coordination of an anilinyl nitrogen could displace the other end of the diphosphine, to give a *P*,*N*-chelated species like **3b**, on the basis that neither ^{31}P resonance has a chemical shift consistent with free dmapm (δ_P –36.0)[30] or the pendent phosphines of other reported dmapm complexes (δ_P –41.3 and –41.8).[45] In addition, the molar conductivity of Λ = 62 $cm^2\ \Omega^{-1}\ mol^{-1}$, which is consistent with a 1:1 electrolyte in nitromethane, is inconsistent with dmapm functioning as

a tridentate ligand in a *P*,*P'*,*N*-chelation mode, through displacement of the second chloro ligand.

The fluxionality of complex **4** is made evident by the SST experiment and by the broad signals in both the ^{1}H and $^{31}P\{^{1}H\}$ NMR spectra which exhibit temperature dependent chemical shifts and line-shapes. Variable temperature $^{31}P\{^{1}H\}$ NMR spectroscopic analysis of **4** shows that the 6:1 ratio of the non-symmetric complex to the C_s-symmetric *P*,*P'*-chelate between –80 and 50 °C remains relatively unchanged (even after replacing CD_2Cl_2 solvent with CD_3NO_2), although all signals sharpen upon cooling. Furthermore, between 50 and 80 °C, the signal belonging to the C_s-symmetric isomer is coincidentally overlapping with the more downfield signal of the non-symmetrical species. Unfortunately, the variable temperature ^{1}H NMR analysis is not useful as a means of characterization for compound **4** due to very broad, overlapping aromatic and *N*-methyl signals over the entire temperature range studied (–80 to 80 °C), rendering the identity of the major solution isomer unknown.

The solid state structure of **4** (Figure 3.9) also fails to provide clues about the nature of the non-symmetrical solution species, showing that the isopropyl

Figure 3.9. ORTEP Diagram of [RuCl(η^6-*p*-cymene)(*P*,*P'*-dmapm)]Cl (**4**). Only one of two crystallographically independent cations of [RuCl(η^6-*p*-cymene)(*P*,*P'*-dmapm)]Cl **4** is shown. Thermal ellipsoids as in Figure 3.3.

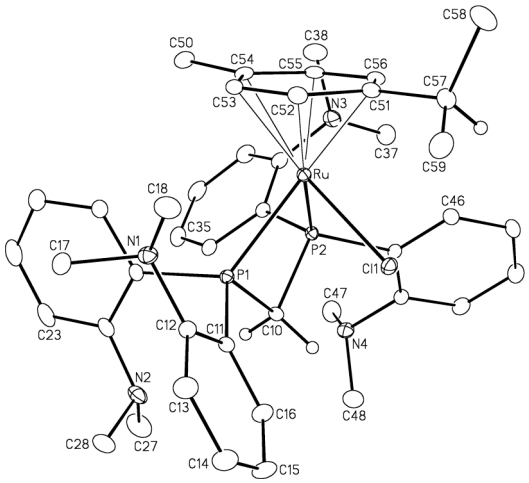

unit of the *p*-cymene fragment should not be restricted from freely rotating about the isopropyl-aryl and ruthenium-arene bond axes, suggesting that this particular geometry should possess chemically equivalent phosphorus nuclei. However, dissolution of the crystalline sample in CD_2Cl_2 and subsequent $^{31}P\{^1H\}$ NMR spectroscopic analysis shows the same 6:1 concentration ratio of C_1- to C_s-symmetric isomers as discussed above. Table 3.6 shows that the Ru–Cl bond

Table 3.6. Selected Structural Parameters for Compound **4**

Atoms	Distances / Å
Ru–Cl(1)	2.3938(6), 2.3928(6)[a]
Ru–P(1)	2.3778(6), 2.3851(7)
Ru–P(2)	2.3313(6), 2.3319(6)
P(1)–C(10)	1.849(2), 1.839(2)
P(2)–C(10)	1.839(2), 1.826(2)
Atoms	Angles / °
Cl(1)–Ru–P(1)	79.60(2), 80.09(2)
Cl(1)–Ru–P(2)	83.60(2), 84.52(2)
P(1)–Ru–P(2)	71.09(2), 71.43(2)
Ru–P(1)–C(10)	91.89(7), 92.03(8)
Ru–P(2)–C(10)	93.67(8), 94.12(8)
P(1)–C(10)–P(2)	95.85(11), 97.43(12)

[a] Two crystallographically independent molecules.

length in **4** (2.3938(6) and 2.3928(6) Å for the two independent molecules) is similar to that of **3b** (2.3944(6) Å). However, complex **4** has slightly greater Ru–P bond lengths (between 2.3851(7) and 2.3313(6) Å) than that of **3b** (2.3059(7) Å), presumably due to the greater strain of the four-membered chelate ring in addition to the increased steric congestion at Ru in **4**. Interestingly, the chelate ring of **4** is quite puckered with Ru–P(1)–C(10)–P(2) and Ru–P(2)–C(10)–P(1) torsional angles for the two independent molecules between 18.5(1)° and 22.99(9)° as the methylene unit is bent slightly out of the plane of the ring toward the chloro ligand.

Although the monophosphinoaniline complexes discussed (*vide supra*) exhibit different coordination tendencies depending on the degree of methyl substitution at the amine, diverse coordination behaviour at ruthenium is even more pronounced when comparing the diphosphinoanilines (mapm *vs.* dmapm). Unlike the reaction described above for dmapm, reaction of mapm with 0.5 equiv of **1** at ambient temperature in dichloromethane results in facile displacement of

the *p*-cymene moiety to generate the complex, [$RuCl_2$(*P*,*P'*,*N*,*N'*-mapm)] (**5**, Scheme 3.4) containing mapm bound as a tetradentate ligand. Both complexes **4** and **5** were synthesized in dichloromethane solution followed by washing with *n*-pentane (to remove any *p*-cymene that may have been produced) and were isolated as orange powders in good yields. Upon exposure to water or prolonged exposure to air, samples of both **4** and **5** turn green, presumably due to oxidative decomposition[46] to yet unidentified species. Although exposure of **5** to water or other protic solvents could promote chloride ion displacement and concomitant coordination of an additional amine to generate a cationic complex, we have not yet investigated this reaction. The formation of such a pentadentate complex could produce numerous stereoisomers which should be expected to complicate spectroscopic analysis.

The ^{1}H and ^{31}P{^{1}H} NMR spectra of **5** show (^{31}P{^{1}H} NMR spectrum in Figure 3.10) a mixture of stereoisomers. Single crystal X-ray structural analysis of

Figure 3.10. ^{31}P{^{1}H} NMR Spectrum of [$RuCl_2$(*P*,*P'*,*N*,*N'*-mapm)] (**5**). Signal ① corresponds to C_2-symmetric stereoisomers; signals ② correspond to C_1-symmetric stereoisomers.

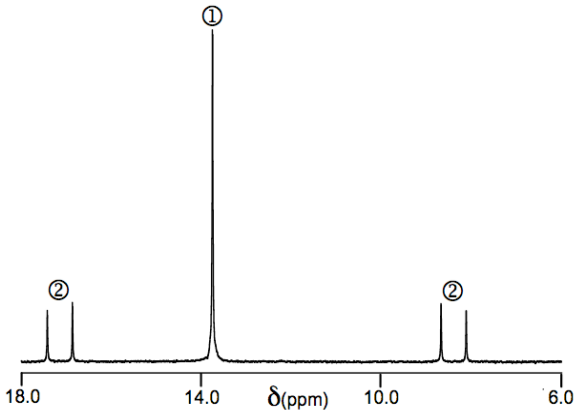

5•0.5CH_2Cl_2 shows disorder in one of the coordinated *N*-methylamino groups over two diastereotopic positions with a 60 : 40 site occupancy ratio representing C_2- and C_1-symmetric stereoisomers, respectively. Dissolution of the crystalline sample in CD_2Cl_2 and subsequent NMR spectroscopic analyses also indicate the presence of these stereoisomers in a ratio similar to that observed in the solid state, confirming that these isomers co-crystallize. The ^{31}P{^{1}H} NMR spectrum of

5 shows a prominent singlet at δ_P 13.7, attributed to the P_R,P'_R,N_R,N'_R configuration (ORTEP shown later) and its corresponding enantiomer. In this configuration, the phosphorus nuclei are equivalent by a C_2-symmetry axis. In addition to this signal are two doublets at δ_P 17.1 and 8.4 ($^2J_{PP}$ = 90 Hz), attributed to the P_R,P'_R,N_S,N'_R configuration and its corresponding enantiomer. The integrated signal intensities show that the ratio of these C_2- to C_1-symmetric stereoisomers is approximately 3 : 2 (mol/mol) and that there is no evidence of the other possible C_1- and C_2-symmetric stereoisomers.

The ^{1}H NMR spectrum of **5** (Figure 3.11) shows two doublets at δ_H 3.06 ($^3J_{HH}$ = 6.0 Hz) and at 2.66 ($^3J_{HH}$ = 4.8 Hz) representing the pendent and

Figure 3.11. ^{1}H NMR Spectrum of (C_1- and C_2-Symmetric Stereoisomers of) [$RuCl_2$(*P*,*N*,*P'*,*N'*-mapm)] (**5**)

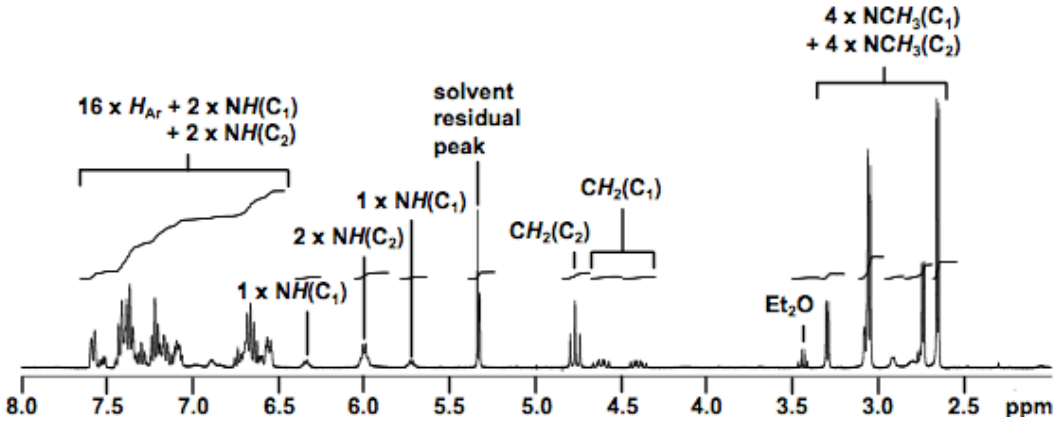

coordinated *N*-methyl protons, respectively, for the C_2-symmetric stereoisomers. These signals exhibit vicinal coupling to the amine hydrogens which resonate at δ_H 6.01 and 6.61, respectively, and appear as broad quartets. The methylene protons of the diphosphine backbone produce a triplet resonance at δ_H 4.78 with $^2J_{PH}$ = 11.6 Hz, confirming the chemical equivalence of the neighboring phosphines. The ^{13}C{^{1}H} NMR spectrum of **5** shows a triplet at δ_C 55.9 ($^1J_{PC}$ = 25 Hz) for the methylene carbon and two singlet resonances at δ_C 47.8 and 30.6 belonging to coordinated and pendent *N*-methylamino groups, respectively. The ambient temperature spectroscopic observation of two well defined *N*-methyl environments within this C_2-symmetric isomer shows no evidence for Type II hemilability,[1] whereby the pendent anilines could, in principle, reversibly displace

the coordinated ones, resulting in coalescence of the *N*-methyl proton signals. The lack of such inherent fluxionality at ruthenium(II) is in contrast to a similar series of rhodium(I) complexes which were shown to display Type II hemilability by ^{1}H NMR spectroscopy.[22] The molar conductivity of **5** was found to be $\Lambda = 7$ cm^2 Ω^{-1} mol^{-1}, consistent with a non-conducting complex.

X-ray structural analysis of compound **5** reveals a centrosymmetric unit cell with a disordered *N*-methyl group (N(3A) and C(37A), Figure 3.12) implying

Figure 3.12. ORTEP Diagrams of [$RuCl_2$(*P*,*P'*,*N*,*N'*-mapm)] (**5**). The P_R,P'_R,N_R,N'_R (left) and P_R,P'_R,N_S,N'_R (right) configurations are depicted. Thermal ellipsoids as in Figure 3.3.

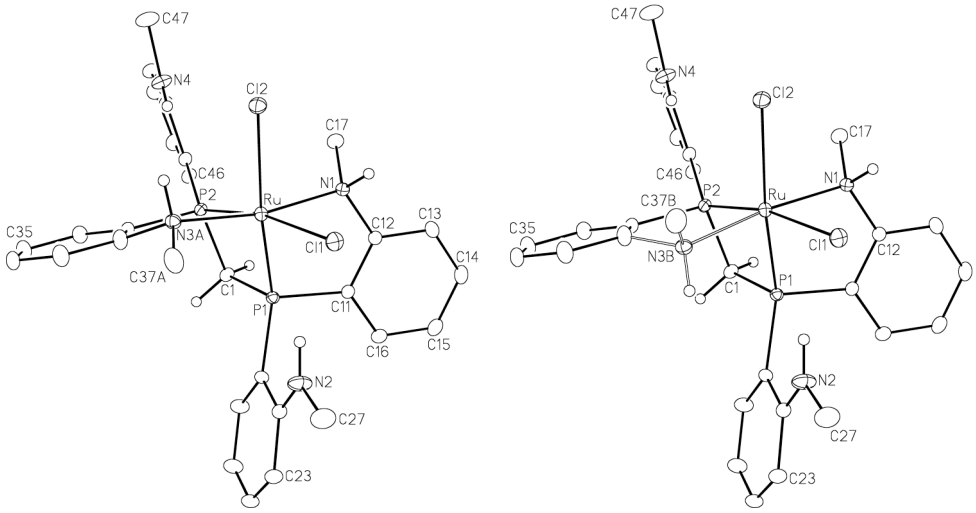

co-crystallization of multiple stereoisomers (*vide supra*). The chelating geometry of the tetradentate, *P,P',N,N'*-ligand at ruthenium is, to the best of our knowledge, unique. The strain of the four-membered chelate ring is made evident by compression of the P(1)–C(1)–P(2) angle from the ideal 109.5° to 91.09(9)° (see Table 3.7) as well as compression of the P(1)–Ru–P(2) angle from the ideal 90° to

Table 3.7. Selected Structural Parameters for Compound **5**

Atoms	Distances / Å	Atoms	Distances / Å
Ru–Cl(1)	2.4793(6)	Ru–P(2)	2.2194(5)
Ru–Cl(2)	2.4903(6)	Ru–N(1)	2.1352(17)
Ru–P(1)	2.2359(9)	Ru–N(3A)	2.168(4)
Atoms	Angles / °	Atoms	Angles / °
Cl(1)–Ru–P(1)	97.215(19)	Cl(2)–Ru–N(3A)	81.72(11)
Cl(2)–Ru–P(2)	103.41(2)	P(1)–Ru–P(2)	72.828(19)
Cl(1)–Ru–N(1)	83.06(5)	Ru–P(1)–C(1)	97.18(6)
Cl(1)–Ru–N(3A)	96.94(11)	Ru–P(2)–C(1)	97.85(6)
Cl(2)–Ru–N(1)	87.08(5)	P(1)–C(1)–P(2)	91.09(9)

72.83(2)°. Within the five-membered *P*,*N*-chelate rings the angles are much less distorted with angles at Ru, P, N and C close to the idealized values. All of the amine hydrogens come into reasonably close contacts (between 2.31 and 2.47 Å) with the two chloro ligands, which are less than the sum of the van der Waals radii[35] (3.05 Å) and suggest weakly attractive interactions.

The reaction of mapm with $[Ru(CO)_4(\eta^2\text{-}C_2H_4)]$ in dichloromethane solution initially produces $[Ru(CO)_4(P\text{-mapm})]$ (**6a**) which, at ambient temperature, over a 24 h period with exposure to ambient light, is completely converted to the thermodynamic product, $[Ru(CO)_3(P,P'\text{-mapm})]$ (**6b**, Scheme 3.5) by photolytic decarbonylation. The $^{31}P\{^1H\}$ NMR spectrum of the reaction

Scheme 3.5. Reaction of mapm with $[Ru(CO)_4(\eta^2\text{-}C_2H_4)]$ in Ambient Light

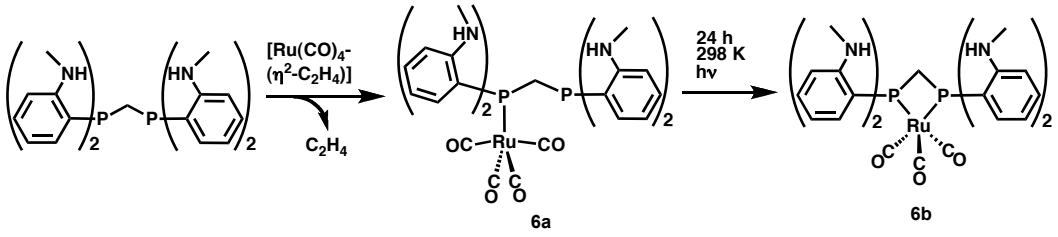

mixture after a few hours of exposure to ambient light shows two doublets at δ_P 15.1 and –66.0 (d, $^2J_{PP}$ = 115 Hz) for the coordinated and pendent phosphines of **6a**, respectively, while the signal for **6b** shows up as a singlet at δ_P –41.3. The ^{31}P signal for the pendent end of the diphosphine of **6a** has an expectedly similar chemical shift to that of the free mapm ligand which appears at δ_P –60.9.[22] ^1H NMR analysis of **6a** shows two broad quartets at δ_H 4.65 and 4.19 corresponding to two chemically distinct pairs of amine hydrogens and were identified (by GCOSY analysis) as having vicinal relationships to the *N*-methyl protons which resonate at δ_H 2.74 and 2.54, respectively. The chemical shifts of the amine protons, which are close to that of the free ligand (δ_H = 4.62)[22] are consistent with pendent amine groups. The fact that only two methyl resonances are observed in the ^1H NMR spectrum of **6a** eliminates the possibility that the kinetic product is $[Ru(CO)_3(P,N\text{-mapm})]$, which would be expected to show four distinct *N*-methyl environments. The monodentate coordination mode of **6a** is analogous to that

reported by Kiel and Takats for [Ru(CO)$_4$(*P*-dppm)] (dppm = $Ph_2PCH_2PPh_2$), which was found to undergo photodissociation, resulting in release of carbon monoxide and generating [Ru(CO)$_3$(*P*,*P'*-dppm)].[47] The methylene proton signal of **6a**, at δ_H 3.53, appears as a doublet of doublets due to coupling with two chemically inequivalent phosphorus nuclei. Although the $^{31}P\{^1H\}$ NMR spectrum of **6b** at ambient temperature (Figure 3.13) appears as a singlet (*vide supra*),

Figure 3.13. $^{31}P\{^1H\}$ NMR Spectra of [Ru(CO)$_3$(*P*,*P'*-mapm)] (**6b**)

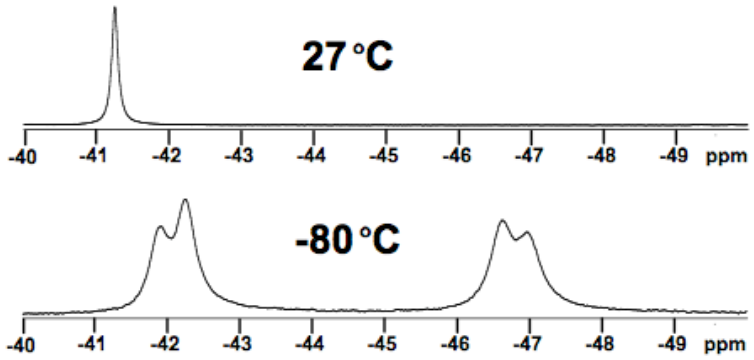

cooling to –80°C results in splitting of this singlet resonance into two broad signals at –42.0 and –46.5, showing that the exchange of axial and equatorial phosphorus nuclei by a Berry-pseudorotation can be slowed to render them distinguishable at this temperature. The ^1H NMR spectrum of **6b** (Figure 3.14)

Figure 3.14. ^1H NMR Spectrum of [Ru(CO)$_3$(*P*,*P'*-mapm)] (**6b**) from nearly complete decarbonylation of [Ru(CO)$_4$(*P*-mapm)] (**6a**).

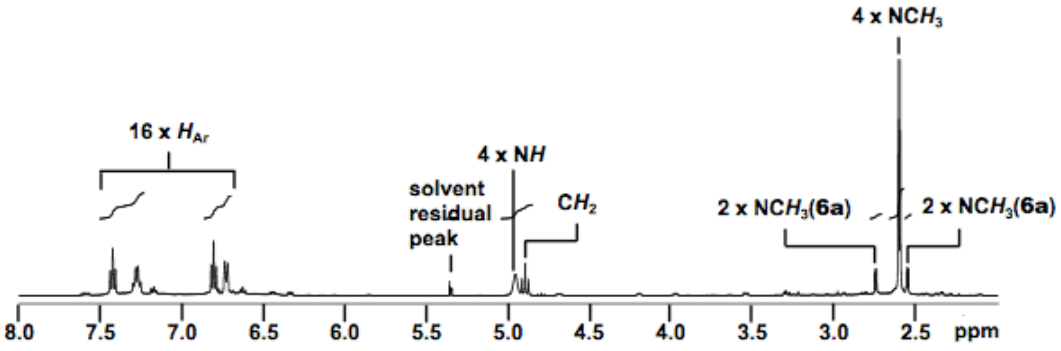

shows a broad quartet at δ_H 4.95 ($^3J_{HH}$ = 5.2 Hz) representing the amine hydrogens, a triplet at 4.89 ($^2J_{PH}$ = 10.0 Hz) representing the methylene protons and a doublet at 2.59 ($^3J_{HH}$ = 5.2 Hz) representing the *N*-methyl protons. The

chemical equivalence of these groups of protons at ambient temperature is consistent with a fluxional process.

X-Ray crystallographic analysis of **6b** illustrates the pseudo-trigonal bipyramidal geometry at ruthenium with clearly distinguishable axial and equatorial phosphine donors (Figure 3.15). The strain of the four-membered

Figure 3.15. ORTEP Diagram of [Ru(CO)$_3$(*P*,*P'*-mapm)] (**6b**). Thermal ellipsoids as in Figure 3.3.

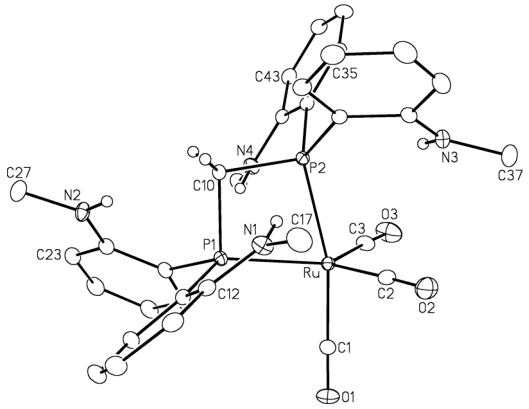

chelate ring is made evident by the compressed P(1)–C(10)–P(2) angle of 97.32(10)° (see Table 3.8) and the compressed P(1)–Ru–P(2) angle of 71.41(2)°.

Table 3.8. Selected Structural Parameters for Compound **6b**

Atoms	Distances / Å
Ru–P(1)	2.3855(6)
Ru–P(2)	2.3878(6)
Ru–C(1)	1.911(2)
Ru–C(2)	1.931(2)
Ru–C(3)	1.905(2)
P(1)–C(10)	1.864(2)
P(2)–C(10)	1.846(2)
Atoms	Angles / °
P(1)–Ru–P(2)	71.41(2)
P(1)–Ru–C(1)	95.99(7)
P(1)–Ru–C(2)	115.59(8)
P(1)–Ru–C(3)	129.55(9)
P(2)–Ru–C(1)	166.34(7)
P(2)–Ru–C(2)	96.74(7)
P(2)–Ru–C(3)	93.43(8)
Ru–P(1)–C(10)	95.44(7)
Ru–P(2)–C(10)	95.83(7)
P(1)–C(10)–P(2)	97.32(10)

The chelate ring is exceptionally planar as is shown by the P(1)–Ru–P(2)–C(10) torsional angle of only 0.18(7)°, while the analogous torsional angles for the four-membered chelate rings of **4** and **5** are 20.48° and 7.23(7)° respectively. Within

the trigonal equatorial plane the angles (113.8(1)° to 129.59(8)°) deviate slightly from the idealized 120°, with the largest angle (P(1)–Ru–C(3)) appearing to have opened up to accommodate the pendent N(4) amine group which projects into this plane from above in Figure 3.15. As is typical for trigonal bipyramidal structures containing a chelate, the Ru–P(2) vector is tilted from the idealized axial orientation, owing to chelate ring strain, such that the P(2)–Ru–C(1) angle (166.34(7)°) deviates from the idealized 180°.

We attempted to exploit the pendent phosphine of **6a** to prepare a dinuclear ruthenium complex of the formulation $[Ru_2(CO)_x(\mu\text{-}P,P'\text{-mapm})]$ by reacting mapm with 2 equiv of $[Ru(CO)_4(\eta^2\text{-}C_2H_4)]$ in complete darkness (to prevent conversion of **6a** to **6b**). However, rather than producing the expected binuclear complex, this reaction generated a mixture, containing approximately equal concentrations of $[Ru_3(CO)_{10}(\mu\text{-}P,P'\text{-mapm})]$ (**7**) and **6a**, the latter of which was gradually converted to **6b** upon exposure to ambient light (Scheme 3.6) as

Scheme 3.6. Reactions of mapm with Ruthenium Carbonyl Precursors

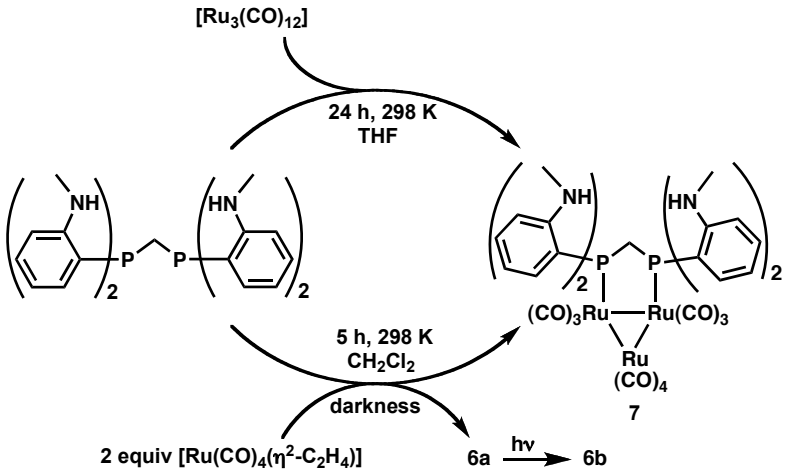

determined by $^{31}P\{^1H\}$ and ^1H NMR spectroscopy. Washing with *n*-pentane easily removed **6b**, allowing **7** to be purified and crystallized for X-ray structural analysis. Complex **7** can also be prepared more directly by reacting mapm with 1 equiv of $[Ru_3(CO)_{12}]$ in tetrahydrofuran solution, and the mixture produced by this method is also spectroscopically devoid of **6b**. The $^{31}P\{^1H\}$ NMR spectrum of **7** shows only a singlet at δ_P 2.2, consistent with a symmetric bridging mode of the

mapm ligand which serves to simplify the ^{1}H NMR spectrum, as does the fact that none of the amines participate in coordination. The methylene protons appear as a triplet at δ_H 4.76 while the amine hydrogen signal appears as a relatively upfield quartet at δ_H 3.94. Interestingly, the *N*-methyl proton signal appears as a slightly broadened doublet due to 2.5 Hz coupling with the amine hydrogen (a typical coupling constant in usually twice as large).[22] The slight broadening of this signal may be a consequence of the fluxionality of the carbonyl moieties on the trinuclear core which has been well documented within the analogous dppm-bridged system.[48] This fluxionality is made evident by the $^{13}C\{^{1}H\}$ spectrum, which shows only a single resonance at δ_C 210.9 representing all carbonyls. The infrared spectrum of **7** in CH_2Cl_2 is similar to that described for the dppm analogue[48] showing multiple carbonyl stretches between 2079 and 1955 cm^{-1}.

The solid state structure of compound **7** (Figure 3.16) clearly illustrates the *P*,*P'*-bridging mode of the mapm ligand across two ruthenium atoms, each of

Figure 3.16. ORTEP Diagram of $[Ru_3(CO)_{10}(\mu\text{-}P,P'\text{-mapm})]$ (**7**). Thermal ellipsoids as in Figure 3.3.

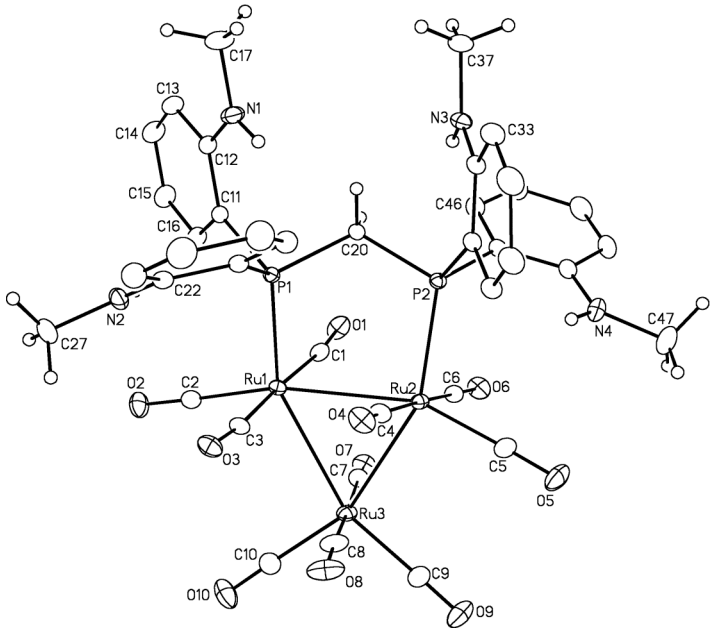

which possesses three terminally bound carbonyl ligands while sharing a bridging $Ru(CO)_4$ unit. Table 3.9 shows that all Ru–Ru bond lengths are very similar

(Ru(1)–Ru(2), 2.8464(3); Ru(2)–Ru(3), 2.8567(3); Ru(1)–Ru(3), 2.8504(3) Å) despite the presence of the bridging diphosphine across the Ru(1)–Ru(2) bond. As

Table 3.9. Selected Structural Parameters for Compound **7**

Atoms	Distances / Å
Ru(1)–Ru(2)	2.8464(3)
Ru(1)–Ru(3)	2.8504(3)
Ru(2)–Ru(3)	2.8567(3)
Ru(1)–P(1)	2.3317(6)
Ru(2)–P(2)	2.3580(6)
Atoms	Angles / °
Ru(1)–Ru(2)–Ru(3)	59.973(7)
Ru(2)–Ru(1)–Ru(3)	60.194(7)
Ru(1)–Ru(3)–Ru(2)	59.833(7)
Ru(1)–Ru(2)–P(2)	94.203(17)
Ru(2)–Ru(1)–P(1)	91.596(7)
P(1)–C(20)–P(2)	118.47(13)

is typical in such clusters, pairs of carbonyls that are almost eclipsed when viewed along the metal-metal bonds are actually staggered slightly in order to avoid unfavorable contacts. As a result, the torsion angles of these carbonyls about Ru–Ru bonds vary between 15.7(1)° and 20.5(1)°.

The preparation of **7**, in which all amine groups were pendent, led us to ponder whether amine coordination could be promoted. Decarbonylation of **7** was attempted by various methods including UV photolysis and carbonyl oxidation with one or more equivalents of trimethylamine-*N*-oxide. However, each of these attempts produced complex mixtures of unidentified products as was observed spectroscopically.

The previously reported dmapm analogue, $[Ru(CO)_3(P,P'\text{-dmapm})]$,[45] had previously been shown to act as a useful precursor for the synthesis of the heterobimetallic complex, $[RhRuCl(CO)_3(\mu\text{-}CO)(\mu\text{-}P,N,P',N'\text{-dmapm})]$. However, instability of the complex was believed to result from the substantial lability of the *N*,*N*-dimethylamino donors of the dmapm ligand. We thought that substituting dmapm by mapm within such a bimetallic complex might better stabilize the soft metal combination by providing less labile *N*-methylamino donors. However, an attempt to synthesize the heterobinuclear complex, $[RhRuCl(CO)_3(\mu\text{-}CO)(\mu\text{-}P,N,P',N'\text{-mapm})]$, from **6b** and 0.5 equiv of [RhCl(μ-

Cl)$(CO)_2]_2$ reveals a number of products by $^{31}P\{^1H\}$ NMR, which curiously includes the previously reported dirhodium species, $[Rh_2Cl_2(CO)_2$(μ-*P*,*N*,*P'*,*N'*-mapm)].[22]

3.4 Conclusions

A number of coordination modes for *ortho*-phosphinoaniline ligands at ruthenium have been reported herein and, as was previously described in related Rh chemistry,[22] the *N*-methyl and *N*,*N*-dimethyl analogues can give rise to rather different chemistries. For example, a comparison of the reactivities of the monophosphinoaniline ligands, Ph_2PAr and Ph_2PAr' (Ar = *o*-C_6H_4NHMe; Ar' = *o*-$C_6H_4NMe_2$) with $[RuCl(\mu\text{-}Cl)(\eta^6\text{-}p\text{-cymene})]_2$ (**1**), illustrates that the degree of *N*-methyl substitution on the ligand influences the barrier to amine coordination. While the *N*,*N*-dimethyl complex, $[RuCl_2(\eta^6\text{-}p\text{-cymene})(P\text{-}Ph_2PAr')]$ (**3a**), rapidly undergoes amine coordination under mild conditions to afford the *P*,*N*-chelated $[RuCl(\eta^6\text{-}p\text{-cymene})(P,N\text{-}Ph_2PAr')]Cl$ (**3b**), the *N*-methyl analogue, $[RuCl_2(\eta^6\text{-}p\text{-cymene})(P\text{-}Ph_2PAr)]$ (**2a**), is stabilized by intramolecular hydrogen bonding in the monodentate *P*-coordinated isomer and requires kinetic assistance from a protic solvent to promote formation of the *P*,*N*-chelate, $[RuCl(\eta^6\text{-}p\text{-cymene})(P,N\text{-}Ph_2PAr)]Cl$ (**2b**). Compound **2b** can be deprotonated to yield the amido complex, $[RuCl(\eta^6\text{-}p\text{-cymene})(P,N\text{-}Ph_2PAr^-)]$ (**2c**), which appears to undergo enantiomerization in solution, presumably through the coordinatively unsaturated species, $[Ru(\eta^6\text{-}p\text{-cymene})(P,N\text{-}Ph_2PAr^-)]Cl$ (**2d**). Although **2c** has been shown to act as a ketone transfer hydrogenation catalyst, the mechanism remains unclear. The role played by the amido-hydrido complex $[RuH(\eta^6\text{-}p\text{-cymene})(P,N\text{-}Ph_2PAr^-)]$ in ketone transfer hydrogenation catalysis by **2c** will be addressed in Chapter 4 of this thesis.

Highly diverse coordination chemistry was observed using the related diphosphine ligands $Ar'_2PCH_2PAr'_2$ (dmapm) and $Ar_2PCH_2PAr_2$ (mapm). Whereas the dmapm ligand reacted with **1** to give the *P*,*P'*-chelate, [RuCl(η^6-*p*-cymene)(*P*,*P'*-dmapm)]Cl (**4**), in which all dimethylanilinyl groups remained pendent, mapm reacted by displacement of the *p*-cymene group to give [$RuCl_2$(*P*,*P'*,*N*,*N'*-mapm)] (**5**) in which both phosphorus and two of the *N*-methylanilinyl groups are bonded to Ru, giving an unprecedented coordination mode for the ligand. Complex **4** is believed to undergo an isomerization between a C_s-symmetric *P*,*P'*-chelate and a yet unidentified species in solution while complex **5**, which exhibits a *P*,*P'*,*N*,*N'*-chelation mode, is prepared as a mixture of stereoisomers. Starting from the Ru(0) precursor, [$Ru(CO)_4(\eta^2$-$C_2H_4)$], the pendent chelate complex [$Ru(CO)_4$(*P*-mapm)] (**6a**) results from displacement of ethylene by mapm which, upon exposure to ambient light for an extended period, is eventually converted to **6b** via photodissociation of CO. Our attempts to prepare binuclear complexes of ruthenium bridged by the diphosphinoanilines, although unsuccessful, have resulted in the generation of the trinuclear compound [$Ru_3(CO)_{10}$(μ-*P*,*P'*-mapm)] (**7**). None of the complexes **6a**, **6b** nor **7** are found to possess coordinated aniline donors and our attempts to displace carbonyl functionalities from compound **7**, to cleanly generate complexes stabilized by coordinated amines, were unsuccessful, presumably reflecting the lack of affinity of the soft Ru(0) center for the hard amine groups. Nevertheless, the pendent amines of complexes **6b** and **7** serve as potential stabilizing functionalities in the event of coordinative unsaturation at the metal centers. Although the trinuclear dmapm complex, [$Ru_3(CO)_{10}$(μ-*P*,*P'*-dmapm)], analogous to **7**, has not yet been synthesized, it can presumably be prepared in an analogous manner since amine coordination does not seem to have an influence on diphosphinoaniline reactivity with ruthenium carbonyl complexes.

3.5 References

1) Braunstein, P.; Naud, F. *Angew. Chem., Int. Ed.* **2001**, *40*, 680 – 699.

2) Slone, C. S.; Weinberger, D. A.; Mirkin, C. A. *Prog. Inorg. Chem.* **1999**, *48*, 233 – 350.

3) Werner, H. *Dalton Trans.* **2003**, 3829 – 3837.

4) Lindner, E.; Pautz, S.; Haustein, M. *Coord. Chem. Rev.* **1996**, *155*, 145 – 162.

5) Espinet, P.; Soulantica, K. *Coord. Chem. Rev.* **1999**, *193 – 195*, 499 – 556.

6) Guiry, P. J.; Saunders, C. P. *Adv. Synth. Catal.* **2004**, *346*, 497 – 537.

7) Jeffrey, J. C.; Rauchfuss, T. B. *Inorg. Chem.* **1979**, *18*, 2658 – 2666.

8) Dabb. S. L.; Messerle, B. A.; Smith, M. K.; Willis, A. C. *Inorg. Chem.* **2008**, *47*, 3034 – 3044.

9) Ziessel, R.; Toupet, L.; Chardon-Noblat, S.; Deronzier, A.; Matt, D. *J. Chem. Soc., Dalton Trans.* **1997**, 3777 – 3784.

10) Costella, L.; Del Zotto, A.; Mezzetti, A.; Zangrando, E.; Rigo, P. *J. Chem. Soc., Dalton Trans.* **1993**, 3001 – 3008.

11) Braunstein, P.; Graiff, C.; Naud. F.; Pfaltz, A.; Tiripicchio, A. *Inorg. Chem.* **2000**, *39*, 4468 – 4475.

12) Yang, H.; Alvarez-Gressier, M.; Lugan, N.; Mathieu, R. *Organometallics* **1997**, *16*, 1401 – 1409.

13) Dahlenburg, L.; Kühnlein, C. *J. Organomet. Chem.* **2005**, *690*, 1 – 13.

14) Braunstein, P.; Naud, F.; Rettig, S. J. *New J. Chem.* **2001**, *25*, 32 – 39.

15) Rahman, M. S.; Prince, P. D.; Steed, J. W.; Hii, K. K. *Organometallics* **2002**, *21*, 4927 – 4933.

16) Bacchi, A.; Balordi, M.; Cammi, R.; Elviri, L.; Pelizzi, C.; Picchioni, F.; Verdolino, V.; Goubitz, K.; Peschar, R.; Pelagatti, P. *Eur. J. Inorg. Chem.* **2008**, 4462 – 4473.

17) Moreno, M. A.; Haukka, M.; Jääskeläinen, S.; Vuoti, S.; Pursiainen, J.; Pakkanen, T. A. *J. Organomet. Chem.* **2005**, *690*, 3803 – 3814.

18) Drommi, D.; Nicolò, F.; Arena, C. G.; Bruno, G.; Faraone, F.; Gobetto, R.

Inorg. Chim. Acta **1994**, *221*, 109 – 116.

19) Zhu, G.; Terry, M.; Zhang, X. *J. Organomet. Chem.* **1997**, *547*, 97 – 101.

20) Tuttle, T.; Wang, D.; Thiel, W.; Köhler, J.; Hofmann, M.; Weis, J. *Dalton Trans.* **2009**, 5894 – 5901.

21) Slugovc, C.; Doberer, D.; Gemel, C.; Schmid, R.; Kirchner, K.; Winkler, B.; Stelzer, F. *Monatsh. F. Chem.* **1998**, *129*, 221 – 233.

22) Hounjet, L. J.; Bierenstiel, M.; Ferguson, M. J.; McDonald, R.; Cowie, M. *Dalton Trans.* **2009**, 4213 – 4226.

23) Clapham, S. E.; Hadzovic, A.; Morris, R. H. *Coord. Chem. Rev.* **2004**, *248*, 2201 – 2237.

24) (a) Noyori, R.; Ohkuma, T. *Angew. Chem. Int. Ed.* **2001**, *40*, 40 – 73. (b) Haack, K.-J.; Hashiguchi, S.; Fujii, A.; Ikariya, T.; Noyori, R. *Angew. Chem., Int. Ed. Engl.* **1997**, *36*, 285 – 288. (c) Yamakawa, M.; Ito, H.; Noyori, R. *J. Am. Chem. Soc.* **2000**, *122*, 1466 – 1478.

25) Lundgren, R. J.; Stradiotto, M. *Chem. – Eur. J.* **2008**, *14*, 10388 – 10395.

26) Lundgren, R. J.; Rankin, M. A.; McDonald, R.; Schatte, G.; Stradiotto, M. *Angew. Chem., Int. Ed.* **2007**, *46*, 4732 – 4735.

27) Standfest-Hauser, C.; Slugovc, C.; Mereiter, K.; Schmid, R.; Kirchner, K.; Xiao, L.; Weissensteiner, W. *J. Chem. Soc. Dalton Trans.* **2001**, 2989 – 2995.

28) (a) Renfrew, A. K.; Phillips, A. D.; Egger, A. E.; Hartinger, C. G.; Bosquain, S. S.; Nazarov, A. A.; Keppler, B. K.; Gonsalvi, L.; Peruzzini, M.; Dyson, P. J. *Organometallics* **2009**, *28*, 1165 – 1172. (b) Bugarcic, T.; Habtemariam, A.; Deeth, R. J.; Fabbiani, F. P. A.; Parsons, S.; Sadler, P. J. *Inorg. Chem.* **2009**, *48*, 9444 – 9453.

29) Fritz, H. P.; Gordon, I. R.; Schwarzhans, K. E.; Venanzi, L. M. *J. Chem. Soc.* **1965**, 5210 – 5216.

30) Jones, N. D.; Meessen, P.; Smith, M. B.; Losehand, U.; Rettig, S. J.; Patrick, B. O.; James, B. R. *Can. J. Chem.* **2002**, *80*, 1600 – 1606.

31) Cooke, J.; Berry, D. E.; Fawkes, K. L. *J. Chem. Educ.* **2007**, *84*, 115 – 118.

32) Programs for diffractometer operation, unit cell indexing, data collection, data reduction and absorption correction were those supplied by Bruker.

33) Beurskens, P. T.; Beurskens, G.; de Gelder, R.; Smits, J. M. M; Garcia-Granda, S.; Gould, R. O. (2008). The *DIRDIF-2008* program system. Crystallography Laboratory, Radboud University Nijmegen, The Netherlands.

34) Sheldrick, G. M. *Acta Crystallogr*. **2008**, *A64*, 112 – 122.

35) Altomare, A.; Burla, M. C.; Camalli, M.; Cascarano, G. L.; Giacovazzo, C.; Guagliardi, A.; Moliterni, A. G. G.; Polidori, G.; Spagna, R. *J. Appl. Cryst.* **1999**, *32*, 115 – 119.

36) Zefirov, Y. V.; Zorkii, P. M. *Russ. Chem. Rev*. **1989**, *58*, 421 – 440.

37) Arena, C. G.; Calamia, S.; Faraone, F.; Graiff, C. and Tiripicchio, A. *J. Chem. Soc., Dalton Trans.* **2000**, 3149 – 3157.

38) Garrou, P. E. *Chem. Rev*. **1981**, *81*, 229.

39) Bain, A. D. *Prog. Nucl. Magn. Reson. Spectrosc*. **2003**, *43*, 63 – 103.

40) Jia, W.; Chen, X.; Guo, R.; Sui-Seng, C.; Amoroso, D.; Lough, A. J.; Abdur-Rashid, K. *Dalton Trans.* **2009**, 8301 – 8307.

41) Rauchfuss, T. B.; Patino F. T.; Roundhill, M. *Inorg. Chem*. **1975**, *14*, 652 – 656.

42) Vinzi, F.; Zassinovich, G.; Mestroni, G. *J. Mol. Catal*. **1983**, *18*, 359 – 366.

43) (a) Meerwein, H.; Schmidt, R. *Justus Liebigs Ann. Chem*. **1925**, *444*, 221. (b) Ponndorf, W. *Z. Angew. Chem*. **1926**, *39*, 138. (c) Verley, A. *Bull. Chem. Soc. Chim. Fr*. **1925**, *37*, 537. (d) Oppenauer, R. V. *Recl. Trav. Chim. Pays-Bas* **1937**, *56*, 137. (e) Wilds, A. L. *Org. React*. **1944**, *2*, 178. (f) Djerassi, C. *Org. React.* **1951**, *6*, 207.

44) Jensen, S. B.; Rodger, S. J.; Spicer, M. D. *J. Organomet. Chem*. **1998**, *556*, 151 – 158.

45) Dennett, J. N. L.; Bierenstiel, M.; Ferguson, M. J.; McDonald, R.; Cowie, M. *Inorg. Chem*. **2006**, *45*, 3705 – 3717.

46) Murray, K. S.; van den Bergen, A. M.; West, B. O. *Aust. J. Chem*. **1978**, *31*, 203 – 207.

47) Kiel, G.-Y.; Takats, J. *Organometallics* **1989**, *8*, 839 – 840.

48) Cotton, F. A.; Hanson, B. E. *Inorg. Chem*. **1977**, *16*, 3369 – 3371.

Chapter 4: Phosphine-Amido Complexes of Ruthenium: Mechanistic Implications for Ketone Transfer Hydrogenation Catalysis

4.1 Introduction

The transfer hydrogenation of ketones represents a useful means of producing value-added alcohols under relatively benign conditions and many effective catalytic systems have been developed involving phosphorus- and nitrogen-ligated ruthenium complexes.[1–5] Transition metal-catalyzed reactions have traditionally relied on the inclusion of a strong base in reaction mixtures, either to activate the metal-containing precatalyst or to play a more direct role as a cocatalyst.[6]

The two mechanisms most commonly involved in the transfer hydrogenation of ketones are the "inner-" and "outer-sphere" cycles. During an "inner-sphere" mechanism (Scheme 4.1, left cycle), the reagent ketone

Scheme 4.1. Inner- (Left Cycle) and Outer-Sphere (Right Cycle) Mechanisms of Transfer Hydrogenation. The reaction of acetophenone with ^{i}PrOH occurs upon the addition of base (^{t}BuOK) to a metal halide precatalyst.

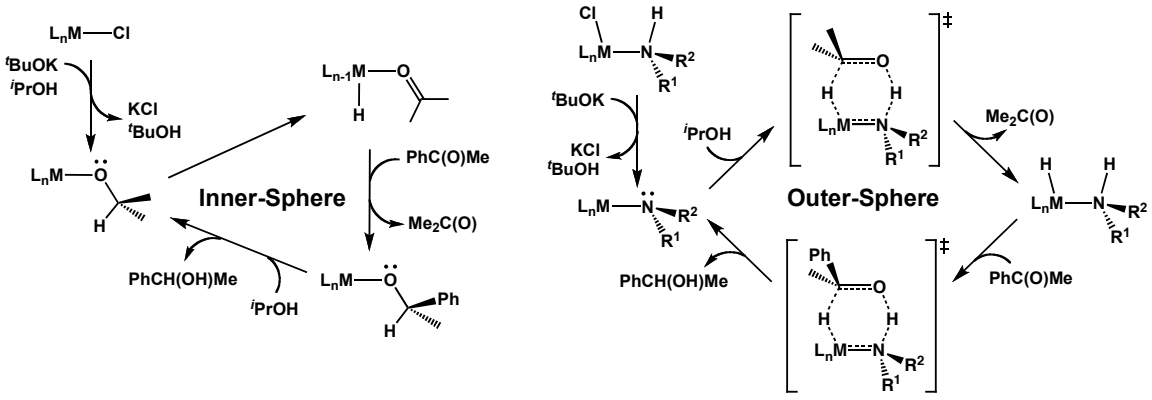

(acetophenone in the example shown) can insert into an M–H bond (generated by β-hydride elimination from the isopropoxo group) with concomitant elimination

of acetone, to form a new alkoxide, which is then protonated by the incoming reagent alcohol, releasing the product alcohol from the metal. In the outer-sphere mechanism, initially proposed by Noyori,[1] the inclusion of a strongly basic amido ligand within ruthenium-containing catalysts can allow for deprotonation of the alcohol (^{i}PrOH in this example) by the nucleophilic nitrogen donor with simultaneous hydride transfer to the adjacent metal atom via a highly ordered transition state (Scheme 4.1, right cycle). Transfer of the protic and hydridic hydrogens from the amine and metal to the polar substrate (acetophenone) then generates the product alcohol. In this case, the non-innocent amido ligand renders the catalyst exceptionally reactive without requiring the use of an external base in reaction media.[1]

A less common mechanism, that is proposed for Al- and Sn-catalyzed processes, but is rarely mentioned in the context of late-metal systems is the Meerwein-Ponndorf-Verley-Oppenauer (MPVO) mechanism (Scheme 4.2). [7,8] In this case, the metal center can act as a scaffold upon which the alkoxide (again, produced by adding base to the reaction mixture) can transfer its hydride directly to the nucleophilic carbonyl functionality of a coordinated ketone, thereby avoiding the intermediacy of a hydrido complex.

Scheme 4.2. MPVO Mechanism of Transfer Hydrogenation.

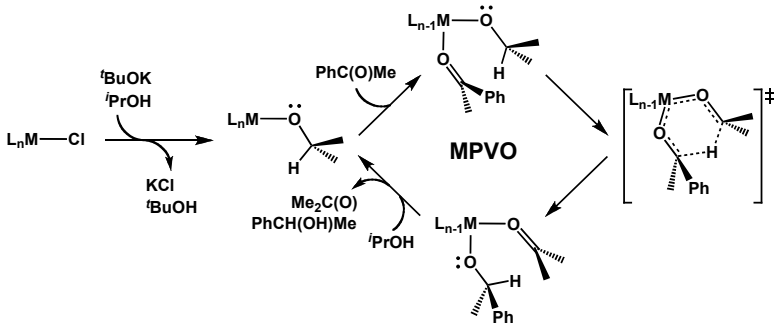

Although most transfer hydrogenation reactions catalyzed by late-metal complexes can be rationalized on the basis of inner- or outer-sphere mechanisms, one possible exception is Stradiotto's highly active zwitterionic catalyst, [RuCl(η^6-*p*-cymene)(*P*,*N*-(1)-P^{i}Pr$_2$-(2)-NMe$_2$-C$_9$H$_5^-$)],[9] for which neither

mechanism seems applicable. Previously, we showed that an *ortho*-phosphinoanilido complex of ruthenium, not unlike Stradiotto's catalyst, functions as a moderately active ketone transfer hydrogenation catalyst in the presence of base.[10] The necessity for base in conjunction with our amido catalyst ruled out an outer-sphere mechanism, but at the time, we did not investigate this further. In the current work, we highlight new evidence that also discounts an inner-sphere process as the catalytically dominant pathway and discuss the possible operation of the less explored (MPVO) alternative.

4.2 Experimental

4.2.1 General Comments

All solvents were deoxygenated, dried (using appropriate drying agents), distilled before use, and stored under nitrogen. All reactions were performed under an Ar atmosphere using standard Schlenk techniques. Isopropanol (^{i}PrOH; > 99%, distilled over Mg turnings and stored under Ar), and acetophenone (99%, deoxygenated and stored under Ar over 5 Å molecular sieves), used for transfer hydrogenation catalysis, as well as ethylmagnesium bromide (EtMgBr; 3.0 M in diethyl ether) and lithium triethylborohydride (Li[$HBEt_3$]; 1.0 M in tetrahydrofuran) were purchased from Aldrich. Sodium borohydride ($NaBH_4$; 98 %) was purchased from Strem Chemicals. The complex, [RuCl(η^6-*p*-cymene)(*P*,*N*-Ph_2PAr^-)] (**1**, Ar^- = $C_6H_4NMe^-$), was prepared as previously reported.[10] NMR spectra were recorded on Varian Inova-400, -500 or Varian Unity-500 spectrometers operating at 399.8, 498.1 or 499.8 MHz, respectively, for ^{1}H, at 161.8, 201.6 or 202.3 MHz, respectively for ^{31}P and at 100.6, 125.3 or 125.7 MHz, respectively, for ^{13}C nuclei. *J* values are given in hertz (Hz). Overlapping or unresolved aromatic signals, observed in the typical 6 – 8 ppm range in the ^{1}H NMR spectrum, and found between 80 – 120 ppm in the ^{13}C{^{1}H} NMR spectrum, are not reported. Spectroscopic data for complexes **2** and **3** are

provided in Table 4.1. Elemental analyses were performed by the Microanalytical Laboratory within the Department.

Table 4.1. $^{31}P\{^1H\}$, ^1H and $^{13}C\{^1H\}$ NMR Data for Ruthenium Compounds[a]

Compound	$\delta(^{31}P\{^1H\})$/ppm[b]	$\delta(^1H)$/ppm[c]	$\delta(^{13}C\{^1H\})$/ppm[c]
[RuH(η^6-*p*-cymene)(*P*,*N*-Ph_2PAr^-)] (**2**)	70.1 (s)	NCH_3: 3.30 (s, 3H) CH(CH_3)$_2$: 2.15 (sept, $^3J_{HH}$ = 6.8 Hz, 1H) ArCH_3:1.56 (s, 3H) CH(CH_3)$_2$: 1.06 (d, $^3J_{HH}$ = 6.8 Hz, 3H), 1.04 (d, $^3J_{HH}$ = 6.8 Hz, 3H) RuH: –7.96 (d, $^2J_{PH}$ = 46.5 Hz, 1H)	NCH$_3$: 48.9 (s) CH(CH$_3$)$_2$: 32.3 (s) CH(CH$_3$)$_2$: 24.1 (s), 23.6 (s) ArCH$_3$: 19.0 (s)
[RuEt(η^6-*p*-cymene)(*P*,*N*-Ph_2PAr^-)] (**3**)	68.7 (s)	NCH_3: 3.26 (s, 3H) CH(CH_3)$_2$: 2.13 (sept, $^3J_{HH}$ = 6.8 Hz, 1H) ArCH_3: 1.68 (s, 3H) CH_2CH_3: 1.38 (pt, $^3J_{HH}$ = 7.5 Hz, 3H) CH_2CH_3: 1.10 (m, 1H), 0.80 (m, 1H) CH(CH_3)$_2$: 0.96 (d, $^3J_{HH}$ = 6.8 Hz, 3H), 0.94 (d, $^3J_{HH}$ = 6.8 Hz, 3H)	NCH$_3$: 48.3 (s) CH(CH$_3$)$_2$: 31.6 (s) CH(CH$_3$)$_2$: 24.2 (s), 22.6 (s) CH_2CH_3: 23.4 (d, $^3J_{PC}$ = 4 Hz) ArCH$_3$: 17.5 (s) CH_2CH_3: 14.0 (d, $^2J_{PC}$ = 14 Hz)

[a] NMR abbreviations: s = singlet, d = doublet, t = triplet, m = multiplet, sept = septet, p = pseudo. NMR data recorded at 27°C in C_6D_6. [b] ^{31}P chemical shifts referenced to external 85% H_3PO_4. [c] ^1H and ^{13}C chemical shifts referenced to external tetramethylsilane. Chemical shifts for aryl groups not given.

4.2.2 Preparation of Metal Complexes

(a) Reaction of [RuCl(η^6-*p*-cymene)(*P*,*N*-Ph_2PAr^-)] (1) with Li[$HBEt_3$]. An NMR tube was charged with **1** (22 mg, 39 μmol), sealed with a septum, then evacuated and backfilled with Ar three times. The compound was dissolved in 0.7 mL of C_6D_6 producing a dark, burgundy solution and a 1.0 M solution of Li[$HBEt_3$] in tetrahydrofuran (42 μL, 42 μmol) was added via a microliter syringe, resulting in a red mixture that was left for several hours, allowing a white precipitate to settle from the bright red solution. The supernatant was transferred via cannula under Ar to a prepared NMR tube and the sample was then analyzed by ^1H and $^{31}P\{^1H\}$ NMR spectroscopy. The resulting spectra indicated the formation of two products, [RuH(η^6-*p*-cymene)(*P*,*N*-Ph_2PAr^-)] (**2**) and [RuEt(η^6-*p*-cymene)(*P*,*N*-Ph_2PAr^-)] (**3**) in approximately equal proportions as judged by the intensities of the only two ^{31}P signals observed (at δ 70.1 and 68.7; see Parts (b) and (c) for independent syntheses).

(b) Hydrido(η^6-*p*-cymene)(*P*,*N*-diphenyl(*o*-*N*-methylanilido)phosphine) ruthenium(II), [RuH(η^6-*p*-cymene)(*P*,*N*-Ph_2PAr^-)] (2). In a 25 mL Schlenk tube under anhydrous conditions and Ar atmosphere, [RuCl(η^6-*p*-cymene)(*P*,*N*-

Ph_2PAr^-)] (**1**; 177 mg, 315 μmol) and sodium borohydride (26 mg, 687 μmol) were dissolved in 10 mL of methanol while stirring. The mixture, which initially turned a blue-green color, turned dark red after 10 min, and was allowed to stir for a total of 30 min before removing the solvent *in vacuo*. Benzene (10 mL) was added to the remaining residue and the resultant slurry was stirred for 10 min before allowing the precipitate to settle. The supernatant was filtered through a Celite® plug and transferred to a prepared 50 mL Schlenk flask via cannula transfer under Ar. The solvent was removed *in vacuo* resulting in an amorphous, red residue (156 mg). Although a satisfactory elemental analysis could not be obtained for this compound, its NMR spectra (^{1}H NMR spectrum provided as Supporting Information) leave no doubt about its formulation.

(c) Ethyl(η^6-*p*-cymene)(*P*,*N*-diphenyl(*o*-*N*-methylanilido)phosphine) ruthenium(II), [RuEt(η^6-*p*-cymene)(*P*,*N*-Ph_2PAr^-)] (3). In a 50 mL Schlenk flask under anhydrous conditions and Ar atmosphere, **1** (84 mg, 149 μmol) was dissolved in 5 mL of benzene at ambient temperature and the solution was stirred for 5 min. Ethyl magnesium bromide (3.0 M in diethyl ether, 60 μL, 180 μmol) was added to the dark burgundy solution via syringe to produce a cloudy, red mixture, which was stirred for 5 min before removing the solvents *in vacuo*. While stirring, 10 mL of benzene was added to produce a cloudy, orange-red mixture that was then filtered through a Celite® plug in a micropipette (via Ar overpressure through a cannula) into a prepared 25 mL Schlenk tube. The solvent volume was reduced to approx 5 mL *in vacuo* and the red solution was layered with 10 mL of *n*-pentane and left undisturbed for 18 h. The supernatant was then removed via cannula and the red crystalline product was dried *in vacuo* (50 mg, 60% yield, found: C, 66.73; H, 6.68; N, 2.66%. Calcd for [$C_{31}H_{36}NPRu$]: C, 67.13; H, 6.54; N, 2.53%).

(d) Reactions of [RuCl(η^6-*p*-cymene)(*P*,*N*-Ph_2PAr^-)] (1) with Alkoxides. In a 50 mL Schlenk flask under anhydrous conditions and Ar atmosphere, **1** (50 mg, 89 μmol) was dissolved in 5 mL of benzene at ambient temperature with stirring.

In a 25 mL Schlenk flask, KOH (5 mg, 90 μmol) was dissolved in 5 mL of alcohol (either methanol or isopropanol) at ambient temparature with stirring and this solution was then transferred (via Ar overpressure through a cannula) to the solution of **1** and the mixture was stirred for 10 min at ambient temperature before removing the solvents *in vacuo*. Benzene (10 mL) was then added to the resulting dark red residue and the mixture was filtered through a Celite® plug in a micropipette (via Ar overpressure through a cannula) into a prepared 50 mL Schlenk flask. The solvent was removed *in vacuo* and the residue was dissolved in 1 mL of C_6D_6 and transferred to a prepared NMR tube via cannula. NMR spectra showed the exclusive formation of [RuH(η^6-*p*-cymene)(*P*,*N*-Ph_2PAr^-)] (**2**), when either alcohol (methanol or isopropanol) was used. Similar reactions performed using ^{t}BuOK rather than KOH as the base yielded identical spectroscopic observations.

4.2.3 Ketone Transfer Hydrogenation Experiment

In a 50 mL Schlenk flask under anhydrous conditions and Ar atmosphere, [RuCl(η^6-*p*-cymene)(*P*,*N*-Ph_2PAr^-)] (**1**; 50.0 mg, 89.0 μmol) and $NaBH_4$ (5.1 mg, 130 μmol) were dissolved in 7.0 mL of MeOH at ambient temperature and stirred for 15 min. The solvent was removed *in vacuo*, acetophenone (10.4 mL, 89.0 mmol) was added to the residue, and the cloudy, red mixture was stirred for 15 min. The precipitate (NaCl) was allowed to settle from the red solution and a 2.08 mL aliquot (17.8 μmol of **2** dissolved in 17.8 mmol acetophenone) was withdrawn via Gastight® syringe and transferred to a prepared 50 mL three-necked, round-bottom flask equipped with a 0.5" stir bar and attached reflux condenser through which an Ar overpressure was applied. While stirring, the solution was heated to 90 °C for 10 min. A solution of ^{t}BuOK (8.0 mg, 71.3 μmol) in ^{i}PrOH (13.6 mL, 178 mmol) was then added via cannula transfer under Ar. A 1.0 mL aliquot of the reaction mixture was immediately withdrawn and passed through a column containing 2 cm of acidic alumina atop 2 cm of Florisil® and collected in a vial so that less than 30 s elapsed between removal of the sample from the mixture and removal of catalyst from the sample. The vial was

then capped and stored at 0 °C until the mixture could be analyzed by NMR spectroscopy and GC-EI-MS. Aliquots were withdrawn and treated as described above at 5, 60 and 120 min relative to the addition of ^{i}PrOH and ^{t}BuOK.

4.2.4 X-Ray Structure Determination

Data were collected using Mo Kα radiation ($\lambda = 0.71073$ Å) on a Bruker APEX-II CCD detector/D8 diffractometer[11] with the crystal of **3** cooled to –100 °C. The data were corrected for absorption through Gaussian integration from indexing of the crystal faces. The structure was solved using direct methods (*SHELXS–97*).[11] Refinements were completed using the program *SHELXL-97*.[12] Hydrogen atoms were assigned positions based on the sp^2 or sp^3 hybridization geometries of their attached carbon atoms, and were given thermal parameters 20% greater than those of their parent atoms. A summary of the crystallographic experimental details for [RuEt(η^6-*p*-cymene)(*P*,*N*-Ph_2PAr^-)] (**3**) is provided in Table 4.2.

Table 4.2. Crystallographic Experimental Details for Compound **3**

Formula	$C_{31}H_{36}NPRu$
Formula Weight	554.65
Crystal Dimensions (mm)	0.60 × 0.22 × 0.12
Crystal System	monoclinic
Space Group	$P2_1/n$ (an alternate setting of $P2_1/c$ [No. 14])
a (Å)	9.8986 (12)
b (Å)	18.572 (2)
c (Å)	14.3074 (18)
β (deg)	94.1510 (10)
V (Å^3)	2623.3 (6)
Z	4
ρ_{calcd} (g cm^{-3})	1.404
μ (mm^{-1})	0.678
Data Collection 2θ Limit (deg)	55.54
Total Data Collected	22472 ($-12 \le h \le 12$, $-24 \le k \le 24$, $-18 \le l \le 18$)
Independent Reflections	6117 ($R_{int} = 0.0382$)
Number of Observed Reflections (*NO*)	5315 [$F_o^2 \ge 2\sigma(F_o^2)$]
Restraints/Parameters	0 / 308
Goodness-of-Fit (*S*)[a] [All Data]	1.042
R_1 [$F_o^2 \ge 2\sigma(F_o^2)$][b]	0.0299
wR_2 [All Data][c]	0.0791
Largest Difference Peak and Hole	1.053 and –0.714 e Å^{-3}

[a] $S = [\Sigma w(F_o^2 - F_c^2)^2/(n-p)]^{1/2}$ (n = number of data; p = number of parameters varied; $w = [\sigma^2 (F_o^2) + (0.0433P)^2 + 1.3930P]^{-1}$ where $P = [\text{Max}(F_o^2, 0) + 2F_c^2]/3$). [b] $R_1 = \Sigma||F_o| - |F_c||/\Sigma|F_o|$. [c] $wR_2 = [\Sigma w(F_o^2 - F_c^2)^2/\Sigma w(F_o^4)]^{1/2}$.

4.3 Results and Discussion

In earlier work, we reported that the phosphine-amido complex [RuCl(η^6-*p*-cymene)(*P*,*N*-Ph_2PAr^-)] (**1**; Ar^- = *o*-$C_6H_4NMe^-$) functions as a ketone transfer hydrogenation catalyst and found that the reaction occurred only in the presence of ^{t}BuOK.[10] This observation eliminated the possibility of an "outer-sphere," hydrogenation mechanism that should operate in the absence of base by catalytic involvement of the amido donor.[1] We speculated that the active catalyst may form by β-hydride elimination from a coordinated alkoxide to produce the hydrido complex, [RuH(η^6-*p*-cymene)(*P*,*N*-Ph_2PAr^-)] (**2**, Scheme 4.3). In the present study, we set out to attempt to determine the role of base in the transfer hydrogenation reaction and to establish whether or not **2** is a catalytically relevant intermediate.

Scheme 4.3. Synthesis of Hydrido (**2**) and Ethyl (**3**) Compounds

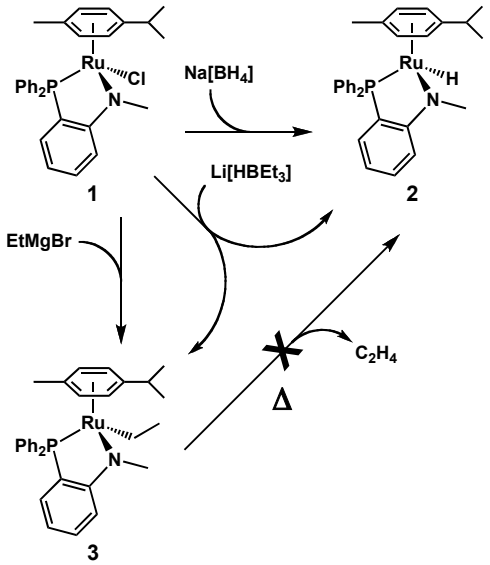

Attempts to prepare this hydride species by reacting compound **1** with 1 equiv of Li[$HBEt_3$] under ambient conditions in C_6D_6, led to the formation of two compounds in approximately equimolar quantities; in addition to the targeted hydride (**2**), the ethyl product, [RuEt(η^6-*p*-cymene)(*P*,*N*-Ph_2PAr^-)] (**3**), was also obtained. Ethyl transfer from superhydride to ruthenium has previously been

demonstrated in similar systems.[13,14] Each compound can be prepared independently as the sole product by reaction of **1**, either with $NaBH_4$ in methanol to give the hydride (**2**) or with EtMgBr in benzene to give the ethyl species (**3**), as outlined in Scheme 4.3.

Compound **2** is represented by a signal at δ 70.1 in the $^{31}P\{^1H\}$ NMR spectrum while the hydride signal is found at δ –7.96 in the ^1H spectrum as a doublet with $^2J_{PH}$ = 46.5 Hz (see Supporting Information). All other proton resonances are similar to those of the precursor chloro species (**1**) and are fully consistent with the proposed geometry. Compound **3** shows a slightly more upfield chemical shift in the $^{31}P\{^1H\}$ NMR spectrum at δ 68.7 and the ^1H spectrum shows three resonances for the ethyl ligand with a pseudo-triplet at δ 1.38 ($^3J_{HH}$ = 7.5 Hz) representing the methyl group and two multiplets at δ 1.10 and 0.80 representing the diastereotopic protons of the methylene unit. Compound **2** decomposes in CD_2Cl_2, reverting predominantly to **1** (among other unidentified species) with concomitant production of CHD_2Cl (as made evident by a pentet signal at δ 3.06 in the ^1H NMR spectrum) equal to the amount of **1** regenerated.

Unfortunately, numerous attempts to purify and isolate **2** as an analytically pure solid were unsuccessful since **2** is quite unstable. For example, attempts to crystallize the complex from dark red (nearly black) benzene solutions using *n*-pentane, while employing our best efforts to provide completely inert conditions, produced a pale green (almost white) precipitate that was much less soluble in benzene, the NMR spectra for which reveal decomposition to numerous unidentified species. However, a benzene solution of **2** handled under strictly inert conditions could be concentrated *in vacuo* to a dark, red, amorphous residue, then quickly redissolved in anhydrous acetophenone and ^{i}PrOH, in which the compound is stable, allowing us to study its capabilities as a catalyst.

While attempts to crystallize complex **2** were unsuccessful, compound **3**, which is also highly air-sensitive, can be easily isolated as large, red crystals by

layering a saturated benzene solution with *n*-pentane. A crystallographic analysis of **3** (Figure 4.1) shows the chelating phosphine-amido ligand having the

Figure 4.1. ORTEP Diagram of [RuEt(η^6-*p*-cymene)(*P*,*N*-Ph_2PAr^-)] (**3**). Gaussian ellipsoids for all non-hydrogen atoms are depicted at the 20% probability level. Hydrogen atoms are shown with arbitrarily small thermal parameters for the methyl, methylene and methine groups, and are not shown for the aryl rings.

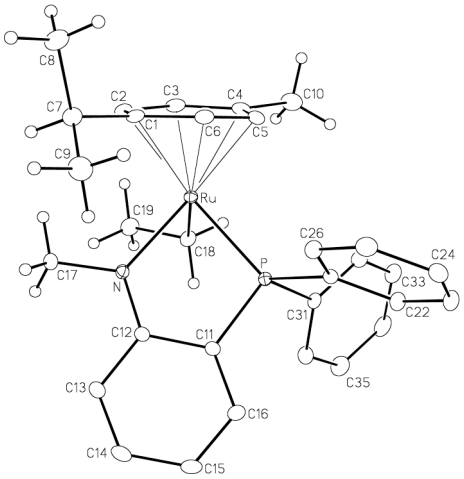

characteristic planar geometry of the amido group[15] as demonstrated by the sum of the angles at nitrogen (359.7°). The ethyl group appears normal and the lack of a β-agostic interaction, made evident by the expanded Ru–C(18)–C(19) angle (114.7(2)°, Table 4.3) and the Ru···H separation of greater than 3.2 Å, illustrates its κ^1-geometry in the solid state and is consistent with coordinative saturation of

Table 4.3. Selected Structural Parameters for Compound **3**

Atoms	Bond Lengths (Å)
Ru–P	2.2837(6)
Ru–N	2.102(2)
Ru–C(1)	2.319(2)
Ru–C(2)	2.261(2)
Ru–C(3)	2.238(2)
Ru–C(4)	2.228(2)
Ru–C(5)	2.186(2)
Ru–C(6)	2.321(2)
Ru–C(18)	2.154(2)
N–C(12)	1.348(2)
C(11)–C(12)	1.430(3)
C(12)–C(13)	1.430(3)
C(13)–C(14)	1.378(3)
C(14)–C(15)	1.394(3)
C(15)–C(16)	1.387(3)
C(11)–C(16)	1.397(3)
Atoms	**Angles (°)**
P–Ru–N	81.30(5)
P–Ru–C(18)	82.97(6)
N–Ru–C(18)	82.52(8)
Ru–C(18)–C(19)	114.7(2)

the complex. The length of the Ru–C(18) bond (2.154(2) Å) appears normal, being comparable to the Ru–C distances within [RuEt(η^6-C_6Me_6)(*S*,*S*'-N(P(^{i}Pr)$_2$S)$_2$] (2.133(3) Å)[13] and [RuEt$_2$((5,5'-^{t}Bu)$_2$-2,2'-Bipy)$_2$] (2.138(7) and 2.142(8) Å).[16] The Ru–N distance (2.102(2) Å) is longer than that within the coordinatively unsaturated anilido-containing complex, [RuH(PPh_3)(*P*,*N*,*N*'-$Ph_2PCH_2P(Ph_2)$=N-(*o*)-$C_6H_4NH^-$)] (2.031(2) Å)[17] suggesting that the presence of the larger *N*-methyl group within our hexacoordinate complex may slightly hinder coordination of the amido nitrogen. This suggestion is supported by the structural parameters for **3**, which show that repulsion between the *p*-cymene isopropyl and amido methyl groups results, not only in the somewhat elongated Ru–N bond, but also in the unsymmetrical binding of the *p*-cymene ligand, in which the Ru–C(1) and Ru–C(6) distances (2.319(2) and 2.321(2) Å, respectively), adjacent to the isopropyl group, are elongated compared with the other Ru–C_{cymene} distances (2.186(2) – 2.261(2) Å). Nevertheless, the Ru–N bond in **3** is still shorter than that within the related phosphine-amine complex, [RuCl(η^6-*p*-cymene)(*P*,*N*-Ph_2PAr)]Cl (2.172(2) Å),[10] consistent with this anionic amido group functioning as a better donor than the amine, and also possibly reflecting some degree of π-donor character to ruthenium by the amido lone pair. It is also noteworthy that the nitrogen-arene bond length within amido complex **3** (N–C(12) = 1.348(2) Å) is much shorter than that within the amine compound [RuCl(η^6-*p*-cymene)(*P*,*N*-Ph_2PAr)]Cl (N–C(12) = 1.458(4) Å),[10] suggesting additional delocalization of the amido lone pair onto the aromatic ring. This proposed resonance delocalization of the lone pair in **3** is further illustrated by elongation of the aromatic C–C bonds involving the carbon atom *ipso* to nitrogen (C(11)–C(12) and C(12)–C(13) = 1.430(3) Å) compared to other C–C bonds within the same group (*ca.* 1.39 Å) or adjacent phenyl groups (*ca.* 1.39 Å). The delocalization of the amido lone pair onto the aryl ring has been previously noted in a related series of phosphine-amido complexes of Rh and was proposed to rationalize the low basicity of the amido nitrogen in these species.[15] A comparison with the structure of **1**[10] shows the same trend in amido-aryl bond lengths and presumably is one reason that this species does not undergo transfer hydrogenation via an outer-sphere mechanism.

Under strictly inert conditions, compound **3** displays remarkable stability, even in refluxing benzene. This species' apparent resistance to β-hydride elimination inspired our attempts to prepare analogous alkoxo complexes, [Ru(OR)(η^6-*p*-cymene)(*P*,*N*-Ph_2PAr^-)] (R = ^{i}Pr or Me), which should be generated upon the addition of a base to **1** in alcohols. However, numerous attempts to prepare such derivatives by reactions of **1** with KOH in MeOH or with one or more equiv of ^{t}BuOK or ^{i}PrONa in ^{i}PrOH consistently reveal the presence of **2**, due to its apparent formation from the putative, but spectroscopically unobserved, target alkoxide intermediates, [Ru(OR)(η^6-*p*-cymene)(*P*,*N*-Ph_2PAr^-)]. Unfortunately, attempts to prepare an alkoxo complex, not having a β-hydride by reaction of **1** with 1 equiv of ^{t}BuOK in C_6D_6 in the absence of alcohol resulted in a complex mixture of products as made evident by $^{31}P\{^1H\}$ NMR analysis. Despite the stability of the ethyl derivative **3**, it appears that β-hydride elimination from isopropoxo and methoxo ligands of transient species, [Ru(OR)(η^6-*p*-cymene)(*P*,*N*-Ph_2PAr^-)] occurs (at least in the absence of reagent ketone) over the time it takes to carry out reactions and obtain NMR spectra. In this case, a classical β-hydride elimination from the coordinated alkoxide would require the generation of a vacant coordination site, either by ring slippage of the η^6-arene[18] or by dissociation of the phosphine donor, although it is difficult to rationalize why such processes should favor β-hydride elimination for an alkoxide, but not for the ethyl analogue **3**. However, Milstein *et al*. have offered another rationale for the apparent β-hydride elimination from a coordinatively saturated alkoxo complex. This proposal involves dissociation of the alkoxide from the metal, allowing for substrate alcohol to form a C–H σ-complex while the alkoxide anion is stabilized by exogenous alcohol. Subsequent hydride abstraction from the alcohol forms the Ru–H bond and a ketone.[19] In our case, the involvement of such an elimination process could explain the stability of the ethyl complex, which contains a relatively inert Ru–C bond. The dissociation of alkoxide anion from ruthenium is consistent with our earlier inference that chloro complex **1** undergoes enantiomerization in dichloromethane solution via chloride ion dissociation to form a coordinatively unsaturated intermediate.

A catalytic study of **2** showed its significantly reduced activity relative to that of its precursor (**1**) for acetophenone transfer hydrogenation in the presence of four catalytic equiv of ^{t}BuOK (see Table 4.4), with turnover frequencies an

Table 4.4. Transfer Hydrogenation of Acetophenone with Catalysts **1** and **2**

Entry	Complex	t_{rxn} (min)	Conversion (%)	TOF (h^{-1})
1[7]	**1**	5	13	1560
2[7]	**1**	60	34	340
3[7]	**1**	120	46	230
4	**2**	5	1	120
5	**2**	60	7	70
6	**2**	120	9	45

[a]Determined by GC and ^{1}H NMR analyses. [b]Turnover frequency determined at the corresponding reaction time (t_{rxn}) in column 4. [c] Reaction conditions: Temperature = 90 °C; Ru/^{t}BuOK/acetophenone/^{i}PrOH = 1 : 4 : 1,000 : 10,000.

order of magnitude less for the hydrido species (**2**) compared to the chloro precursor (**1**) in the presence of alkoxide ion. Such an observation suggests that the hydrido complex (**2**) may represent a means of catalyst deactivation, rather than the active species in the cycle involving **1**. Consistent with our observations, Stradiotto *et al.* have recently reported a catalyst system comprised of a zwitterionic indenyl species, [RuCl(η^6-*p*-cymene)(*P*,*N*-(1)-P^{i}Pr$_2$-(2)-NMe$_2$-C$_9$H$_5^-$)], that is catalytically active in the presence of base, and have also ruled out the involvement of the related hydrido complex, [RuH(η^6-*p*-cymene)(*P*,*N*-(1)-P^{i}Pr$_2$-(2)-NMe$_2$-C$_9$H$_5^-$)], in transfer hydrogenation reactions carried out under conditions similar to our own.[9] The fact that these hydrido complexes are not active in both cases indicates that an inner-sphere mechanism is not the catalytically dominant pathway (Scheme 4.1, left cycle). The catalytic dependence on external base also rules out the involvement of an outer-sphere mechanism for transfer hydrogenation.[10]

A remaining mechanistic possibility that deserves consideration is the Meerwein-Ponndorf-Verley-Oppenauer (MPVO)[2,7,8] pathway, in which an alkoxo ligand transfers its hydride directly to a coordinated ketone without the intermediacy of a metal-bound hydrogen atom (Scheme 4.2). In our case, an MPVO mechanism requires either dissociation of the phosphine donor from the (yet unobserved), coordinatively saturated isopropoxo complex, [Ru(^{i}PrO)(η^6-*p*-

cymene)(*P*,*N*-Ph_2PAr^-)], or ring slippage[18] of the η^6-*p*-cymene group, to generate a second vacant coordination site for complexation of substrate ketone. The latter possibility seems viable based on the crystallographically observed distortions of the coordinated arene in **3** (discussed above). In the event of coordinative unsaturation at this complex, binding of the *O*-donor substrate, acetophenone to Ru would give rise to mutually *cis* ketone and isopropoxo ligands, leading to direct hydride transfer from the isopropoxo ligand to the ketone. While the MPVO mechanism has been proposed to operate within transfer hydrogenation reactions catalyzed by tin[20] and aluminum[21] species, there is a lack of evidence supporting its involvement within ruthenium-catalyzed processes (although this possibility has been suggested by Morris *et al.*).[2]

The above requirement for coordinative unsaturation in the MPVO mechanism is troublesome in the context of the stability of the ethyl complex **3** since such unsaturation would presumably also result in facile β-H elimination from this species. However, given the requirement for base in reaction mixtures, and the possibility for stabilization of outer-sphere alkoxide by exogenous alcohol (or even potassium ions), a variant of the classical MPVO mechanism might involve replacement of the dissociated isopropoxide anion by acetophenone and subsequent direct hydride transfer from alkoxide to ketone via a six-membered transition state, diagrammed in Figure 4.2, without requiring a vacant coordination site at ruthenium.

Figure 4.2. Possible Variations of an MPVO Transition State

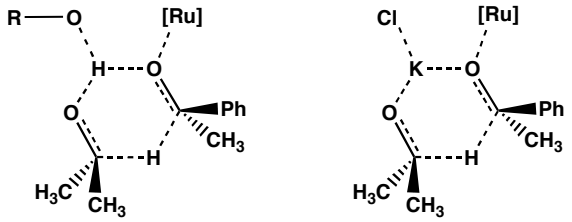

Noyori's diamido ruthenium catalyst, [Ru(η^6-*p*-cymene)(*N*,*N*-(*S*,*S*)-$TsDPEN^{2-}$)] (Figure 4.3), which operates in the absence of base, cannot be rationalized by an MPVO pathway based on the observation that its

enantioselectivity is not affected when a chiral hydrogen donor is used (during such a process, a chiral alkoxo ligand should promote enantioselective hydrogen

Figure 4.3. Noyori's Asymmetric Transfer Hydrogenation Catalyst

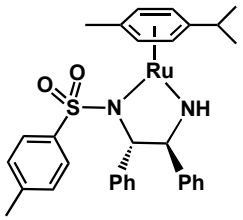

transfer to an adjacent prochiral ketone).[1,22] One might suggest conducting a similar experiment with our catalyst (**1**) using enantiomerically pure 2-butanol as the hydrogen donor and probing for enantiomeric excess as additional support for an MPVO mechanism. However, such an observation would fail to rule out an inner-sphere process since some degree of enantioselectivity should be expected for either pathway. Our chiral precatalyst (**1**) exists as a racemate, therefore, coordination of an enantiomerically pure alkoxide may favor one of two diastereoisomeric alkoxo complexes. In the case of an MPVO mechanism, the resulting stereochemical influence on a coordinated prochiral ketone is apparent. In the case of an inner-sphere mechanism, two energetically distinct β-hydride elimination pathways also exist, one of which may be more kinetically accessible, thereby favoring formation of one enantiomer of **2** over the other. The resulting stereochemical bias prevents us from discounting an inner-sphere mechanism based on the observation of an enantiomeric excess. However, in the case of Noyori's complex, the fact that enantioselectivity does not differ when either racemic or enantiomerically pure alcohols are used appears to rule out both inner-sphere and MPVO hydrogen transfer processes. A comparison of the catalytic features of complex **1** (containing a relatively inert amido functionality)[15] to those of Noyori's catalyst, shows how differences in the basicity of amido groups can influence their involvement during catalysis, resulting in entirely different reaction mechanisms.

4.4 Conclusion

Hydrido and ethyl derivatives of ruthenium complexes containing chelating phosphine-amido ligands have been prepared and characterized. The hydrido complex, [RuH(η^6-*p*-cymene)(*P*,*N*-Ph_2PAr^-)] (**2**) is found to be much less catalytically active than the analogous chloro complex (**1**) for the transfer hydrogenation of acetophenone with ^{i}PrOH in the presence of base, suggesting the role of a highly reactive, yet unobserved isopropoxo intermediate, analogous perhaps to the ethyl derivative, [RuEt(η^6-*p*-cymene)(*P*,*N*-Ph_2PAr^-)] (**3**). The reaction of **1** with Li[$HBEt_3$] provides an interesting example of carbon-boron bond activation (a fundamental process in Suzuki-Miyaura coupling reactions)[23] to afford an ethyl ruthenium complex.[13,14,16] The stability of **3**, in light of our observation that hydrido complex **2** is formed upon the addition of basic ^{i}PrOH to **1**, also provides support for the likely involvement of [Ru(^{i}PrO)(η^6-*p*-cymene)(*P*,*N*-Ph_2PAr^-)] in a catalytic mechanism. We have now ruled out the possibility of both traditional inner- and outer-sphere mechanisms for this reaction and have discussed the likelihood of an MPVO pathway or a variant thereof, the involvement of which in late-metal systems could be more prominent than previously thought.

4.5 References

1) Haack, K.-J.; Hashiguchi, S.; Fujii, A.; Ikariya, T.; Noyori, R. *Angew. Chem. Int. Ed. Engl.* **1997**, *36*, 285 – 288.

2) Clapham, S. E.; Hadzovic, A.; Morris, R. *Coord. Chem. Rev.* **2004**, *248*, 2201 – 2237.

3) Noyori, R. *Angew. Chem. Int. Ed.* **2002**, *41*, 2008 – 2022.

4) Ohkuma, T.; Hattori, T.; Ooka, H.; Inoue, T.; Noyori, R. *Org. Lett.* **2004**, *6*, 2681 – 2683.

5) Gao, J.-X.; Ikariya, T.; Noyori, R. *Organometallics* **1996**, *15*, 1087 – 1089.

6) (a) Noyori, R.; Ohkuma, T. *Angew. Chem., Int. Ed.* **2001**, *40*, 40 – 73. (b) Abdur-
Rashid, K.; Faatz, M.; Lough, A. J.; Morris, R. H. *J. Am. Chem. Soc.* **2001**, *123*, 7473 – 7474.

7) Vinzi, F.; Zassinovich, G.; Mestroni, G. *J. Mol. Catal.* **1983**, *18*, 359 – 366.

8) (a) Meerwein, H.; Schmidt, R. *Justus Liebigs Ann. Chem.* **1925**, *444*, 221. (b) Ponndorf, W. Z. *Angew. Chem.* **1926**, *39*, 138. (c) Verley, A. Bull. *Chem. Soc. Chim. Fr.* **1925**, *37*, 537. (d) Oppenauer, R. V. *Recl. Trav. Chim. Pays-Bas* **1937**, *56*, 137. (e) Wilds, A. L. *Org. React.* **1944**, *2*, 178. (f) Djerassi, C. *Org. React.* **1951**, *6*, 207.

9) Lundgren, R. J.; Rankin, M. A.; McDonald, R.; Schatte, G.; Stradiotto, M. *Angew. Chem. Int. Ed.* **2007**, *46*, 4732 – 4735.

10) Hounjet, L. J.; Bierenstiel, M.; Ferguson, M. J.; McDonald, R.; Cowie, M. *Inorg. Chem.* **2010**, *49*, 4288 – 4300.

11) Programs for diffractometer operation, unit cell indexing, data collection, data reduction, and absorption correction were those supplied by Bruker.

12) Sheldrick, G. M. *Acta Crystallogr.* **2008**, *A64*, 112 – 122.

13) Cheung, W.-M.; Chiu, W.-H.; Williams, I. D.; Leung, W.-H. *Eur. J. Inorg. Chem.* **2009**, 792 – 798.

14) Arikawa, Y.; Tashita, S.-Y.; Yamaguchi, S.; Miyahara, H.; Asayama, T.; Umakoshi, K.; Onishi, M. *Chem. Lett.* **2010**, *39*, 940 – 941.

15) Hounjet, L. J.; McDonald, R.; Ferguson, M. J.; Cowie, M. Submitted to *Inorg. Chem.* Sept. 14, 2010. Manuscript ID: ic-2010-01883u.

16) Black, S. I.; Skapski, A. C.; Young, G. B. *J. Chem. Soc., Chem. Commun.* **1989**, 911 – 913.

17) Boubekeur, L.; Ulmer, S.; Ricard, L.; Mézailles, N.; Le Floch, P. *Organometallics*, **2006**, *25*, 315 – 317.

18) (a) Muetterties, E. L.; Bleeke, J. R.; Wucherer, E. J. *Chem. Rev.* **1982**, *82*, 499 – 525. (b) Bianchini, C.; Caulton, K. G.; Chardon, C.; Eisenstein, O.; Folting, K.; Johnson, T. J.; Meli, A.; Peruzzini, M.; Rauscher, D. J. *J. Am. Chem. Soc.*

1991, *113*, 5127 – 5129. (c) Zhang, S.; Shen, J. K.; Basolo, F.; Ju, T. D.; Lang, R. F.; Kiss, G.; Hoff, C. D. *Organometallics*, **1994**, *13*, 3692 – 3702.

19) Blum, O.; Milstein, D. *J. Organomet. Chem.* **2000**, *593 – 594*, 479 – 484.

20) Boronat, M.; Corma, A.; Renz, M. *J. Phys. Chem. B* **2006**, *110*, 21168 – 21174.

21) Campbell, E. J.; Zhou, H.; Nguyen, S. T. *Org. Lett.* **2001**, *3*, 2391 – 2393.

22) Alonso, D. A.; Brandt, P.; Nordin, S. J. M.; Andersson, P. G. *J. Am. Chem. Soc.* **1999**, *121*, 9580 – 9588.

23) Yu, Y.; Brennessel, W. W.; Holland, P. L. *Organometallics*, **2007**, *26*, 3217 – 3226.

Chapter 5: A Comparison of Structure and Reactivity of Phosphine-Amido and Hemilabile Phosphine-Amine Chelates of Rhodium

5.1 Introduction

The rich and varied chemistry of transition metal complexes bearing chelating, bifunctional ligands includes the development of increasingly efficient and unique homogeneous catalytic systems.[1-11] Within metal complexes, these bifunctional hybrid ligands are known to exhibit hemilability, whereby at least one of the donors is strongly coordinating and anchored to the metal, while the more labile donor(s) can be displaced by catalytic substrates, but can also offer chelate stabilization in the event of coordinative unsaturation.[12-17] Low-valent, late transition metals, which form strong bonds with softer phosphines and weak bonds with harder amines are commonly ligated by phosphine-amines to generate hemilabile complexes.[18-25] Furthermore, the use of incompletely *N*-substituted amine donors within such hybrid *P*,*N*-ligands allows for deprotonation of the coordinated amines to generate non-labile phosphine-amido complexes, some of which have found catalytic applications.[26-30] Late-metal amido complexes (particularly of ruthenium) are widely used as catalysts for the hydrogenation of polar unsaturates whereby dihydrogen heterolysis is achieved through metal-ligand cooperativity to generate hydrido-amine complexes, which can then undergo hydride and proton transfer to the substrate via an outer-sphere, bifunctional mechanism.[8, 31-33]

In earlier studies involving a series of hybrid *P*,*N*-ligands based on *ortho*-phosphinoanilines, we investigated mono- and binuclear complexes of rhodium in which the degree of methyl substitution at nitrogen was found to have a significant influence on both structure and hemilability.[22] In related chemistry

with ruthenium, the structural diversity was again demonstrated in which alteration of the *N*-donor was found to give rise to a number of different coordination modes,[26] although the hemilability observed at rhodium was not exhibited by these ruthenium complexes. One of our primary interests in the protic *ortho*-phosphinoaniline ligands was the possibility for deprotonation of the amine groups to yield phosphine-amido chelates, the reactivity of which could then be compared to the phosphine-amine analogues. In keeping with the well established reactivity of amido complexes (particularly involving ruthenium)[31–33] one of our phosphine-amido complexes was found to be active as a ketone transfer hydrogenation catalyst.[26] In the current study, we set out to extend our original investigation of phosphine-amine complexes of rhodium and to compare their reactivities with those of the related phosphine-amido species.

In order to compare the reactivity of amido and amine complexes we targeted the silylation of olefins, for which rhodium is known to be effective.[11,34,35] The hydrosilylation of organic reagents to generate organosilanes has many potential applications for the production of new electronic materials and polymers.[36] Olefin hydrosilylation catalyzed by late metal complexes is often accompanied by dehydrogenative silylation side-reactions, particularly when rhodium is the metal used.[11,34,35] However, the selective formation of unsaturated organosilicon compounds could be useful for generating a variety of functionalized silanes by subjecting the alkene functionality of the product vinylsilane to further substrate addition. The possibility of metal-metal cooperativity in reactions catalyzed by amido or amine complexes prompted us to prepare binuclear complexes and to compare their reactivities with those of the mononuclear analogues.

5.2 Experimental

5.2.1 General Comments

All solvents were deoxygenated, dried (using appropriate drying agents) distilled before use, and stored under nitrogen. Unless indicated otherwise, all reactions were performed under an Ar atmosphere using standard Schlenk techniques. The reagents, diphenyl(*o*-*N*-methylanilinyl)phosphine (Ph_2PAr),[22] di(*o*-*N*-methylanilinyl)phenylphosphine ($PhPAr_2$),[22] bis(di(*o*-*N*-methylanilinyl)-phosphino)methane (mapm),[22] diphenyl(*o*-*N*,*N*-dimethylanilinyl)phosphine (Ph_2PAr'),[37] bis(*o*-*N*,*N*-dimethylanilinyl)phenylphosphine ($PhPAr'_2$),[37] bis(di(*o*-*N*,*N*-dimethylanilinyl)phosphino)methane (dmapm)[38] and $[Rh(\mu\text{-}OMe)(COD)]_2$[39] were prepared according to literature procedures. Styrene (≥ 99%, deoxygenated and stored under Ar over 4 Å molecular sieves), trifluoromethanesulfonic acid (HOTf; ≥ 99%, stored under Ar), hydrogen tetrafluoroborate (HBF_4; 54 % (w/w) in Et_2O, stored under Ar), iodomethane (99.5%), trimethyloxonium tetrafluoroborate (Me_3OBF_4; 95%) and 1,2-bis(diphenylphosphino)ethane (dppe; 97%) were purchased from Aldrich. Triethylsilane ($HSiEt_3$; ≥ 98%, deoxygenated and stored under Ar over 4 Å molecular sieves) was purchased from Alfa-Aesar while $[Rh(NBD)_2][BF_4]$ (≥ 96%, stored under Ar) was purchased from Strem Chemicals. NMR spectra were recorded on Varian Inova-400, -500 or Varian Unity-500 spectrometers operating at 399.8, 498.1 or 499.8 MHz, respectively, for ^1H, at 161.8, 201.6 or 202.3 MHz, respectively, for ^{31}P and at 100.6, 125.3 or 125.7 MHz, respectively, for ^{13}C nuclei. Coupling constants are given in Hz. Overlapping or unresolved aromatic ^1H signals, observed in the typical δ 6 – 8 range, and aromatic $^{13}C\{^1H\}$ signals, found between δ 80 – 120, are not reported. Spectroscopic data for metal complexes (**1a** – **9**) are provided in Tables 5.1 and 5.2. Elemental analyses were performed by the Microanalytical Laboratory of this department. Electrospray ionization mass spectra were run on a Micromass Zabspec spectrometer in the departmental MS facility. In all cases, the distribution of isotope peaks for the appropriate parent ion matched very closely that calculated from the formulation given.

Table 5.1. $^{31}P\{^{1}H\}$ NMR Spectroscopic Data for the Compounds. [a]

Compound	$\delta(^{31}P\{^{1}H\})$ / ppm [b]
[Rh(COD)(*P*,*N*-Ph_2PAr^-)] (**1a**)	41.2 (d, $^{1}J_{RhP}$ = 163 Hz, 1P)[c]
[Rh(COD)(*P*,*N*-PhP(Ar^-)Ar)] (**1b**)	25.9 (d, $^{1}J_{RhP}$ = 157 Hz, 1P)[c]
$[Rh_2(COD)_2(\mu$-*P*,*N*,*P'*,*N'*-$mapm^{2-})]$ (**2**)	11.7 (m, $^{1}J_{RhP}$ = 165 Hz, 2P)[c,d]
[Rh(*P*,*P'*-dppe)(*P*,*N*-Ph_2PAr^-)] (**3**)	67.9 (ddd, $^{1}J_{RhP}$ = 142 Hz, $^{2}J_{PP}$ = 37 Hz, $^{2}J_{PP}$ = 33 Hz, 1P),[e] 59.0 (ddd, $^{1}J_{RhP}$ = 159 Hz, $^{2}J_{PP}$ = 312 Hz, $^{2}J_{PP}$ = 33 Hz, 1P),[e] 46.0 (ddd, $^{1}J_{RhP}$ = 143 Hz, $^{2}J_{PP}$ = 312 Hz, $^{2}J_{PP}$ = 37 Hz, 1P)[e]
$[RhO_2$(*P*,*P'*-dppe)(*P*,*N*-Ph_2PAr^-)] (**4**)	52.3 (ddd, $^{1}J_{RhP}$ = 130 Hz, $^{2}J_{PP}$ = 20 Hz, $^{2}J_{PP}$ = 9 Hz, 1P), 50.8 (ddd, $^{1}J_{RhP}$ = 134 Hz, $^{2}J_{PP}$ = 13 Hz, $^{2}J_{PP}$ = 9 Hz, 1P), 41.0 (ddd, $^{1}J_{RhP}$ = 106 Hz, $^{2}J_{PP}$ = 20 Hz, $^{2}J_{PP}$ = 13 Hz, 1P)
$[RhI(CH_3)$(*P*,*P'*-dppe)(*P*,*N*-Ph_2PAr^-)] (**5**)	49.2 (ddd, $^{1}J_{RhP}$ = 107 Hz, $^{2}J_{PP}$ = 445 Hz, $^{2}J_{PP}$ = 25 Hz, 1P),[c] 38.0 (ddd, $^{1}J_{RhP}$ = 101 Hz, $^{2}J_{PP}$ = 445 Hz, $^{2}J_{PP}$ = 12 Hz, 1P)[c] 36.7 (dm, $^{1}J_{RhP}$ = 102 Hz, 1P)[c]
[Rh(*P*,*P'*-dppe)(*P*,*N*-Ph_2PAr')] $[BF_4]$ (**6**)	69.2 (ddd, $^{1}J_{RhP}$ = 130 Hz, $^{2}J_{PP}$ = 35 Hz, $^{2}J_{PP}$ = 31 Hz, 1P), 55.0 (ddd, $^{1}J_{RhP}$ = 149 Hz, $^{2}J_{PP}$ = 291 Hz, $^{2}J_{PP}$ = 31 Hz, 1P), 43.1 (ddd, $^{1}J_{RhP}$ = 142 Hz, $^{2}J_{PP}$ = 291 Hz, $^{2}J_{PP}$ = 35 Hz, 1P)
[Rh(NBD)(*P*,*N*-Ph_2PAr')][BF_4] (**7a**)	37.7 (d, $^{1}J_{RhP}$ = 177 Hz, 1P)
[Rh(NBD)(*P*,*N*-$PhPAr'_2$)][BF_4] (**7b**)	27.5 (d, $^{1}J_{RhP}$ = 171 Hz, 1P)
$[Rh_2(NBD)_2(\mu$-*P*,*N*,*P'*,*N'*-dmapm)$][BF_4]_2$ (**8**)	12.0 (m, $^{1}J_{RhP}$ = 180 Hz, 2P)[d] 9.7 (m/br, $^{1}J_{RhP}$ = 177 Hz, 2P)[d,g] 7.4 (m/br, $^{1}J_{RhP}$ = 183 Hz, 2P)[f,g]
[Rh(COD)(*P*,*N*-Ph_2PAr)][OTf] (**9**)	38.3 (d, $^{1}J_{RhP}$ = 159 Hz, 1P)

[a] NMR abbreviations: s = singlet, d = doublet, t = triplet, m = multiplet, br = broad. All NMR data recorded at 27°C in CD_2Cl_2 unless otherwise indicated. [b] ^{31}P chemical shifts referenced to external 85% H_3PO_4. [c] NMR data recorded in C_6D_6. [d] C_2-symmetric isomer. [e] NMR data recorded in C_4D_8O. [f] C_s-symmetric isomer. [g] NMR data recorded at –80°C.

Table 5.2. ^{1}H and $^{13}C\{^{1}H\}$ NMR Spectroscopic Data for the Compounds.[a]

Compound	δ(^{1}H) / ppm	δ(^{13}C{^{1}H}) / ppm
[Rh(COD)(*P*,*N*-Ph_2PAr^-)] (**1a**)	H_{COD}: 5.26 (m/br, 2H), 3.33 (m/br, 2H), 2.13 (m/br, 4H), 1.82 (m/br, 4H)[b] RhNCH_3: 2.94 (s, 3H)[b]	RhNCH_3: 39.1 (s)[b]
[Rh(COD)(*P*,*N*-PhP(Ar^-)Ar)] (**1b**)	N*H:* 6.95 (m/br, 1H)[b] H_{COD}: 5.31 (m/br, 1H), 5.10 (m/br, 1H), 3.29 (m/br, 2H), 1.92 (m/br, 8H)[b] RhNCH_3: 2.93 (s, 3H)[b] HNCH_3: 2.43 (d, $^{3}J_{HH}$ = 4.4 Hz, 3H)[b]	RhNCH_3: 39.0 (s)[b] HNCH_3: 29.0 (s)[b]
[Rh_2(COD)$_2$(μ-*P*,*N*,*P'*,*N'*-$mapm^{2-}$)] (**2**)	*H*NCH_3: 6.51 (m/br, 2H)[b,c] H_{COD}: 5.27 (m, 2H), 4.66 (m, 2H), 2.97 (m, 2H), 2.74 (m, 2H), 2.31 (m, 2H), 2.05 (m, 4H), 1.84 (m, 4H), 1.55 (m, 6H)[b,c] PCH_2P: 3.17 (t, $^{2}J_{PH}$ = 10.0 Hz, 2H)[b,c] RhNCH_3: 2.63 (s, 6H)[b,c] HNCH_3: 2.34 (d, $^{3}J_{HH}$ = 5.2 Hz, 6H)[b,c]	RhNCH_3: 39.1 (s)[b,c] HNCH_3: 30.4 (s)[b,c] PCH_2P: 18.9 (t, $^{1}J_{PC}$ = 17 Hz)[b,c]
[Rh(*P*,*P'*-dppe)(*P*,*N*-Ph_2PAr^-)] (**3**)	NCH_3: 2.93 (s, 3H)[d] P(CH_2)$_2$P: 2.00 (m, 4H)[d]	NCH_3: 47.0 (d, $^{3}J_{PC}$ = 12 Hz)[d] P(CH_2)$_2$P: 30.2 (m) 26.3 (m)[d]
[RhO_2(*P*,*P'*-dppe)(*P*,*N*-Ph_2PAr^-)] (**4**)	NCH_3: 2.91 (d, $^{4}J_{PH}$ = 4.4 Hz, 3H) P(CH_2)$_2$P: 2.11 (m, 4H)	N/A (decomposes in CD_2Cl_2; poor solubility in other solvents)
[RhI(CH_3)(*P*,*P'*-dppe)(*P*,*N*-Ph_2PAr^-)] (**5**)	P(CH_2)$_2$P: 3.60 (m, 1H), 2.68 (m, 1H), 2.47 (m, 1H), 2.02 (m, 1H)[b] NCH_3: 3.41 (s, 3H)[b] RhCH_3: 0.79 (d, $^{2}J_{RhH}$ = 2.0Hz, 3H)[b]	NCH_3: 49.9 (d, $^{2}J_{RhC}$ = 6 Hz)[b] P(CH_2)$_2$P: 31.8 (m), 26.9 (m)[b] RhCH_3: 13.2 (m, $^{1}J_{RhC}$ = 22 Hz)[b]
[Rh(*P*,*P'*-dppe)(*P*,*N*-Ph_2PAr')][BF_4] (**6**)	N(CH_3)$_2$: 3.03 (s, 6H) P(CH_2)$_2$P: 2.06 (m, 4H)	N/A
[Rh(NBD)(*P*,*N*-Ph_2PAr')][BF_4] (**7a**)	H_{NBD}: 5.62 (s/br, 2H), 4.12 (s/br, 4H), 1.72 (m/br, 2H) N(CH_3)$_2$: 3.02 (s, 6H) H_{NBD}: 5.56 (s/br, 2H), 4.05 (s/br, 2H), 4.02 (s/br, 2H), 1.66 (d, $^{2}J_{HH}$ = 8.8 Hz, 1H), 1.60 (d, $^{2}J_{HH}$ = 8.8 Hz, 1H)[e] N(CH_3)$_2$: 2.94 (s, 6H)[e]	N(CH_3)$_2$: 52.3 (s)
[Rh(NBD)(*P*,*N*-$PhPAr'_2$)][BF_4] (**7b**)	H_{NBD}: 4.49 (s/br, 4H), 4.00 (s/br, 2H), 1.62 (s/br, 2H) N(CH_3)$_2$: 2.84 (s, 12H)	N(CH_3)$_2$: 50.4 (s)
[Rh_2(NBD)$_2$(μ-*P*,*N*,*P'*,*N'*-dmapm)][BF_4]$_2$ (**8**)	H_{NBD}: 5.40 (s/br, 4H), 3.76 (s, 4H), 3.40 (s/br, 4H), 1.50 (s, 4H)[c] PCH_2P: 3.15 (t, $^{2}J_{PH}$ = 9.9 Hz, 2H)[c] N(CH_3)$_2$: 2.75 (s/br, 24H)[c]	N(CH_3)$_2$: 49.8 (s/br)[c] PCH_2P: 24.1 (m/br)[c]
[Rh(COD)(*P*,*N*-Ph_2PAr)][OTf] (**9**)	N*H*: 7.08 (m/br, 1H), H_{COD}: 6.05 (m/br, 1H), 5.47 (m/br, 1H), 4.23 (m/br, 1H), 3.44 (m/br, 1H), 2.33 (br, 8H) NCH_3: 2.82 (d, $^{3}J_{HH}$ = 6.0, 3H)	NCH_3: 46.1 (s)

[a] NMR abbreviations: s = singlet, d = doublet, t = triplet, m = multiplet, br = broad. All NMR data recorded at 27°C in CD_2Cl_2 unless otherwise indicated. ^{1}H and ^{13}C chemical shifts referenced to external tetramethylsilane. Chemical shifts for aryl groups not given. [b] NMR data recorded in C_6D_6. [c] C_2-symmetric isomer. [d] NMR data recorded in C_4D_8O. [e] NMR data recorded at –80°C.

5.2.2 Preparation of Metal Complexes

(a) η^2:η^2-1,5-Cyclooctadiene(*P*,*N*-diphenyl(*o*-*N*-methylanilido)phosphine) rhodium(I), [Rh(COD)(*P*,*N*-Ph_2PAr^-)] (1a). In a 100 mL Schlenk flask under anhydrous conditions and Ar atmosphere, Ph_2PAr (768 mg, 2.64 mmol) and [Rh(μ-OMe)(COD)]$_2$ (638 mg, 1.32 mmol) were dissolved in 10 mL of benzene at ambient temperature resulting in a brilliant red-orange solution. The solvent volume was reduced to approx 5 mL *in vacuo* and 20 mL of *n*-pentane was then added resulting in the formation of an orange precipitate. The slurry was stirred for 10 min before allowing the precipitate to settle. The supernatant was removed by cannula transfer under Ar, then the solid was dried *in vacuo* and recovered as an orange powder (1.13 g, 74% yield, found: C, 66.67; H, 5.97; N, 2.59%. Calcd for $[C_{27}H_{29}NPRh]\cdot 0.5C_6H_6$: C, 66.96; H, 6.02; N, 2.75%). Although the crystal structure indicates one equiv of benzene per formula unit, a non-crystalline sample was analyzed here and ^{1}H NMR analysis in CD_2Cl_2 (obtained at approximately the same time as the elemental analysis) was used to verify benzene content. Single crystals suitable for X-ray diffraction were obtained by layering a saturated benzene solution with *n*-pentane in an NMR tube.

(b) η^2:η^2-1,5-Cyclooctadiene(*P*,*N*-((*o*-*N*-methylanilido)(*o*-*N*-methylanilinyl) phenylphosphine))rhodium(I), [Rh(COD)(*P*,*N*-PhP(Ar^-)Ar)] (1b). The compound was prepared in a manner similar to that of **1a** using $PhPAr_2$ (224 mg, 698 μmol) and [Rh(μ-OMe)(COD)]$_2$ (169 mg, 349 μmol) and was isolated as a red-orange powder (220 mg, 59% yield, found: C, 63.55; H, 6.00; N, 5.20%. Calcd for $[C_{28}H_{32}N_2PRh]$: C, 63.40; H, 6.08; N, 5.28%). HRMS (ESI): *m*/*z* 531.1432 $[M + H]^+$. Calcd for $C_{28}H_{33}N_2PRh$: *m*/*z* 531.1431.

(c) bis(η^2:η^2-1,5-Cyclooctadiene)(μ-*P*,*N*,*P'*,*N'*-di((*o*-*N*-methylanilido)(*o*-*N*-methylanilinyl)phosphino)methane)dirhodium(I,I), [Rh_2(COD)$_2$(μ-*P*,*N*,*P'*,*N'*-mapm^{2-})] (2). *Method a*. In a 50 mL Schlenk tube under anhydrous conditions and Ar atmosphere, mapm (71 mg, 142 μmol) and [Rh(μ-OMe)(COD)]$_2$ (68 mg, 140 μmol) were dissolved in 2 mL of tetrahydrofuran at ambient temperature

resulting in a dark red solution. To the stirred solution was then added 10 mL of *n*-pentane, which resulted in the formation of an orange precipitate. The slurry was stirred for 10 min before allowing the precipitate to settle. The supernatant was removed by cannula transfer under Ar, then the solid was dried *in vacuo* and recovered as an orange powder (99 mg, 71% yield, found: C, 59.13; H, 6.58; N, 5.43%. Calcd for $[C_{45}H_{56}N_4P_2Rh_2]\cdot C_4H_8O$: C, 59.28; H, 6.50; N, 5.64%). Single crystals suitable for X-ray diffraction were obtained by slow evaporation from a tetrahydrofuran solution in an NMR tube. *Method b*. The reaction above was also carried out using 5 mL of benzene rather than 2 mL of tetrahydrofuran, and in this case, a red slurry was immediately produced rather than a dark red solution. Product isolation was identical to that of *Method a*.

(d) *P*,*P'*-1,2-bis(Diphenylphosphino)ethane(*P*,*N*-diphenyl(*o*-*N*-methylanilido) phosphine)rhodium(I), [Rh(*P*,*P'*-dppe)(*P*,*N*-Ph_2PAr^-)] (3). In a 50 mL Schlenk flask under anhydrous conditions and Ar atmosphere, dppe (71 mg, 178 μmol) and [Rh(COD)(*P*,*N*-Ph_2PAr^-)] (**1a**, 103 mg, 178 μmol) were dissolved in 7 mL of tetrahydrofuran at ambient temperature producing a red solution, which was stirred for 10 min. Stirring was stopped, the solution was carefully layered with 20 mL of *n*-pentane and the mixture was left undisturbed for 18 h. The supernatant was removed by cannula transfer under Ar, then the solid was dried *in vacuo* and recovered as large red crystals (103 mg, 79% yield, found: C, 68.17; H, 5.70; N, 1.73%. Calcd for $[C_{45}H_{41}NPRh]\cdot C_4H_8O$: C, 68.14; H, 5.72; N, 1.62%). Single crystals suitable for X-ray diffraction were obtained by slow evaporation from a tetrahydrofuran solution in an NMR tube.

(e) η^2-Peroxo(*P*,*P'*-1,2-bis(diphenylphosphino)ethane)(*P*,*N*-diphenyl(*o*-*N*-methylanilido)phosphine)rhodium(III), [RhO_2(*P*,*P'*-dppe)(*P*,*N*-Ph_2PAr^-)] (4). In a 50 mL Schlenk flask under anhydrous conditions and Ar atmosphere, 10 mL of tetrahydrofuran was added to [Rh(*P*,*P'*-dppe)(*P*,*N*-Ph_2PAr^-)] (**3**, 31 mg, 36 μmol) and the mixture was stirred for 30 min resulting in a bright red solution. Oxygen was passed through the solution for 10 min with no noticeable color

change and 20 mL of *n*-pentane was then added resulting in an orange slurry, which was stirred for 30 min before allowing the precipitate to settle. The supernatant was removed by cannula transfer, and the red solid was then dried *in vacuo* (25 mg, 68% yield. HRMS (ESI): *m/z* 824.1473 $[M + H]^+$. Calcd for $C_{45}H_{42}NO_2P_3Rh$: 824.1478). Single crystals suitable for X-ray diffraction were obtained by slow evaporation from a benzene solution in an NMR tube.

(f) Iodo(methyl)(*P*,*P'*-1,2-bis(diphenylphosphino)ethane)(*P*,*N*-diphenyl(*o*-*N*-methylanilido)phosphine)rhodium(III), [RhI(CH_3)(*P*,*P'*-dppe)(*P*,*N*-Ph_2PAr^-)] (5). In a 50 mL Schlenk flask under anhydrous conditions and Ar atmosphere, [Rh(COD)(*P*,*N*-Ph_2PAr^-)] (**1a**, 157 mg, 271 μmol) and dppe (108 mg, 271 μmol) were dissolved in 10 mL of benzene at ambient temperature while stirring. Iodomethane (17 μL, 270 μmol) was then added via microsyringe resulting in an instantly noticeable darkening of the solution color. The solvent volume was reduced to approx 5 mL *in vacuo* and 20 mL of diethyl ether was added while stirring to produce a red precipitate. The precipitate was allowed to settle from the mixture and the supernatant was removed by cannula under Ar. The solid was dried *in vacuo* and isolated as a red powder (152 mg, 49% yield, found: C, 58.78; H, 5.13; N, 1.35%. Calcd for $[C_{46}H_{44}INP_3Rh]$: C, 59.18; H, 4.75; N, 1.50%). Although the crystal structure indicates 1 equiv of $C_4H_{10}O$ and 2 equiv of C_4H_8O per formula unit, a non-crystalline sample was analyzed here. ^1H NMR analysis in C_6D_6 (obtained at approximately the same time as the elemental analysis) was used to verify solvent content. Single crystals suitable for X-ray diffraction were obtained by layering a saturated tetrahydrofuran solution with diethyl ether in an NMR tube.

(g) *P*,*P'*-1,2-bis(Diphenylphosphino)ethane(*P*,*N*-diphenyl(*o*-*N*,*N*-dimethyl-anilinyl)phosphine)rhodium(I) tetrafluoroborate, [Rh(*P*,*P'*-dppe)(*P*,*N*-Ph_2PAr')][BF_4] (6). In an NMR tube under Ar atmosphere, [Rh(*P*,*P'*-dppe)(*P*,*N*-Ph_2PAr^-)] (**3**, 21 mg, 24 μmol) and Me_3OBF_4 (4.0 mg, 27 μmol) were dissolved in 0.7 mL of CD_3NO_2 producing a dark yellow solution. $^{31}P\{^1H\}$ and ^1H NMR

spectra reveal **6** as the major product along with [Rh(*P*,*P'*-dppe)(*P*,*N*-Ph_2PAr)][BF_4], suggesting the presence of moisture in the reaction mixture (generating HBF_4, which protonates at nitrogen). Despite our best efforts, we have not been able to isolate **6** as an analytically pure substance.

(h) η^2:η^2-1,4-Norbornadiene(*P*,*N*-diphenyl(*o*-*N*,*N*-dimethylanilinyl) phosphine)rhodium(I) tetrafluoroborate, [Rh(NBD)(*P*,*N*-Ph_2PAr')][BF_4] (7a). In a 50 mL Schlenk flask under anhydrous conditions and Ar atmosphere, Ph_2PAr' (94 mg, 308 μmol) and [$Rh(NBD)_2$][BF_4] (115 mg, 308 μmol) were dissolved in 5 mL of dichloromethane at ambient temperature resulting in an orange solution, which was stirred for 5 min. Stirring was stopped, the solution was carefully layered with 10 mL of *n*-pentane and the mixture was left undisturbed for 18 h. The supernatant was removed by cannula transfer under Ar then the solid was dried *in vacuo* and recovered as large orange crystals (134 mg, 71% yield, found: C, 53.89; H, 4.89; N, 2.34%. Calcd for [$C_{27}H_{28}NPRh$][BF_4]·0.25CH_2Cl_2: C, 53.79; H, 4.72; N, 2.30%). ^{1}H NMR analysis in $CDCl_3$ (obtained at approximately the same time as the elemental analysis) was used to verify dichloromethane content. HRMS (ESI): *m*/*z* 500.1003 $[M]^+$. Calcd for $C_{27}H_{28}NPRh$: *m*/*z* 500.1009.

(i) η^2:η^2-1,4-Norbornadiene(*P*,*N*-di(o-*N*,*N*-dimethylanilinyl)phenyl-phosphine)rhodium(I) tetrafluoroborate, [Rh(NBD)(*P*,*N*-$PhPAr'_2$)][BF_4] (7b). The compound was prepared in a manner similar to that of **7a** using $PhPAr'_2$ (153 mg, 439 μmol) and [$Rh(NBD)_2$][BF_4] (164 mg, 439 μmol) and was isolated as a yellow-orange powder (231 mg, 83% yield, found: C, 55.42; H, 5.35; N, 4.37%. Calcd for [$C_{29}H_{33}N_2PRh$][BF_4]: C, 55.26; H, 5.28; N, 4.44%). HRMS (ESI): *m*/*z* 543.1425 $[M]^+$. Calcd for $C_{29}H_{33}N_2PRh$: *m*/*z* 543.1431.

(j) bis(η^2:η^2-1,4-Norbornadiene)(μ-*P*,*N*,*P'*,*N'*-bis(di(*o*-*N*,*N*-dimethylanilinyl) phosphino)methane)dirhodium(I,I) bis(tetrafluoroborate), [$Rh_2(NBD)_2$(μ-*P*,*N*,*P'*,*N'*-dmapm)][BF_4]$_2$ (8). In a 50 mL Schlenk tube under anhydrous

conditions and Ar atmosphere, dmapm (225 mg, 404 μmol) and $[Rh(NBD)_2][BF_4]$ (302 mg, 808 μmol) were dissolved in 10 mL of dichloromethane at ambient temperature resulting in an orange-red solution, which was then stirred for 5 min. To the stirred solution was added 20 mL of *n*-pentane resulting in the formation of a yellow precipitate. The slurry was stirred for 5 min before allowing the precipitate the settle. The supernatant was then removed by cannula transfer under Ar and the product was isolated as a yellow powder (414 mg, 85% yield, found: C, 48.94; H, 5.10; N, 4.58%. Calcd for $[C_{47}H_{58}N_4P_2Rh_2][BF_4]_2 \cdot 0.5CH_2Cl_2$: C, 49.06; H, 5.11; N, 4.82%). Although the crystal structure indicates 1 equiv of CH_2Cl_2 per formula unit, a non-crystalline sample was analyzed here, which was exposed to air before analysis. ^{1}H NMR analysis in $CDCl_3$ (obtained at approximately the same time as the elemental analysis) was used to verify dichloromethane content. Single crystals suitable for X-ray diffraction were obtained by layering a saturated dichloromethane solution with tetrahydrofuran in an NMR tube. HRMS (ESI): *m/z* 473.1117 $[M]^{2+}$. Calcd for $C_{47}H_{58}N_4P_2Rh_2$: *m/z* 473.1118.

(k) η^2:η^2-1,5-Cyclooctadiene(*P*,*N*-diphenyl(*o*-*N*-methylanilinyl)phosphine) rhodium(I) trifluoromethanesulfonate, [Rh(COD)(*P*,*N*-Ph_2PAr)][OTf] (9). In a 25 mL Schlenk tube under anhydrous conditions and Ar atmosphere, [Rh(COD)(*P*,*N*-Ph_2PAr^-)] (**1a**, 100 mg, 173 μmol) was dissolved in 2 mL of dichloromethane at ambient temperature producing an orange-red solution. While stirring, HOTf (16 μL, 180 μmol) was added, which turned the solution yellow after 5 min. To the stirred solution, 10 mL of *n*-pentane was added resulting in the formation of a yellow precipitate. Stirring was stopped, the precipitate was allowed to settle and the supernatant was removed by cannula transfer under Ar. The solid was then dried *in vacuo* and isolated as a yellow powder (76 mg, 63% yield, found: C, 49.36; H, 4.33; N, 2.14%. Calcd for $[C_{27}H_{30}NPRh][CF_3O_3S] \cdot 0.5CH_2Cl_2$: C, 49.33; H, 4.50; N, 2.02%). ^{1}H NMR analysis in $CDCl_3$ (obtained at approximately the same time as the elemental analysis) was used to verify dichloromethane content. Single crystals suitable for

X-ray diffraction were obtained by slow evaporation from a dichloromethane solution in an NMR tube. HRMS (ESI): *m/z* 502.1170 $[M]^+$. Calcd for $C_{27}H_{30}NPRh$: 502.1165.

5.2.3 Low Temperature Protonation of [Rh(*P*,*P'*-dppe)(*P*,*N*-Ph_2PAr^-)] (3)

In an NMR tube under anhydrous conditions and Ar atmosphere, **3** (25 mg, 29 μmol) was dissolved in 0.7 mL of CD_2Cl_2 at ambient temperature and the bright red solution was immediately cooled to –80 °C in acetone/dry ice. Using a microsyringe, $HBF_4 \cdot xEt_2O$ (4.0 μL, 29 μmol) was added, resulting in a brilliant blue-green solution and the temperature of the tube was maintained at –80 °C throughout the duration of subsequent ^1H, $^1H\{^{31}P\}$ and $^{31}P\{^1H\}$ NMR analyses (approximately five minutes).

5.2.4 General Protocol for Olefin Silylation Experiments

A representative procedure for the reaction of triethylsilane with styrene using [Rh(COD)(*P*,*N*-Ph_2PAr^-)] (**1a**) as the catalyst (Entry 3, Table 5.8) is as follows: In a 50 mL three-necked round-bottom flask equipped with a stir bar and attached reflux condenser, under anhydrous conditions and Ar atmosphere, **1a** (10.0 mg, 17.3 μmol) was dissolved in styrene (9.91 mL, 86.5 mmol) and the resulting red solution was heated to 60 °C for 10 min while stirring. Triethylsilane (2.76 mL, 17.3 mmol) was then added such that the molar ratio of Rh : $HSiEt_3$: styrene = 1 : 1,000 : 5,000. The reaction temperature was maintained at 60 °C and an overpressure of Ar was applied throughout the course of the reaction. The reaction mixture was sampled every 15 min for 3 h (relative to the addition of triethylsilane) by withdrawing a 0.5 mL aliquot from the reaction mixture and immediately adding it to 2.5 mL of dichloromethane containing 1.0 μL of HOTf. A 1.0 mL aliquot of this diluted solution was then quickly passed through a 4 cm Florisil® column using an overpressure so that less than 30 s elapsed between removal of the sample from the reaction mixture and removal of the catalyst from the sample. The eluent was collected in a vial and stored at 0 °C in the dark until the reaction mixture could be analyzed by GC-MS and ^1H NMR spectroscopy.

Reactions carried out in the presence of nitrobenzene were performed by first dissolving the catalysts in the appropriate volume of $C_6H_5NO_2$, followed by addition of the reagents as described above, so that the mole ratio of solution components was Rh : $HSiEt_3$: styrene : $C_6H_5NO_2$ = 1 : 1,000 : 5,000 : 1,000 in each case. Removal of cationic catalysts (**7a**, **7b** and **8**) was easily accomplished (without HOTf) by passing reaction mixtures directly through a 4 cm Florisil® column.

5.2.5 X-Ray Structure Determinations

(a) General. Crystallographic experimental details for compounds **1a**, **2**, **3** and **4** are provided in Table 5.3 while those of compounds **5**, **8** and **9** are provided in Table 5.4. See Appendix III for information about accessing additional crystallographic data. Crystals were grown via slow diffusion of *n*-pentane into a benzene (**1a**) solution of the compound, diffusion of diethyl ether into a tetrahydrofuran (**5**) solution of the compound, diffusion of tetrahydrofuan into a dichloromethane (**8**) solution of the compound or by evaporation of a tetrahydrofuran (**2**, **3**), benzene (**4**), or dichloromethane (**9**) solution of the compound. Data were collected using Mo Kα radiation (λ = 0.71073 Å) on a Bruker APEX-II CCD detector/D8 diffractometer[40] with the crystals cooled to – 100 °C. The data were corrected for absorption through use of a multi-scan model (*SADABS*[40]) (**1a**, **2**) or through Gaussian integration from indexing of the crystal faces (**3**, **4**, **5**, **8**, **9**). Structures were solved using direct methods/structure expansion (*SIR97*[41]) (**1a**, **5**, **8**), direct methods (*SHELXS–97*[42]) (**2**, **4**, **9**), or Patterson search/structure expansion (*DIRDIF-2008*[43]) (**3**). Refinements were completed using the program *SHELXL-97*.[42] Hydrogen atoms were assigned positions based on the sp^2 or sp^3 hybridization geometries of their attached carbon or nitrogen atoms, and were given thermal parameters 20% greater than those of their parent atoms, except in the case of **2**, for which the positions of hydrogen atoms were refined.

(b) Special Refinement Conditions. Compound 4: One of the solvent benzene molecules was disordered over three sites; each was constrained as an idealized hexagon with C–C distances of 1.39 Å, and the carbon atoms were refined with occupancies of 1/3 and with a common isotropic displacement parameter.

Table 5.3. Crystallographic Experimental Details for **1a** and **2** – **4**

Compound	**1a**·C_6H_6	**2**·C_4H_8O	**3**·C_4H_8O	**4**·2.5C_6H_6
Formula	$C_{33}H_{35}NPRh$	$C_{49}H_{64}N_4OP_2Rh_2$	$C_{49}H_{49}NOP_3Rh$	$C_{60}H_{56}NO_2P_3Rh$
Formula Weight	579.50	992.80	863.71	1018.88
Crystal Dimens (mm)	0.62 × 0.40 × 0.24	0.32 × 0.29 × 0.12	0.51 × 0.25 × 0.15	0.38 × 0.23 × 0.17
Crystal System	triclinic	Monoclinic	triclinic	Monoclinic
Space Group	$P\bar{1}$ (No. 2)	$C2$ (No. 5)	$P\bar{1}$ (No. 2)	$P2_1/c$ (No. 14)
a (Å)	9.3000 (3)	15.1371 (17)	11.4776 (3)	10.6143 (11)
b (Å)	11.3914 (3)	11.9719 (14)	13.9888 (4)	25.953 (3)
c (Å)	14.3271 (4)	12.1833 (14)	14.1445 (4)	18.329 (2)
α (deg)	72.4250 (2)		93.0113 (3)	
β (deg)	82.6184 (3)	96.5980 (10)	105.1022 (3)	97.0481 (12)
γ (deg)	68.1805 (3)		108.5004 (3)	
V (Å^3)	1343.08 (7)	2193.2 (4)	2056.47 (10)	5011.0 (9)
Z	2	2	2	4
ρ_{calcd} (g cm^{-3})	1.433	1.503	1.395	1.351
μ (mm^{-1})	0.718	0.868	0.571	0.481
$2\theta_{max}$ (deg)	55.04	52.98	55.02	55.08
Total Data Collected	11885 (–12 ≤ h ≤ 12, –14 ≤ k ≤ 14, –18 ≤ l ≤ 18)	8765 (–18 ≤ h ≤ 18, –14 ≤ k ≤ 15, –15 ≤ l ≤ 15)	18507 (–14 ≤ h ≤ 14, –18 ≤ k ≤ 18, –18 ≤ l ≤ 18)	43868 (–13 ≤ h ≤ 13, –33 ≤ k ≤ 33, –23 ≤ l ≤ 23)
Independent Reflns (R_{int})	6116 (0.0079)	4528 (0.0248)	9400 (0.0110)	11523 (0.0255)
Obsd Reflns [$I \geq 2\sigma(I)$]	5995	4464	8749	10092
Restraints/Params	0 / 326	0 / 292	0 / 497	0 / 570
Flack Abs Struct Parameter		0.50(3)		
Goodness-of-Fit (All Data)[b]	1.030	1.212	1.039	1.126
R_1 [$I \geq 2\sigma(I)$][c]	0.0186	0.0275	0.0236	0.0432
wR_2 [All Data][d]	0.0507	0.0670	0.0655	0.1159
Largest Diff Peak, Hole (e Å^{-3})	0.396, –0.430	0.545, –0.637	0.651, –0.622	1.076, –0.772

[a] An alternate setting of $P2_1/c$ (No. 14). [b] $S = [\Sigma w(F_o^2 - F_c^2)^2/(n-p)]^{1/2}$ where n = number of data; p = number of parameters varied; $w = [\sigma^2 (F_o^2) + (a_0P)^2 + a_1P]^{-1}$ where $P = [\text{Max}(F_o^2, 0) + 2F_c^2]/3$, and a_0 and a_1 are optimized by the refinement program; for **1a**, $a_0 = 0.0269$, $a_1 = 0.7218$; for **2**, $a_0 = 0$, $a_1 = 4.3520$; for **3**, $a_0 = 0.0326$, $a_1 = 1.2582$; for **4**, $a_0 = 0.0413$, $a_1 = 9.3155$. [c] $R_1 = \Sigma||F_o| - |F_c||/\Sigma|F_o|$. [d] $wR_2 = [\Sigma w(F_o^2 - F_c^2)^2/\Sigma w(F_o^4)]^{1/2}$.

Table 5.4. Crystallographic Experimental Details for **5**, **8** and **9**

Compound	**5**·$C_4H_{10}O$·$2C_4H_8O$	**8**·CH_2Cl_2	**9**
Formula	$C_{58}H_{70}INO_3P_3Rh$	$C_{48}H_{60}B_2Cl_2F_8N_4P_2Rh_2$	$C_{28}H_{30}F_3NO_3PRhS$
Formula Weight	1151.87	1205.28	651.47
Crystal Dimens (mm)	0.43 × 0.39 × 0.13	0.33 × 0.27 × 0.17	0.47 × 0.23 × 0.13
Crystal System	monoclinic	orthorhombic	triclinic
Space Group	$P2_1/n^a$	$P2_12_12_1$ (No. 19)	$P\bar{1}$ (No. 2)
a (Å)	16.0575 (9)	14.4151 (5)	10.0204 (5)
b (Å)	14.3966 (8)	15.3563 (5)	13.4944 (7)
c (Å)	23.1868 (13)	22.5030 (8)	21.7084 (11)
α (deg)			105.8209 (6)
β (deg)	91.6909 (7)		90.9298 (6)
γ (deg)			103.7044 (6)
V (Å^3)	5357.8 (5)	4981.3 (3)	2733.5 (2)
Z	4	4	4
ρ_{calcd} (g cm^{-3})	1.428	1.607	1.583
μ (mm^{-1})	1.029	0.903	0.811
$2\theta_{max}$ (deg)	55.38	55.00	55.32
Total Data Collected	47936 ($-20 \le h \le 20$, $-18 \le k \le 18$, $-30 \le l \le 30$)	43948 ($-18 \le h \le 18$, $-19 \le k \le 19$, $-29 \le l \le 29$)	24354 ($-13 \le h \le 13$, $-17 \le k \le 17$, $-28 \le l \le 28$)
Independent Reflns (R_{int})	12477 (0.0243)	11415 (0.0235)	12536 (0.0158)
Obsd Reflns [$I \ge 2\sigma(I)$]	10553	11029	11122
Restraints/Params	0 / 606	0 / 613	0 / 757
Flack Abs Struct Parameter		–0.002(15)	
Goodness-of-Fit (All Data)[b]	1.074	1.045	1.088
R_1 [$I \ge 2\sigma(I)$][c]	0.0306	0.0249	0.0396
wR_2 [All Data][d]	0.0884	0.0632	0.0918
Largest Diff Peak, Hole (e Å^{-3})	1.408, –0.559	0.923, –0.482	0.958, –1.525

[a] An alternate setting of $P2_1/c$ (No. 14). [b] $S = [\Sigma w(F_o^2 - F_c^2)^2/(n-p)]^{1/2}$ where n = number of data; p = number of parameters varied; $w = [\sigma^2(F_o^2) + (a_0P)^2 + a_1P]^{-1}$ where $P = [\text{Max}(F_o^2, 0) + 2F_c^2]/3$, and a_0 and a_1 are optimized by the refinement program; for **5**, $a_0 = 0.0472$, $a_1 = 4.3211$; for **8**, $a_0 = 0.0331$, $a_1 = 3.1675$; for **9**, $a_0 = 0.0228$, $a_1 = 6.1661$. [c] $R_1 = \Sigma||F_o| - |F_c||/\Sigma|F_o|$. [d] $wR_2 = [\Sigma w(F_o^2 - F_c^2)^2/\Sigma w(F_o^4)]^{1/2}$.

5.3 Results and Discussion

5.3.1 Phosphine-Amido Complexes

Reactions of $[Rh(\mu\text{-OMe})(COD)]_2$ with the protic monophosphinoaniline ligands, Ph_2PAr or $PhPAr_2$ (Ar = *o*-C_6H_4NHMe), in benzene at ambient temperature generate brilliant, red-orange solutions containing the neutral phosphine-amido complexes, [Rh(COD)(*P*,*N*-Ph_2PAr^-)] (**1a**, Ar^- = *o*-$C_6H_4NMe^-$) or [Rh(COD)(*P*,*N*-$PhP(Ar^-)Ar$)] (**1b**), resulting from *N*-deprotonation by the methoxide ion (Scheme 5.1). Replacement of a phenyl group in **1a** by an anilinyl group in **1b** creates a stereogenic center at phosphorus, and as a result, **1b** is chiral. The $^{31}P\{^1H\}$ NMR spectrum of **1a** displays the expected doublet at δ 41.2 with $^1J_{RhP}$ = 163 Hz, while

the ^{1}H NMR spectrum shows a sharp singlet at δ 2.94 representing the *N*-methyl group, two distinct olefinic proton signals at δ 5.26 and 3.33, and the aliphatic ^{1}H

Scheme 5.1. Synthesis of Phosphine-Amido Compounds **1a**, **1b** and **2**

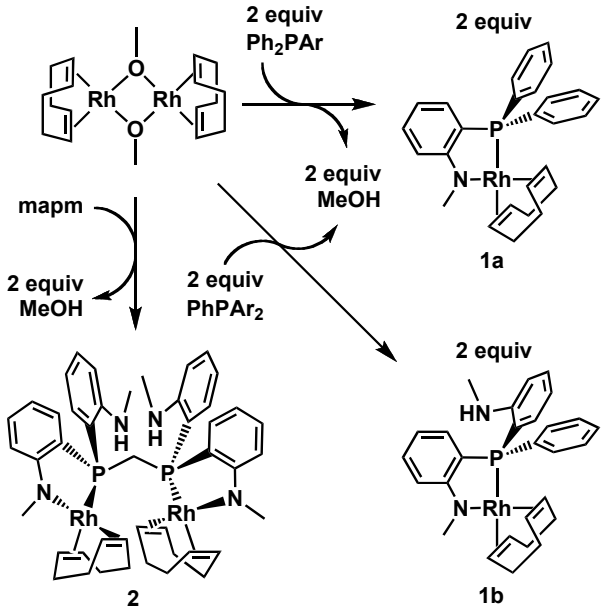

resonances of the cyclooctadiene ligand as complex multiplets between δ 1.82 and 2.13. The ^{13}C{^{1}H} NMR spectrum shows the singlet *N*-methyl resonance at δ 39.1, which was identified by gradient heteronuclear multiple quantum coherence (GHMQC) analysis. For complex **1b**, the ^{31}P signal is shifted upfield (to δ 25.9) relative to that of **1a**, as is usually observed when the number of aniline groups is increased.[22] The ^{1}H NMR spectrum shows two sharp, distinct signals at δ 2.93 and 2.43 representing *N*-methyl groups belonging to the coordinated amido and pendent amine functionalities, respectively. Otherwise, the spectral parameters for both compounds are comparable.

The solid-state structure of **1a** (Figure 5.1) illustrates a square-planar ligand arrangement at rhodium in addition to a trigonal-planar geometry around the amido nitrogen atom; relevant bond lengths and angles are given in Table 5.5. The planarity of this amido group is demonstrated by the sum of the angles about nitrogen (359.9°), and the Rh–N distance (2.063(1) Å) is significantly shorter than the Rh–N single bond present in the related phosphine-amine compound,

[RhCl(CO)(*P*,*N*-Ph_2PAr)] (2.129(2) and 2.140(2) Å for the two independent molecules),[22] demonstrating a favorable π-interaction of the amido group with the

Figure 5.1. ORTEP Diagram of [Rh(COD)(*P*,*N*-Ph_2PAr^-)] (**1a**). Gaussian ellipsoids for all non-hydrogen atoms are depicted at the 20% probability level. Hydrogen atoms are shown with arbitrarily small thermal parameters for the cyclooctadiene and methyl groups, and are not shown for the aryl rings.

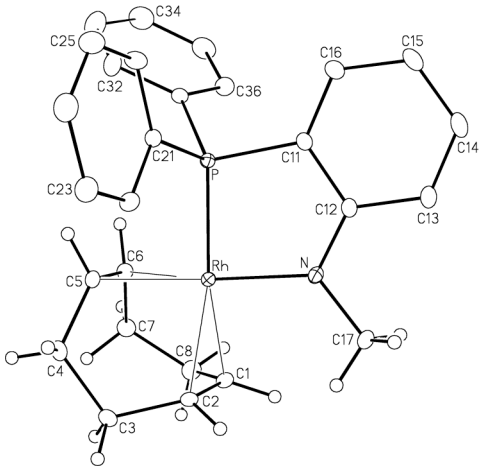

metal. The C–C bond length of the alkene coordinated *trans* to the amido nitrogen (C(5)–C(6) = 1.405(2) Å) is significantly longer than that coordinated *trans* to the phosphine (C(1)–C(2) = 1.377(2) Å), while the Rh–C bond lengths opposite

Table 5.5. Selected Structural Parameters for Compounds **1a** and **2**

	1a·C_6H_6	**2**·C_4H_8O
Atoms	Bond Lengths (Å)	Bond Lengths (Å)
Rh–P	2.2534(3)	2.261(1)
Rh–N(1)	2.063(1)	2.056(4)
C(1)–C(2)	1.377(2)	1.355(8)
C(5)–C(6)	1.405(2)	1.401(8)
N(1)–C(12)	1.374(2)	1.340(6)
N(2)–C(22)	–	1.367(7)
C(11)–C(12)	1.423(2)	1.421(5)
C(12)–C(13)	1.424(2)	1.411(7)
C(13)–C(14)	1.385(2)	1.375(8)
C(14)–C(15)	1.393(2)	1.373(6)
C(15)–C(16)	1.386(2)	1.401(7)
C(16)–C(11)	1.392(2)	1.399(6)
Rh–C(1)	2.231(1)	2.204(5)
Rh–C(2)	2.221(1)	2.220(4)
Rh–C(5)	2.140(1)	2.136(5)
Rh–C(6)	2.137(1)	2.139(5)
Atoms	Angles (º)	Angles (º)
P–Rh–N(1)	81.82(3)	81.3(1)
Rh–N(1)–C(17)	124.43(9)	123.3(3)
Rh–N(1)–C(12)	121.05(9)	123.1(3)
C(17)–N(1)–C(12)	114.4(1)	112.8(4)
P–C(10)–P'	–	122.8(3)
C(27)–N(2)–H(2N)	–	115(3)
C(22)–N(2)–H(2N)	–	113(3)
C(27)–N(2)–C(22)	–	121.3(5)

nitrogen are shorter (Rh–C(5) and Rh–C(6) = 2.140(1) and 2.137(1) Å, respectively) than those opposite phosphorus (Rh–C(1) and Rh–C(2) = 2.231(1) and 2.221(1) Å, respectively). While structural differences between the coordinated olefins perhaps reflect the π-donor character of the amido functionality, strengthening back-bonding to the olefin *trans* to it, the Rh–N–C(17) angle of 124.43(9)° is slightly expanded relative to that of a trigonal plane, suggesting that steric repulsion between the olefinic hydrogen atoms on C(1) and C(2) with the neighboring *N*-methyl group may also weaken the interaction of this olefin with rhodium. Indeed, the shortest H···H contact between these groups (2.12 Å) is slightly shorter than a normal van der Waals contact of 2.3 Å.[44]

A binuclear analogue of **1b** can be prepared much as reported above for the monophosphinoaniline complexes by using the previously reported mapm ligand ($Ar_2PCH_2PAr_2$).[22] Reaction of this protic diphosphinoaniline ligand with one equiv of $[Rh(\mu\text{-OMe})(COD)]_2$ in tetrahydrofuran produces the binuclear species, $[Rh_2(COD)_2(\mu\text{-}P,N,P',N'\text{-mapm}^{2-})]$ (**2**, $mapm^{2-}$ = $Ar(Ar^-)PCH_2P(Ar^-)Ar$; Scheme 5.1), in which two of the four available amines are deprotonated to give amido functionalities at each metal, leaving two pendent amine groups. A $^{31}P\{^1H\}$ NMR spectrum shows a second order multiplet at δ 11.7 with $^1J_{RhP}$ = 165 Hz. The ^1H NMR spectrum shows a triplet resonance at δ 3.17 with $^2J_{PH}$ = 10.0 Hz corresponding to two chemically equivalent hydrogen atoms of the PCH_2P unit; the appearance of a single methylene resonance indicates that this species possesses C_2-symmetry (as depicted in Scheme 5.1) since for a C_s-symmetric complex with mutually *syn* coordination planes, these hydrogen atoms would be chemically distinct. When the above reaction was carried out in C_6D_6, an additional product in approx 15% yield was observed together with **2**. This minor, unidentified impurity displays a low intensity doublet in the $^{31}P\{^1H\}$ NMR spectrum at δ 15.1 with $^1J_{RhP}$ = 166 Hz, and may either be a C_s-symmetric isomer of **2** or a mononuclear tetradentate species with chemically equivalent phosphorus atoms. Whatever its identity, this impurity can be easily separated from **2** by

precipitation of the latter with *n*-pentane and removal of the supernatant by cannula transfer.

We anticipated that coordination of a pendent amine at rhodium might produce a transient, 18-electron, five-coordinate intermediate, and that subsequent proton transfer from this amine to the adjacent amido nitrogen might invert one square plane with respect to the other. However, it appears that such amido/amine donor exchange does not occur at a spectroscopically observable rate and there is no evidence to suggest that isomerization of the C_2-symmetric enantiomers, *via* a C_s-symmetric intermediate, is occurring in solution. The same is true for **1b**, the ^{1}H NMR spectrum of which shows sharp, well-resolved resonances for the *N*-methyl groups belonging to coordinated (amido) and pendent (amine) functionalities. Complexes **1a**, **1b** and **2** are air-stable as solids, can be prepared in good yields and are soluble in benzene, tetrahydrofuran and dichloromethane.

A crystallographic analysis of **2** (Figure 5.2) illustrates the preferred *anti*-configuration of the rhodium coordination planes with respect to each other such that the molecule possesses C_2-symmetry in the solid state and crystallizes in a chiral space group (*C*2; see Supporting Information). The *anti*-arrangement of the

Figure 5.2. ORTEP Diagram of $[Rh_2(COD)_2(\mu\text{-}P,N,P',N'\text{-mapm}^{2-})]$ (**2**). Thermal ellipsoids as in Figure 5.1. Hydrogen atoms are shown with arbitrarily small thermal parameters for the cyclooctadiene, methyl, methylene and amine groups, and are not shown for the aryl rings.

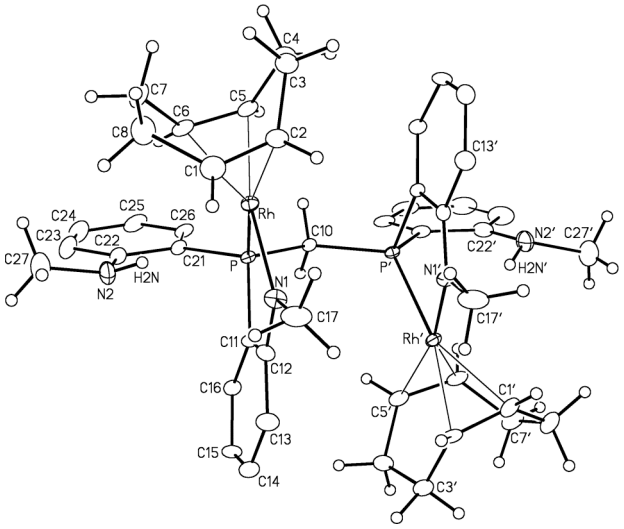

two Rh square planes allows the bulky COD ligands to avoid each other, and twisting of the diphosphine backbone about the P–CH_2 bonds further staggers the metal positions, as seen by the Rh–P–P'–Rh' torsion angle of 86.26(3)° and the 5.0994(6) Å separation of the metals. The large P–C(10)–P' angle of 122.8(3) ° is significantly expanded from the ideal tetrahedral arrangement at the methylene carbon, presumably a result of steric interactions between the COD group on one rhodium center with the anilido group on the other (see Figure 5.2). An analysis of the parameters in Table 5.5 shows that the environment of each Rh center in **2** appears similar to that of **1a** as demonstrated by comparable bond lengths and angles in each complex; each half of **2** appears to be structurally similar to complex **1a**, with the obvious exception of the pendent amine groups in the former.

Inspection of the metrical parameters of the anilido groups in compounds **1a** and **2** reveals that the amido-aryl bonds (N–C(12) = 1.374(2) Å for **1a** and 1.340(6) Å for **2**) are significantly shorter than those within the previously reported phosphine-amine complex, [RhCl(CO)(*P*,*N*-Ph_2PAr)] (1.468(3) and 1.465(4) Å for the two independent molecules),[22] while the arene C–C bonds involving the carbon atom *ipso* to an amido nitrogen, C(11)–C(12) and C(12)–C(13) within **1a** and **2** (*ca.* 1.42 Å), are comparable with those of the previously reported amido ruthenium complex, [RuCl(η^6-*p*-cymene)(*P*,*N*-Ph_2PAr$^-$)] (*ca.* 1.43 Å).[26] These bonds are also significantly longer than all other C–C bonds within the amido-aryl groups (*ca.* 1.39 Å), or those of the adjacent phenyl groups (*ca.* 1.39 Å), as well as analogous bonds within the anilinyl ring of [RhCl(CO)(*P*,*N*-Ph_2PAr)] (*ca.* 1.39 Å).[22] The significantly shorter *N*-aryl distances, and the distortions within the aryl group, suggest delocalization of the amido lone pair over the aromatic ring, as represented by the valence bond structures shown in Scheme 5.2. Such lone pair delocalization has been suggested to result in the lower Brønsted basicity of aniline,[45] and it is anticipated that the electron withdrawing effect imposed by the aryl substituent at nitrogen within these amido complexes may play a role in their reactivity. A portion of this study aims to

highlight some of the diverse means by which substrates can undergo activation by phosphine-amido complexes. Although the resonance contributor depicted at the bottom-left of Scheme 5.2 appears possible, a comparison of the phosphorus-aryl bond length of **1a** (P–C(11) = 1.796(1) Å) with those of the adjacent phosphorus-phenyl bonds (P–C(21) = 1.823(1) Å and P–C(31) = 1.814(1) Å) suggests that this resonance description is less significant.

Scheme 5.2. Possible Resonance Description of Compound **1a**

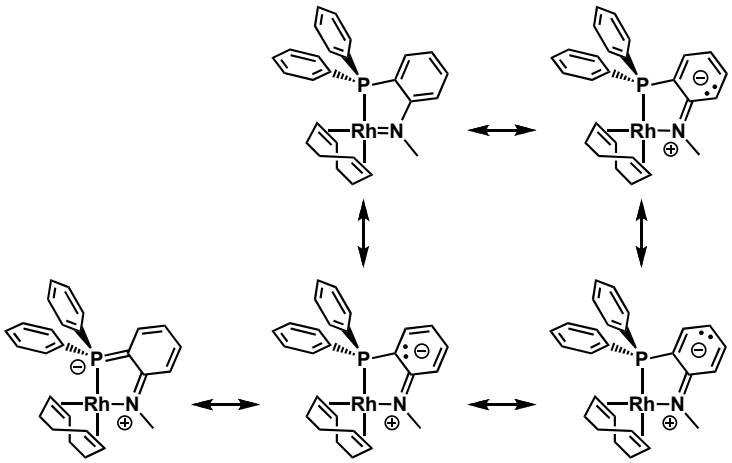

Although **1a** may appear similar in many respects to Grützmacher's ketone hydrogenation catalyst, [Rh(P(Tol)Ph_2)(η^2:η^2,*N*-(dibenzotropylidenyl)$_2$N$^-$)] (which rapidly reacts with molecular hydrogen to form an amine hydride),[8] reactions of either **1a** or **2** with hydrogen at ambient pressure and temperature in tetrahydrofuran solutions result in decomposition, presumably by hydrogenation of the diolefin. In an attempt to produce a species that would react cleanly with molecular hydrogen to produce a stable complex, the cyclooctadiene ligand of **1a** was replaced by a chelating diphosphine. The reaction of **1a** with one equiv of 1,2-bis(diphenylphosphino)ethane (dppe) in tetrahydrofuran under inert conditions results in the facile generation of [Rh(*P*,*P'*-dppe)(*P*,*N*-Ph_2PAr$^-$)] (**3**, Scheme 5.3), which can be isolated as large, red crystals in good yield.

The $^{31}P\{^1H\}$ NMR spectrum of **3** (Figure 5.3) shows the expected signal pattern for an ABCX spin-system with a downfield resonance at δ 67.9

corresponding to the phosphine unit *trans* to the amido donor. The resonances of the mutually *trans* phosphine donors appear at δ 59.0 and 46.0 and are identified

Scheme 5.3. Synthesis of Phosphine-Amido Compounds **3** – **6**

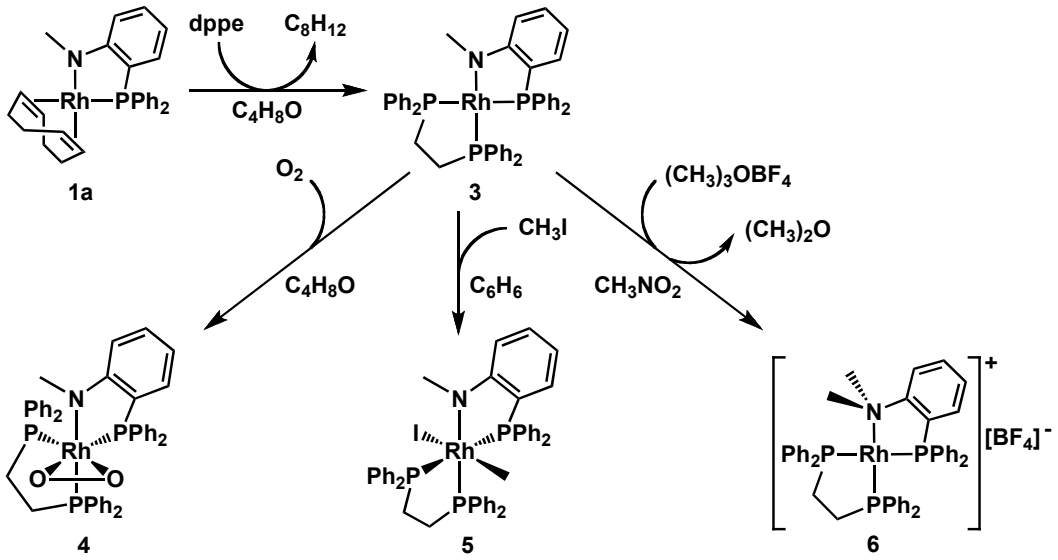

by their strong mutual coupling ($^2J_{PP}$ = 311 Hz). The ^{1}H NMR spectrum of **3** shows a singlet *N*-methyl signal at δ 2.93 and complex multiplets for the dppe

Figure 5.3. ^{31}P{^{1}H} NMR Spectrum of [Rh(*P*,*P'*-dppe)(*P*,*N*-Ph_2PAr^-)] (**3**)

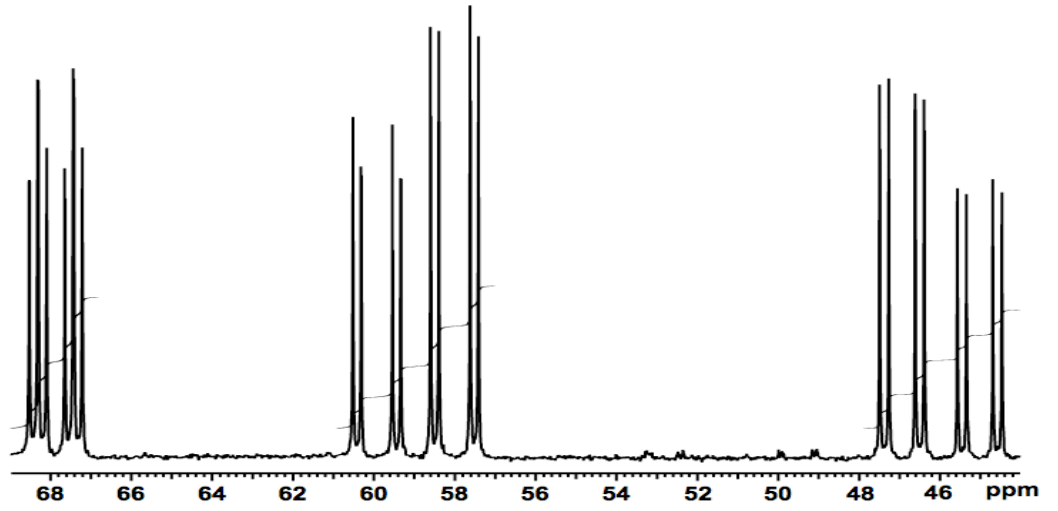

methylene protons centered around δ 2.00. The aliphatic ^{13}C resonance, found at δ 47.0, was identified as belonging to the *N*-methyl group by GHMQC analysis *via* correlation to the attached protons, while the signals at δ 30.2 and 26.3 correlate to the dppe methylene protons.

The X-ray structure of compound **3** (Figure 5.4) depicts the square-planar complex with a somewhat shortened Rh–P(3) bond of only 2.2120(4) Å for the

Figure 5.4. ORTEP Diagram of [Rh(*P*,*P'*-dppe)(*P*,*N*-Ph_2PAr^-)] (**3**). Thermal ellipsoids as in Figure 5.1. Hydrogen atoms are shown with arbitrarily small thermal parameters on methyl and methylene groups, and are not shown for the aryl rings.

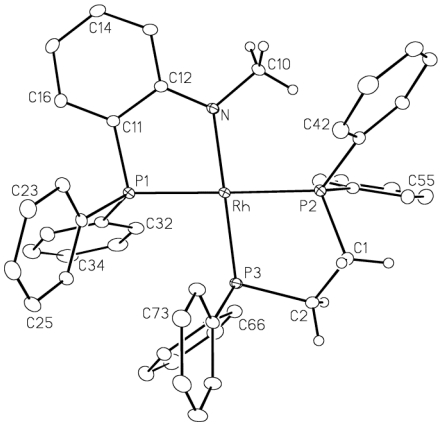

end of the diphosphine donor *trans* to the amido functionality, and relatively long Rh–P(1) and Rh–P(2) bonds for the mutually *trans* phosphines at 2.2939(4) and 2.2737(4) Å, respectively (Table 5.6), consistent with the greater *trans*-influence

Table 5.6. Selected Structural Parameters for Compounds **3** – **5**

	3·C_4H_8O	**4**·2.5C_6H_6	**5**·$C_4H_{10}O$·2C_4H_8O
Atoms	Bond Lengths (Å)	Bond Lengths (Å)	Bond Lengths (Å)
Rh–P(1)	2.2939(4)	2.3096(7)	2.3228(6)
Rh–P(2)	2.2737(4)	2.3009(8)	2.4006(6)
Rh–P(3)	2.2120(4)	2.2914(7)	2.3183(6)
Rh–N	2.085(1)	2.098(2)	2.117(2)
Rh–O(1), Rh–O(2)	–	2.024(2), 2.054(2)	–
O(1)–O(2)	–	1.440(3)	–
Rh–I	–	–	2.8028(3)
Rh–C(1)	–	–	2.098(2)
N–C(12)	1.359(2)	1.350(4)	1.347(3)
Atoms	Angles (°)	Angles (°)	Angles (°)
P(1)–Rh–P(2)	178.50(1)	100.00(3)	173.72(2)
P(3)–Rh–N	178.04(4)	176.99(7)	178.65(6)
P(1)–Rh–N	81.98(4)	81.44(7)	80.07(6)
P(2)–Rh–P(3)	83.73(1)	84.96(3)	84.27(2)
P(1)–Rh–P(3)	97.28(1)	96.88(3)	100.66(2)
I–Rh–C(1)	–	–	176.16(7)

of the phosphine groups. An interesting structural feature of this complex involves the close-to-parallel arrangement of the phenyl groups on P(1) and P(3) on the same side of the rhodium coordination plane. Despite the proximity of the carbon atoms on adjacent phenyl groups (i.e., C(66)···C(32) = 3.35 Å), which are comparable to those between layers of graphite,[47] the expanded P(1)–Rh–P(3)

angle of 97.28(1) ° suggests that the parallel arrangement of these groups simply minimizes steric contacts and is not the result of attractive π-π interactions. The Rh–N distance in **3** (2.085(1) Å) is slightly elongated relative to those of **1a** (2.063(1) Å) and **2** (2.056(4) Å) perhaps illustrating decreased π-donor character of the amido group due to the absence of the *trans* olefin π-acceptor. Again, the short N–C(12) distance (1.359(2) Å) is indicative of partial double bond character and delocalization of the lone pair over the aryl group.

Surprisingly, compound **3** in tetrahydrofuran at ambient temperature is inert to dihydrogen as judged by NMR analysis, even after a 24 h exposure. It appears that the amido group is neither nucleophilic enough to deprotonate hydrogen, nor a strong enough donor to promote H_2 oxidative addition at rhodium under ambient conditions. The delocalization of the nitrogen lone pair over the aryl ring, as noted above, is undoubtedly playing a role in modulating the basicity of the amido group. A structurally related complex, [$Rh(PPh_3)_2$(*P*,*N*-$Ph_2PC_6H_4NH^-$)], has also been prepared, and although it was found to be inactive as a ketone hydrogenation catalyst, its direct reaction with hydrogen was not reported.[46] Although unreactive toward H_2, compound **3** does display the ability to undergo oxidative addition in two other cases examined. Compound **3** is stable in air for days as a crystalline solid, but solutions of this complex react immediately with molecular oxygen upon exposure to air (unlike **1a**, **1b** or **2**) to afford the peroxo derivative, [RhO_2(*P*,*P'*-dppe)(*P*,*N*-Ph_2PAr^-)] (**4**, Scheme 5.3). This sparingly soluble compound can be dissolved in CD_2Cl_2 in order to allow NMR characterization, however slow decomposition is observed in this solvent. The $^{31}P\{^1H\}$ NMR spectrum of **4** shows three ddd signals at δ 52.7, 50.1 and 38.7 with the largest $^2J_{PP}$ coupling constant of only 20 Hz, indicating the absence of mutually *trans* phosphines in this complex. In contrast to compound **3**, a ^1H NMR analysis of **4** shows splitting of the *N*-methyl resonance into a doublet with $^4J_{PH}$ = 4.4 Hz and the coupling interaction (most likely due to the *trans* phosphine) was verified by $^1H\{^{31}P\}$ NMR analysis, showing collapse of the doublet resonance to a singlet.

A crystallographic analysis of **4** shows a pseudo-trigonal bipyramidal geometry at rhodium (Figure 5.5) in which the axial sites are occupied by one end

Figure 5.5. ORTEP Diagram of [RhO_2(*P*,*P'*-dppe)(*P*,*N*-Ph_2PAr^-)] (**4**). Thermal ellipsoids as in Figure 5.1. Hydrogen atoms are shown with arbitrarily small thermal parameters on methyl and methylene groups, and are not shown for the aryl rings.

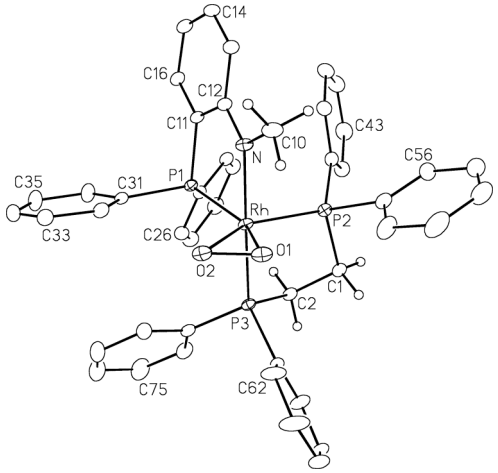

of the dppe group and the amido donor, while the other end of the dppe group, the O_2 moiety and the *P*-terminus of the phosphine-amido group occupy the equatorial positions. A structural comparison of **3** and **4** demonstrates that O_2 binding to **3** retains the mutually *trans* arrangement of the amido group and one end of the dppe ligand, with the other ends of both chelates bending back to accommodate O_2. Table 5.6 shows that the O–O bond length (1.440(3) Å) is comparable to that found in the O_2 adduct of Vaska's complex (1.47(1) Å),[48] in which O_2 is reversibly bound.[49] However, **4** shows no evidence of O_2 loss after being subject to an Ar purge for 10 min or to vacuum for 1.5 h as made evident by the unchanged $^{31}P\{^1H\}$ NMR spectrum. The P(1)–Rh–P(2) angle of 100.00(3) ° is intermediate between the angles expected for octahedral and trigonal bipyramidal geometries; the former geometric description is appropriate when considering the complex as a Rh(III)-peroxide, and the latter as a Rh(I)-dioxygen adduct. A comparison of structures **3** and **4** illustrates elongation of the mutually *trans* Rh–P(3) and Rh–N bonds in the latter – a feature that is particularly interesting considering that the spectroscopically observed $^4J_{PH}$ in compound **4** (*vide supra*) is not seen in the ^1H NMR spectrum of compound **3**. As expected, all Rh–L

distances in **4** are longer than those in **3** owing to increased steric crowding caused by coordination of the O_2 ligand.

Compound **3** bears some resemblance to a phosphine-amido complex prepared by Fryzuk *et al.*, which was shown to undergo oxidative additions of halomethanes.[50] We thought that **3** might react with iodomethane in an analogous manner, but were also curious about the possibility that subsequent methyl migration to the amido group could occur to generate a complex with a labile *N*,*N*-dimethylanilinyl substituent. We find that addition of iodomethane to one equiv of **3** in benzene results in an immediate darkening of the initially red solution, signaling the formation of the oxidative addition product, [RhI(CH_3)(*P*,*P'*-dppe)(*P*,*N*-Ph_2PAr^-)] (**5**, Scheme 5.3). The pattern observed in the $^{31}P\{^1H\}$ NMR spectrum, is typical of an ABCX spin system and demonstrates a large coupling constant ($^2J_{PP}$ = 445 Hz) between a pair of ^{31}P nuclei indicating the presence of mutually *trans* phosphine donors in the product. The ^1H NMR spectrum reveals a singlet resonance at δ 3.41 corresponding to one *N*-methyl group, as well as four distinct multiplets between δ 3.60 and 2.02, each representing one of the chemically unique methylene protons of the dppe ligand. An upfield doublet at δ_H 0.79 ($^2J_{RhH}$ = 2.0 Hz) represents the rhodium-bound methyl group. Compound **5** is remarkably stable in refluxing benzene and methyl migration to the amido group to produce [Rh(*P*,*P'*-dppe)(*P*,*N*-Ph_2PAr')]I or [RhI(*P*,*P'*-dppe)(*P*-Ph_2PAr')] is never observed.

A crystallographic study of **5** was carried out in order to unambiguously establish the geometry (*cis* or *trans* arrangement of CH_3 and I ligands) and to compare structural characteristics with those of its square planar precursor (**3**) and pseudo-trigonal bipyramidal peroxo complex (**4**). The X-ray structure of **5** (Figure 5.6) shows the anticipated octahedral geometry at rhodium having the iodo and methyl groups in a mutually *trans* arrangement (as is often observed),[51] and is consistent with nucleophilic displacement of I^- from CH_3I by the Rh complex (**3**). The structure of **5** reveals an expanded square plane of pnictogen donor atoms

relative to **3**, made evident by a comparison of bond lengths at rhodium within these two species (Table 5.6), presumably a result of steric crowding in this 6-

Figure 5.6. ORTEP Diagram of [RhI(CH_3)(*P*,*P'*-dppe)(*P*,*N*-Ph_2PAr^-)] (**5**). Thermal ellipsoids as in Figure 5.1. Hydrogen atoms are shown with arbitrarily small thermal parameters on methyl and methylene groups, and are not shown for the aryl rings.

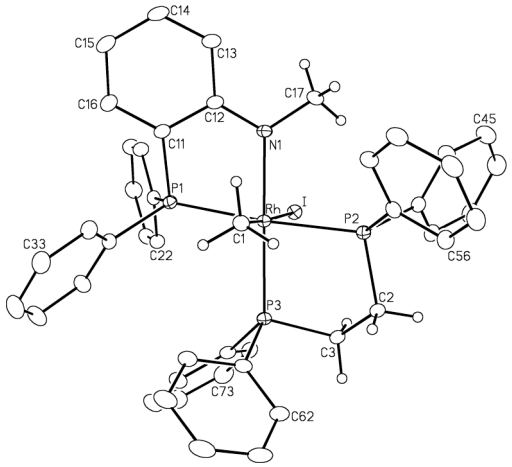

coordinate complex, bearing the large iodo ligand. With the exception of a slight deviation of the P(1)–Rh–P(2) angle from linearity in **5**, other angles at rhodium are similar to those of complex **3**. As was described above for compounds **1a** and **2**, the N–C(12) bond lengths in each of the phosphine-amido compounds **3**, **4** and **5** (1.359(2), 1.350(4) and 1.347(3) Å, respectively) are also significantly contracted relative to those of the previously reported phosphine-amine compound, [RhCl(CO)(*P*,*N*-Ph_2PAr)] (1.468(3) and 1.465(4) Å for the two independent molecules),[22] suggesting some degree of electron delocalization over the aromatic rings.

The propensity for oxidative addition of iodomethane to **3**, rather than its heterolysis by the amido-rhodium functionality, reflects an electron-rich rhodium atom and a relatively inert amido group consistent with the crystallographically inferred delocalization of electron density over both the metal and the aromatic system. However, the well established existence of *P*,*N*-coordinated *N*,*N*-dimethylanilinylphosphines,[22,26] including our synthesis of [Rh(*P*,*P'*-dppe)(*P*,*N*-Ph_2PAr')][BF_4] (**6**, Ar' = *o*-$C_6H_4NMe_2$), generated by sequential reactions of Ph_2PAr' and dppe ligands with [$Rh(NBD)_2$][BF_4] (discussed later), suggests that

alkylation of the amido nitrogen in **3**, to give an *N*,*N*-dimethylanilinyl group should be possible, perhaps by using a harder methyl cation. Indeed, the addition of trimethyloxonium tetrafluoroborate (Me_3OBF_4) to **3** in nitromethane produces [Rh(*P*,*P'*-dppe)(*P*,*N*-Ph_2PAr')][BF_4] (**6**, Scheme 5.3). Compound **6** appears as three ddd signals in the $^{31}P\{^1H\}$ spectrum at δ 69.2, 55.0 and 43.1, and the ^1H spectrum shows a singlet at δ 3.03 representing the two chemically equivalent *N*-methyl groups, consistent with the representation provided in Scheme 5.3. In principle, this complex could undergo isomerization to an analogue of **5** by an oxidative 1,2-methyl migration from N to Rh. However, the absence of an upfield Rh-methyl resonance in the ^1H NMR spectrum shows that such a process has not occurred, presumably due to the poor coordinating ability of the tetrafluoroborate counterion, which cannot provide electronic saturation that would favor a rhodium(III) species. Even the addition of KI to **6** in CD_3NO_2 did not result in its conversion to **5**. We thought that perhaps the opposite might also be possible, in which the iodo/methyl complex **5** could be converted into **6** by reductive elimination of methyl and amido groups. However, attempts to produce **6** by iodide abstraction from **5** with $AgBF_4$ in dichloromethane, nitromethane or benzene under anhydrous, inert conditions in the dark consistently resulted in complex intractable mixtures.

Having observed alkyl group addition at either rhodium or the amido nitrogen, we sought to determine the possible site(s) of protonation in **3**. The reaction of **3** with one equiv of $HBF_4 \cdot xEt_2O$ in CD_2Cl_2 at ambient temperature initially produces a blue-green solution that turns yellow within a few seconds. The yellow solution can be shown to contain [Rh(*P*,*P'*-dppe)(*P*,*N*-Ph_2PAr)][BF_4], in which the proton is *N*-bound, as made evident by a doublet resonance in the ^1H NMR spectrum, representing the *N*-methyl group at δ 2.39 (with $^3J_{HH}$ = 4.8 Hz), a broad quartet for the amine hydrogen at δ 8.21, and no hydride signal. We thought that the initially observed blue-green color might represent protonation at rhodium to generate a hydrido intermediate, from which 1,2-proton migration to nitrogen generates the thermodynamic product. However, when the reaction is repeated at

–80 °C, low temperature NMR analysis of the blue-green solution reveals two kinetic intermediates in the $^{31}P\{^{1}H\}$ spectrum in an approximate 1 : 1 ratio, each with an ABCX signal pattern. Interestingly, the ^{1}H and $^{1}H\{^{31}P\}$ NMR spectra show no evidence of a hydride signal from δ 1.5 through –20.0. However, numerous, unprecedented multiplets appearing between δ 4.5 to 6.5 suggest that protonation occurs kinetically at the *ortho* or *para* positions of the anilinyl ring to produce cationic phosphine-imine intermediates that isomerize to the thermodynamic product via imine-enamine tautomerization, as shown for protonation at one of the *ortho* positions in Scheme 5.4. The absence of a hydride

Scheme 5.4. Protonation of **3** via a Possible Phosphine-Imine Intermediate

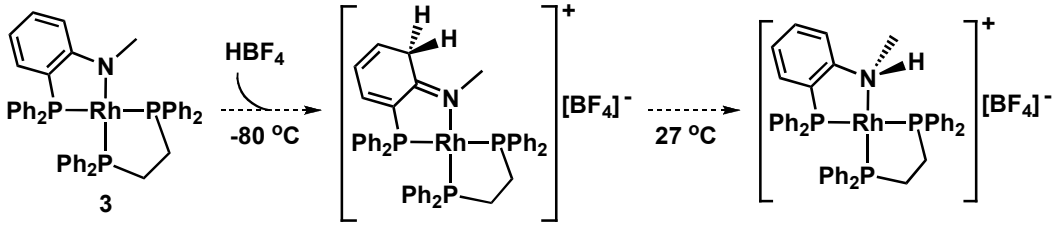

resonance in the upfield region and the presence of several new signals in the downfield region of the ^{1}H spectrum at –80 °C seem to indicate that the arene is the most nucleophilic site in **3**. Warming to ambient temperature then quickly produces a yellow solution, accompanied by disappearance of many of the signals between δ 4.5 – 6.5 to give [Rh(*P*,*P'*-dppe)(*P*,*N*-Ph_2PAr)][BF_4]. Protonation at either the *ortho* or *para* positions of the aryl group is consistent with the crystallographically inferred delocalization of the amido lone pair over the aromatic ring (see Scheme 5.2), as are the dramatic color changes observed as aromaticity is broken (upon protonation at carbon) and subsequently regenerated (upon proton migration to nitrogen). Reversible dearomatization has also been shown to occur within Milstein's dehydrogenation catalyst, which employs a pyridine-based *P*,*N*,*N*-ligand.[52]

5.3.2 Phosphine-Amine Complexes

(a) Generation from Phosphine-Amines

Hemilabile complexes are readily formed by the displacement of a norbornadiene group in $[Rh(NBD)_2]^+$ by a phosphine-amine ligand. Reactions of $[Rh(NBD)_2][BF_4]$ with one equiv of Ph_2PAr' or $PhPAr'_2$ (Ar' = *o*-$C_6H_4NMe_2$) in dichloromethane result in the formation of phosphine-amine products, $[Rh(NBD)(P,N\text{-}Ph_2PAr')][BF_4]$ (**7a**) or $[Rh(NBD)(P,N\text{-}PhPAr'_2)][BF_4]$ (**7b**, Scheme 5.5), respectively. Compound **7a** shows the expected doublet in the

Scheme 5.5. Synthesis of Phosphine-Amine Compounds **7a**, **7b** and **8**

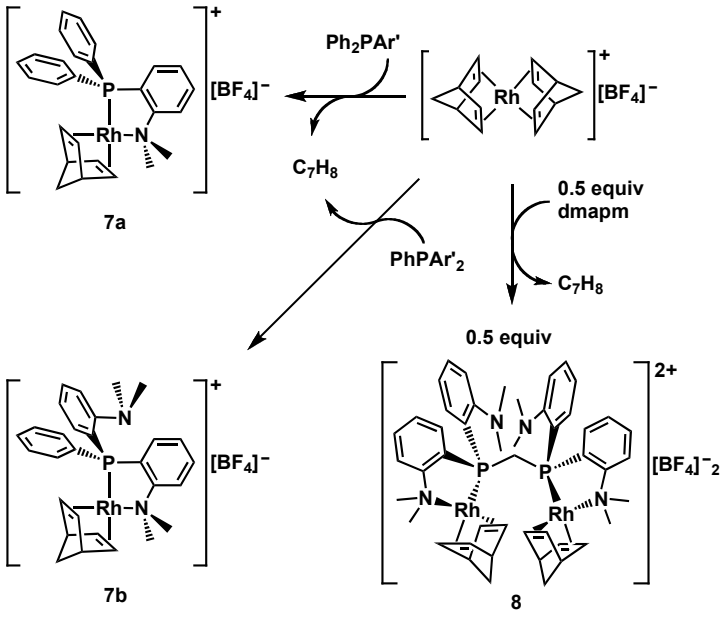

$^{31}P\{^1H\}$ NMR spectrum at δ 37.7, while its ambient temperature ^1H NMR spectrum shows three broad signals at δ 5.62, 4.12 and 1.72, in a 1 : 2 : 1 intensity ratio, representing the norbornadiene methine, olefin and methylene hydrogen atoms, respectively. The observation of only three ^1H signals for the norbornadiene group (rather than five signals in a 2 : 2 : 2 : 1 : 1 ratio, expected for the static geometry shown in Scheme 5.5), suggests chemical exchange via a fluxional process in which the olefinic groups opposite P and N are exchanging. At –80 °C, the spectrum shows two partially resolved olefinic proton resonances as well as two distinct doublets representing the methylene protons. At –60 °C, coalescence of the olefinic proton signals is observed with an exchange rate

constant of k_{coal} = 18 s^{-1} corresponding to an activation barrier of $\Delta G^{\ddagger}$ (213 K) = 11 kcal/mol. This chemical exchange can be rationalized either by a process involving Rh–N bond rupture *trans* to one olefin, *via* a transient 14 e^- intermediate, rotation about the Rh–P bond, followed by reformation of the Rh–N bond *cis* to this olefin, or by lability of the norbornadiene ligand. In order to test whether lability of the norbornadiene or Ph_2PAr' ligands accounts for the observed fluxionality, **7a** was reacted with 1 equiv of dppe in CD_2Cl_2. The resulting $^{31}P\{^1H\}$ NMR spectrum shows a 1 : 1 : 1 mixture of [Rh(NBD)(*P*,*P'*-dppe)][BF_4] (δ 57.0, $^1J_{RhP}$ = 153 Hz),[53] [Rh(*P*,*P'*-dppe)(*P*,*N*-Ph_2PAr')][BF_4] (**6**), and free Ph_2PAr' (δ –12.2) suggesting that both the norbornadiene and Ph_2PAr' ligands are susceptible to displacement by the chelating diphosphine. Compound **6** displays a signal pattern characteristic of an ABCX spin system in the $^{31}P\{^1H\}$ NMR spectrum similar to that of **3**, inspiring its preparation by addition of Me_3OBF_4 to **3** (*vide supra*).

The displacement of both phosphine-amine and norbornadiene ligands by dppe suggests that their labilities are comparable, and that the observation of chemical exchange may be the result of more than one fluxional process. Although hemilability of the related $PhPAr'_2$ and PAr'_3 ligands at rhodium has already been found to occur by rapid and reversible displacement of the coordinated amine by a pendent one,[22] in this case, hemilability of the Ph_2PAr' ligand implies the involvement of a coordinatively unsaturated species, which may allow for more facile substrate coordination/activation in catalysis. The $^{31}P\{^1H\}$ NMR spectrum of **7b** shows a signal at δ 27.5, shifted upfield relative to that of **7a**. Like that of **7a**, the ambient temperature ^1H NMR spectrum of **7b** also shows three broad resonances representing the norbornadiene group, as well as a single resonance at δ 2.84 representing all four rapidly exchanging *N*-methyl groups. The observation of only one *N*-methyl signal indicates exchange of the amines at rhodium by a Type II[2] hemilabile process similar to those occurring within the previously reported species, [RhCl(CO)(*P*,*N*-$PhPAr'_2$)] and [RhCl(CO)(*P*,*N*-$PhPAr_2$)].[22]

Reaction of the diphosphinoaniline, dmapm ($Ar'_2PCH_2PAr'_2$), with 2 equiv of $[Rh(NBD)_2][BF_4]$ in dichloromethane results in the generation of the binuclear analogue of **7b**, namely, $[Rh_2(NBD)_2(\mu\text{-}P,N,P',N'\text{-dmapm})][BF_4]_2$ (**8**, Scheme 5.5), which like compound **2**, places the rhodium coordination planes *anti* to each other so that the dication is C_2-symmetric. The ambient temperature $^{31}P\{^1H\}$ NMR spectrum of this compound shows a broadened second order multiplet at δ 12.0 with $^1J_{RhP}$ = 180 Hz (Figure 5.7). Upon cooling however, the

Figure 5.7. $^{31}P\{^1H\}$ NMR Spectra of Compound **8** (in 6 : 1 (v/v) CD_2Cl_2/CD_3NO_2)

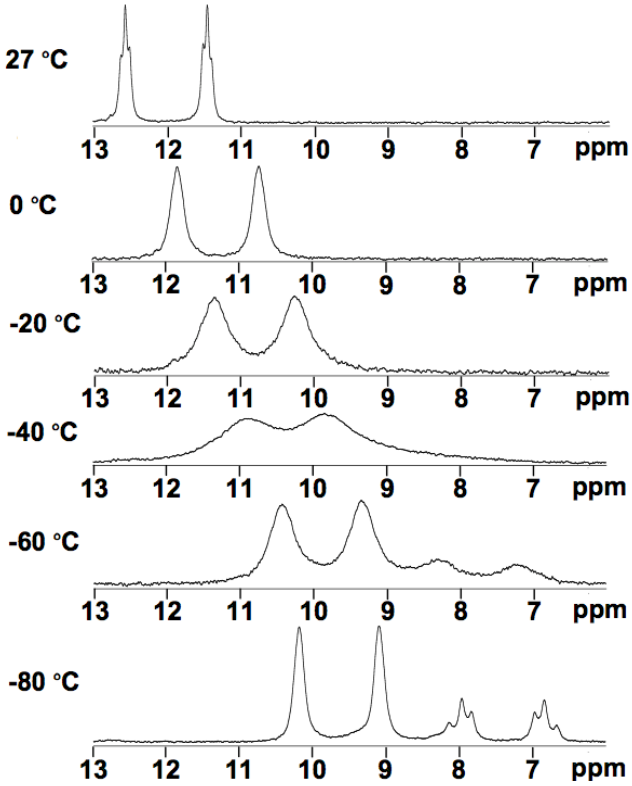

signal shows further broadening, followed by decoalescence (at approx –60 °C), finally producing a less intense multiplet at δ 7.4 in addition to a more intense multiplet at δ 9.7 (at –80 °C). We propose that the less intense, more upfield signal results from the C_s-symmetric isomer of **8**, having mutually *syn* coordination planes, acting as an intermediate through which interconversion of C_2-symmetric enantiomers occurs. Such a transformation, which may involve sequential displacement of each coordinated amine by the adjacent, pendent one was observed for a similar complex, although in this case the speculated C_s-

symmetric intermediate could not be directly observed.[22] An ambient temperature, ^{1}H NMR analysis of **8** shows a triplet at δ 3.15 representing the chemically equivalent PCH_2P hydrogens of the C_2-symmetric species as well as a single broad resonance at δ 2.75 representing all *N*-methyl protons. Unfortunately, all ^{1}H signals broaden dramatically and irregularly upon cooling to –80 °C, precluding low temperature characterization.

The solid state structure of **8** (dication shown in Figure 5.8) has the expected *anti* arrangement of the coordination planes as was observed for **2** (*vide*

Figure 5.8. ORTEP Diagram of $[Rh_2(NBD)_2(P,N,P',N'\text{-dmapm})][BF_4]_2$ (**8**). Only the dication, $[Rh_2(NBD)_2(\mu\text{-}P,N,P',N'\text{-dmapm})]^{2+}$, is shown. Non-hydrogen atoms are represented by Gaussian ellipsoids at the 20% probability level. Hydrogen atoms are shown with arbitrarily small thermal parameters on methylene and norbornadiene groups, and are not shown for the methyl and aryl groups.

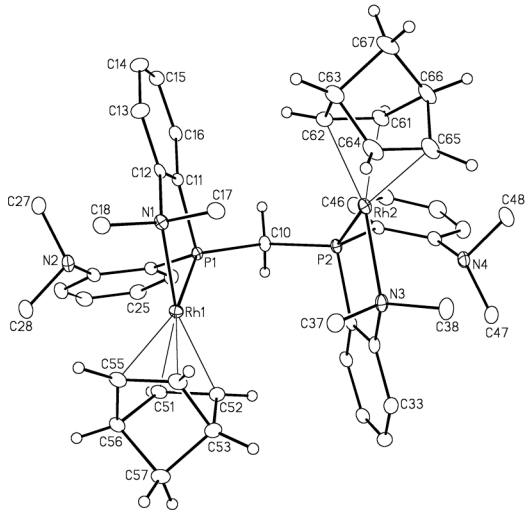

supra) and all other structural parameters appear normal with the exception of the expanded P(1)–C(10)–P(2) angle of 123.0(1)° (Table 5.7), which appears to be due to transannular steric relief, much as observed for **2**. As was also observed for **2**, the staggering of the Rh positions about the bridging diphosphine backbone is seen in the Rh(1)–P(1)–P(2)–Rh(2) torsion angle of 57.29(2)°. The nitrogen atoms within the pendent *N*,*N*-dimethylaniline groups of **8**, are pyramidalized, as made evident by the sums of the angles at N(2) and N(4) (*ca.* 333°), contrasting the somewhat more planar geometry observed for the pendent *N*-methylaniline group in **2** (sum of angles at N(2) = 349°). Whether this difference in

pyramidalization at nitrogen upon substitution of a hydrogen atom by a methyl group is an artifact arising from the greater uncertainty in the X-ray determined hydrogen positions, or whether if reflects the more electropositive nature of H[54,55] favoring sp^2 over sp^3 hybridization, as rationalized by Bent's rules,[56] is not clear.

Table 5.7. Selected Structural Parameters for Compounds **8** and **9**

	8·CH_2Cl_2	**9**
Atoms	Bond Lengths (Å)	Bond Lengths (Å)
Rh(1)–P(1)	2.2514(6)	2.2642(7), 2.2590(7)[a]
Rh(2)–P(2)	2.2292(6)	–
Rh(1)–N(1)	2.194(2)	2.148(2), 2.161(4)
Rh(2)–N(3)	2.205(2)	–
N(1)–C(12)	1.485(3)	1.464(4), 1.456(6)
Atoms	Angles (°)	Angles (°)
P(1)–Rh(1)–N(1)	84.25(5)	82.18(7), 80.84(8)
P(2)–Rh(2)–N(3)	84.16(6)	–
P(1)–C(10)–P(2)	123.00(12)	–
C(22)–N(2)–C(27)	110.6(2)	–
C(22)–N(2)–C(28)	112.8(2)	–
C(27)–N(2)–C(28)	109.6(2)	–
C(42)–N(4)–C(47)	112.0(2)	–
C(42)–N(4)–C(48)	111.1(2)	–
C(47)–N(4)–C(48)	110.4(2)	–

[a] Two crystallographically independent molecules.

(b) Generation from Phosphine-Amido Complexes

The reactivity of phosphine-amido complexes discussed earlier has indicated that the amido functionality is inert to covalent substrates (H_2 and CH_3I) and structural data provide an explanation based on resonance delocalization of amido electron density. However, these species can be readily protonated or methylated at the nitrogen atom, indicating that electrophilic addition to the amido group is possible. Conveniently, protonation of the non-labile phosphine-amido species serves as an alternate route to hemilabile phosphine-amine complexes. The phosphine-amido complex, [Rh(COD)(*P*,*N*-Ph_2PAr^-)] (**1a**), can be converted into the hemilabile phosphine-amine compound, [Rh(COD)(*P*,*N*-Ph_2PAr)][OTf] (**9**) by protonation with trifluoromethanesulfonic acid (HOTf). The ^1H NMR spectrum of **9** displays a doublet resonance for the *N*-methyl group at δ 2.62 showing coupling ($^3J_{HH}$ = 6.0 Hz) with the amine hydrogen at δ 7.08, the resonance for which was identified by GCOSY analysis. In this spectrum, the COD protons appear as broad resonances suggesting fluxionality, however a variable temperature NMR study was not undertaken in this case. The ambient temperature $^{31}P\{^1H\}$ NMR spectrum

appears as a sharp doublet at δ 38.3 with $^{1}J_{RhP}$ = 159 Hz. This complex was isolated and characterized for proof of concept since the addition of HOTf to reaction mixtures employing amido complexes **1a**, **1b** and **2** as catalysts (followed by passing solutions through Florisil®) is a rapid and efficient means of removing catalysts from reaction mixtures. Although the reaction was not attempted, compound **9**, or its norbornadiene analogue can presumably also be synthesized directly from the corresponding *ortho*-phosphinoaniline (Ph_2PAr) and either of the cationic precursors, $[Rh(COD)_2][OTf]$ or $[Rh(NBD)_2][BF_4]$, much as outlined earlier for the synthesis of **7a**.

The X-ray structure of phosphine-amine complex **9** (Figure 5.9) displays a shortened olefinic bond opposite the amine donor (C(5)–C(6) = 1.383(5) and

Figure 5.9. ORTEP Diagram of [Rh(COD)(*P*,*N*-Ph_2PAr)][OTf] (**9**). Only one of two crystallographically independent cations (A) is shown. Non-hydrogen atoms are represented by Gaussian ellipsoids at the 20% probability level. Hydrogen atoms, where shown, have been given arbitrarily small thermal parameters.

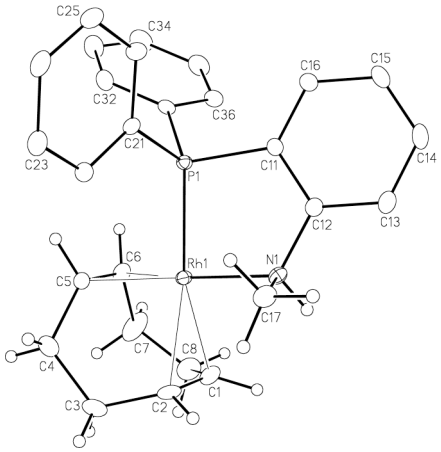

1.388(6) Å for the two crystallographically independent molecules) when compared with that of the parent (**1a**, 1.405(2) Å) bearing the π-donating amido group. Conversion of the amido group to an amine has also resulted in a lengthening of the Rh–N bonds of **9** (2.148(2) and 2.161(4) Å) relative to that of **1a** (2.063(1) Å), presumably due to the lack of a π-interaction with rhodium in the former, although in **9** this bond remains shorter than those of **8** (2.194(2) and 2.205(2)Å) presumably, in this case, a result of decreased steric bulk of the *N*-methylamine donor in **9** relative to those of the *N*,*N*-dimethylamine donors of **8**.

In attempts to prepare the binuclear phosphine-amine compound, $[Rh_2(NBD)_2(\mu\text{-}P,N,P',N'\text{-mapm})][BF_4]_2$ (**10**), reactions of mapm with 2 equiv of $[Rh(NBD)_2][BF_4]$ in CD_2Cl_2 were performed under a range of conditions. The major product from these reactions shows spectroscopic characteristics consistent with those expected for **10**, appearing as a second order multiplet at δ 7.0 ($^1J_{RhP}$ = 170 Hz) in the ambient temperature $^{31}P\{^1H\}$ NMR spectrum and having a signal pattern similar to the other binuclear analogues described herein (**2** and **8**) and elsewhere.[22] A similar, but less intense, broadened resonance at δ 3.7 ($^1J_{RhP}$ = 172 Hz) is also seen in this spectrum. The observation of two distinct $^{31}P\{^1H\}$ signals for **10** is similar to that observed for the *N*,*N*-dimethyl analogue (**8**; *vide supra*), and we again attribute the less intense, more upfield signal to a C_s-symmetric intermediate, through which the C_2-symmetric enantiomers interconvert. Interestingly, variable temperature $^{31}P\{^1H\}$ NMR analysis of **10** shows that decreasing the temperature to –80 °C results in broadening of the downfield resonance (now at δ 5.6) along with sharpening and increasing intensity of the more upfield resonance (now at δ 1.9) consistent with a temperature-dependent shift in the equilibrium concentrations of C_2- and C_s-symmetric isomers. Unfortunately, the ^1H NMR spectra, at both ambient temperature and –80 °C, show broad, unresolved signals due to the presence of several other unidentified species, which also precludes our successful isolation of **10** as an analytically pure substance. An alternate method for the preparation of $[Rh_2(NBD)_2(\mu\text{-}P,N,P',N'\text{-mapm})]^{2+}$ by protonation of **2** with 2 equiv of HOTf in dichloromethane was also attempted; however, $^{31}P\{^1H\}$ and ^1H NMR analyses produced spectra similar to those described above.

5.3.3 Catalytic Olefin Silylation

The complexes, $[Rh(COD)(P,N\text{-}Ph_2PAr^-)]$ (**1a**, Ar^- = $o\text{-}C_6H_4NMe^-$), $[Rh(COD)(P,N\text{-}PhP(Ar^-)Ar)]$ (**1b**), $[Rh_2(COD)_2(\mu\text{-}P,N,P',N'\text{-}mapm^{2-})]$ (**2**), $[Rh(NBD)(P,N\text{-}Ph_2PAr')][BF_4]$ (**7a**), $[Rh(NBD)(P,N\text{-}PhPAr'_2)][BF_4]$ (**7b**) and $[Rh_2(NBD)_2(\mu\text{-}P,N,P',N'\text{-dmapm})][BF_4]_2$ (**8**), which are all air stable as solids and

can be isolated in good to excellent yields, were studied as catalysts for styrene silylation (Scheme 5.6). The spectroscopic observation of hemilability within

Scheme 5.6. Possible Products from Reaction of Triethylsilane with Styrene

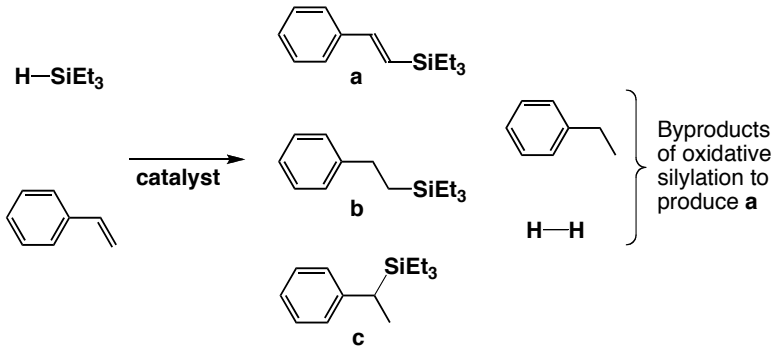

complexes **7a**, **7b** and **8** inspired us to compare the catalytic activities of these compounds with the non-labile phosphine-amido analogues, **1a**, **1b** and **2**. Specifically, we aimed to determine how the different *N*-donor functionalities might alter the rates of competing hydrosilylation and oxidative silylation processes by examining selectivities for vinylsilane **a**, and hydrosilylation products **b** and **c** (Scheme 5.6). Oxidative (dehydrogenative) silylation to produce **a** can either occur by direct liberation of molecular hydrogen from the reagents, or by hydrogen transfer from each reagent to an additional equiv of styrene (necessitating the use of excess styrene in reaction mixtures to promote selectivity for **a**).[11,34,35] We also wanted to examine whether or not the presence of adjacent metal atoms in the binuclear complexes would have a positive effect on reactivity (through metal-metal cooperativity)[57] by comparisons with mononuclear congeners. In addition, we sought to compare the catalytic characteristics of mononuclear compounds **1a** and **1b**, as well as **7a** and **7b**, to determine what influence the presence of an additional, pendent amine donor may have on reactivity.

The excellent solubility of the neutral amido complexes **1a**, **1b** and **2** directly in styrene eliminated the need for any additional solvent, and indeed several reactions were performed neat in reagents (See Table 5.8, Entries 1 – 5). Despite their excellent solubilities, rapid separation of these catalysts from

reaction mixtures was made possible by protonation of the amido groups with HOTf to generate ionic species that could then be easily removed using a Florisil®

Table 5.8. Catalytic Reactions of Triethylsilane and Styrene at 60 °C

Entry	Catalyst	Rh : $HSiEt_3$: Styrene	t_{rxn} (min)	Conversion[a]	a[a]	b[a]	c[a]	o[a]	[Rh] (mM)
1	**1a**	1 : 20 : 100	15 30	59 100	62 71	36 27	1 1	1 1	68.0
2	**1a**	1 : 100 : 500	30 60	62 100	61 67	36 30	3 3	<1 <1	13.6
3	**1a**	1 : 1,000 : 5,000	90 180	72 93	56 60	33 30	10 9	<1 <1	1.36
4	**1b**	1 : 1,000 : 5,000	90 180	54 90	50 64	36 28	14 8	<1 <1	1.36
5	**2**	1 : 1,000 : 5,000	90 180	40 68	57 61	42 38	<1 <1	<1 <1	1.36
6[b]	**1a**	1 : 1,000 : 5,000	120 300	71 100	67 69	27 27	<1 <1	6 4	1.20
7[b]	**1b**	1 : 1,000 : 5,000	120 300 1,440	57 93 100	58 68 72	29 24 21	1 1 1	12 8 6	1.20
8[b]	**2**	1 : 1,000 : 5,000	120 300 1,440	54 79 100	65 66 65	34 33 32	1 1 1	0 0 2	1.20
9[b]	**7a**	1 : 1,000 : 5,000	120 300 1,440	58 82 100	55 58 64	35 34 29	6 4 3	4 4 4	1.20
10[b]	**7b**	1 : 1,000 : 5,000	120 300 1,440	41 84 100	47 62 64	36 28 26	1 1 1	16 9 9	1.20
11[b]	**8**	1 : 1,000 : 5,000	120 300 1,440	40 71 100	42 60 67	20 19 19	2 1 1	36 20 13	1.20
12[c]	other	1 : 20 : 100	1,440	98	96	2	<1	<1	5

[a] Conversions and selectivities (%) for *E*-$Ph(CH)_2SiEt_3$ (**a**), $Ph(CH_2)_2SiEt_3$ (**b**), (+/–)-$PhCH(CH_3)SiEt_3$ (**c**) and other (**o**) silicon-containing products determined by GC-MS and ^1H NMR analysis on samples obtained at corresponding reaction times (t_{rxn}) in column 4. Reactions were carried out neat in styrene and triethylsilane unless indicated otherwise. [b] Reactions were carried out in the presence of 1,000 equiv of $C_6H_5NO_2$ per equiv of Rh. [c] Data obtained from reference 11; here the values reported in **a**, **b**, **c** and **o** columns represent yields (%) rather than selectivities. Reaction was carried out in toluene.

column. Cationic species **7a**, **7b** and **8**, which were insoluble in styrene, were dissolved in an appropriate volume of nitrobenzene prior to reagent addition so that the mole ratio of components in the reaction mixtures was Rh : $HSiEt_3$: styrene : $C_6H_5NO_2$ = 1 : 1,000 : 5,000 : 1,000 in each case (Entries 9 – 11, respectively). These cationic phosphine-amine catalysts are readily removed from reaction mixtures (without protonation by HOTf) using a Florisil® column, as described above.

At the outset, we intended to investigate the reactivities of the phosphine-amido compounds (**1a**, **1b** and **2**), anticipating that the possibility of metal-metal cooperativity[57] might result in a rate enhancement for catalyst **2** relative to **1b**. However, a comparison of Entries 3 – 5 shows that both mononuclear complexes (**1a** and **1b**) are actually somewhat more active than **2**, indicating that the presence of two adjacent metal centers actually appears to have an adverse effect, perhaps due to crowding within the binuclear complex. Comparisons of **1a** and **1b** as catalysts (Entries 3, 4, 6 and 7) demonstrate that the presence of a pendent amine appears to result in somewhat slower initial activity, but does not seem to affect the overall activity of the complex at longer reaction times.

Entries 3 – 5 provide representative data obtained from a more detailed kinetic analysis of the phosphine-amido catalysts, undertaken to compare their activities at predetermined intervals as reactions progressed (see Chart 5.1). A

Chart 5.1. Reaction Profiles for Catalysts **1a**, **1b** and **2**. Catalysts were dissolved in styrene and resultant mixtures were heated at the reaction temperature (60 °C) for 10 min prior to the addition of triethylsilane. The molar ratio of reaction components in each case was Rh : $HSiEt_3$: styrene = 1 : 1,000 : 5,000. Aliquots withdrawn from reaction mixtures at 15 min intervals for 180 min were treated and analyzed as described in the Experimental section.

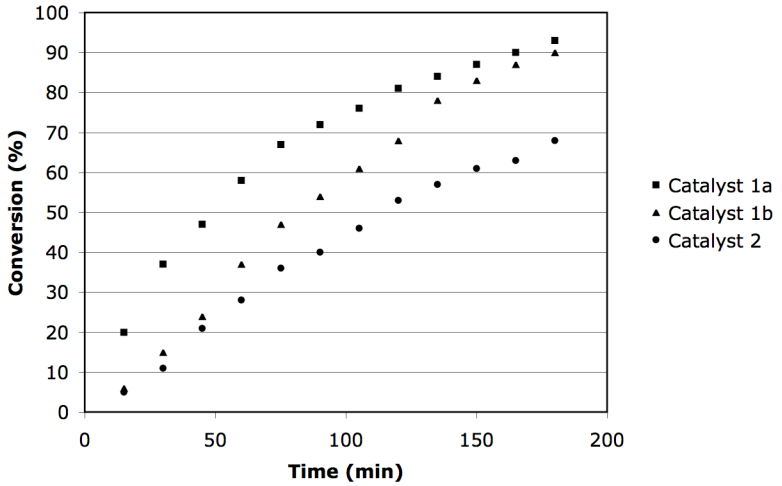

comparison of the reaction profiles shows superior activity of **1a** over both **1b** and **2** at early stages of the reaction; however, as reactions progress, the activity of **1a** slows noticeably relative to that of **1b**. Although replicate experiments, which may have allowed for a more quantitative comparison of the reactivities of **1a** and

1b were not performed, the data provided in both Chart 5.1 and Table 5.8 clearly demonstrate that binuclear complexes **2** and **8** are each somewhat less active catalysts than their mononuclear counterparts, ruling out the possibility for metal-metal cooperativity with respect to catalytic activity in these systems. Certainly, no improvement in catalytic properties is seen within the binuclear systems. It is interesting, from the preliminary data provided in Chart 5.1, that **1a** appears to be more active than **1b** at early reaction times, while at longer reaction times the conversion rates for these two catalysts seem comparable. Such an observation is consistent with the presence of the pendent amine donor in **1b**, which could stabilize catalytic intermediates against coordinative unsaturation, thereby slowing the rate of catalyst decomposition. The lack of a noticeable induction period in each case suggests that homogenous catalysis by molecular species predominates under these conditions since induction periods are often observed when molecular systems decompose over time to form more catalytically active, colloidal species.[58,59]

In order to compare the neutral and cationic species as catalysts under identical conditions, reactions were initially carried out in the presence of nitromethane, in which the cationic species are soluble. However, we find that the phosphine-amido series is unstable in the presence of this Brønsted acidic solvent (pK_a = 10.2),[60] resulting in decomposition of these catalysts at the reaction temperature. For example, heating **1a** to 60 °C for 3 h in the presence of 10 equiv of CH_3NO_2 in C_6D_6 reveals decomposition to at least four other species as indicated by $^{31}P\{^1H\}$ NMR analysis. In nitrobenzene, however, compounds **1** and **2** are quite stable at the reaction temperature, as shown by $^{31}P\{^1H\}$ NMR spectra of the compounds obtained after 3 h at 60 °C. Nitrobenzene was therefore chosen a common solvent for each of the catalysts in order to make more meaningful comparisons between the amido- and amine-containing species. An analysis of Table 5.8 (Entries 6 – 11) shows that the neutral phosphine-amido catalysts are more active than their cationic phosphine-amine counterparts, possibly due to greater propensity for silane oxidative addition by the former series containing the

more electron-rich metal centers. Consistent with the trends discussed above for the phosphine-amido series, a comparison of Entries 9 – 11 in Table 5.8 shows that the phosphine-amine catalyst **7a** exhibits enhanced initial reactivity relative to **7b**, bearing the pendent amine donor, and that as reactions approach completion, the activities of these species are comparable. Again, the binuclear complex (**8**) is shown to be the least active catalyst within this series.

During each of the reactions detailed in Table 5.8, initially orange reaction mixtures quickly became lighter in color upon the addition of triethylsilane, followed by eventual darkening of the color at or near complete conversions, effectively signaling the end of a reaction. In general, it was noticed that more gradual darkening of solution colors correlated with slower, more steady conversions of triethylsilane. This darkening of solution colors as reactions progress, along with the change in product selectivity that is observed during the course of any given reaction, seems to indicate some degree of catalyst decomposition over time. Unfortunately, the low concentrations of catalysts used in reaction mixtures precluded NMR spectroscopic analyses of rhodium-containing species remaining after reactions were stopped.

The catalysts studied show comparable selectivities for vinylsilane product **a** (see Scheme 5.6) and in general, selectivities for this product are found to increase slightly as reactions progress, suggesting that the catalysts may undergo transformation(s) as the number of turnovers increases, resulting in variable product distributions that depend on the extent of reaction. Entry 12 shows catalytic data for the reaction reported by Stradiotto *et al.*, which was carried out using an analogous zwitterionic *P*,*N*-catalyst lacking the amido functionality.[11] Although our complexes appear to be more active than this zwitterionic catalyst, as made evident by significantly lower catalyst loadings (compare Entries 6 – 11 with 12) and faster conversions in our case, the latter is shown to be far more selective for unsaturated organosilane, **a**.

We suggest that the phosphine-amido complexes achieve silane activation by oxidative addition rather than by invoking reactivity of the amido group since the reaction of iodomethane with **3** shows that the polar covalent substrate prefers oxidative addition at rhodium – certainly the phosphine-amine complexes must activate the silane in such a manner. Interestingly, CG-MS data from every reaction reported in Table 5.8 indicates that significantly less of the hydrogen transfer byproduct, phenylethane, is produced than **a** (often less than 50 % (mol/mol)). Such an observation implies the role of a process involving direct liberation of molecular hydrogen from reaction mixtures in addition to loss of hydrogen via hydrogenation of excess styrene. Each of the catalysts generally favors *anti*-Markovnikov regiochemistry and there is no evidence for the unsaturated products *Z*-$Ph(CH)_2SiEt_3$ or $PhC(SiEt_3)=CH_2$ in any of the reaction mixtures analyzed in this study. However, small quantities of $O(SiEt_3)_2$ were often identified among the products, presumably due to the presence of adventitious water in reaction mixtures.

The addition of stoichiometric quantities of various silanes (including, $HSiEt_3$, $HSi(OEt)_3$, $HSiPh_3$ and H_2SiPh_2) to compound **1a** in the absence of olefinic reagents results in very slow reactivity, often over a few days at ambient temperature, or over a period of hours at 60 °C, consistently and gradually decomposing to afford complex mixtures of multiple products as observed by $^{31}P\{^1H\}$ and ^1H NMR spectroscopy. The halosilanes, $ClSiEt_3$ and $ISiMe_3$ also react with **1a**, albeit more readily, to produce complex mixtures. Complexes **1a**, **1b** and **2** are each stable in the presence of excess styrene per equiv of rhodium at 60 °C for 3 h as judged by NMR analyses. The amido complex, [Rh(*P*,*P'*-dppe)(*P*,*N*-Ph_2PAr^-)] (**3**), was not tested as a catalyst since it failed to react with triethyl-, triphenyl- or diphenylsilanes in refluxing tetrahydrofuran. However, this compound was found to react exothermically upon the addition of one equiv of phenylsilane at ambient temperature, generating a yellow solution comprised of many spectroscopically unidentifiable species. The reactivity of **3** with the monosubstituted silane could make this complex suitable for a catalytic

application similar to that described above. However, such an investigation was not undertaken during this study.

5.4 Conclusions

A new series of mono- and binuclear rhodium complexes containing anionic or neutral *P*,*N*-ligands has been prepared. Deprotonation of phosphine-amine ligands, Ph_2PAr, $PhPAr_2$ or $Ar_2PCH_2PAr_2$, by the base-containing precursor, $[Rh(\mu\text{-}OMe)(COD)]_2$, generates the phosphine-amido complexes [Rh(COD)(*P*,*N*-Ph_2PAr^-)] (**1a**), [Rh(COD)(*P*,*N*-$Ph_2P(Ar^-)Ar$)] (**1b**) or $[Rh_2(COD)_2(\mu\text{-}P,N,P',N'\text{-}mapm^{2-})]$ (**2**), respectively. Replacement of the cyclooctadiene functionality of **1a** with 1,2-bis(diphenylphosphino)ethane (dppe) yields [Rh(*P*,*P'*-dppe)(*P*,*N*-Ph_2PAr^-)] (**3**) while protonation of **1a** with HOTf occurs at nitrogen to produce [Rh(COD)(*P*,*N*-Ph_2PAr)]][OTf] (**9**). Displacement of a diolefin ligand in $[Rh(NBD)_2][BF_4]$ by the phosphine-amine ligands, Ph_2PAr', $PhPAr'_2$, dmapm, or mapm produces the hemilabile compounds [Rh(NBD)(*P*,*N*-Ph_2PAr')]$[BF_4]$ (**7a**), [Rh(NBD)(*P*,*N*-$PhPAr'_2$)]$[BF_4]$ (**7b**), $[Rh_2(NBD)_2(\mu\text{-}P,N,P',N'\text{-dmapm})][BF_4]_2$ (**8**) and $[Rh_2(NBD)_2(\mu\text{-}P,N,P',N'\text{-mapm})][BF_4]_2$ (**10**), respectively.

A comparison of the structures of amido and amine complexes shows the expected planarity at the amido nitrogen, as well as shorter Rh–N bond lengths in the amido complexes. However, these species also display shorter N-aryl bonds and variations in the C–C bond lengths within the aryl group that are consistent with delocalization of the amido lone pair over the aromatic ring, which has significant chemical implications as demonstrated by the lack of reactivity of phosphine-amido complex **3** with H_2. The electron-withdrawing effect of the aryl group at nitrogen renders the lone pair unavailable for heterolytic activation of H_2, while also lowering the basicity of rhodium, effectively preventing H_2 oxidative addition at the metal. However, compound **3** does readily undergo oxidative additions of O_2 and CH_3I to give the expected Rh(III) products, $[RhO_2(P,P'\text{-}$

dppe)(*P*,*N*-Ph_2PAr^-)] (**4**) and [RhI(CH_3)(*P*,*P'*-dppe)(*P*,*N*-Ph_2PAr^-)] (**5**), respectively. Attempts to induce 1,2-methyl migration from rhodium to the amido nitrogen in the iodo/methyl product **5** were unsuccessful, although direct methylation at nitrogen is observed upon reaction of **3** with Me_3OBF_4, to generate [Rh(*P*,*P'*-dppe)(*P*,*N*-Ph_2PAr')][BF_4] (**6**). Protonation of **3** also yielded a phosphine-amine product at ambient temperature. Surprisingly perhaps, low temperature protonation suggests greater nucleophilicity of the aryl group, with subsequent proton migration to nitrogen upon warming; certainly no sign of protonation at Rh was observed.

The neutral phosphine-amido complexes were found to be more active as silylation catalysts than the cationic phosphine-amine derivatives, and although it was anticipated that the binuclear complexes might exhibit metal-metal cooperativity effects with respect to catalytic activity or selectivity, a comparison of these species with their mononuclear congeners shows that the binuclear complexes are less effective catalysts. These observations contrast the reactivity displayed by tetraphosphine complexes, which were found to be more active as hydroformylation catalysts than their mononuclear analogues, presumably as a result of metal-metal cooperativity.[57] From preliminary data, the presence of pendent amine donors within the catalysts appears to result in more steady conversions to products and it appears that catalyst decomposition may be inhibited relative to species lacking these groups, suggesting that the addition of a pendent hemilabile functionality to a catalyst may enhance its robustness. While the complexes studied are quite active as catalysts for the dehydrogenative silylation of styrene favoring a single unsaturated product, none of the catalysts studied exhibited excellent selectivity for this vinylsilane. The neutral phosphine-amido complexes were exceedingly soluble in styrene, negating the use of a solvent in reaction media, and could be easily removed from product mixtures by protonation to afford the cationic phosphine-amine species.

Although the phosphine-anilido complexes described in this paper display interesting reactivity, including their catalytic activity, the modulating influence of the aryl group attached to the amido nitrogen suggests that their reactivity will differ significantly from that of the alkyl-amido complexes conventionally used in "outer-sphere" transfer hydrogenation catalysis. In our case, the electron-withdrawing character of the aryl group at nitrogen, in combination with a relatively electron-rich Rh(I) center results in the apparent nucleophilicity of the arene upon protonation, which contrasts the previously demonstrated electrophilicity of the anilido ligand within an electron-poor Os(IV) complex.[61]

5.5 References

1) Keim, W.; Kowaldt, F. H.; Goddard, R.; Krüger, C. *Angew. Chem., Int. Ed. Engl.* **1978**, *17*, 466 – 467.

2) Braunstein, P.; Naud. F.; Rettig, S. J. *New J. Chem.* **2001**, *25*, 32 – 39.

3) Holz, J.; Kadyrov, R.; Borns, S.; Heller, D.; Börner, A. *J. Organomet. Chem.* **2000**, *603*, 61 – 68.

4) Shirakawa, E.; Kurahashi, T.; Yoshida, H.; Hiyama, T. *Chem. Commun.* **2000**, 1895 – 1896.

5) Yang, H.; Alvarez-Gressier, M.; Lugan, N.; Mathieu, R. *Organometallics*, **1997**, *16*, 1401 – 1409.

6) Espinet, P. Soulantica, K. *Coord. Chem. Rev.* **1999**, *193 – 195*, 499 – 556.

7) Gunanathan, C.; Ben-David, Y.; Milstein, D. *Science* **2007**, *317*, 790 – 792.

8) Maire, P.; Büttner, T.; Breher, F.; Le Floch, P.; Grützmacher, H. *Angew. Chem., Int. Ed.* **2005**, *44*, 6318 – 6323.

9) Lundgren R. J.; Rankin, M. A.; McDonald, R.; Schatte, G.; Stradiotto, M. *Angew. Chem., Int. Ed.* **2007**, *46*, 4732 – 4735.

10) Lundgren, R. J.; Stradiotto, M. *Chem. – Eur. J.* **2008**, *14*, 10388 – 10395.

11) Cipot, J.; McDonald, R.; Ferguson, M. J.; Schatte, G.; Stradiotto, M. *Organometallics*, **2007**, *26*, 594 – 608.

12) Jeffrey, J. C.; Rauchfuss T. B. *Inorg. Chem.* **1979**, *18*, 2658 – 2666.

13) Braunstein, P.; Naud, F. *Angew. Chem., Int. Ed.* **2001**, *40*, 680 – 699.

14) Lindner, E.; Pautz, S.; Haustein, M. *Coord. Chem. Rev.* **1996**, *155*, 145 – 162.

15) Slone, C. S.; Weinberger, D. A.; Mirkin, C. A. *Prog. Inorg. Chem.* **1999**, *48*, 233 – 350.

16) Werner, H. *Dalton Trans.* **2003**, 3829 – 3837.

17) Bassetti, M. *Eur. J. Inorg. Chem.* **2006**, 4473 – 4482.

18) Jones, N. D.; James, B. R. *Adv. Synth. Catal.* **2002**, *344*, 1126 – 1134.

19) Foo, S. J. L.; Jones, N. D.; Patrick, B. O.; James, B. R. *Chem. Commun.* **2003**, 988 – 989.

20) Jones, N. D.; Foo, S. J. L.; Patrick, B. O.; James, B. R. *Inorg. Chem.* **2004**, *43*, 4056 – 4063.

21) Jones, N. D.; Meessen, P.; Losehand, U.; Patrick, B. O.; James, B. R. *Inorg. Chem.* **2005**, *44*, 3290 – 3298.

22) Hounjet, L. J.; Bierenstiel, M.; Ferguson, M. J.; McDonald, R.; Cowie, M. *Dalton Trans.* **2009**, 4213 – 4226.

23) Fernández-Galán, R.; Jalón, F. A.; Manzano, B. R.; Rodríguez-de-la-Fuente *Organometallics* **1997**, *16*, 3758 – 3768.

24) Bertini, I.; Dapporto, P.; Fallani, G.; Sacconi, L. *Inorg. Chem.* **1971**, *10*, 1703 – 1707.

25) Baker, K. V.; Brown, J. M.; Cooley, N. A.; Hughes, G. D.; Taylor, R. J. *J. Organomet. Chem.* **1989**, *370*, 397 – 406.

26) Hounjet, L. J.; Bierenstiel, M.; Ferguson, M. J.; McDonald, R.; Cowie, M. *Inorg. Chem.* **2010**, *49*, 4288 – 4300.

27) Bacchi, A.; Balordi, M.; Cammi, R.; Elviri, L.; Pelizzi, C.; Picchioni, F.; Verdolino, V.; Goubitz, K.; Peschar, R.; Pelagatti, P. *Eur. J. Inorg. Chem.* **2008**, 4462 – 4473.

28) Liang, L.-C.; Chien, P.-S.; Huang, M.-H. *Organometallics* **2005**, *24*, 353 – 357.

29) Huang, M.-H.; Liang, L.-C. *Organometallics* **2004**, *23*, 2813 – 2816.

30) Gao, J.-X.; Ikariya, T.; Noyori, R. *Organometallics* **1996**, *15*, 1087 – 1089.

31) Haack, K.-J.; Hashiguchi, S.; Fujii, A.; Ikariya, T.; Noyori, R. *Angew. Chem., Int. Ed. Engl.* **1997**, *36*, 285 – 288.

32) Casey, C. P.; Johnson, J. P. *J. Org. Chem.* **2003**, *68*, 1998 – 2001.

33) Clapham, S. E.; Hadzovic, A.; Morris, R. H. *Coord. Chem. Rev.* **2004**, *248*, 2201 – 2237.

34) Takeuchi, R.; Yasue, H. *Organometallics* **1996**, *15*, 2098 – 2102.

35) Kakiuchi, F.; Nogami, K.; Chatani, N.; Seki, Y.; Murai, S. *Organometallics* **1993**, *12*, 4748 – 4750.

36) Zhang, Z.; Sherlock, D.; West, R.; West, R. *Macromolecules* **2003**, *36*, 9176 – 9180.

37) Fritz, H. P.; Gordon, I. R.; Schwarzhans, K. E.; Venanzi, L. M. *J. Chem. Soc.* **1965**, 5210 – 5216.

38) Jones, N. D.; Meessen, P.; Smith, M. B.; Losehand, U.; Rettig, S. J.; Patrick, B. O.; James, B. R. *Can. J. Chem.* **2002**, *80*, 1600 – 1606.

39) Uson, R.; Oro, L. A.; Cabeza, J. A. *Inorg. Synth.* **1985**, *23*, 126 – 130.

40) Programs for diffractometer operation, unit cell indexing, data collection, data reduction and absorption correction were those supplied by Bruker.

41) Altomare, A.; Burla, M. C.; Camalli, M.; Cascarano, G. L.; Giacovazzo, C.; Guagliardi, A.; Moliterni, A. G. G.; Polidori, G.; Spagna, R. *J. Appl. Cryst.* **1999**, *32*, 115 – 119.

42) Sheldrick, G. M. *Acta Crystallogr.* **2008**, *A64*, 112 – 122.

43) Beurskens, P. T.; Beurskens, G.; de Gelder, R.; Smits, J. M. M; Garcia-Granda, S.; Gould, R. O. (2008). The *DIRDIF-2008* program system. Crystallography Laboratory, Radboud University Nijmegen, The Netherlands.

44) Zefirov, Y. V.; Zorkii, P. M. *Russ. Chem. Rev. (Engl. Transl.)* **1989**, *58*, 421 – 440.

45) Bruice, P. Y. *Organic Chemistry, 4th edn.*, Pearson, Upper Saddle River, NJ, **2004**, p. 271.

46) Dahlenburg, L.; Herbst, K.; Zahl, A. *J. Organomet. Chem.* **2000**, *616*, 19 – 28.

47) Bacon, G. E. *Acta Cryst.* **1951**, *4*, 558 – 561.

48) Lebel, H.; Ladjel, C.; Bélanger-Gariépy, F.; Schaper, F. *J. Organomet. Chem.*

2008, *693*, 2645 – 2648.

49) Vaska, L. *Science* **1963**, *140*, 809 – 810.

50) Fryzuk, M. D.; MacNeil, P. A.; Rettig, S. J. *Organometallics*, **1986**, *5*, 2469 – 2476.

51) Feliz, M.; Freixa, Z.; van Leeuwen, P. W. N. M.; Bo, C. *Organometallics* **2005**, *24*, 5718 – 5723.

52) Gunanathan, C.; Ben-David, Y.; Milstein, D. *Science*, **2007**, *317*, 790 – 792.

53) Dorta, R.; Shimon, L.; Milstein, D. *J. Organomet. Chem.* **2004**, *689*, 751 – 758.

54) Allred, A. L. *J. Inorg. Nucl. Chem.* **1961**, *17*, 215 – 221.

55) Huheey, J. E. *J. Phys. Chem.* **1965**, *69*, 3284 – 3291.

56) (a) Bent, H. A. *J. Chem. Phys.* **1959**, *33*, 1258 – 1259. (b) Bent, H. A. *Chem. Rev.* **1961**, *61*, 275 – 311. (c) Alabugin, I. V.; Manoharan, M.; Buck, M.; Clark, R. J. *J. Mol. Struct.* **2007**, *813*, 21 – 27.

57) Broussard, M. E.; Juma, B.; Train, S. G.; Peng, W.-J.; Laneman, S. A.; Stanley, G. S. *Science* **1993**, *260*, 1784 – 1788.

58) Lewis, L. N.; Lewis, N. *J. Am. Chem. Soc.* **1986**, *108*, 7228 – 7231.

59) Stein, J.; Lewis, L. N.; Gao, Y.; Scott, R. A. *J. Am. Chem. Soc.* **1999**, *121*, 3693 – 3703.

60) Murata, K.; Konishi, H.; Ito, M.; Ikariya, T. *Organometallics*, **2002**, *21*, 253 – 255.

61) Soper, J. D.; Saganic, E.; Weinberg, D.; Hrovat, D. A.; Benedict, J. B.; Kaminsky, W.; Mayer, J. M. *Inorg. Chem.* **2004**, *43*, 5804 – 5815.

Chapter 6: Conclusions

6.1 Concluding Remarks

Initial objectives for the work described in this dissertation were: (1) To prepare a new series of *P*,*N*-ligands and investigate their coordination chemistry and hemilability[1] within mono- and binuclear complexes of late transition metals, (2) to study how hemilability might affect the reactivity of these complexes by comparisons with non-labile analogues in both stoichiometric and catalytic contexts, and (3) to examine the possibility for metal-metal cooperativity[2] within a series of binuclear derivatives by comparison with analogous mononuclear species in both stoichiometric and catalytic contexts. While many of these objectives have been met, comparisons of complex reactivity focussed largely on one type of catalytic reaction (olefin silylation[3]), and the results of this study have, in both cases, contradicted initial hypotheses that hemilability and metal-metal cooperativity should result in enhanced reactivity.[4] Nevertheless, a thorough spectroscopic study has provided an improved understanding of the fluxional processes that give rise to hemilability in *ortho*-phosphinoaniline complexes, and a comparison of *N*-methyl- and *N*,*N*-dimethylaniline moieties shows how steric alteration of the nitrogen donor can affect the rates of hemilabile exchange processes at rhodium(I).[5] We have also shown how such differences can significantly influence the coordination chemistry of these ligands at ruthenium(II).[6] In addition, we have developed new catalyst systems for ketone transfer hydrogenation and olefin silylation reactions. The transfer hydrogenation studies reported herein have raised some interesting questions about the possibility of an unprecedented reaction mechanism.[6] The comparison of *P*,*N*-chelates of rhodium as olefin silylation catalysts could have important implications for the design of more efficient catalyst systems incorporating hemilabile ligands and also demonstrates an efficient means for the removal of

highly soluble molecular catalysts from reaction mixtures by exploiting the reactivity of the amido funtionality.[4]

In Chapter 2, the preparation of a new series of hemilabile *ortho*-phosphinoaniline ligands containing the *N*-methylanilinyl functionality was described. These ligands, in addition to their previously reported *N*,*N*-dimethylaniline derivatives, were then complexed to the "[RhCl(CO)]" fragment. A detailed spectroscopic analysis of these [RhCl(CO)L] (L = *ortho*-phosphinoaniline) complexes shows that, within the *N*,*N*-dimethyl series, chemical exchange of labile amine donors is significantly faster than within the *N*-methyl series. A crystallographic comparison of the two sets of compounds demonstrates how steric interactions of the bulkier *N*,*N*-dimethyl donors with neighboring chloro ligands weaken their interactions with rhodium, providing a rationale for their enhanced lability relative to the smaller *N*-methyl donor. Diphosphinoaniline ligands were shown to bridge two metals via the diphosphine moiety while also chelating at each metal via the amine groups so that each half of a binuclear complex is structurally similar to mononuclear species. Interestingly, the binuclear *N*-methyl compound, $[Rh_2Cl_2(CO)_2(\mu\text{-}P,N,P',N'\text{-mapm})]$, exhibits a short intermetallic separation in the solid state due to transannular hydrogen bonding interactions between the chloro group on one metal and the amine hydrogen at the other. Conversely, within the *N*,*N*-dimethyl (dmapm-containing) derivative, a transannular steric repulsion between *N*-methyl and chloro groups at opposite metals forces the rhodium coordination planes apart. Our anticipation that metal-metal cooperativity should be more likely to occur for the *N*-methyl complex with the shorter intermetallic distance has not been realized. In fact, a comparison of similar species as olefin silylation catalysts (described in Chapter 5) showed that both (*N*-methyl and *N*,*N*-dimethyl) types of bimetallic complexes are somewhat catalytically inferior to their mononuclear counterparts indicating, at least in this case, that bringing the metals into close proximity via a bridging ligand actually appears to have an adverse effect on reactivity.

Chapter 3 discussed diverse coordination chemistries of four *ortho*-phosphinoanilines at ruthenium. Within the monophosphinoanilines, the *N*-methyl derivative was reluctant to chelate to ruthenium(II) since, in dichloromethane, the pendent amine hydrogen is engaged through a metastable hydrogen-bond with a chloro ligand resulting in the N lone pair being directed away from ruthenium. In refluxing methanol however, chelation can be irreversibly promoted as a chloro ligand is ejected from the inner-sphere to allow for coordination of the amine donor. The resulting cation can then be deprotonated by a weak base to generate a phosphine-amido complex, found to be effective as a transfer hydrogenation catalyst, but only in the presence of base, prompting the mechanistic investigation discussed in Chapter 4. Interestingly, the *N*,*N*-dimethyl analogue is never observed as a monodentate ligand at ruthenium(II) despite its greater lability at rhodium(I), discussed in Chapter 2. The diphosphinoanilines also show distinct coordination behaviours. While the *N*-methylaniline ligand displaces the coordinated arene in $[RuCl(\mu\text{-}Cl)(\eta^6\text{-}p\text{-cymene})]_2$ to generate a neutral species containing mapm bound as a tetradentate *P*,*P'*,*N*,*N'*-ligand, the *N*,*N*-dimethylaniline derivative displaces a chloro ligand to form a cationic, bidentate *P*,*P'*-chelate. Unfortunately, binuclear ruthenium carbonyl species were found to be unstable relative to a mixture of mono- and trinuclear complexes and mixed-metal complexes containing rhodium and ruthenium could not be isolated despite attempts by a number of synthetic routes. It appears that the mapm ligand ($Ar_2PCH_2PAr_2$; Ar = *o*-C_6H_4NHMe) prefers to bridge two rhodium nuclei, even upon the addition of a rhodium(I) precursor to a *P*,*P'*-mapm-chelated ruthenium(0) complex.

In Chapter 5, two new series of *ortho*-phosphinoaniline complexes of rhodium are described, again containing either *N*-methyl- or *N*,*N*-dimethylaniline groups. One objective of this study was to compare cationic, hemilabile amine and neutral, non-labile amido complexes as olefin silylation catalysts. The latter are found to be more active, possibly owing to a greater propensity for Si–H oxidative addition at the more nucleophilic rhodium center within these amido

species. While comparisons of mono- and binuclear species were carried out to probe for evidence of metal-metal cooperativity during catalysis, this investigation failed to show evidence for such an effect, actually demonstrating superior activity of the former. Despite this shortcoming, the catalysts prepared are shown to be highly active at low catalyst loadings, exhibiting some selectivity for dehydrogenative olefin silylation. From a preliminary kinetic analysis, we propose that the addition of a labile, pendent amine functionality within these catalysts may improve their longevity and efficiency. The neutral phosphine-amido complexes, which are quite effective catalysts in the absence of solvent owing to their solubility in the substrate, can be easily removed from reaction mixtures by protonation to generate insoluble cationic species. The potential for reactivity at the amido functionality was also investigated by stoichiometric reactions, which demonstrated its relative inertness, showing a propensity for oxidative addition at rhodium. The crystallographically inferred delocalization of amido electron density over both the arene and rhodium provides a rationale for the poor nucleophilicity of nitrogen, suggesting that activation of the silane does not involve its heterolysis across the Rh–N bond.

In Chapter 3 ketone transfer hydrogenation catalysis was carried out in the presence of a phosphine-amido complex of ruthenium. The observation that catalysis only occurred in the presence of an added base ruled out the involvement of an "outer-sphere" mechanism involving simultaneous deprotonation of substrate alcohol by the amido group and hydride transfer to ruthenium. The objective of Chapter 4 was to further investigate the mechanism of this reaction. We were able to directly discount the catalytic involvement of a hydrido complex since its independent preparation and subsequent reactivity study showed significantly inferior activity relative to the chloro-containing precatalyst used in combination with a strong base. The fact that the hydrido complex can be prepared by reaction of the chloro derivative with basic isopropanol suggests its formation by β-hydride elimination from a (yet unobserved) transient isopropoxo intermediate, structurally analogous to a surprisingly stable ethyl derivative. The

likely catalytic intermediacy of an isopropoxo species points to the possible involvement of a less explored Meerwein-Ponndorf-Verley-Oppenauer mechanism, the likes of which has not yet been shown to occur within ruthenium-catalyzed transfer hydrogenation processes.

The work described in this thesis illustrates how subtle differences in steric and electronic characteristics of *ortho*-phosphinoaniline ligands can drastically affect their behaviour at rhodium and ruthenium. These ligands are shown to be particularly useful because the tunability of the nitrogen donor allows for a range of differences in coordination chemistry, lability and reactivity. Deprotonation of *ortho*-phosphinoanilines at late metals is also shown to generate a number of amido complexes. While the presence of an aryl substituent at nitrogen allows for the isolation and characterization of many stable amido-metal species, the weaker basicity of this amido donor greatly hinders its involvement in the activation of small molecules. Nevertheless, these phosphine-amido compounds are quite useful as catalysts because of their strong donor character, which enhances reactivity of the metal while simultaneously providing stability to the complex as a chelating unit.

6.2 References

1) (a) Jeffrey, J. C.; Rauchfuss, T. B. *Inorg. Chem.* **1979**, *18*, 2658 – 2666. (b) Slone, C. S.; Weinberger, D. A.; Mirkin, C. A. *Prog. Inorg. Chem.* **1999**, *48*, 233 – 350. (c) Braunstein, P.; Naud, F. *Angew. Chem. Int. Ed.* **2001**, *40*, 680 – 699.

2) Broussard, M. E.; Juma, B.; Train, S. G.; Peng, W.-J.; Laneman, S. A.; Stanley, G. G. *Science*, **1993**, *260*, 1784 – 1788.

3) (a) Cipot, J.; McDonald, R.; Ferguson, M. J.; Schatte, G.; Stradiotto, M. *Organometallics*, **2007**, *26*, 594 – 608. (b) Karstedt, B. D. (General Electric) *US Patent* 3 715 334. (c) Hitchcock, P. B.; Lappert, M. F.; Warhurst, N. J. W.

Angew. Chem., Int. Ed. Engl. **1991**, *30*, 438 – 440. (d) Stein, J.; Lewis, L. N.; Gao, Y.; Scott, R. A. *J. Am. Chem. Soc.* **1999**, *121*, 3693 – 3703. (e) Speier, J. L. *Adv. Organomet. Chem.* **1979**, *17*, 407 – 447.

4) Hounjet, L. J.; McDonald, R.; Ferguson, M. J.; Cowie, M. *Inorg. Chem.* **2011**, DOI: ic-2010-01883u.

5) Hounjet, L. J.; Bierenstiel, M.; Ferguson, M. J.; McDonald, R.; Cowie, M. *Dalton Trans.* **2009**, 4213 – 4226.

6) Hounjet, L. J.; Bierenstiel, M.; Ferguson, M. J.; McDonald, R.; Cowie, M. *Inorg. Chem.* **2010**, *49*, 4228 – 4300.

Appendices

Appendix I: Drying Agents for Solvents

Solvent	**Drying Agent / Indicator**
Dichloromethane	P_2O_5
n-Pentane	Na
Tetrahydrofuran	Na / benzophenone
Diethyl Ether	Na / benzophenone
Benzene	Na / benzophenone
Methanol	$MgSO_4$
Isopropanol	Mg
Nitromethane	CaH_2
Nitrobenzene	CaH_2
Acetonitrile	CaH_2
Acetone	$CaCl_2$ / benzophenone

Appendix II: Coauthor Contributions

AII.1 Chapters 1 and 6

Martin Cowie assisted with revising and editing.

AII.2 Chapter 2

Matthias Bierenstiel first prepared and partially characterized the ligands Ph_2PAr (Ar = *o*-C_6H_4NMe) and mapm ($Ar_2PCH_2PAr_2$). In addition, he also first prepared and partially characterized the complexes [RhCl(CO)(*P*,*N*-Ph_2PAr)] (**5**), [RhCl(CO)(*P*,*N*-PAr'_3)] (**9**) and [$Rh_2Cl_2(CO)_2$(μ-*P*,*P'*,*N*,*N'*-mapm)] (**10**). Michael J. Ferguson and Robert McDonald collected all crystallographic data. Martin Cowie supervised the project and assisted with revising and editing.

AII.3 Chapter 3

Matthias Bierenstiel first prepared and partially characterized the complex [RuCl(η^6-*p*-cymene)(*P*,*N*-Ph_2PAr')]Cl (**3b**). Michael J. Ferguson and Robert McDonald collected all crystallographic data. Martin Cowie supervised the project and assisted with revising and editing.

AII.4 Chapter 4

Michael J. Ferguson collected all crystallographic data. Martin Cowie supervised the project and assisted with revising and editing.

AII.5 Chapter 5

Michael J. Ferguson and Robert McDonald collected all crystallographic data. Martin Cowie supervised the project and assisted with revising and editing.

Appendix III: Crystallographic Data

Structure reports, crystallographic information files (CIFs) and checkCIF reports for the structures discussed in Chapters 2 – 5 can be obtained free of charge by contacting either Dr. Robert McDonald or Dr. Michael Ferguson at the address below and quoting the internal reference number(s) for the appropriate compound(s) provided in the following sections:

X-Ray Crystallography Laboratory (Room E3-13)
Department of Chemistry, University of Alberta
11227 Saskatchewan Drive NW
Edmonton, AB, Canada, T6G 2G2
Tel.: 1 780 492 2485
Fax.: 1 780 492 8231
E-mail: bob.mcdonald@ualberta.ca
michael.ferguson@ualberta.ca

AIII.1 Chapter 2

Compound #	Internal Reference Number
5	COW0529
6	COW0813
7	COW0812
9	COW0517
10	COW0611
11	COW0709
14	COW0838

AIII.2 Chapter 3

Compound #	Internal Reference Number
2a	COW0821
2b	COW0936
2c	COW0937
3b	COW0524
4	COW0904
5	COW0712
6b	COW0802
7	COW0923

AIII.3 Chapter 4

Compound #	Internal Reference Number
3	COW1008

AIII.4 Chapter 5

Compound #	Internal Reference Number
1a	COW0931
2	COW0921
3	COW1016
4	COW1017
5	COW1044
8	COW0910
9	COW1022